

Proceedings of the International Atomic Energy Agency Specialists' Meeting on Subcritical Crack Growth

Sessions I and II

**Held at Freiburg, Federal Republic of Germany
May 13-15, 1981**

Edited by W. H. Cullen

**Sponsored by
International Atomic Energy Agency
U.S. Nuclear Regulatory Commission**

**Proceedings prepared by
Materials Engineering Associates, Inc.**

The views expressed in these proceedings are not necessarily those of the U. S. Nuclear Regulatory Commission.

The submitted manuscript has been authored by a contractor of the U.S. Government under contract. Accordingly the U.S. Government retains a nonexclusive, royalty-free license to publish or reproduce the published form of this contribution, or allow others to do so, for U.S. Government purposes.

Available from

GPO Sales Program
Division of Technical Information and Document Control
U.S. Nuclear Regulatory Commission
Washington, DC 20555

Printed copy price: \$7.50

and

National Technical Information Service
Springfield, VA 22161

Proceedings of the International Atomic Energy Agency Specialists' Meeting on Subcritical Crack Growth

Sessions I and II

**Held at Freiburg, Federal Republic of Germany
May 13-15, 1981**

Date Published: May 1983

**Edited by
W. H. Cullen**

**Sponsored by
International Atomic Energy Agency
U.S. Nuclear Regulatory Commission
Office of Nuclear Regulatory Research**

**Proceedings prepared by
Materials Engineering Associates, Inc.
9700B George Palmer Highway
Lanham, MD 20706**

**Under subcontract to:
ENSA, Inc.
3320 Bailey Avenue
Buffalo, NY 14215
NRC FIN B8133**

ABSTRACT

This report is a compilation of papers which were presented at the IAEA Specialists' Meeting on Subcritical Crack Growth, held at the Fraunhofer-Institute for Fracture Mechanics, Freiburg, FRG, May 13-15, 1981. These papers describe the experimental procedures for and interpretation of results of fatigue crack growth rate testing of pressure vessel and piping steels in pressurized, high-temperature water.

CONTENTS

	<u>Page</u>
ABSTRACT.....	111
1. EXECUTIVE SUMMARY.....	1
2. INTRODUCTION.....	3
3. SESSION I - CRACK GROWTH OF PV STEEL IN THE LOWER OXYGEN CONTENT WATER RELEVANT TO PRESSURIZED WATER REACTOR (PWR) CONDITIONS	
3.1 "Corrosion Fatigue Crack Growth of Pressure Vessel Welds in PWR Environment," W. H. Bamford, L. N. Ceschini, D. M. Moon.....	7
3.2 "An Investigation of Fatigue Crack Growth in SA508-2 in a 288°C PWR Environment by a Constant ΔK Test Method," W. A. Van der Sluys, D. S. DeMiglio.....	41
3.3 "Cyclic Crack Growth in High-temperature Water: Results of an International Testing Round Robin," R. L. Jones.....	65
3.4 "Fatigue Crack Growth Rates of Irradiated Pressure Vessel Steels in Simulated Nuclear Coolant Envi- ronment," W. H. Cullen.....	91
3.5 "Design-, Operation-, and Inspection-Relevant Fac- tors of Fatigue Crack Growth Rates for Pressure Vessel and Piping Steels," W. H. Cullen.....	109
3.6 "Experience with an Autoclave-Refreshing-System for Crack-Growth Measurements under PWR- and BWR- Environmental Conditions, " A. Gerscha, E. Klausnitzer, N. Wieling.....	129
4. SESSION IIA - CRACK GROWTH OF PV STEELS IN THE HIGH OXY- GEN CONTENT WATER RELEVANT TO BOILING WATER REACTOR (BWR) CONDITIONS	
4.1 "Crack Growth Resistance of Low Alloy Steel in High- temperature Oxygenated Water," D. A. Hale, C. H. Lange, J. N. Kass.....	141

CONTENTS

	<u>Page</u>
4.2 "Fatigue Crack Growth Through Typical Weld HAZ Microstructures of SA-533 GR B Steel in BWR Environment," T. Kondo, H. Nakajima, H. Takahashi, T. Shoji.....	179
5. SESSION IIB - PIPE WORK	
5.1 "Crack Growth Behavior of Sensitized Stainless Steel in High-Temperature, High-Purity Oxygenated Water," R. M. Horn, D. A. Hale, C. W. Jewett, C. H. Lange, J. N. Kass.....	191
5.2 "Low Temperature Sensitization of Weld Heat-Affected Zones in Type 304 Stainless Steel," R. D. Caligiuri, L. E. Eiselstein, M. J. Fox.....	231
5.3 "Effect of PWR Environment on the Fatigue Crack Growth of Different Stainless Steels and Inconel Type Alloy," C. Amzallag, G. Baudry, J. L. Bernard.....	261
5.4 "The Role of Uncertainty in the Measurement of Crack Length by Compliance Technique," R. G. Ballinger, R. M. Latanision, W. C. Moshier, R. M. N. Pelloux.....	293

1. EXECUTIVE SUMMARY

This specialists' meeting grew out of the work of the International Cyclic Crack Growth Rate Group. The proceedings consist of contributions representing the work of scientists and engineers from seven nations. The topics center on fatigue crack growth of pressure vessel and piping steels in light-water reactor environments. Several papers describe measurement of growth rates for a variety of steels; others discuss fractographic observations, postulate micromechanistic processes of subcritical crack growth, and describe methods of applying these data sets to reactor-typical geometries.

Since many laboratories have recently begun the development of the techniques necessary for research in high-temperature, aqueous environments, most of the projects deal with a specific material-environment-loading description. Similarly, the micromechanistic descriptions which are postulated, are usually based on a specific set of test results. For many of the laboratories, these results were among the first generated with the test facilities, and the data sets occasionally contain artifacts which reflect experimental difficulties.

Several laboratories are rapidly advancing the state-of-the-art in the areas of test practice, data interpretation, applications of data to structural models, and micromechanistic model development. While the bulk of the experimental programs address pressure vessel steels, research results from piping steels and steam generator alloys is also presented. Many of the basic observations of the effects of a single variable (load ratio, waveform, material chemistry) seem to be in hand, and current research seeks to investigate the combined effects of several variables and to develop more complete micromechanistic models.

2. INTRODUCTION

Because of the complex testing systems and technological sophistication which is required for pressurized high-temperature water fatigue crack growth rate (FCGR) testing, the development of data for nuclear applications has been slowed relative to that for marine environments or other near-ambient situations. The first published reports include work from Westinghouse Nuclear Energy Systems (Refs. 1,2), Japan Atomic Energy Research Institute (Refs. 3,4) and General Electric-Nuclear Energy Division (Ref. 5). Beginning in 1975, other laboratories began to provide data addressing various aspects of environmentally-assisted fatigue crack growth in reactor-component materials.

By 1977, the interest level and the number of laboratories capable of performing research in reactor-water environments had risen to the point that it was possible to pool these technical resources to better address the difficulties of testing, interpretation of data and application of results. Under the guidance of K. Lynn (NRC) and K. Stahlkopf (EPRI) and with the organizational help of H. E. Watson of the Naval Research Laboratory an International Cyclic Crack Growth Rate (ICCGR) Group was formed. Representatives from seven nations agreed to contribute their efforts to the goals of the Group. From that start, the Group has grown to include members from forty-one organizations, representing eleven nations. The growth and vitality of the ICCGR Group has both fueled and drawn from the concurrent growth and vitality of the world-wide research programs in environmentally-assisted crack growth rate testing.

In addition to providing a forum for the discussion of recent results and for the exchange of information on test techniques, the ICCGR Group inaugurated specific projects aimed at standardizing test practices and data processing techniques. Two round robin programs, one on data processing and one on test conduct were carried out in the 1979-1981 time frame. The results of the data processing program have ultimately led to revised guidelines for data acquisition, processing and plotting. The data from the experimental round robin (Ref. 6) have led to a new awareness of certain critical variables, especially environment and waveform.

By 1981, the intensity and productivity of these programs warranted a more open forum than the semiannual meetings of the ICCGR Group would allow. Under the sponsorship of the International Atomic Energy Agency this symposium was held at the Institut für Werkstoffmechanik (IFW) in Freiburg, FRG. About sixty attendees heard thirty-one contributions, interlaced with discussions and summaries. While most of the presentations were contributed by personnel from ICCGR-member laboratories, papers were also contributed by authors involved in other nuclear-component areas of interest, principally in structural applications.

A large amount of crack growth data, spanning all types of pressure vessel and piping steels as well as steam generator materials (Inconel and other high alloy materials) was presented for the first time. Several papers discussed models for crack growth based on the micromechanistic processes of hydrogen assistance and anodic dissolution. Fractographic results were presented in an attempt to define crack growth mechanisms. A session on data applications contained contributions describing the use of data for design and in-service inspection procedures as well as some specialized applications. It was clear that the state-of-the-art had been successfully presented to the attendees over the duration of this meeting.

Since this symposium was held, significant additional progress has been made both within the ICCGR Group and by the individual member laboratories working on their own programs. The overall data base has been significantly expanded, and the influence of several critical variables has been explored and more accurately assessed. Several programs have been initiated to specifically address the micromechanistic crack tip chemistry and deformation processes. Many laboratories have established expertise in the use of high-temperature reference electrodes and are able to measure the free corrosion potential of the specimens under test. This quantity can suggest whether hydrogen evolution is occurring (at low potentials) on the specimen surface, or whether passivation, or oxidation is occurring (at higher potentials). Such information is invaluable support for model development.

The ICCGR has designed a second experimental round robin, this time using a larger specimen (50 mm thick compact specimen) and a higher load ratio ($R = Q.7$). Additionally, several laboratories are cooperating in other kinds of specific exchange programs, involving testing or post-test examination of certain types of steels of a specific interest to two or three laboratories. A description of the current status of the ICCGR Group activities can be found in Reference 8.

The proceedings of this meeting were originally published in a very limited edition and were issued mainly to participants and attendees. In response to requests from researchers in this field, they are being reprinted to achieve a more widespread distribution. The ICCGR Executive Committee has tentatively planned a second specialists' meeting to be held in 1984.

REFERENCES

1. T. R. Mager and V. J. McLoughlin, "The Influence of an Environment of High Temperature Primary Grade Nuclear Reactor Water on the Fatigue Crack Growth Characteristics of A 533 Grade B Class 1 Plate and Weldment Material," Heavy Section Steel Technology Program Technical Report No. 16, HSST-TM-16, Oct. 1971.
2. T. R. Mager, J. D. Landes, V. McLoughlin and D. M. Moon, "The Effect of Low Frequencies on the Fatigue Crack Growth Characteristics of A 533B Class 1 Plate in an Environment of High Temperature Primary Grade Nuclear Reactor Water," Heavy Section Steel Technology Program Technical Report No. 35, HSST-TM-35, Dec. 1973.
3. T. Kondo, T. Kikuyama, H. Nakajima and M. Shindo, "Fatigue of Low-Alloy Steels in Aqueous Environment at Elevated Temperatures," in Proc. of the 1971 Int. Conf. on Mechanical Behavior of Materials, Vol.III, 1972, pp. 319-327.
4. T. Kondo, T. Kikuyama, H. Nakajima, M. Shindo and R. Nagasaki, "Corrosion Fatigue of ASTM A302B Steel in High Temperature Water, the Simulated Nuclear Reactor Environment" in Corrosion Fatigue: Chemistry, Mechanics and Microstructure, NACE-2, eds. O. Devereux et al., National Association of Corrosion Engineers, Houston, TX 77027, 1973, pp. 539-556.
5. T. L. Gerber, J. D. Heald and E. Kiss, "Fatigue Crack Growth in SA508-C1.2 Steel in a High Temperature, High Purity Water Environment," Trans. ASME, Ser. H, J. Eng. Mat. and Technology, 96, 1974, pp. 255-261.
6. R. L. Jones, "Cyclic Crack Growth in High-Temperature Water: Results of a Testing Round Robin," in this volume, pp. 65 - 88.
7. G. Slama and R. Jones, "International Cooperative Group on Cyclic Crack Growth Rate, in Proceedings of the 5th SMIRT Post-Conference Seminar, Paris, France, Aug, 1981, pp. 311-325.
8. W. H. Cullen, "Work of the International Cyclic Crack Growth Rate Group on Environmentally-affected Crack Growth," in Proceedings of the U.S. Nuclear Regulatory Commission Tenth Water Reactor Safety Research Information Meeting, NUREG/CP-0041, Vol. 4, 1983, pp. 9-22.

CORROSION FATIGUE CRACK GROWTH OF PRESSURE VESSEL
WELDS IN PWR ENVIRONMENT

W. H. Bamford, L. J. Ceschini, and D. M. Moon

Westinghouse Electric Corporation
Pittsburgh, PA. USA

ABSTRACT

The fatigue crack growth rate behavior of several pressure vessel steel welds in PWR environment will be discussed. The behavior will be compared with associated heat-affected zone behavior, and with comparable base metal results. The welds show different degrees of susceptibility to the environmental influence, and this will be discussed in some detail, along with fractographic observations on the tested specimens.

INTRODUCTION

During the past several years a program has been conducted to study the corrosion fatigue characteristics of automatic submerged arc weldments used for nuclear reactor pressure vessels. Three different fluxes were studied, representing the range of fluxes employed by United States manufacturers. These are all produced by the Linde Division of Union Carbide Corporation and are designated Linde 124, 0091 and 80.

The chemical composition of the welds and associated heat-affected zones studied is summarized in Table 1. Several heats of A533B class 1 plate and A508 class 2 forging steel were also studied, and these added significantly to the interpretation of the observed behaviors. The composition of these heats was also included in Table 1 for reference.

A test matrix was constructed to study these welds, so that they could be suitably compared under similar test conditions. As may be seen in Table 2, two loading effects variables were investigated. The R/ratio (minimum stress/maximum stress) is known to be the major factor influencing fatigue crack growth rates of these materials in water environments. The second loading variable investigated was the wave form, for which the sine wave was compared to a ramp/reset condition. Both load forms resulted in a 17 mHZ frequency.

Results of the testing indicate that there are significant differences in the corrosion fatigue crack growth rate behavior of the three types of welds studied. These behavioral differences arise from metallurgical differences in these welds, which can be separated from environmental and loading variables. Although the explanation for all the observed behavior is not yet complete, significant progress has been made in characterizing the corrosion fatigue behavior of these welds.

The primary variables which were found to affect crack growth rates in the simulated PWR environment were

- R ratio
- Loading wave form
- Sulfur content

Fatigue crack growth rates were increased with higher R ratio values and with sinusoidal wave forms as opposed to ramp/reset loadings. It also appears that the sulfur content of the steel or weld has a very strong influence on the environmental susceptibility, with high sulfur resulting in more susceptibility. The R ratio affected all materials equally, while the latter two effects were material dependent.

TEST PROCEDURES

The fatigue crack growth rate tests were conducted in a pressurized water environment produced in autoclaves which were heated to the desired temperature with electrical heaters embedded in the chamber wall. Complete details of the test chamber have been previously discussed.⁽¹⁾ Test conditions used in the present study were primarily water at 288°C (550°F) and 14 Mpa (2000 lb/in²). The pressurized water chemistry is maintained by a flowing system with carefully monitored oxygen and thermal conductivity.

The tests were carried out using 2 in. thick (5.08 cm) precracked fatigue specimens of the compact and WOL configurations which were sinusoidally stressed under load control. Test autoclaves contained single specimens, and employed independent water systems. The specimens were machined from the center of the weld, oriented as shown in Figure 1, with the crack propagating in the direction of welding. The heat-affected zone specimens were oriented similarly, except that the plane of the specimen was set at a slight angle so that the crack could follow the boundary of the weld.

Crack growth was monitored continuously with an externally mounted linear variable differential transformer (LVDT) which reflects the face opening displacement of the specimen. The LVDT reading was then converted to crack length using a compliance method based on beach marks purposely produced on the specimen. The resulting crack length vs. cycles data was then converted to crack growth rate data, using the incremental polynomial method recommended by ASTM. This method has the dual advantages of being the least subjective method of data processing, as well as producing a large amount of data, which aids in establishing trends and making comparisons.

As a result of exposure to the high temperature water the fracture surfaces were covered with a dense oxide obscuring any fractographic information. An electrolytic cleaning technique involving scrubbing with cathodic hydrogen was used to remove this oxide scale.

All of the fractographic examinations were conducted using a scanning electron microscope. Due to the obliterating action of the oxidation on the fine fracture surface features, no advantage was found in using the higher resolving power of the transmission electron microscope and replicating procedures. The finest striation spacing measured on the cleaned fracture surface using the scanning electron microscope was 5.08×10^{-5} cm (2×10^{-5} in.).

To study the density and size distribution of the carbides in the weld and base metal samples, an extraction replica technique was employed using a 10% solution of bromine in methanol.

CRACK GROWTH RATES IN WELDS

Of the three fluxes studied, there is little to separate one from the other in terms of general observations on quality, weldability or general corrosion resistance. There are some differences in the chemical makeup which can be seen from Table 1. The Linde 124 and Linde 80 flux are similar in that they contain higher levels of silicon and manganese than the Linde 0091 flux. This is true in general for these fluxes, and the approximate ranges of content observed on a large number of heats are shown in terms of weight percent below:

	Mn	Si
Linde 124	1.25 - 1.35	0.4 - 0.5
80	1.25 - 1.35	0.4 - 0.5
0091	1.10 - 1.20	< 0.3

In the welds tested, the sulfur levels were considerably different, with the Linde 0091 containing much less sulfur than the other two. This cannot be said to be true in general, however, as opposed to the comments above on

manganese and silicon. The sulfur content of a given weld is a strong function of the date of manufacture of the nuclear vessel, with sulfur levels having dropped gradually with time, to the point where today the weight percentage is seldom as high as 0.010, regardless of the flux used. A detailed review of available crack growth results is provided below for each of the fluxes, followed by appropriate comparisons.

LINDE 124 FLUX

The first weld to be studied was a submerged arc weld of the type now used for most reactor vessel welds. The results available to date are summarized in Figures 2 and 3 for R ratio values of 0.2 and 0.7, and there is a very clear R ratio effect, typical of that observed on all the materials studied. Also shown in all figures are the ASME Section XI reference curves^[2] for these steels in air and light water reactor environments. The most striking result of these tests in Figure 2 is that there is considerable scatter in the results, with the crack growth rates showing small increases and decreases along the overall advance of growth rate with applied ΔK . The growth rates observed were in general somewhat less than for base metal specimens of the same chemistry. The heat affected zone specimen in Figure 2 behaved very similarly to the welds, and there is no definite effect of the ramp-reset loading form as compared to the sine wave. This lack of wave form effect is in marked contrast to results for another weld, to be discussed later.

The results obtained for higher R ratio, and summarized in Figure 3 are less well behaved. This was true in general for the high R tests of all the materials. It was apparently very difficult for the crack growth acceleration due to the environment to sustain itself. Only one of the four weld specimens tested could produce a growth rate above 10^{-3} mm/cycle; all the others arrested, as can be seen in the figure. The cracks failed to advance far enough to produce applied ΔK values greater than 20 MPa \sqrt{m} . In one case, a specimen was tested for 7 months, amassing 166,000 cycles. (Typical test time was 40,000 cycles). Based on results from other tests, the fact that the single specimen which grew was tested under a ramp-reset loading is probably not signifi-

cantly related to the choice of waveform. The heat-affected zone specimen did show a more conventional behavior, typical of that of the A533 B plate specimens tested at high R. Thus even though it was a heated-affected zone, the fact that it was plate material was probably the governing factor.

LINDE 80 FLUX

These welds were also made by the submerged arc process, and were primarily used in vessels made entirely of forgings. Test results are summarized in Figures 4 and 5 for the welds, and in Figures 6 and 7 for the heat affected zones. An effect not found in other materials was exhibited in these welds: after the initial part of the test, the crack growth rate often decreased tremendously, producing in effect a deep "V" in the data plots. The effect is particularly pronounced for the ramp-reset loading, but also was produced in one sine wave specimen to a considerably smaller degree. At present, these results cannot be effectively explained, but since the sinusoidal wave form is more typical of actual reactor system loading conditions, these results must be considered more typical for in service behavior prediction, and the ramp reset results set aside for further study.

Considering the sinusoidal results, it is apparent that the same R ratio effect is observed as for the other materials, and it is also worthy of note that the crack growth at high R ratio does not show the arrest phenomenon observed in the Linde 124 weld, even though the sulfur and other chemical content is reported to be nearly the same. The available results appear to be in much better agreement in the high R case than the low R case (Fig. 5).

The reversal effect noted above for the ramp-reset condition is even more noticeable in the case of the heat-affected zones where test results are reported in Figures 6 and 7. Again the sine loading results were typically the same as those of other materials, although a reversal did occur in the high R sine specimen, as shown in Figure 7.

LINDE 0091 FLUX

This weld type has been used on a large number of reactor pressure vessels made of plate material, as opposed to forgings. The welds studied under the test matrix were both very low in sulfur compared with the other two weld types tested, as may be seen in Table 1. This low sulfur content is not a special characteristic of the Linde 0091 flux; it is simply a coincidence that both of these welds were low in sulfur.

The welds made with this flux both showed very little environmental enhancement when tested at low R ratio as shown in Figure 8. The crack growth rate behavior was parallel with the ASME reference air line, and remained a straight line. On the other hand, a heat-affected zone specimen tested at $R = 0.2$ showed a considerable amount of environmental sensitivity, but a look at the chemistry of the adjoining plate in Table 1 shows that its sulfur content is very high, about 0.020 weight percent. Accordingly, the growth rates observed for this heat-affected zone specimen are higher than any of the other welds or heat affected zones, which all had lower sulfur contents.

There is a significant R ratio effect for the Linde 0091 welds, just as for the other welds as shown in Figure 9. It is interesting to note that the R ratio effect shows up even for a material which has no significant environmental enhancement at low R ratio, and the amount of enhancement due to R ratio increase is approximately equal to that which was observed on the other materials. Thus, even though the magnitude of environmental enhancement in crack growth is apparently proportional to the sulfur content of the material, the R ratio effect may be independent of this factor, providing the same relative increase in crack growth rate irrespective of the sulfur content.

The effect of loading wave form has not been addressed adequately for this material, because there is no single heat where both wave forms have been used. Indications are that for these low sulfur welds the wave form is an important effect, perhaps even comparable with the magnitude of the R ratio enhancement, as suggested by Figure 9.

COMPARISONS

It is clear from the above discussion that a great many comparisons of different welds tested under the same conditions are now possible. Some possibilities can be developed from study of Table 2, and for this reason all the figures in

this paper have been drawn on a common scale. Two examples of comparisons have been included here as Figures 10 and 11.

In Figure 10 it can be seen that the Linde 80 weld tested shows more environmental sensitivity at low R ratio than does the Linde 0091 weld. The next figure shows a similar conclusion for the Linde 124 weld. It is postulated that these differences are due more to the weld chemistry than to any fundamental differences in the flux types. Table 1 shows that the sulfur content of the Linde 80 and Linde 124 welds is nearly the same, and over fifty percent higher than that of the Linde 0091 weld "D".

The welds in general, show more scatter in the fatigue crack growth rate data than base metal specimens, and of the welds studied the most scatter appears in the Linde 124 samples. This scatter manifests itself in waves or "wiggles" in the portrayal of crack growth rate vs applied stress intensity factor range ΔK . The most likely explanation for this behavior is that there are many microstructural variations in the fusion zone. This scatter appears to decrease as the sulfur level decreases.

The trends observed with sulfur content are similar to those observed in a number of heats of base metal, in that steels with sulfur content less than 0.010 weight percent are inherently less susceptible to environmental enhancement.

FRACTOGRAPHY OF TESTED SPECIMENS

Fracture surface examination has been carried out on a considerable number of the tested specimens. A detailed list is included as part of Table 2. Many of the specimens so studied have been discussed in earlier reports [e.g. 3] but only occasionally have comparisons been made. This section will attempt to provide a more comprehensive comparison of the materials tested and examined to date, which include plate, forging, submerged arc welds using three different flux types, and heat affected zones in both plate and forging materials.

Specimens were examined from nearly all the materials which have been tested in this program, including base metals, welds and associated heat-affected zones. The fracture surfaces indicate that corrosion fatigue crack

growth proceeds by a number of different modes, some of which can operate simultaneously in a single specimen. The dominant mode for a given material appears to be most strongly dependent on the microstructure present, and is not related directly to the crack growth rates observed macroscopically, or the levels of environmental enhancement.

In forgings, regardless of R ratio, crack growth proceeds by well-developed ductile striation formation. This remains the dominant mode of propagation in the plate material as well, but striations are often less well-defined, and are often accompanied by areas which show a cleavage-like appearance. Considerable differences appeared in the welds studied, as discussed next.

LINDE 124 FLUX

The fracture surfaces of all specimens of this weld exhibit a predominance of dimpled rupture, whether tested in air or in the PWR environment. The fracture surface tested in air is the cleanest, and clearly shows the role being played by the large carbide particles in the weld metal, serving as nucleation sites for dimpled rupture. A minor amount of ductile striation formation can also be seen under close examination.

The fracture surface features of the specimens tested in water are considerably obscured by oxidation, but at both $R = 0.2$ and $R = 0.7$ the surfaces are very similar to the air specimen, with a preponderance of dimpled rupture. This behavior is shown for both R ratios in Figure 12, where it can be seen that the amount of dimples is enhanced at the higher R ratio.

LINDE 80 FLUX

The Linde 80 flux has been primarily used in welding forgings, while the Linde 124 flux discussed above is primarily used for welding plates, and the welds tested in this program are typical in this respect. In contrast to the Linde 124 weld metal, the Linde 80 weld metal specimens are characterized more by ductile striation formation than dimpled rupture, which may be related to the relative ease of ductile striation formation in the forging as compared to plates.

At the low R ratio and low to intermediate values of applied ΔK the fracture surface has a rough texture, with occasional ductile striations discernable on about half the surface. The density of carbide-nucleated dimples is very low. At higher applied K, the incidence of secondary cracking and dimples increases, along with a decrease in density of well defined ductile striations, as seen in Figure 13. At higher R ratio, again the density of carbide assisted dimples is very low, with the dominant fractographic feature being ductile striations as shown in the bottom portion of Figure 13.

LINDE 0091 FLUX

The Linde 0091 flux has been generally used to weld A533B plates together. The fracture appearance of these specimens appears to be intermediate between the predominantly dimpled structure of the Linde 124 weld and the ductile striations seen in the Linde 80 weld. The fracture surface at the low R - ratios appears to be a mixture of carbide nucleated dimples interspaced throughout with poorly defined ductile striations, as seen for example in Figure 14. At higher R ratio (0.7) the structure has less well-defined striations and is more dominated by dimples, as seen in the bottom portion of the figure.

HAZ

Heat-affected-zone specimens were examined from both a forging (C-3 HAZ) and a plate (D-1HAZ). In both specimens the results were similar, and results are shown in Figure 15. At low magnification the familiar rumpled markings that characterize fatigue (region A in both figures) were the predominant feature, but there were occasional regions exhibiting a more brittle appearance. Noted previously only in the plate material, these areas have river markings that lie nearly perpendicular to the direction of main crack propagation. At higher magnification these brittlelike areas are generally devoid of any distinctive pattern which could indicate the mechanism responsible for their appearance. The area surrounding these regions does contain ductile fatigue striations, however.

SUMMARY AND CONCLUSIONS

Corrosion fatigue crack growth rate tests conducted over the past several years in simulated PWR environments have enabled identification of the major loading variables which can affect the level of crack growth rate. These are R ratio and loading frequency. Recent studies of this body of data have uncovered new material - related variables which can also have a significant impact on the level of growth observed. The primary variable observed thus far is the level of sulfur in the material. Results have shown a remarkable increase in the environmental sensitivity with increasing sulfur level. This variable appears to explain a number of previously observed results, and appears to be applicable to all pressure vessel steels welds and heat-affected zones.

Among the welds and HAZ materials studies there are considerable differences in behavior, but these are at present thought to be of secondary importance to the R ratio and sulfur content.

The fractographic results further reflect the conclusion that there are significant differences in the crack growth behavior from material to material. Unlike the rather clearly defined trend in macroscopic crack growth results which appears related to sulfur content, however, the fracture morphology appears to be more related to the basic microstructure of the material.

Studies to date have found no evidence in the fractography to suggest that this sulfur effect is directly related to mechanical mechanisms such as accelerated growth due to tearing at sulfide inclusions. In no case was evidence for such effects seen, although they had been previously noted by Wilson [5] to influence the fatigue crack growth of A533B Class 1 steel in air.

In the tests conducted to date in PWR water, the only correlation between high sulfur and fractographic features occurs in specimens D-1HAZ and C-3HAZ which were both relatively high in sulfur and showed enhanced growth. The brittle-appearing component is present in both specimens, although not present in the weld or forging material. As noted previously, however, this component was present in the plate material fracture surfaces, and may be associated more with the bainitic/martensitic microstructure than with the sulfur effect.

The fractography of the sample having the lowest sulfur and the least enhancement in crack growth behavior at $R = 0.2$, D-1WLD, gives little indication of the reason for this unusual behavior. The fracture surface is intermediate between the heavily dimpled structure of the Linde 124 weld, and the striation-dominated appearance of the Linde 80 welds. Although more microstructural characterization work needs to be done to explain this variation in fractography among the weld specimens, the large amount of dimpling and microcracks present in the Linde 124 weld metal is probably related to the density and size of the large globular carbide particles present. The microstructure of the Linde 124 weld contains a much higher density of these particles than is present in the plate material.

Although studies of the mechanisms of corrosion fatigue are in their infancy at present, and relatively few heats of weld and HAZ materials have been characterized, it is clear that crack growth rates of these materials in PWR water environments are not significantly different than those of the base metals involved. Although the crack growth is less regular than that of the base metals, the actual magnitude is overall slightly lower, which reinforces conclusions reached by many earlier investigators of these materials from air tests.

ACKNOWLEDGEMENT

This work was sponsored by the Reactor Safety Research Division of the U.S. Nuclear Regulatory Commission, through a subcontract from the U.S. Naval Research Laboratory. The continuing support of this agency is appreciated.

REFERENCES

1. Bamford, W. H., "The Effect of Pressurized Water Reactor Environment on Fatigue Crack Propagation" in The Influence of Environment on Fatigue, Institution of Mechanical Engineers London 1977.
2. ASME Boiler and Pressure Vessel Code, Winter addendum, 1980 Edition Section XI, Appendix A, New York, N.Y.
3. Bamford, W. H. and Moon, D. M., "Some Mechanistic Observations on the Crack Growth Characteristics of Pressure Vessel and Piping Steels in PWR Environment" Corrosion vol. 36, no. 6, June 1980.
4. Wilson, A. D., "Fatigue Crack Propagation in A533B Steels - Metallographic and Fractographic Analysis" ASME Trans. Journal of Pressure Vessel Technology, Vol. 101 May 1979 p. 155.

TABLE 1
Materials Chemistries

MATERIAL	C	Mn	P	S	Si	Ni	Cr	Mo	Cu	V	Co
Linde 124 Weld "C"	.085	1.32	.013	.012	.48	.91	.14	.49	.05	.005	-
Linde 124 Weld HAZ "C" (adjoining plate plate)	.23	1.33	.009	.014	.22	.58	-	.55	.12	-	-
Linde 80 Weld "C"	.14	1.36	.019	.014	.42	.54	.06	.37	.18	-	-
Linde 80 Weld "C" HAZ adjoining forging	.23	.58	.005	.008	.28	.72	.39	.60	.05	.03	.02
Linde 0091 Weld "D"	.14	1.06	.012	.008	.20	-	-	.48	.15	-	-
Linde 0091 Weld "D- HAZ	.25	1.37	.010	.020	.27	.61	-	.55	.13	-	-
A533B C1 1 "L83" "2D", "02GB" "04A" "1HT" "IN" "TW" "W7"	.22	1.37	.008	.008	.22	.66	.15	.54	.18	-	-
	.22	1.45	.011	.019	.22	.69	.12	.53	-	-	-
	.23	1.29	.010	.018	.24	.60	.09	.50	.14	-	-
	.19	1.28	.009	.013	.25	.61	.04	.55	.10	.005	-
	.21	1.26	.012	.026	.25	.47	-	.47	.19	-	-
	.21	1.38	.008	.004	.21	.67	-	.56	.08	-	-
	.23	1.40	.005	.004	.25	.70	-	.57	-	-	-
A508 C1 2 "R", "R2", } "R1" "F", "F1" "V82" "Q71"	.19	.64	.010	.009	.23	.69	.42	.60	-	-	-
	.19	.60	.010	.012	.26	.70	.33	.56	-	.02	.008
	.20	.60	.013	.012	.20	.73	.35	.56	-	-	-
	.19	.69	.007	.009	.31	.82	.38	.62	.01	-	-

+

TABLE 2
TEST SPECIMENS COMPLETED

MATERIAL	Test Conditions			
	R = 0.2		R = 0.7	
	One Cycle Per Minute SINE	One Min-Ramp No Hold	One Cycle Per Minute SINE	One Min-Ramp No Hold
Linde 124 Weld (2TWOL)	*C-2 *C-3	C-7 C-9	* C-1 C-6	C-8 C-10
Linde 124 Weld HAZ (In A533B C1 1 Plate) (2TCT)		*C-24-HAZ-1		C-23-HAZ-1
Linde 80 Weld (2TCT)	* C-3-WLD C-6-WLD	C-1-WLD	C-4-WLD C-7-WLD	* C-2-WLD
Linde 80 Weld HAZ (In A508 C1 2 Forging) (2TCT)	*C-3-HAZ	* C-1-HAZ	C-4-HAZ	C-2-HAZ
Linde 0091 Weld (2TCT)	D-1-WLD * D-3-WLD		* D-2-WLD	
Linde 0091 Weld HAZ (In A533B C1 1 Plate) (2TCT)	*D-1-HAZ			

(*denotes specimens studied fractographically)

TABLE 3

MAKEUP WATER CHEMISTRY - PRESSURIZED WATER REACTOR

Electrical Conductivity	< 20 μ mhos/cm @ 25°C
ph	5-9
Oxygen	< 0.10 ppm
Chloride	< 0.15 ppm
Fluoride	< 0.15 ppm
Total Solids	< 0.5 ppm
Carbon Dioxide	< 2.0 ppm
Particulates	Filtered to < 25 microns
Silica	< 0.2 ppm
Li ⁷ OH	1×10^{-4} molal Li (~ 0.68 ppm Li ⁷)
Boric Acid	Variable (0 for ph = 9) (~ 1500 ppm B for ph = 5)
Hydrogen	25 - 35 cc/Kg H ₂ O

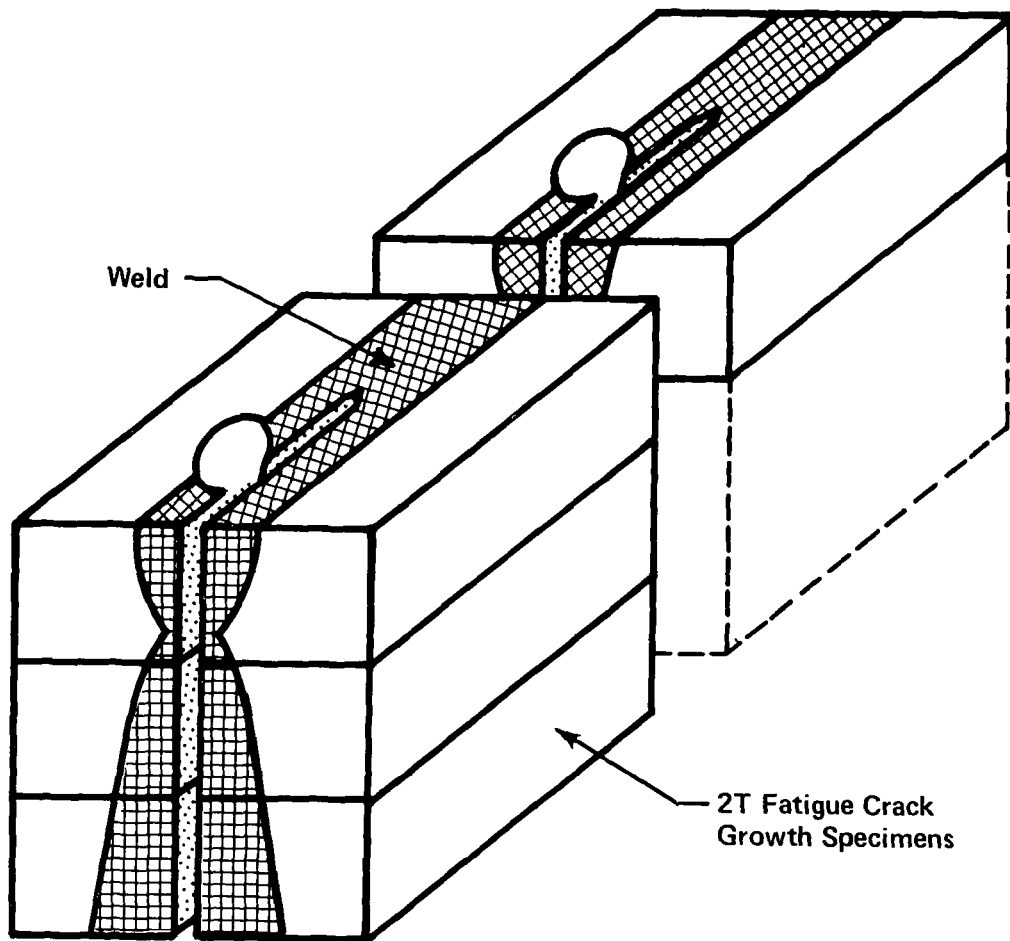


Figure 1. Orientations of Weldment Specimens

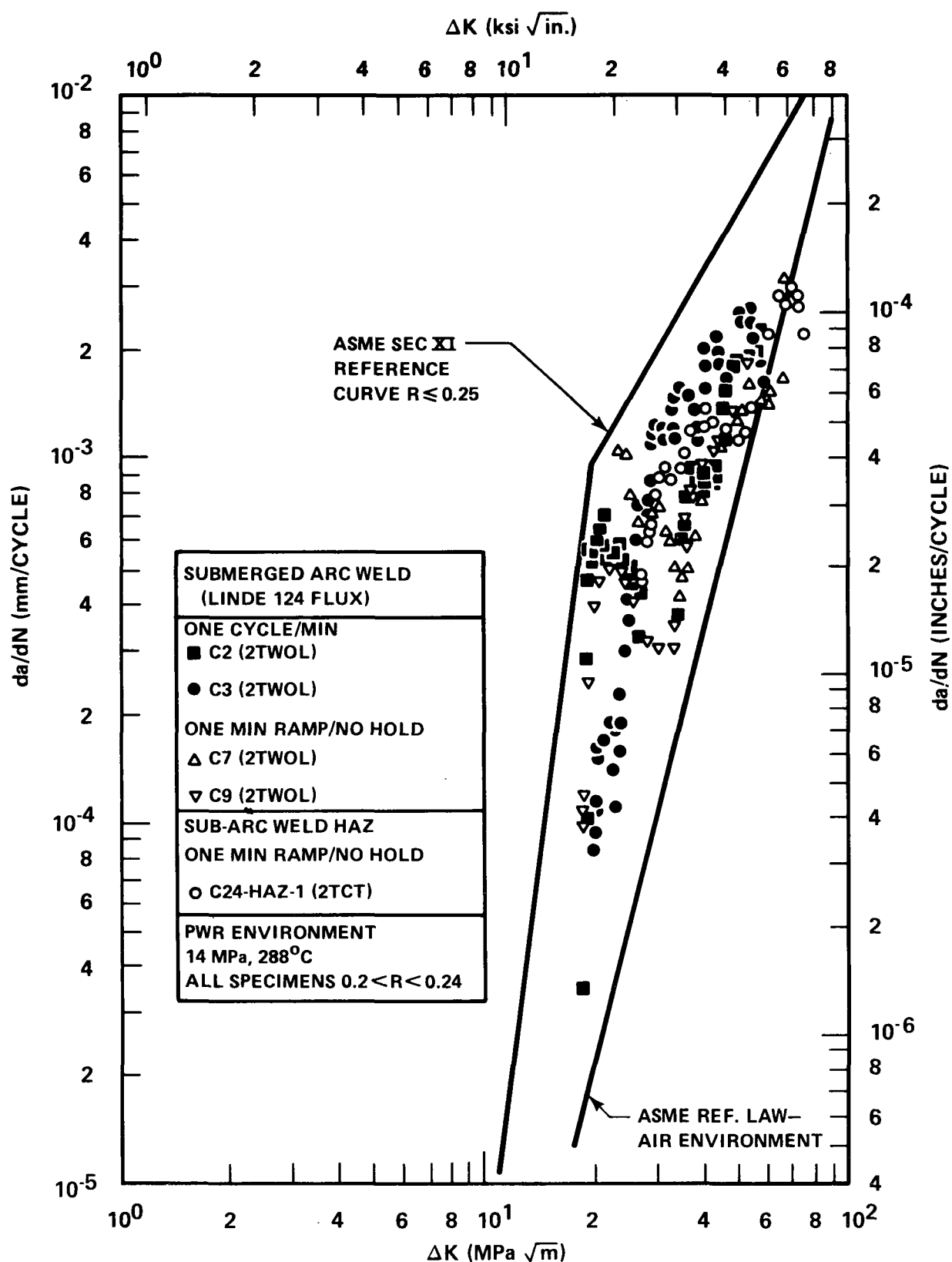


Figure 2. Results for Linde 124 Weld Tested in PWR Environment, $R = 0.2$

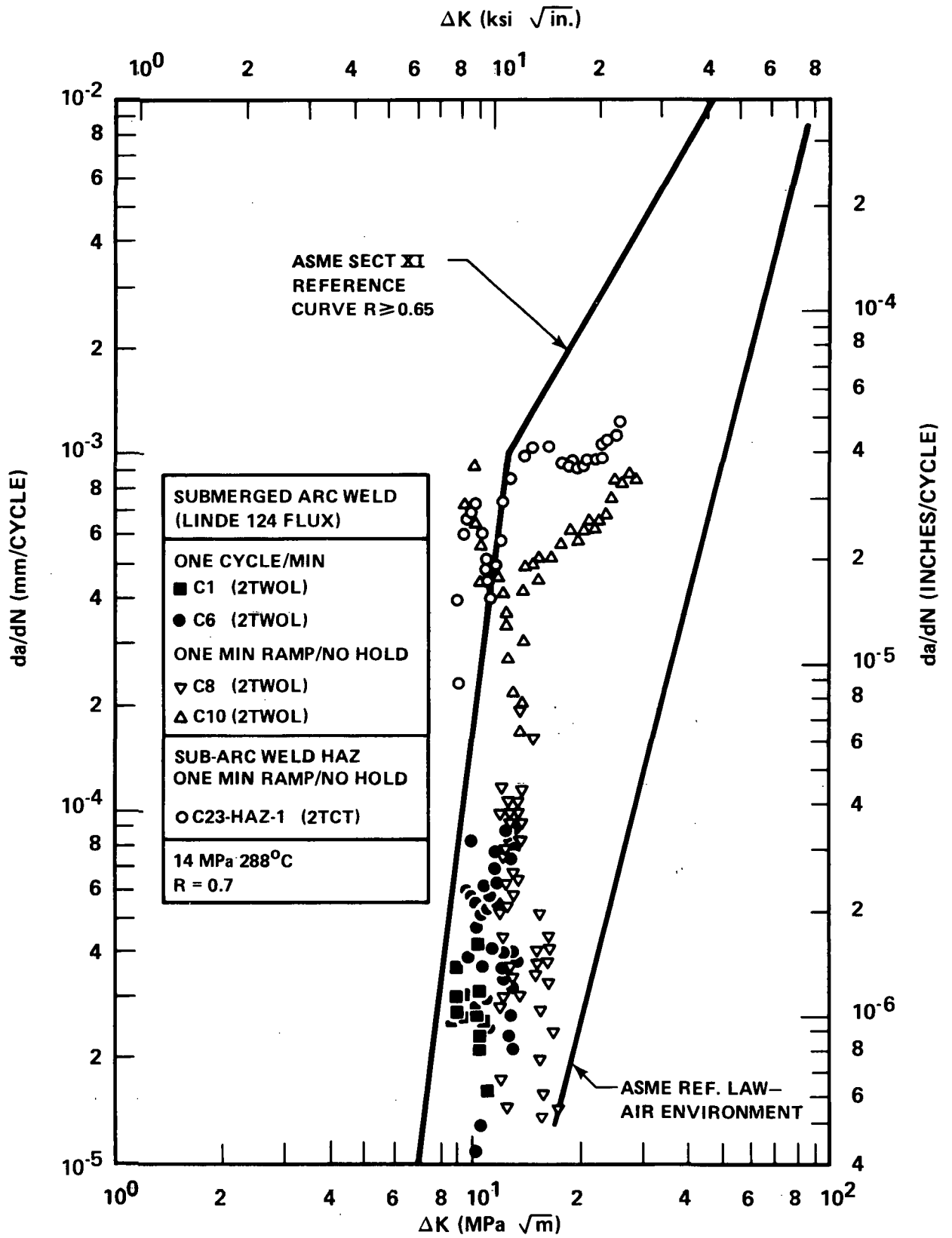
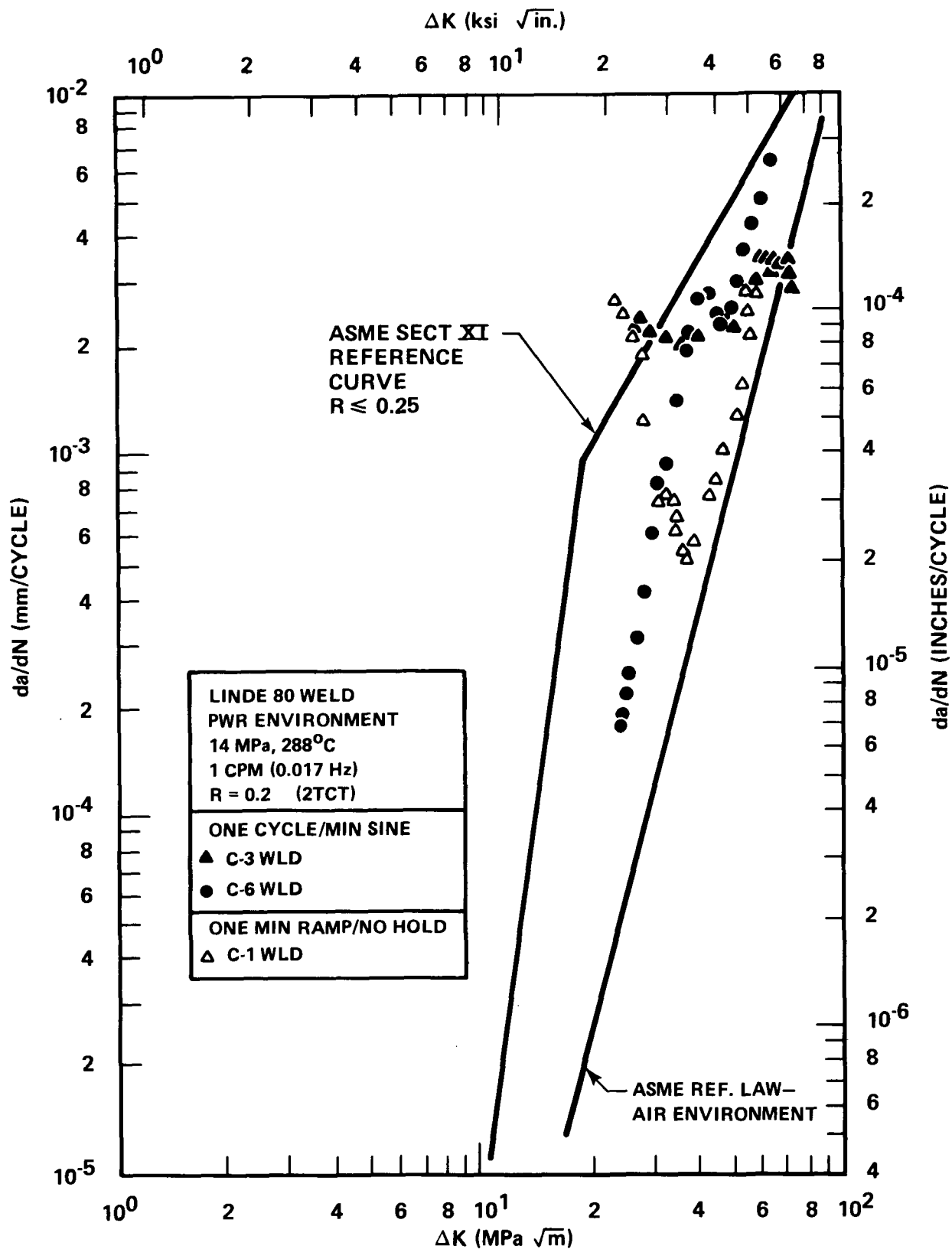
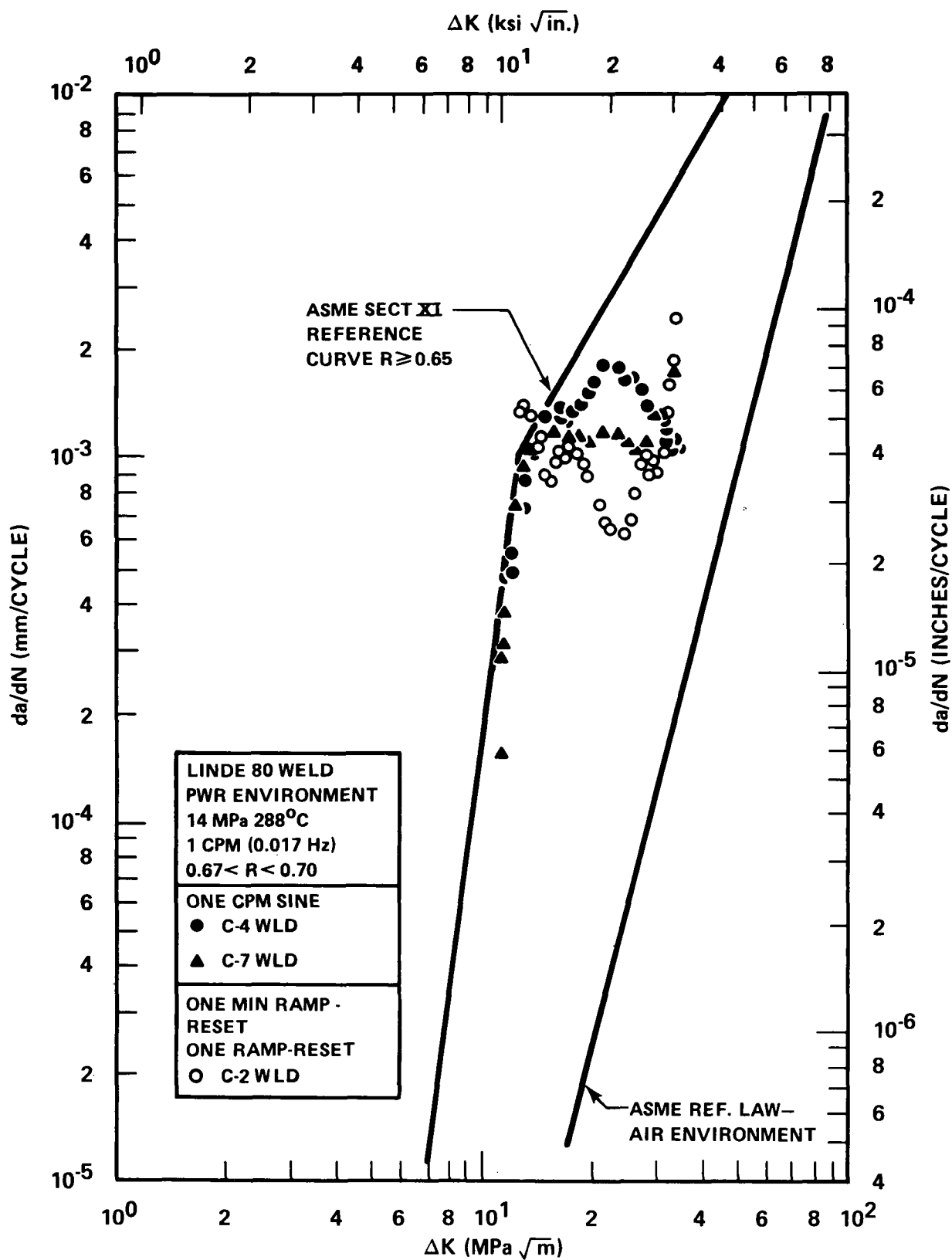
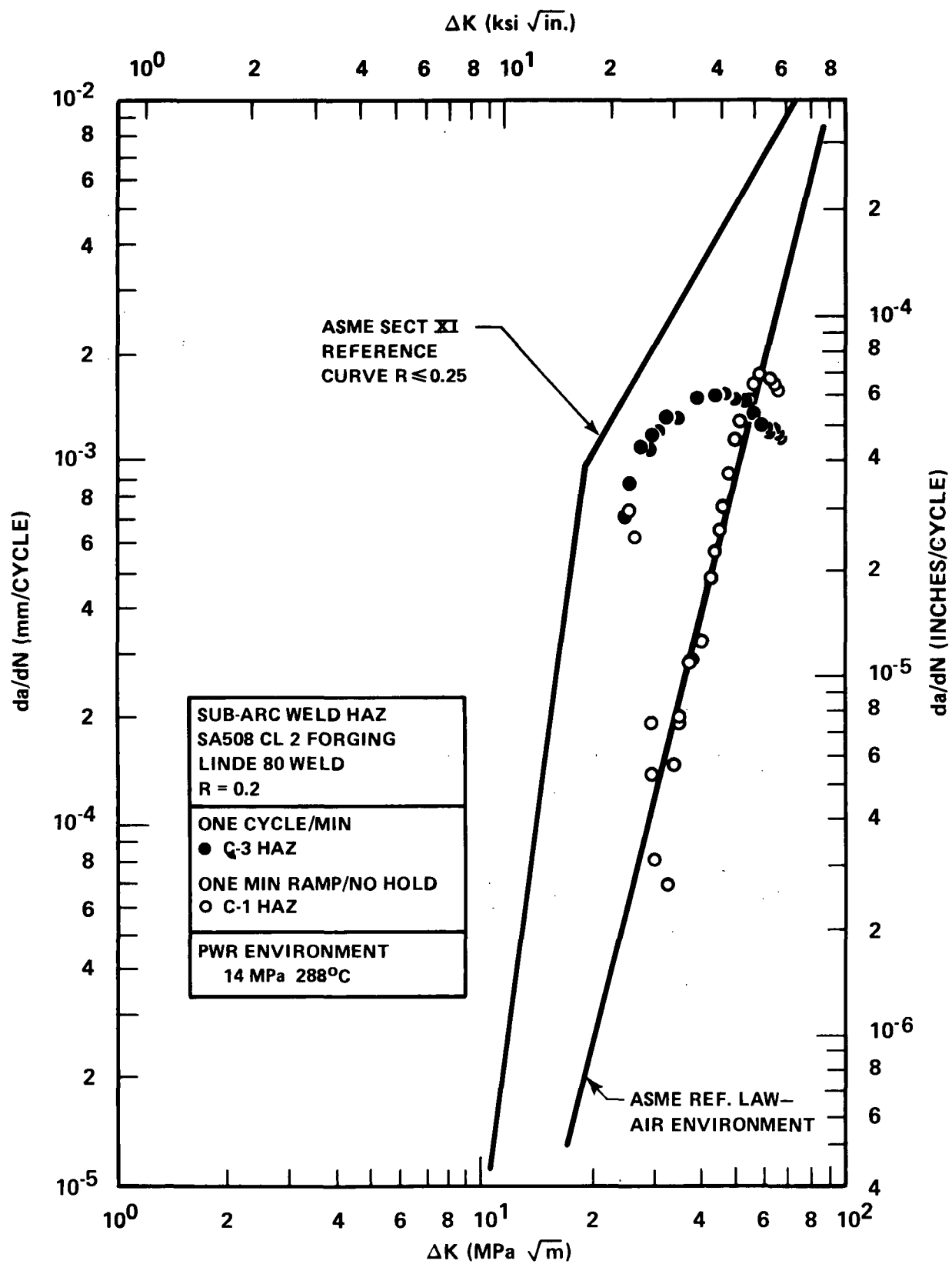
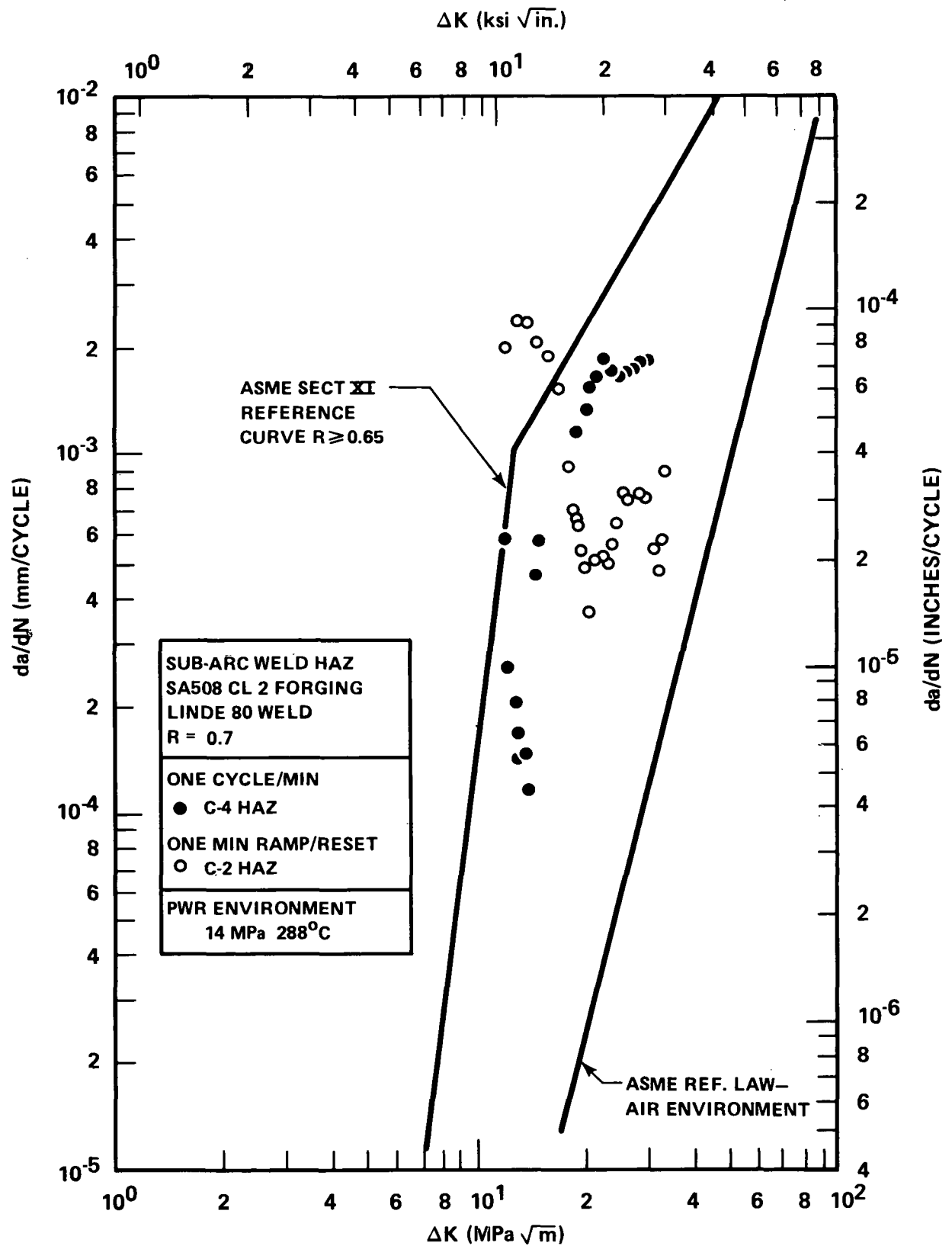


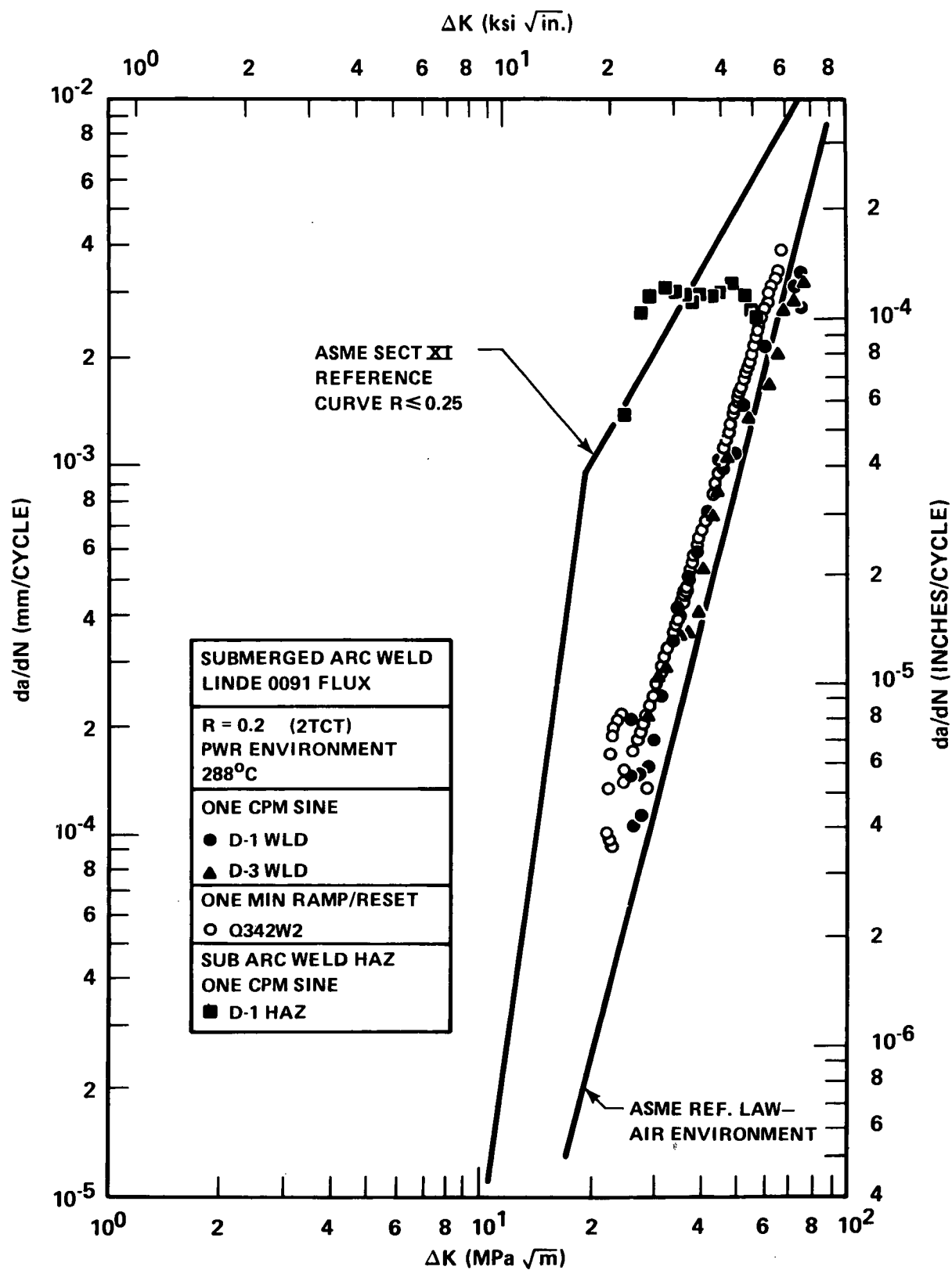
Figure 3. Results for Linde 124 Weld Tested in PWR Environment, $R = 0.7$

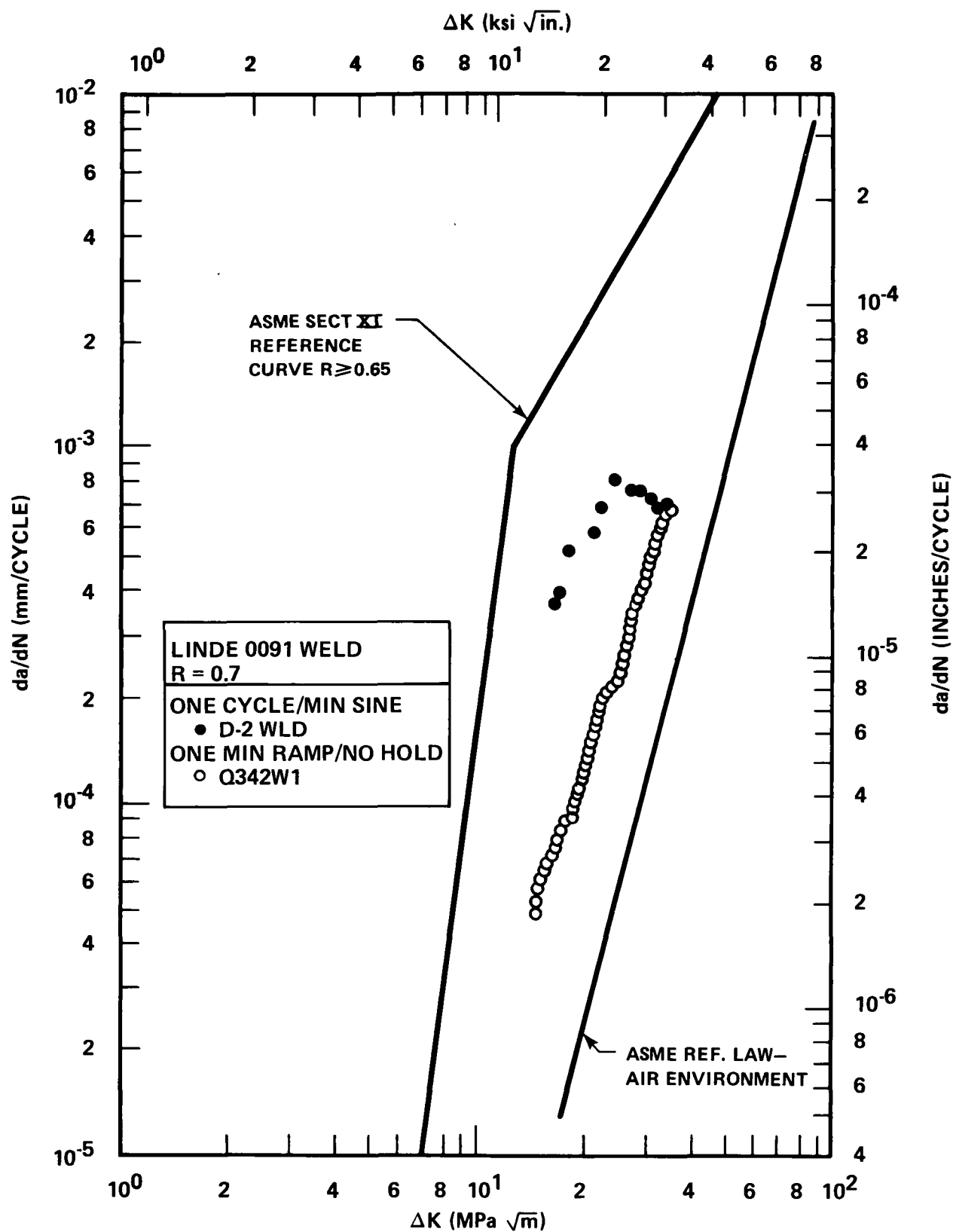
Figure 4. Results for Linde 80 Welds Tested at $R = 0.2$

Figure 5. Results for Linde 80 Welds Tested at $R = 0.7$

Figure 6. Results for Forging HAZ Tested at $R = 0.2$

Figure 7. Results for Forging HAZ Tested at $R = 0.7$

Figure 8. Results for Linde 0091 Welds Tested at $R = 0.2$

Figure 9. Results for Linde 0091 Welds Tested at $R = 0.7$

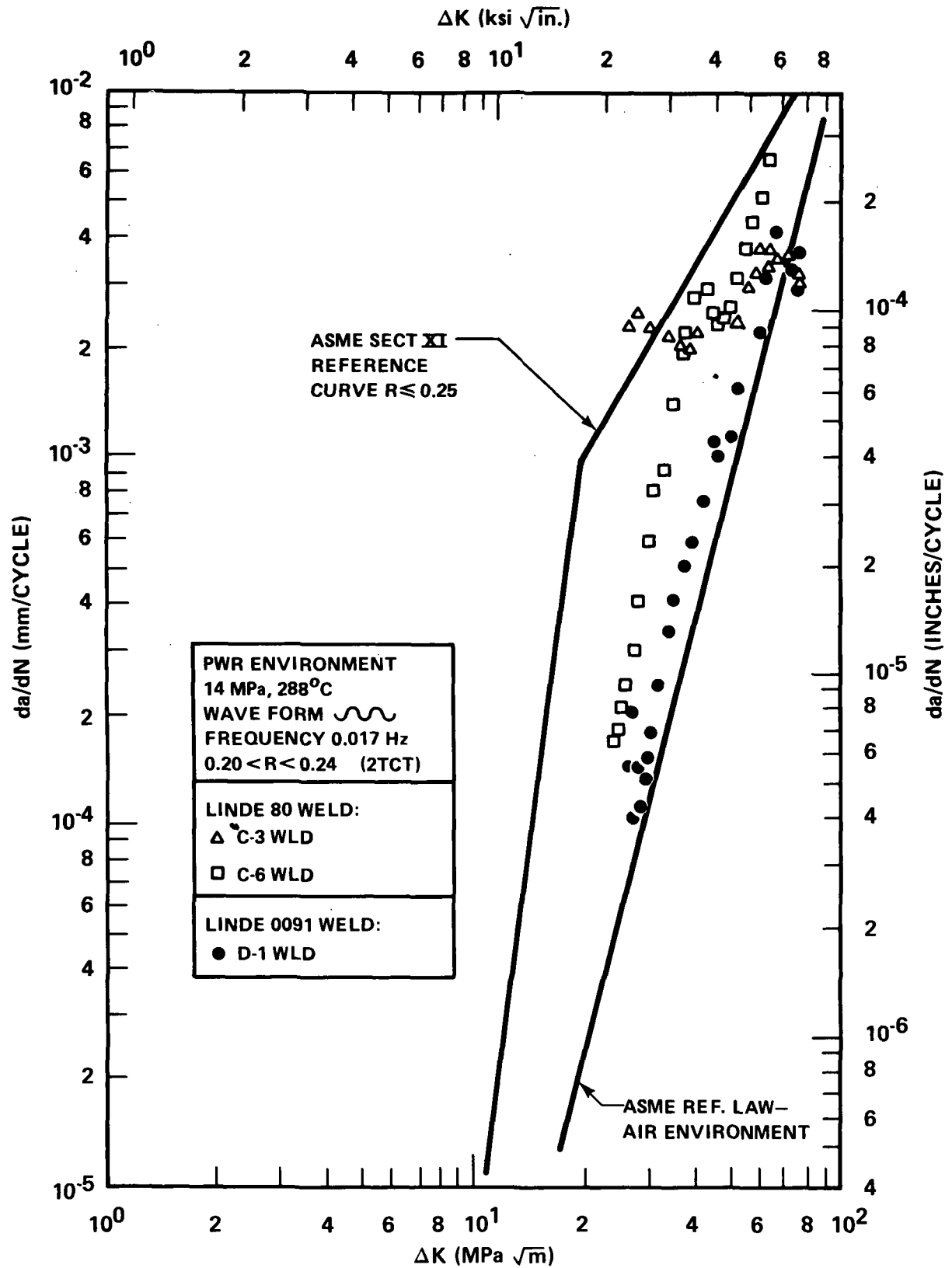


Figure 10. Comparison of Crack Growth for Linde 80 and Linde 0091 Welds

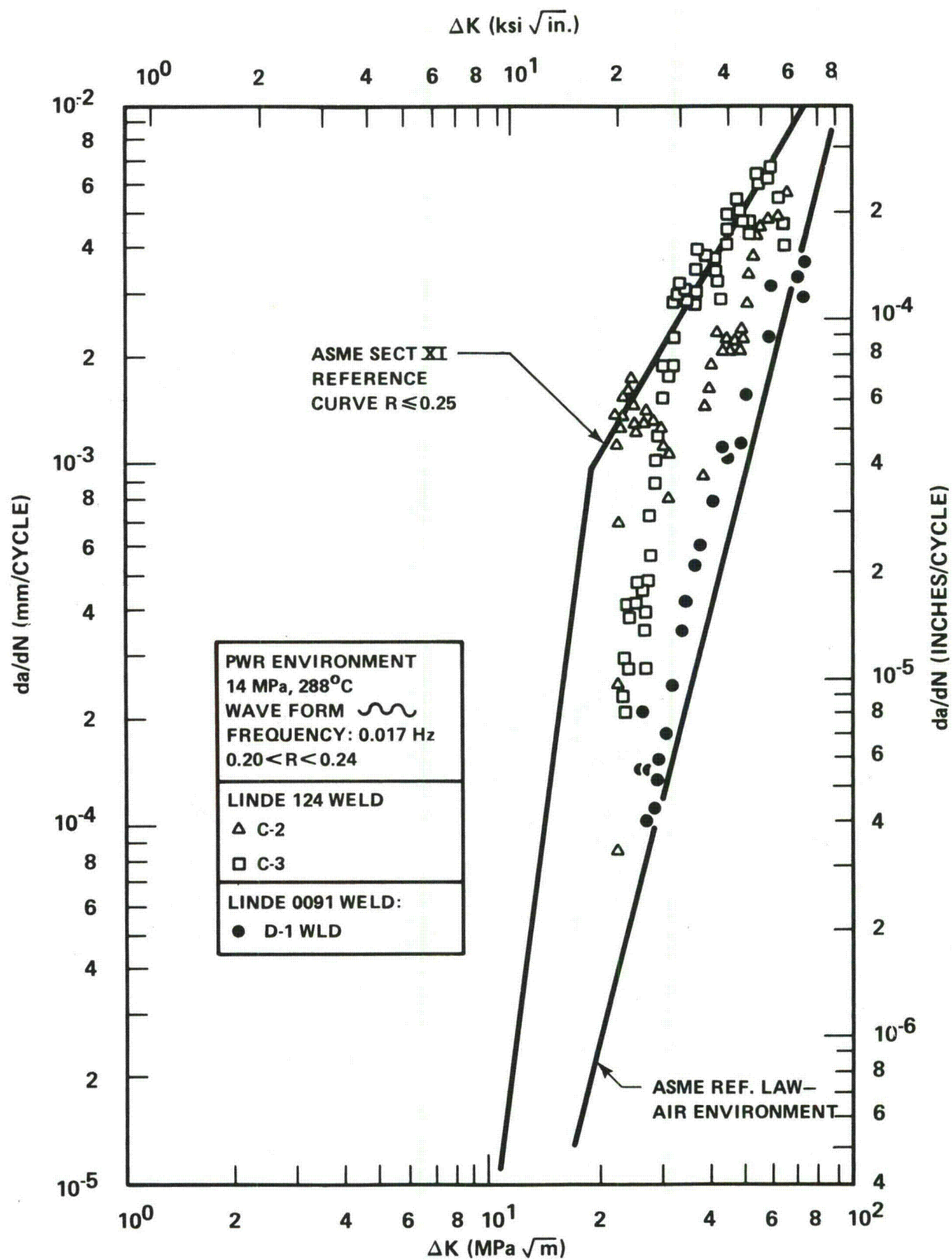
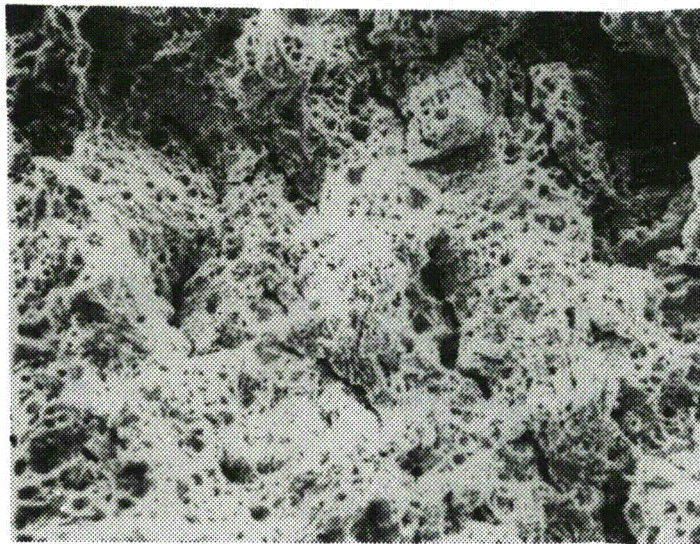
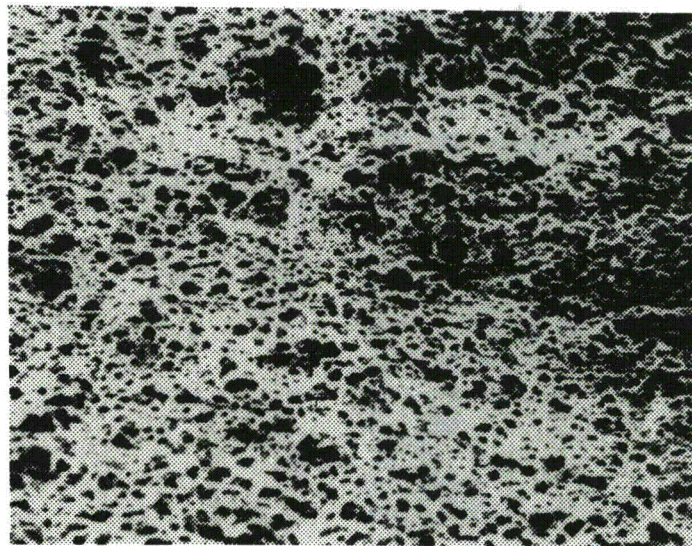


Figure 11. Comparison of Crack Growth in Linde 124 and Linde 0091 Welds



Specimen C-2, $R = 0.2$

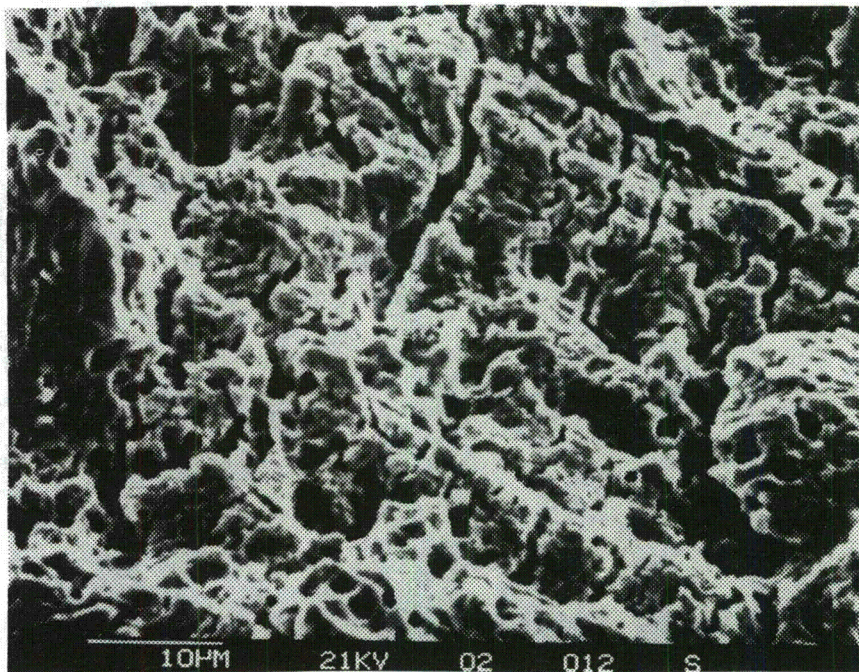
500X



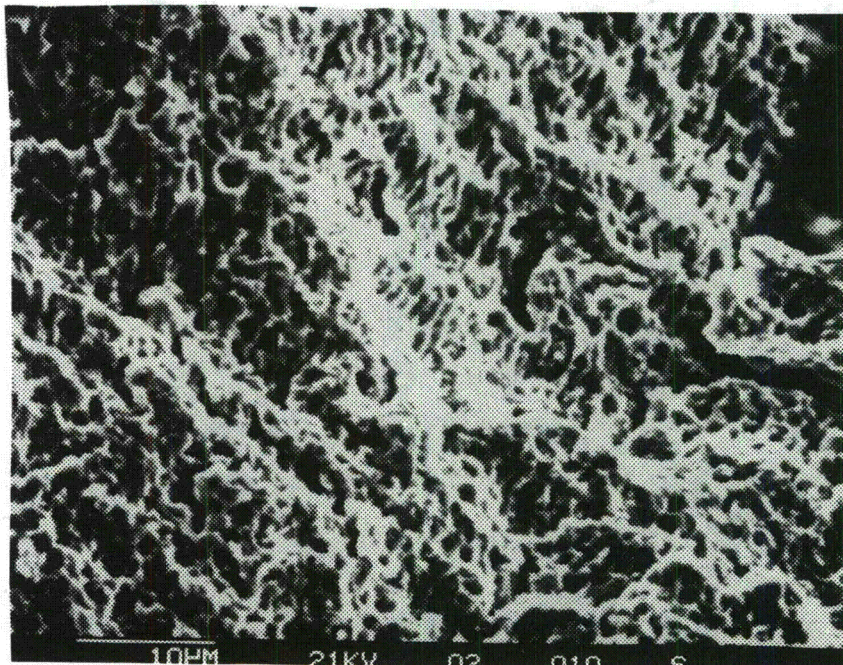
Specimen C-1, $R = 0.7$

500X

Figure 12. Linde 124 Specimens Tested at One Cycle/Minute

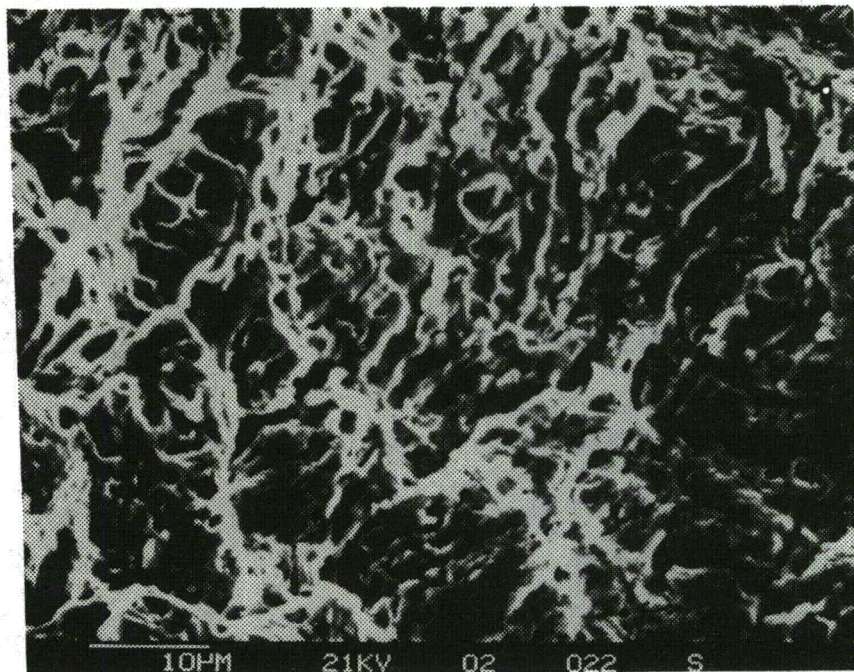


Specimen C-3WLD, R = 0.2

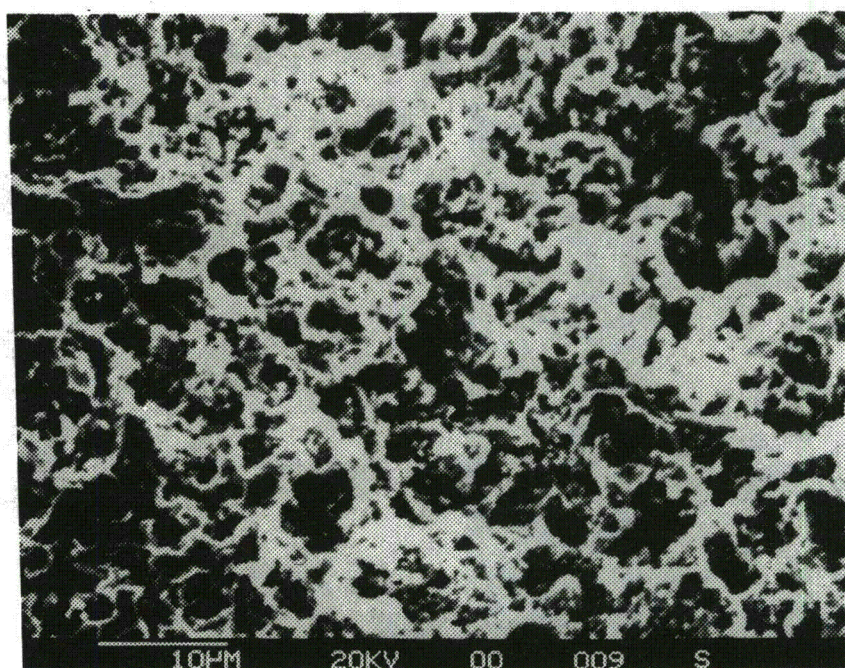


Specimen C-4WLD, R = 0.7

Figure 13. Linde 80 Weld Specimens Tested at One Cycle/Minute

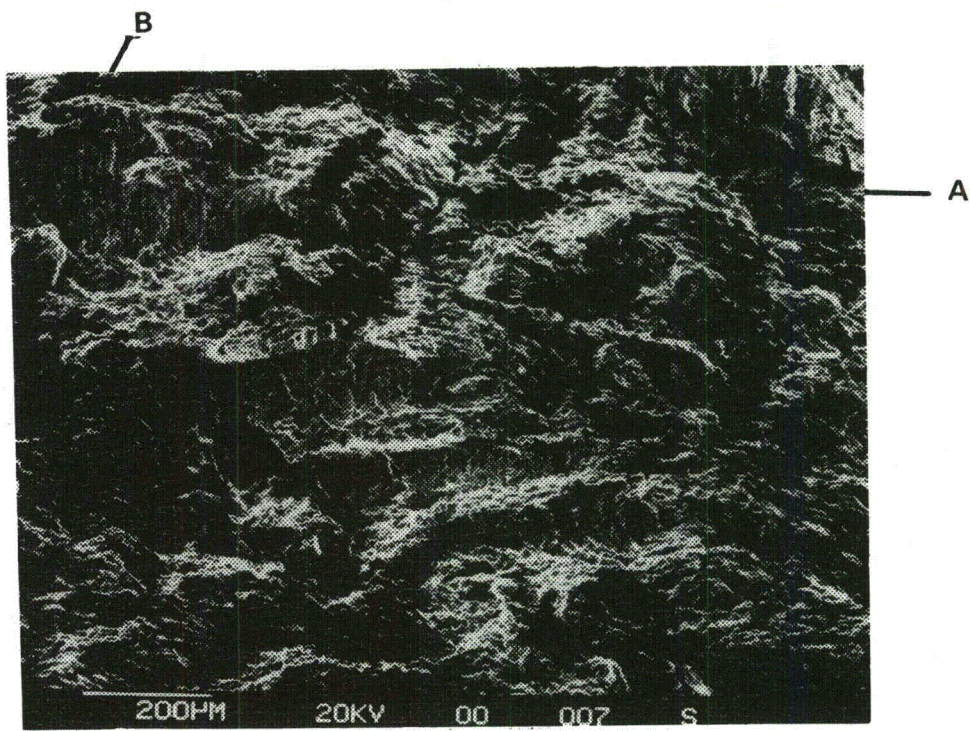


Specimen D-3 WLD Tested at $R = 0.2$

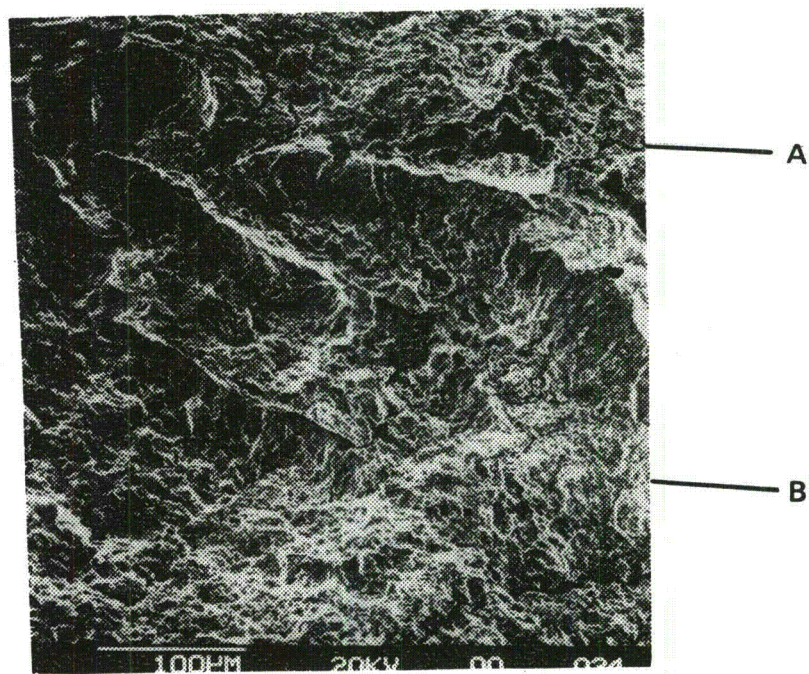


Specimen D-2 WLD Tested at $R = 0.7$

Figure 14. Linde 0091 Weld Specimens Tested at One Cycle/Minute

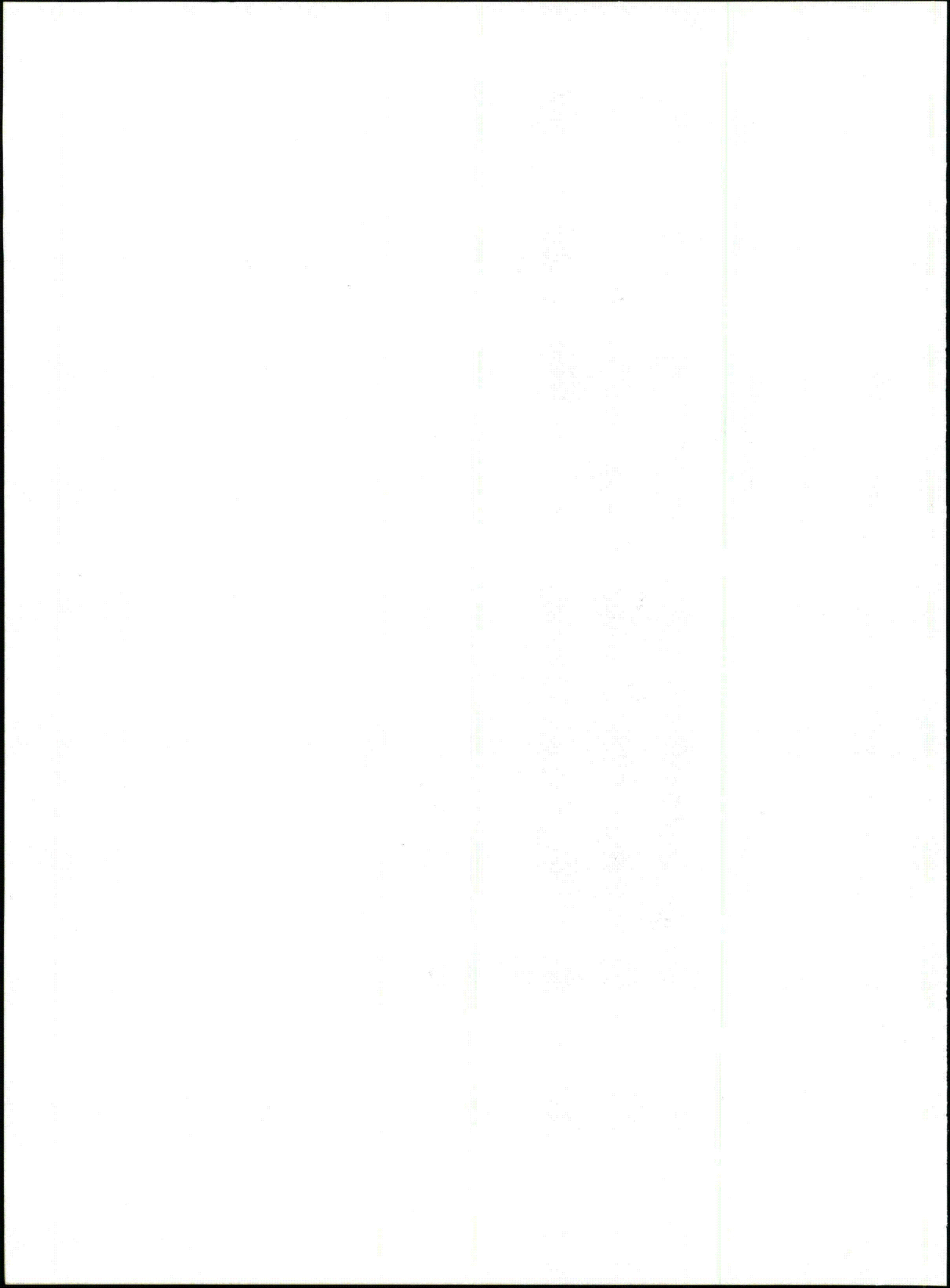


D-1HAZ Tested at $R = 0.2$



C-3HAZ Tested at $R = 0.2$

**Figure 15. Heat-Affected Zone Specimens Tested at $R = 0.2$, One Cycle/Minute
Region A Shows Typical Fatigue Features, Region B is a Brittle-
Appearing Component**



AN INVESTIGATION OF FATIGUE CRACK GROWTH IN SA508-2
IN A 288°C PWR ENVIRONMENT BY A CONSTANT ΔK TEST METHOD

to be presented at: The International Atomic Energy Agency Symposium
Freiburg, Federal Republic of Germany
May 13 - 15, 1981

W. A. Van Der Sluys
Manager, Metallurgy Section
Babcock & Wilcox, a McDermott Company
Alliance Research Center
Alliance, Ohio 44601 U.S.A.
(216) 821-9110

and

D. S. DeMiglio
Research Engineer
Babcock & Wilcox, a McDermott Company
Alliance Research Center
Alliance, Ohio 44601 U.S.A.

The research work reported in this paper was co-sponsored by Babcock & Wilcox, a McDermott Company, and Electric Power Research Institute, Research Project 1325-1

ABSTRACT

Fatigue crack growth experiments using a constant ΔK test technique were conducted on three 50.8 mm thick compact fracture specimens of SA508-2 in a 288°C simulated PWR water environment. Alternating stress intensity factor (ΔK) values were investigated in the range 16.5 to 44 MPa $\sqrt{\text{m}}$ at sinusoidal loading frequencies ranging from 10 to .017 Hz (1 cpm) and R ratios 0.03 to 0.72. For a given ΔK and frequency, ΔK was held constant to within 1%. A steady-state rate of crack growth per cycle of stress (da/dN) was determined for each test condition. Over a typical crack extension of 1.3 mm, the crack growth rate in many cases was a constant. As many as 14 separate experiments were conducted on a single specimen.

There was no influence of prior loading history or crack length on the crack growth rate. It was found that the crack growth rate was controlled by the ΔK , frequency, and R ratio of the test.

Large changes in the crack growth rate did not occur as the frequency of loading was decreased from >1 Hz to .017 Hz (1cpm). As compared to high frequency results (>1 Hz) the crack growth rate increased slightly at 1 cpm for $\Delta K > 22 \text{ MPa}\sqrt{\text{m}}$ and decreased slightly for $\Delta K < 22 \text{ MPa}\sqrt{\text{m}}$.

At 1 cpm the R ratio was observed to influence the crack growth rate; however, the magnitude of this effect was not well-defined.

INTRODUCTION

In the nuclear industry, the ability to quantitatively predict the growth of any flaw that has been introduced in a nuclear pressure vessel (either during fabrication or service) is essential in the establishment of realistic design criteria or meaningful in-service inspection programs. Since pressure vessels are subjected to alternating stress transients during operation, fatigue and environment-assisted fatigue are mechanisms of growth relevant to flaws in nuclear pressure vessels.

Over the past ten years linear elastic fracture mechanics (LEFM) has been used quite extensively to study the growth of flaws in nuclear pressure vessel steels. However, at present, a realistic crack growth law does not exist which will provide a good description of the relationship between the alternating stress intensity factor (ΔK) and the crack growth per cycle of stress (da/dN). Such a law should be applicable to either the pressurized water reactor environment (PWR) or boiling water reactor environment (BWR) and should predict a crack growth rate for realistic water chemistry conditions, neutron fluences, ΔK levels, cyclic frequencies and stress intensity ratios ($R = K_{\min}/K_{\max}$) observed in the nuclear industry.

The goal of the experimental work presented in this paper was to provide fracture mechanics information on the fatigue crack growth properties of an unirradiated nuclear pressure vessel steel (SA508-2) in a simulated PWR water environment. Areas which were investigated include: the dependency of steady-state crack growth rates on prior loading history and the effect of cyclic frequency, R ratio and crack extension on steady-state crack growth rates.

This project was jointly sponsored by Babcock & Wilcox, a McDermott Company and the Electric Power Research Institute.

PROCEDURE

A computer controlled 90,000 N MTS servohydraulic system was used to test 50.8 mm thick compact fracture specimens of SA508-2 in a simulated PWR water environment at 288°C. Specimens were machined according to ASTM E647-78 specifications. (1) A software program (2) (developed at B&W) was used to conduct constant ΔK experiments. For a given ΔK , R ratio and crack length, the applied load was automatically decreased after every .08 mm increment of crack extension in order to hold ΔK constant. As the crack grew, the mean load and the change in applied load would decrease while the specimen's mean deflection and change of deflection would increase. As many as 14 separate experiments were performed on a single specimen.

Crack lengths were determined by a compliance method. During an experiment, after a given number of cycles, load (P) and deflection (δ) readings were collected by a computer during a series of specimen unloadings from P_{max} to P_{min} . The compliance of the specimen was determined by the change in deflection per change in load ($\Delta\delta/\Delta P$). A least squares linear analysis was performed on approximately 80 (P, δ) pairs to obtain a specimen compliance value. The compliance was then correlated to a crack length value from results of an analytical study of compliance and crack length in compact fracture specimens. (3) Typical crack length precisions of ± 0.051 mm were obtained in a 288°C PWR water environment. This high degree of precision was matched by an accuracy of >95% in predicting the true crack length of the specimen for various ΔK conditions as denoted by beachmarkings on the fracture surface.

Load was measured by a load cell external to the autoclave while the deflection of the specimen was measured by a transducer located inside the autoclave on top of the specimen. This transducer was designed and built at B&W and consisted of a tapered beam on which two high temperature strain gauges were mounted. A wire was used to connect the beam to the bottom half of the specimen. The displacement gauge was calibrated in 288°C air over a linear range of 2.54 mm with a maximum deviation from linearity of ± 0.0025 mm. A high gain low-noise amplifier was used to measure deflection readings through a voltage window about a given mean deflection.

In addition to the test method described above, a technique, referred to as " ΔK shedding", was developed to decrease ΔK exponentially from one level to another as the crack grew. A similar technique has been employed by Donald and Schmidt (4) to conduct computer controlled ΔK increasing experiments on compact fracture specimens. A ΔK shed was used to decrease the size of the plastic zone ahead of the crack tip when, for a given R ratio, it was desirable to go from a high to a low ΔK level. During a ΔK -shedding experiment, da/dN would decrease continuously as the crack grew. The equation that describes ΔK -shedding is:

$$\Delta K = \Delta K_0 \exp (C (a-a_0)) \quad (\text{eq. 1})$$

where

- a_0 = initial crack length at beginning of K shed
- a = instantaneous crack length during the K shed
- ΔK_0 = initial alternating stress intensity factor at crack length a_0
- ΔK = instantaneous alternating stress intensity factor at crack length a
- C = decay constant = (-0.12 (1/mm))

In addition to a more efficient use of specimen crack length, (hence, more experiments on a single specimen) this technique was useful in the study of ΔK history effects. That is, for a single specimen, a ΔK level was repeated several times at various crack lengths after many different load histories in the course of the overall test matrix.

The material under investigation was a nuclear pressure vessel material SA508-2. The material chemistry, mechanical properties and heat treatment of this low carbon - low alloy steel similar to 22 NiMoCr37 steel are listed in Table 1⁽⁵⁾. Compact fracture specimens (50.8 mm thick) were machined such that the crack propagation direction was parallel to the final forging direction (T-L as defined by ASTM E399-74). A notch 60.5 mm in length was machined in each specimen and a 0.33 mm fatigue precrack was generated in room temperature air at a ΔK of 16.5 MPa m.

TABLE 1
PROPERTIES OF SA508-2 (HEAT BBB)

Material Chemistry (Weight %)

C	Mn	P	S	Si	Ni	Cr	Mo	Cu
0.22	0.64	0.007	0.012	0.28	0.63	0.34	0.58	0.022

Mechanical Properties

Temp. (°C)	Yield Stress 0.2% Offset (MPa)	Ultimate Tensile Stress (MPa)	Elong. %	Reduction of Area, %
21	488	625	26.5	68.7
288	441	612	25.0	68.0

Heat Treatment

866°C \pm 5°C, (held for 4 hr.) Water Quench
 677°C \pm 5°C, (held for 6 hr.) Air Cooled
 607°C \pm 14°C, (held for 34 hr.) Furnace Cooled

An autoclave fabricated from 347 stainless steel was used for all experiments. Operating temperatures were controlled to 288°C \pm 6°C while pressures were in the range 13.8 MPa \pm 276 KPa. A once-through autoclave water refreshed system was used in which deoxygenated water (O_2 <10 ppb) within the specifications listed in Table 2 was pumped through a preheater and into the autoclave at a flow rate of \sim 2 liters/hr. The water was then cooled and discarded. An on-line Beckman meter was used to continuously monitor the

dissolved oxygen concentration. The start-up procedure for the autoclave consisted of a nitrogen gas purge prior to filling with water of the desired chemistry.

A heating rate of 27°C/hr. was used until the specimen and autoclave reached 288°C. Testing began within 24 hours after the autoclave was filled. Each specimen had approximately an eight hour soak at temperature and pressure before testing began.

TABLE 2

<u>Water Chemistry</u>	<u>Specifications</u>
Dissolved Oxygen	< .01 ppm
Boric Acid	2000 - 8000 ppm
Lithium	0.2 - 2.0 ppm
pH	4.6 - 8.5
Conductivity	< 20 μ mhos/cm
Dissolved Hydrogen	15 - 50 std cc/kg H ₂ O
Chloride	< .01 ppm
Fluoride	< .01 ppm

To maintain a dissolved hydrogen gas content in the feed water, the 200 liter storage tank was continuously sprayed through a hydrogen cover gas. In an operating nuclear power plant, the dissolved hydrogen combines with oxygen in the presence of gamma radiation. In these experiments there was no decrease in dissolved oxygen due to the presence of hydrogen gas.

Periodically, effluent water chemistry was checked during the course of a series of tests on a given specimen.

RESULTS

The fatigue crack growth rate data obtained for SA508-2 material is presented in Tables 3A - 3C and Figures 1 - 9. A total of three test programs were conducted in PWR water at 288°C. Each of these programs used a single specimen for a given number of individual experiments. The variables which were investigated in each of these experiments are presented in Tables 3A - 3C along with the measured crack growth rates.

The objectives of the first two test programs were to determine if prior loading history or crack length influenced the measured crack growth rate; and to demonstrate that the constant ΔK procedure worked. For these reasons the crack growth rate (for a particular value of applied ΔK and loading frequency) was determined a number of times. The purpose of the third test program was to investigate R ratio effects and the amount of crack extension necessary to achieve a steady state crack growth rate.

First Test Program

In Test Program #1 (Spec. 2T03) it was not possible to conduct all the experiments which were planned. For this reason the objective could not be met to determine if a history effect existed. However, as shown in Table 3A, it was demonstrated that constant ΔK tests could be performed. Figure 1 presents the results of this test in the form of a plot of crack growth rate versus crack length.

TABLE 3A
FATIGUE CRACK GROWTH DATA FOR TEST PROGRAM #1
(288°C PMR WATER ENVIRONMENT)

Test Program	Spec.	Exp. No.	ΔK (MPa \sqrt{m})	R	Loading Frequency (Hz)	Crack Extension (mm)	(da/dN) overall (x10 ⁻⁸ m/cycle)
1	2T03	1	16.5	0.3	5	5.2	3.37
		2	16.5		.017	0.4	1.20
		3	16.5		5	0.8	5.40
		4	27.5		.017	0.7	27.6
		5	44.0		.017	0.3	61.4

In the first experiment, the crack propagated 5 mm at an applied ΔK of 16.5 MPa \sqrt{m} at an R ratio of 0.3 for a loading frequency of 5 Hz. Very little variation in crack growth rate with crack length was observed.

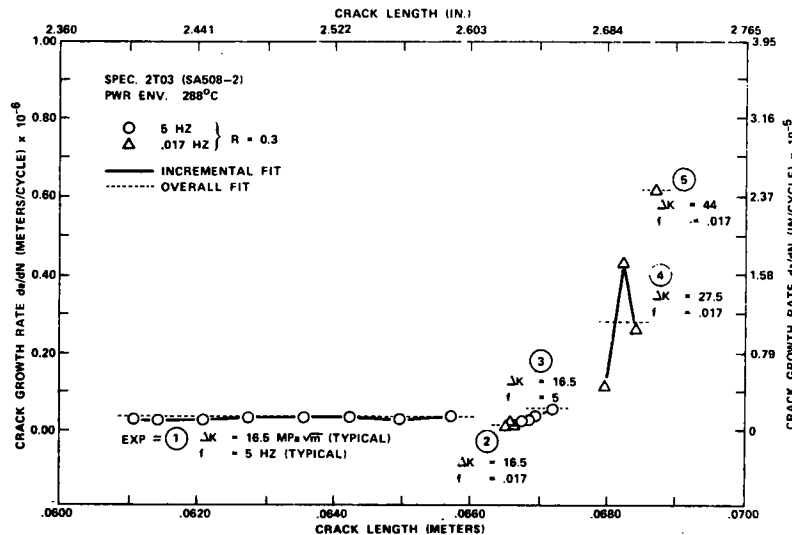


FIGURE 1 CRACK GROWTH RATE (da/dN) VS. CRACK LENGTH FOR EXPS. 1-5
ON SPEC. 2T03 (FIRST TEST PROGRAM)

In the second experiment, the ΔK and R ratio were not changed but the frequency was lowered to .017 Hz (1 cpm). Experimental difficulties, however, were encountered. This was the first attempt to conduct a constant ΔK experiment at 1 cpm. Noise in the extensometer system, which had not interfered with crack length measurements at high frequencies, made it difficult to measure the crack length to a sufficient precision required to conduct the experiment. It was determined that the noise was due to rapid local temperature fluctuations of the water in the autoclave near the specimen. The temperature fluctuation was due to

the water cooling of the load rod seal assembly at the top of the autoclave. Strain gauges mounted on the tapered beam of the displacement transducer were extremely sensitive to this thermal fluctuation. As a temporary fix to this problem, it was found that data of sufficient precision could be obtained if the seal cooling was interrupted periodically during the test. After the test was completed, the problem was solved. An interesting result of this 1 cpm experiment was that the crack growth rate was substantially slower than the crack growth rate measured at 5 Hz in the first experiment. It had been expected that the environment would have a greater influence at the lower frequency and the crack growth rate would, therefore, be greater than the rate measured at high frequency. The lower crack growth rate greatly increased the length of time required to grow the crack a given distance. This experiment was conducted for three weeks over a crack extension of 0.4 mm at a steady state crack growth rate.

Experiment 3 was conducted under the same conditions as Experiment 1. The crack growth rate was approximately equal to the rate observed in Experiment 1. Experiments 4 and 5 were higher ΔK experiments at a test frequency of 1 cpm. These ΔK values were chosen in an attempt to find a ΔK region where a sustained environmental effect existed. These low frequency results would be compared to future high frequency experiments.

Second Test Program

The results of Test Program #2 (Spec. 2T05) are presented in Table 3B and in a plot of crack growth rate versus crack length as shown in Figure 2. In this test program a total of 14 experiments were conducted. As a result of a number of experiments conducted under identical test conditions, the crack growth rate was controlled by ΔK , R ratio and loading frequency independent of prior loading history. The ΔK -shedding technique, described earlier, was used in order to repeat various test conditions.

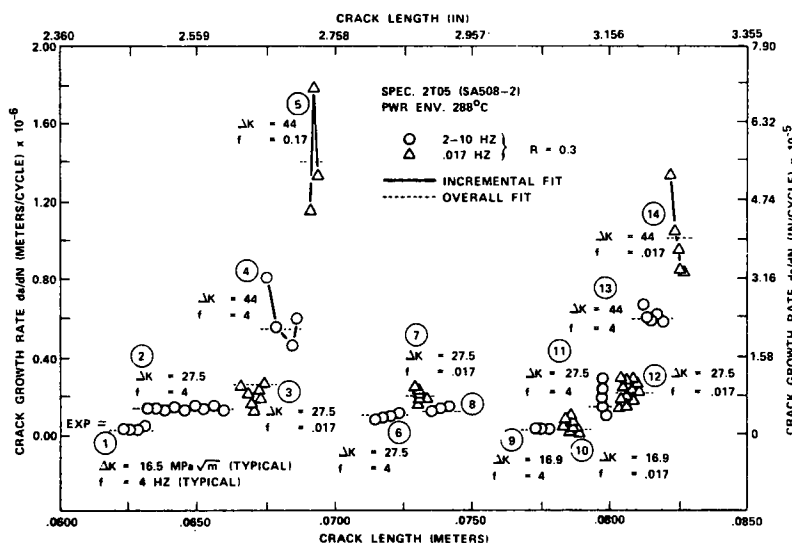


FIGURE 2 CRACK GROWTH RATE (da/dN) VS. CRACK LENGTH FOR EXPS. 1-14 ON SPEC. 2T05 (SECOND TEST PROGRAM)

TABLE 3B
FATIGUE CRACK GROWTH DATA FOR TEST PROGRAM #2
(288°C PWR WATER ENVIRONMENT)

<u>Test Program</u>	<u>Spec.</u>	<u>Exp. No.</u>	<u>ΔK (MPa\sqrt{m})</u>	<u>R</u>	<u>Frequency (Hz)</u>	<u>Crack Extension (mm)</u>	<u>(da/dN) (x10⁻⁸ m/cycle)</u>
2	2T05	1	26.5	0.3	4	0.9	3.6
		2	27.5		10	3.2	14.7
		3	27.5		.017	1.2	27.5
		4	44.0		4	1.5	55.6
		5	44.0		.017	0.4	141
		6	27.5		4	1.2	10.8
		7	27.5		.017	0.4	20.4
		8	27.5		2	1.2	14.3
		9	16.9		4	0.9	3.52
		10	16.9		.017	0.8	2.46
		11	27.5		4	0.6	14.5
		12	27.5		.017	0.8	22.2
		13	44.0		4	1.0	61.0
		14	44.0		.017	0.8	96.8

Figures 3 - 5 present typical plots of crack length versus cycles which were obtained during these experiments. Although in a paper such as this, it is not possible to present all of the crack length versus cycles information obtained in these tests, References 2, 6, 7, and 8 contain this information for all constant ΔK fatigue crack growth experiments.

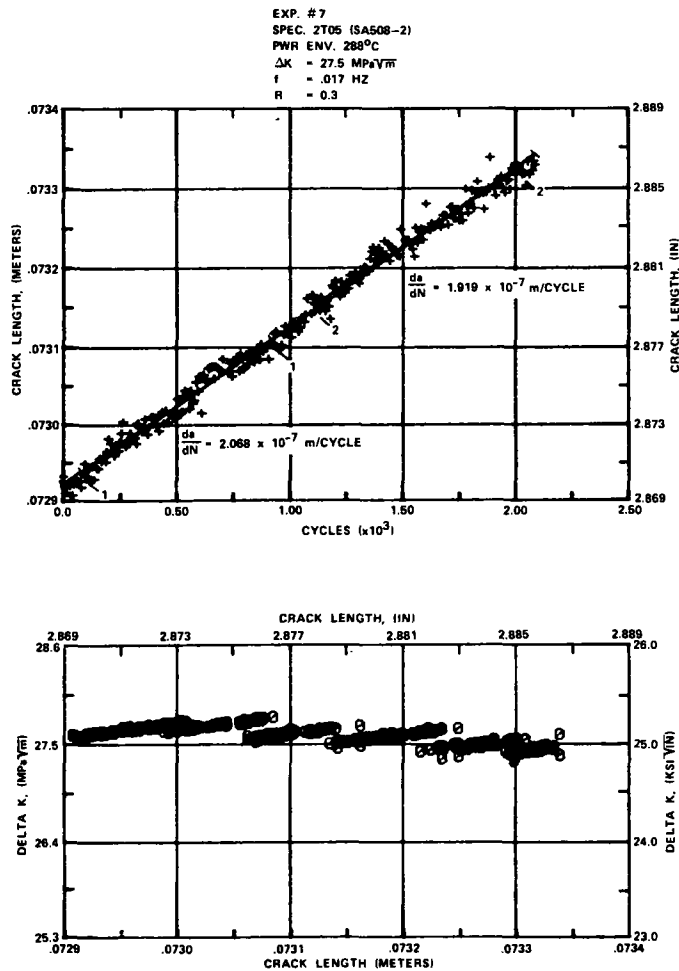


FIGURE 3 CRACK LENGTH VS. CYCLES AND ΔK VS. CRACK LENGTH FOR EXP. 7 - SECOND TEST PROGRAM - SPEC. 2T05

Figure 3 is typical of most of the crack length versus cycles information obtained in a constant ΔK experiment. There are a number of approaches which can be used to determine the crack growth rate from this type of information. There have been three different ones used to interpret the data presented in this paper. The first is a linear regression analysis of all of the data from a single experiment to determine a single average rate. The second is a number of linear regression analyses over regions of the data that the investigator chooses to examine. The third is an incremental linear regression analysis of the data to determine average crack growth rates over intervals of test cycles.

The data points shown on Figures 1, 2, and 6 are the results of an incremental technique to determine crack growth rates where the number of crack length determinations in each increment varied from 10 to 100 depending on how often the crack length was measured during the experiment. The dashed lines (used to indicate overall crack growth rates) on these figures were determined by one of the first two of the above methods of analysis. If the crack length

versus cycles information showed no transients, then the overall crack growth rate was taken as the rate determined by a linear regression analysis of all the data. If significant transient behavior was observed, the overall crack growth rate was determined by a linear regression analysis of all the data after the transient.

The experiment shown in Figure 3 does not show a transient behavior and the crack growth rate changed very little during the experiment. The incremental analysis of this data, which is presented as Experiment 7 in Figure 2, shows that there is some variation in the growth rate; however, the overall growth rate represented by the dashed line is a good representation of the growth rate observed during the experiment.

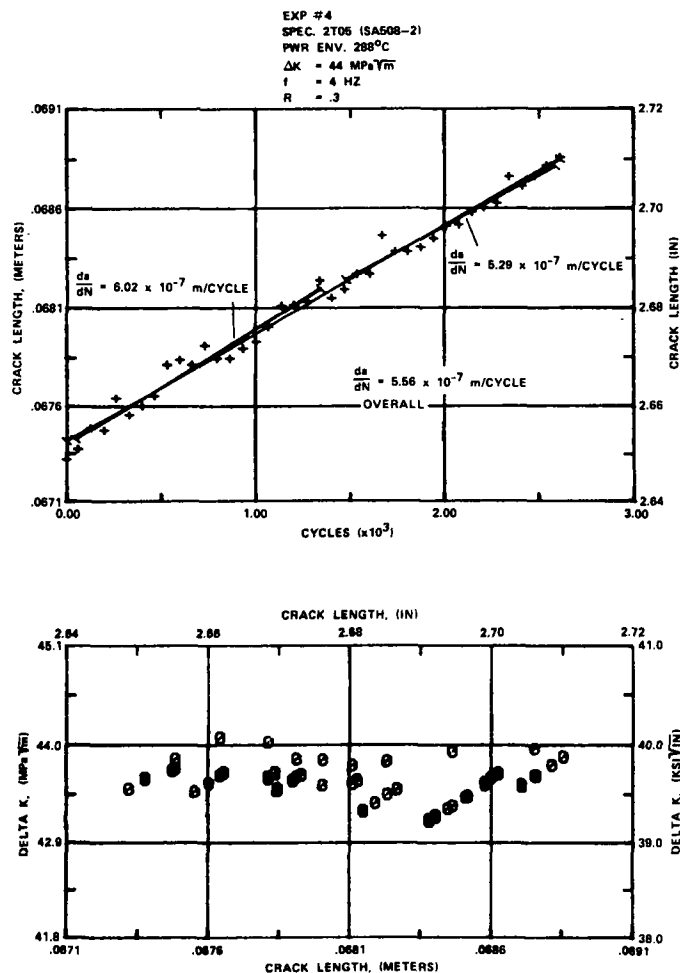


FIGURE 4 CRACK LENGTH VS. CYCLES AND ΔK VS. CRACK LENGTH FOR EXP. 4 - SECOND TEST PROGRAM - SPEC. 2T06

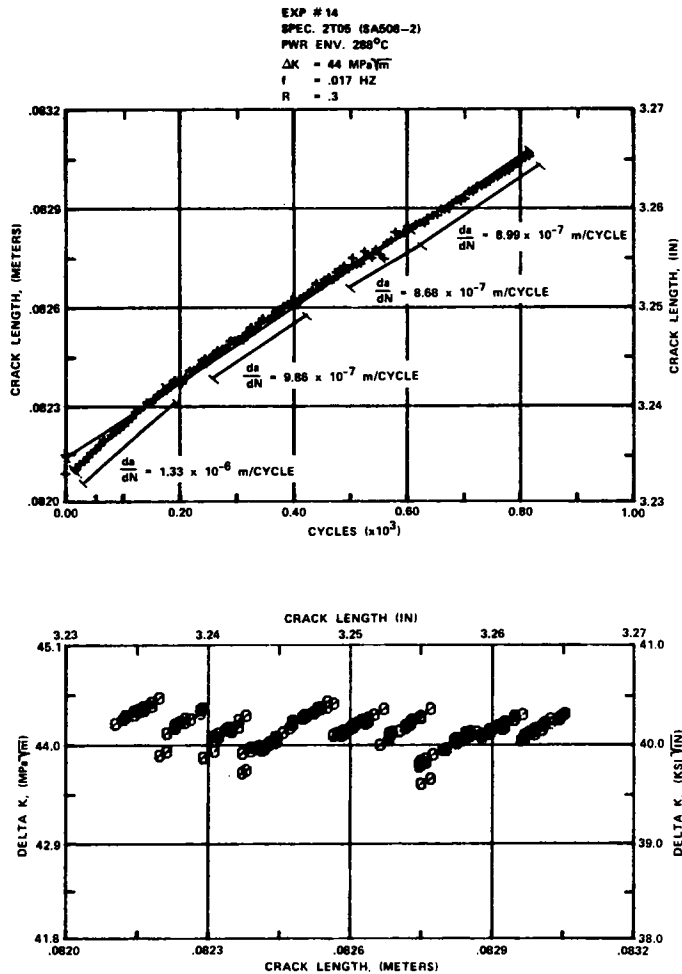


FIGURE 5 CRACK LENGTH VS. CYCLES AND ΔK VS. CRACK LENGTH FOR EXP. 14 - SECOND TEST PROGRAM - SPEC. 2T05

The experiments which do not appear to exhibit a uniform crack growth rate (such as Experiments 4, 5, and 14 shown in Figure 2) represent experiments where either transient behavior was observed (Experiment 14) or, more than usual scatter in crack length data was obtained (Experiments 4 and 5). Figures 4 and 5 present the a versus N data for Experiments 4 and 14, respectively. An observation that can be made is that nonuniform crack growth rates seem to occur at relatively high ΔK values where the crack grew rapidly. Under these conditions, a fewer number of (a , N) pairs were obtained.

Third Test Program

The results from Test Program #3 (Spec. 2T06) are presented in Table 3C and Figure 6. There were two objectives in this set of experiments. The first objective was to demonstrate that a constant crack growth rate could be obtained if the crack grew a long distance at a constant ΔK and a low loading frequency (1 cpm). The second objective was to investigate R ratio effects. In the first

experiment, the crack propagated 4.8 mm at an applied ΔK of $31.5 \text{ MPa}\sqrt{\text{m}}$ for a frequency of 0.017 Hz (1 cpm) and an R ratio of 0.162. As shown in Figure 6, the crack growth rate obtained from this experiment was a constant.

TABLE 3C
FATIGUE CRACK GROWTH DATA FOR TEST PROGRAM #3
(288°C PWR WATER ENVIRONMENT)

<u>Test Program</u>	<u>Spec.</u>	<u>Exp. No.</u>	<u>ΔK ($\text{MPa}\sqrt{\text{m}}$)</u>	<u>R</u>	<u>Frequency (Hz)</u>	<u>Crack Extension (mm)</u>	<u>(da/dN) overall ($\times 10^{-8}$ m/cycle)</u>
3	2T06	1	31.5	.162	.017	4.8	35.5
		2	31.5	.162	1.7	1.3	22.0
		3	38.5	.4	1.7	1.5	42.1
		4	38.5	.4	.017	2.1	86.4 60.8
		5	31.5	.638	1.7	1.5	19.3
		6	20.6	.72	1.7	2.6	8.92
		7	20.6	.72	.017	1.0	11.8
		8	20.6	.4	5	5.6	5.82
		9	20.6	.03	.017	1.4	12.0
		10	20.6	.03	5	1.5	4.32
		11	20.6	.03	.017	1.0	8.43

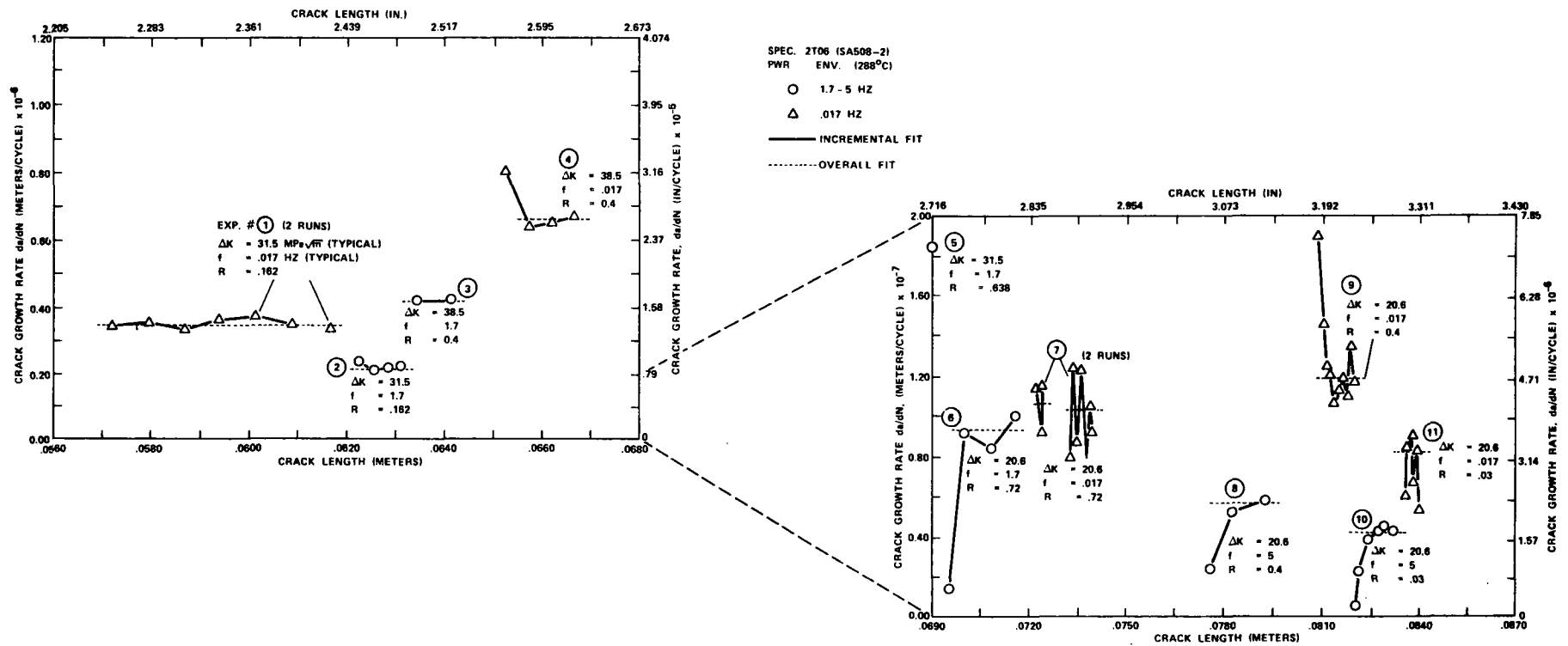


FIGURE 6 CRACK GROWTH RATE (da/dN) VS. CRACK LENGTH FOR EXPS. 1 - 11 ON SPEC. 2T06 (THIRD TEST PROGRAM)

Experiments 6, 7, 8, 9, 10 and 11 were all conducted with an applied ΔK of $20.6 \text{ MPa}\sqrt{\text{m}}$. The effect of three R ratios and two frequencies were investigated. In previous experiments, it was necessary to change test conditions and reduce K from one experiment to the next. The ΔK shedding procedure discussed earlier was used. Ideally, for this set of experiments, the R ratio (hence, K_{max}) was to be reduced from one level to the next and the ΔK was to be held constant. Since an R ratio shedding procedure did not exist at the time of these experiments, the R ratio was reduced to the next test condition and a transient in the crack growth rate was observed until a steady state condition occurred after a sufficient amount of crack extension. In order to save time, the first experiment after a drop in R ratio was always a high loading frequency experiment (5 Hz). In Figure 6 experiments of this type are Experiments 8 and 10. In both of these experiments, a transient occurred in the crack growth rate prior to a steady state condition. Although transients were observed at the beginning of Experiments 6 and 9, it was not clearly understood why they occurred.

Experiments 6, 8, and 10 show the effect on the crack growth rate of a reduction in R ratio when the loading frequency is 5 Hz. The crack growth rate decreased with each decrease in R ratio for a ΔK of $20.6 \text{ MPa}\sqrt{\text{m}}$.

Experiments 7, 9 and 11 were conducted for the same range in R ratio with a loading frequency of .017 Hz (1 cpm). Under these conditions, the crack growth rate did not decrease with decreasing R ratio in the range 0.72 to 0.4. However, for R ratios in the range 0.4 to 0.03, a decrease in crack growth rate was observed.

Figure 7 is a summary of all of the crack growth rate data obtained in all PWR Experiments (Specs. 2T03, 2T05 and 2T06). These data are plotted in the manner of crack growth rate versus alternating stress intensity factor ΔK . The solid points in the figure represent results of experiments conducted at loading frequencies of .017 Hz (1 cpm) while open points represent experiments conducted at loading frequencies of 1.7 Hz or greater. At applied ΔK levels greater than $22 \text{ MPa}\sqrt{\text{m}}$ the crack growth rates obtained at low loading frequencies tend to be faster than the crack growth rates obtained at high loading frequencies. At applied ΔK levels of less than $22 \text{ MPa}\sqrt{\text{m}}$ crack growth rates at low loading frequencies tend to be slower than crack growth rates obtained at high loading frequencies. In order to more clearly quantify this effect, more experiments in the lower ΔK regime must be performed at high and low loading frequencies over a range of R ratios.

The Effect of R Ratio

In general, regardless of frequency, the crack growth rates obtained at high R ratios are greater than or equal to the rates obtained at low R ratio. A summary of all test results for all loading frequencies and R ratios is presented in Figure 7.

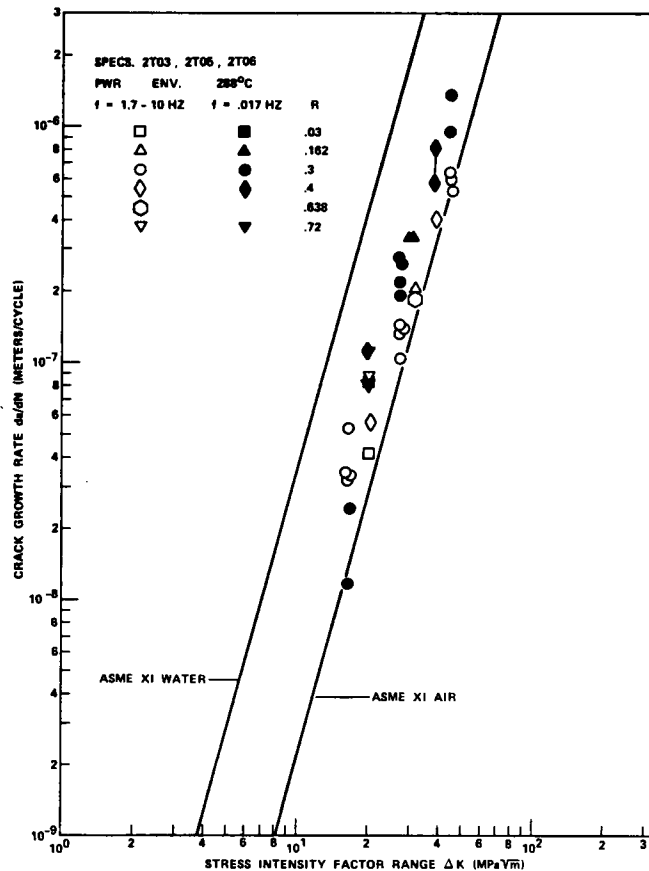


FIGURE 7 CRACK GROWTH RATE (da/dN) VS. ΔK FOR ALL PWR FATIGUE CRACK GROWTH EXPS.

In order to eliminate the effect of R ratio for all experiments, a ΔK effective was computed using Walker's⁽⁵⁾ equation:

$$K_{\text{eff}} = K_{\text{max}} (1 - R)^n \quad (\text{eq. 2})$$

Values of n were determined that best fit the equation for both high and low frequency data. That is, a value of n was chosen such that the correlation coefficient (r) - for a linear regression analysis of crack growth rate versus K_{eff} - was maximized. The results of these analyses are shown in Figure 8 (high frequency data) and Figure 9 (low frequency data). The best fit for the high frequency data was obtained with an n value of .92. The low frequency data had an n value of .90.

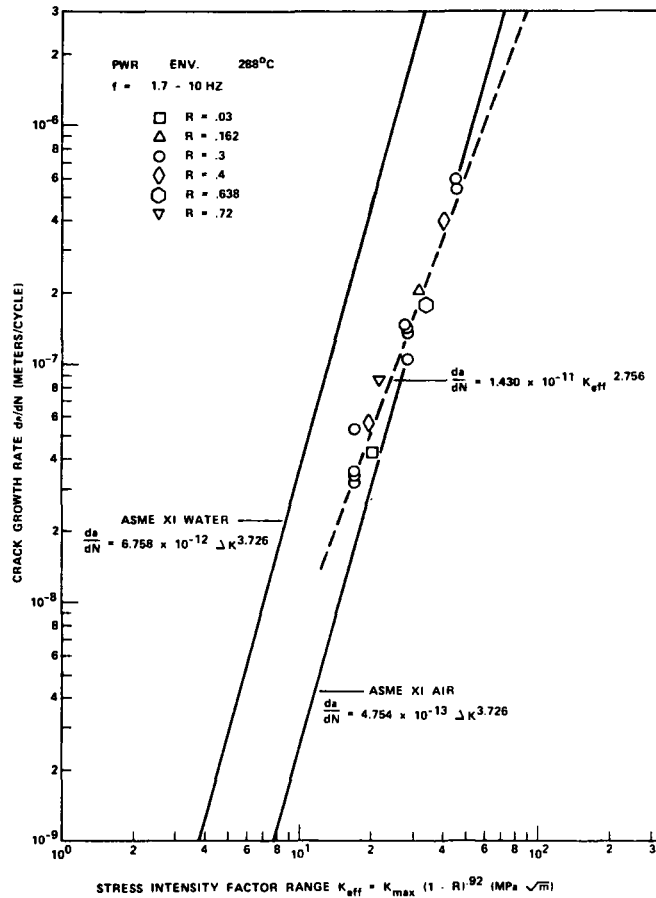


FIGURE 8 CRACK GROWTH RATE (da/dN) VS. K_{eff} FOR ALL PWR EXPERIMENTS AT FREQUENCIES IN THE RANGE 1.7 - 10 HZ

The best fit linear regression line was then determined for both sets of data:

$$(f > 1 \text{ Hz}) \quad \frac{da}{dN} = 1.430 \times 10^{-11} K_{eff}^{2.756}, (r = .9808) \quad (\text{eq. 3})$$

$$(f = 1 \text{ cpm}) \quad \frac{da}{dN} = 7.171 \times 10^{-13} K_{eff}^{3.747}, (r = .9574) \quad (\text{eq. 4})$$

where da/dN = (change in crack length/cycle) = meters/cycle
 $K_{eff} = \text{MPa}\sqrt{m}$

Note that the low frequency line (Figure 9) is parallel to the ASME Sec XI, air line (10) and only slightly above it, while the high frequency line (Figure 8) is closer to the Sec XI air line with a shallower slope. It must also

be noted that the crack growth data that was used to generate equations (3) and (4) was limited (especially in the lower ΔK regime of $<22 \text{ MPa}\sqrt{\text{m}}$). Future results will be necessary to give a better statistical understanding of an appropriate K_{eff} to be used in the formulation of a crack growth law.

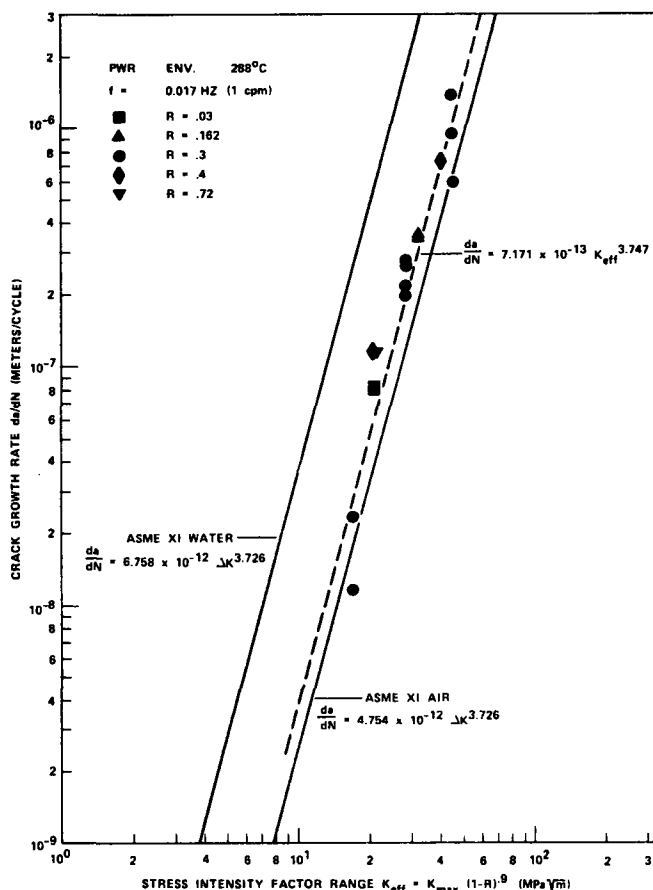


FIGURE 9 CRACK GROWTH RATE (da/dN) VS. K_{eff} FOR ALL PWR FATIGUE CRACK GROWTH EXPERIMENTS AT A FREQUENCY OF 1 cpm

The crack path of Specimen 2T03 (Figure 1) has been examined by optical metallography, SEM and Auger spectroscopy. A transgranular crack path through the bainitic/ferritic microstructure was observed with small amounts of secondary crack branchings over a distance of several grain diameters. Aside from wider spaced tearing striations (with increasing ΔK) there were no other characteristics that distinguished one experiment from another. An Auger analysis revealed a homogeneous distribution of elements on the fracture surface. The atomic percentages of oxygen and iron were in the ratio of 1:1 with an average value of 0.6 atomic percent sulphur.

DISCUSSION OF RESULTS

The results of the tests conducted on the three specimens reported here demonstrate the usefulness of the constant ΔK approach to fatigue crack growth testing. The results from the first two test programs demonstrate that (for a PWR environment) the fracture mechanics parameter of alternating stress intensity factor (ΔK) is the controlling stress variable in the experiment. It is necessary for this result to be clearly defined before the constant ΔK approach can be made useful to explore the significance of other variables, and, also, before a fracture mechanics analysis procedure can be used to predict fatigue crack growth in a fatigue life analysis.

There are three major advantages of the constant ΔK method over the conventional constant load amplitude approach⁽¹⁾ to fatigue crack growth:

1. Steady-state conditions can be achieved. The early portion of the crack length versus cycles data presented in Figure 5 is a good example of a transient in the fatigue crack growth rate in a mildly aggressive environment. After a short interval of crack extension, a steady-state condition was attained. In the constant load amplitude approach, steady state conditions for a given ΔK will never be reached since ΔK is changing as crack length increases. Crack growth rates may be strongly dependent on the initial alternating stress intensity factor (ΔK_1).⁽¹¹⁾ The determination of a crack growth rate may be misleading¹ by a strong dependency of da/dn on ΔK_1 .
2. The effect of a single test variable or a combination of variables can be easily investigated on a single specimen. An example of this is the R ratio study conducted in Test Program #3 (Spec. 2T06) where the influence of two loading frequencies and three R ratios were investigated on a single specimen. R ratio and frequency effects were generated and analyzed without specimen to specimen variability.
3. The laboratory time to conduct a set of experiments is greatly reduced over the constant load amplitude approach. In order to determine crack growth rates for three different R ratios and two loading frequencies with the constant load amplitude approach, three to six specimens would be tested over an autoclave time of many months. Experiments 6 through 11 of Test 3 (Figure 6) required a total of six autoclave weeks over a small crack extension in one specimen.

In general, the magnitude of the environmental effect observed during these experiments was relatively small. As shown in Figure 7, little or no effect of the environment was observed at loading frequencies greater than 1 Hz.

At a loading frequency of .017 Hz (1 cpm), the environment was observed⁽¹²⁾ to influence the crack growth rate in a way different than reported elsewhere. Investigators have reported that, for various conditions, an increase in the crack growth rate (by as much as a factor of ten) was observed for a decrease in loading frequency from greater than 1 Hz to less than 1 cpm for ΔK values greater than 15 MPa \sqrt{m} . This increase in crack growth rate was directly attributed to the environment in that at low loading frequency, the environment has more time to

interact at the crack tip to cause embrittlement. However, in this investigation (as shown in Figure 7) the environment appears to only slightly enhance the rate of crack growth at applied ΔK values greater than $22 \text{ MPa}\sqrt{\text{m}}$ and slightly decrease crack growth rates at applied ΔK values less than $22 \text{ MPa}\sqrt{\text{m}}$.

Bamford used Walker's equation to incorporate R ratio effects into a continuous function of ΔK effective. Fatigue crack growth rate information obtained for pressure vessel steels in light water reactor environments over a range of R ratio of .0 to 0.75 was used. Equations 5 and 6 are the results of this analysis.

$$K_{\text{eff}} = K_{\text{max}} (1 - R)^{0.3} \quad (\text{eq. 5})$$

$$\frac{da}{dN} = 4.754 \times 10^{-13} K_{\text{eff}}^{3.726} \quad (\text{eq. 6})$$

where $\frac{da}{dN}$ = (change in crack length/cycle) = meters/cycle

$$K_{\text{max}}, K_{\text{eff}} = \text{MPa}\sqrt{\text{m}}$$

It is interesting to note that equation (6) would be identical to the ASME XI air line where $K_{\text{eff}} = \Delta K$. However, equation (6) could not be applied to Bamford's crack growth trends to realistically predict crack growth rates at very high R ratios (0.95). To realistically account for R ratio, two statistical models were developed⁽¹³⁾. These statistical models have been approved by the ASME Nuclear Pressure Vessel Code Committee Section XI as a replacement for the air and water flaw growth lines as specified in Reference (10).

The ΔK regime, described above, where an environmental effect at low loading frequency appears to change from positive to negative, could, perhaps, be identified in terms of a number of variables other than ΔK . Some of the variables to be considered are: the crack tip opening displacement (CTOD); the strain rate at the crack tip ($\dot{\epsilon}$); and the time rate of change of the stress intensity factor (\dot{K}).

Each of these variables varies with the applied ΔK over the range of crack extension. In the experiments conducted thus far, critical values of $\dot{\epsilon}$ and CTOD were not investigated. All experiments were conducted with an applied load (P) varying in the form of a sine wave where at any instant of time, t:

$$K(t) = F(a) P(t) = F(a) [\Delta P(\sin(2\pi ft)) + \bar{P}]$$

$$\frac{\partial K(t)}{\partial t} = \dot{K} = F(a) \Delta P (2\pi f) \cos (2\pi ft) \quad (\text{eq. 7})$$

(assume crack length does not change significantly for a single half cycle: K_{\min} to K_{\max})

where \bar{P} = mean load
 $P = P_{\max} - P_{\min}$
 f = loading frequency
 $F(a)$ = geometric factor for compact fracture specimens which is a function of crack length, a , as specified in ASTM E399

Thus, for each cycle of applied load, at a given crack length and test frequency, the K for all experiments varied continuously from zero to a maximum value of $[F(a) \Delta P (2\pi f)]$. No experiments were conducted where another type of loading wave form would be used to conduct a \dot{K} controlled experiment.

Unfortunately, the number of tests conducted to date are too limited to allow for any definite conclusions to be reached as to the behavior of the environmental effect observed in this investigation. The results do, however, serve to stimulate more questions and provide more information to aid in the design of future experiments.

At the ΔK level investigated in Test Program #3, it appears that the effect of R ratio on the growth rate saturates at a value of R greater than or equal to 0.4. Scott⁽¹⁴⁾ has obtained some limited data in seawater at $R = 0.85$ which indicates a saturation of the R ratio effect for R greater than or equal to 0.75.

No change in crack growth rate was observed at an applied ΔK level of 20.6 MPa \sqrt{m} when the R ratio was changed from 0.72 to 0.4; however, a substantial drop in crack growth rate did occur when the R ratio was lowered further to 0.03.

It is interesting to note that although some crack growth rate experiments were conducted at fairly high R ratio (0.72) the crack growth rates (regardless of frequency) are more than ten times slower than the rates measured by Bamford⁽¹³⁾ for a ΔK value of 20.6 MPa \sqrt{m} .

Although the test results are too limited at this time to draw many conclusions, this R ratio effect appears to warrant further investigation.

CONCLUSIONS

The following conclusions can be reached based on the experimental results reported in this paper:

1. The constant ΔK technique is a meaningful and useful approach to conduct fatigue crack growth experiments in an aggressive environment.
2. For the material and environmental conditions investigated, the crack growth rate was controlled by the applied ΔK , R ratio and loading frequency. Crack growth rates were not influenced by prior loading history or crack length.
3. Although small, there is a significant environmental effect when the loading frequency is low (1 cpm). No influence of the environment was observed at frequencies greater than 1 Hz.
4. As compared to the results of tests done at high frequency (> 1 Hz) the environmental effect on crack growth rates at 1 cpm moved from an enhancement in the rate for $\Delta K > 22 \text{ MPa}\sqrt{\text{m}}$ to a reduction in the rate at a $\Delta K < 22 \text{ MPa}\sqrt{\text{m}}$.
5. At a test frequency of 1 cpm the R ratio was observed to influence crack growth rates. However, the magnitude of this effect was not well-defined by these tests.

ACKNOWLEDGMENTS

This work was supported jointly by Babcock & Wilcox, a McDermott Company and the Electric Power Research Institute. The authors acknowledge the valuable assistance of R. H. Merryman and P. F. Harold during the experimental phase of this work, and the assistance of R. L. Jones (EPRI) for insightful discussion and analysis of results.

REFERENCES

1. "Constant Amplitude Fatigue Crack Growth Rates Above 10^{-8} m/cycle", Annual Book of ASTM Standards 1980, E 647-78.
2. W. A. Van Der Sluys, et al, "Corrosion Fatigue Characterization of Reactor Pressure Vessel Steels", First Semi-Annual Report, Electric Power Research Institute, Project No. RP1325-1, September 1979.
3. A. Saxena and S.J. Hudak, Jr., "Review and Extension of Compliance Information for Common Crack Growth Specimens Westinghouse R&D Center, May 3, 1977.
4. J.K. Donald, and D.W. Schmidt, "Computer-Controlled Stress Intensity Gradient Technique for High Rate Fatigue Crack Growth Testing," Journal of Testing and Evaluation, Vol. 8, No. 1, Jan. 1980, pp 19-24.
5. W. L. Server and W. Oldfield, "Nuclear Pressure Vessel Steel Data Base" Topical Report, Electric Power Research Institute, Research Project No. 886-1, December 1978.
6. W. A. Van Der Sluys, et al, "Corrosion Fatigue Characterization of Reactor Pressure Vessel Steels," Second Semi-Annual Report, Electric Power Research Institute, March 1980.
7. W. A. Van Der Sluys, et al, "Corrosion Fatigue Characterization of Reactor Pressure Vessel Steels," Third Semi-Annual Report, Electric Power Research Institute, September 1980.
8. W. A. Van Der Sluys, et al, "Corrosion Fatigue Characterization of Reactor Pressure Vessel Steels," Fourth Semi-Annual Report, Electric Power Research Institute, (in preparation), March 1981.
9. K. Walker, "The Effect of Stress Ratio During Crack Propagation and Fatigue for 2024-T3 and 7075-T6 Aluminum", Effects of Environment and Complex Load History on Fatigue Life, ASTM STP 462 American Society of Testing and Materials, 1970.
10. Rules for In Service Inspection of Nuclear Power Plant Components, ASME XI, July 1980, p. 237.
11. S. J. Hudak, Jr. and R. P. Wei, "Considerations of Non-Steady State Crack Growth in Materials Evaluation and Design," International Journal of Pressure Vessels and Piping, Vol. 9, Jan. 1981, pp 63-74.
12. W. H. Cullen and K. Torronen, "A Review of Fatigue Crack Growth of Pressure Vessel and Piping Steels in High Temperature, Pressurized Reactor - Grade Water", Naval Research Laboratory, NRL Report 4298, September 19, 1980.
13. W. H. Bamford, "Application of Corrosion Fatigue Crack Growth Rate Data to Integrity Analyses of Nuclear Reactor Vessels", Transactions of the ASME, Volume 101, July 1979.

14. P. M. Scott and D. R. V. Silvester, "The Influence of Mean Tensile Stress on Corrosion Fatigue Crack Growth in Structural Steel Immersed in Seawater", Tech. Report UKOSRP 3/02 Harwell Corrosion Service, UKAEA, May 1977.

CYCLIC CRACK GROWTH IN HIGH-TEMPERATURE
WATER--RESULTS OF AN INTERNATIONAL TESTING ROUND ROBIN

by

Robin L. Jones*

Abstract

The results are reported of a testing round robin performed under the auspices of the International Cyclic Crack Growth Group. Fourteen members of the Group participated in the round robin, in which measurements of cyclic crack growth rate were made on nominally identical compact tension specimens of SA533B pressure vessel steel immersed in high purity water at 561K. The plots of crack growth per cycle versus stress intensity factor range obtained by the participants were in acceptable agreement for specimens tested at a frequency of 1 Hz but differed by up to an order of magnitude (in terms of crack growth rate) for tests at 0.017 Hz. Possible sources of interlaboratory scatter are discussed and it is suggested that the observed variations in the environmental contribution to crack growth arise because of inadvertent differences between the chemical environments to which the specimens were exposed during testing. Plans for a second testing program are reviewed.

*Program Manager, Nuclear Plant Materials, Electric Power Research Institute, 3412 Hillview Avenue, P. O. Box 10412, Palo Alto, CA 94303, USA

INTRODUCTION

If a fatigue crack forms in a reactor pressure vessel (RPV) and is detected by in-service inspection, Section XI, Appendix A of the ASME Boiler and Pressure Vessel Code gives a procedure for estimating the remaining useful service life. The procedure combines a fatigue crack growth analysis with a failure margin analysis to determine whether or not repair of the crack is necessary to assure an adequate margin against vessel failure for the remainder of its planned service life. When it first appeared in the Code in 1972, the fatigue crack growth analysis was based on using the relation

$$\frac{da}{dN} = C (\Delta K)^n \quad (1)$$

to calculate the crack growth rate $\frac{da}{dN}$ associated with a transient that generates a stress intensity range ΔK at the crack tip. Values of the constants C and n were given in Appendix A for both subsurface flaws (inert environment) and internal surface flaws (reactor water environment). The values given in the Code were intended to ensure that upper bound estimates of crack growth were obtained.

Research since 1972 has confirmed that the use of equation (1) is appropriate for subsurface flaws and can also be used for surface flaws at cyclic frequencies $\geq 1\text{Hz}$. However, equation (1) is not a good representation of the cyclic crack growth behavior observed in water-environment tests at reactor operating temperatures at lower frequencies ($\leq 0.1\text{Hz}$) and many data are now available that transgress the original Appendix A "upper bound" relationship. Accordingly, a revised analysis procedure for surface flaws was introduced in the 1980 Addenda to the Code. The new procedure provides two different sets of constants for surface flaws at low and high values of ΔK together with a method of including the effect of R ratio (K_{\min}/K_{\max}) within the range $0.25 < R < 0.65$.

The data on which the current version of Appendix A are based were mostly generated in simulated PWR coolant at a frequency of 0.017Hz, ΔK levels of 10 to 60 MPa $\cdot m^{\frac{1}{2}}$ and R values of 0.2 to 0.7. In contrast, reactor transients feature ΔK levels well below 10 MPa $\cdot m^{\frac{1}{2}}$, R values ranging from > 0.95 to < 0 , and wide spectra of cyclic frequency and environment. Recognizing that accurate prediction of in-reactor crack growth would require an extensive program to generate additional test data and to develop a detailed understanding of the mechanisms leading to accelerated cracking in reactor water so that those data could be extrapolated to the service case, EPRI, in conjunction with the U.S. NRC organized the International Cooperative Group on Cyclic Crack Growth Rate Testing and Evaluation (the ICCGR Group).

The goal of the ICCGR Group, which was formally chartered in November 1978, is to coordinate work on cyclic flaw growth in RPV steels undertaken in Western Europe, North America and Japan to maximize the value of the data generated and minimize unnecessary duplication of effort. EPRI, which is in possession of large quantities of well characterized steel, undertook to provide test specimens for the use of the Group in collaborative test programs.

Prior to beginning any experiments, sixteen members of the Group participated in an interlaboratory comparison of methods for calculating crack growth rates from raw corrosion fatigue data (1). Three sets of crack length versus cycles data were distributed to the sixteen participants who were asked to use their own procedures to deduce plots of da/dN versus ΔK . The initial compilation of the results of this exercise showed unacceptable scatter. However, satisfactory explanations for the scatter were found and it was concluded that data reduction from experimental observations was not a major problem, although substantial differences were noted in the degree of curve smoothing favored by different members of the Group. Following the satisfactory conclusion of the data reduction exercise, the Group embarked on the testing round robin reported in the present paper as a final preparation

for a meaningful, interlaboratory collaborative research effort. The fourteen test laboratories listed in Table 1 agreed to participate in the round robin.

EXPERIMENTAL DETAILS

Materials and Test Specimen

The material selected for use in the test program was an SA533B Class 1 plate 0.203m thick manufactured in the U.S. by Lukens Steel. A substantial quantity of this plate, which is referred to as Heat H in the Nuclear Pressure Vessel Steel Data Base (2), was available to EPRI and detailed characterization information had been generated in the course of previous programs. Table 2 presents a summary of the fabrication history, composition and mechanical properties of the plate: additional details can be found in reference 2.

Slabs centered on the quarter thickness and three quarter thickness planes were cut from the plate and standard ASTM compact tension specimens 25.4mm thick were machined from the slabs in the T-L orientation (3). The specimens were precracked in dry air to an a/W of ~ 0.3 at a final ΔK level of $\sim 15 \text{ MPa} \cdot \text{m}^{1/2}$ with $R \sim 0$. Initially, two specimens were shipped to each participant together with detailed data sheets for reporting the results of each test. Each specimen was given a number which could be used to identify that specimens' original location in the plate. Specimens were selected at random for shipment to the participants.

Test Method

The participants were asked to test one of their specimens in accordance with the conditions given in Table 3 and to hold their second specimen pending analysis of the results of the first series of tests. Because of the varying capabilities of the participants autoclave systems, the test specification given in Table 3 is quite loose. Features of note include:

- No specification for the dissolved oxygen content of the water or the method of achieving a "low" level
- No test startup procedure
- No limitations on water flow rate or refreshment of the autoclave environment
- No requirement to electrically isolate the specimen from the autoclave or to make electrochemical potential measurements
- No criteria for aborting an unsuccessful test or for terminating a successful one
- No indication of how to measure load, or crack length.

It was hoped that the results of the tests would provide an indication of the desirability of including such features in the test specifications for future collaborative efforts of the Group.

RESULTS AND DISCUSSION

Seven of the participants were able to complete their first tests quickly. The da/dN versus ΔK plots reported by these participants are shown in Figure 1. (There are nine sets of data shown because two of the participants each had two autoclave systems available for ICCGR work.) Also shown are the ASME Section XI Appendix A reference curves for subsurface flaws and surface flaws ($R < 0.25$). Two types of da/dN versus ΔK curves are apparent in Figure 1: some specimens show linear behavior approximately parallel to the subsurface flaw reference curve but displaced to slightly faster growth rates; the remaining specimens show convex upward behavior with maximum rates close to the surface flaw reference curve. There is considerable scatter in the results from the different laboratories--typically a factor of about five in

terms of crack growth rate but as much as an order of magnitude at some values of ΔK . Interestingly, the two organizations that tested two specimens in different autoclaves were able to duplicate their own results to within a factor of less than two.

The data shown in Figure 1 were reviewed by the Group at a meeting in August 1979 and it was decided that the degree of interlaboratory variability was unacceptably large and that an attempt should be made to identify the source of the scatter. Three separate efforts were mounted, focussed on material variability, differences in the mechanical aspects of the tests, and differences in the environmental aspects of the tests. Differences in data reduction methods were not considered, based on the successful result of the previous interlaboratory comparison (1).

Material Variability

It was thought that variations in the composition and/or microstructure of the plate might be a contributor to the scatter of the test data. Accordingly an attempt was made to correlate the behavior of specimens in the crack growth tests with their location in the plate. No consistent pattern emerged--specimens from adjacent positions in the plate sometimes showed similar behavior in the crack growth experiments and sometimes showed widely different behavior. This suggests that material variability was not a major source of the observed scatter, a conclusion that is consistent with the small between-specimens scatter observed by the two organizations who tested two specimens.

A further effort in this area, involving post-test metallography and fractography, is reported elsewhere in this meeting (4).

Test Method Variability - Mechanical Aspects

A review of the data sheets for the specimens included in Figure 1 revealed several differences in the mechanical aspects of the tests of potential importance including:

- Differences in methods of measuring load and crack length
- Out-of-specification tests, such as
 - constant ΔK used instead of constant load range
 - triangle waveform instead of sine wave
 - additional precracking to a/W of 0.5 prior to testing

A questionnaire was circulated to all participants asking for details of their load and crack length measuring methods. The responses to this questionnaire revealed many different approaches but no obvious sources of interlaboratory variability.

To provide a further check on the importance of differences in crack length and load measurement methods, several additional tests were performed. Three organizations performed tests in 561K air at a frequency of 0.0167 Hz and obtained data consistent with the subsurface flaw reference curve, as shown in Figure 2. Eight organizations conducted tests at a frequency of about 1 Hz in 561K water and again observed behavior consistent with the subsurface flaw reference curve, as shown in Figure 3. The lack of significant interlaboratory scatter in Figures 2 and 3 suggests rather strongly that differences in methods of measuring load and crack length are not important sources of interlaboratory variability.

The importance of waveform was investigated to a limited extent. Two organizations conducted tests at 0.0167 Hz with a triangular waveform in 561K water and obtained the data plotted with triangular and circular symbols in Figure 4. Then one of the organizations repeated its test with a sinusoidal waveform and obtained the data plotted with square symbols. This result indicates that loading waveform is an important part of the test specification for low frequency tests in high temperature water.

Additional constant ΔK tests were also conducted to explore their comparability with constant load range tests. An important observation is illustrated in Figure 5 which shows the initial portion of the a versus N behavior seen in a test at a constant ΔK of $33 \text{ MPa m}^{\frac{1}{2}}$. The test frequency was 0.0167 Hz, the temperature was 561K, R was 0.2, and the dissolved oxygen content was 10 to 30 ppb. Even though the mechanical driving force was constant throughout, the crack growth rate increased by a factor of five during the first 3000 cycles. This behavior, which clearly corresponds to the initial rapid rise in crack growth rate observed in some of the constant load data in Figure 1, indicates that there is at least one variable of importance not covered at all in the Table 3 test specification. Possibilities include a progressive change of crack tip pH during the first few days of the test or hydrogen changing of the specimen. The mechanistic aspects of environmental cracking are covered by several other papers at this meeting, but irrespective of the mechanism, the behavior illustrated in Figure 5 suggests that it will be difficult to compare the result of a constant ΔK experiment conducted in one laboratory with the result of a constant load range experiment conducted in another.

Test Method Variability - Environmental Aspects

A review of the environmental aspects of the test methods used to generate the data plotted in Figure 1 was conducted and supplemented by a questionnaire to all participants. Differences of potential importance found included

- A variety of methods of obtaining and maintaining high purity water and of controlling the dissolved oxygen content leading to
 - oxygen contents ranging from near zero to >100 ppb
 - differences of pH and dissolved hydrogen content and probable differences of other dissolved species

- Differences of startup procedure resulting in the specimens being exposed to widely different environments prior to beginning cycling and following any test interruptions
- Large differences of water flow rate through the autoclave system
- Probable differences of corrosion potential due to the specimens being either electrically coupled to different autoclave materials or electrically isolated.

Analysis did not reveal any systematic correlation with the Figure 1 test results but it was concluded that much tighter specification of environmental factors would be desirable in future test programs. The effect of dissolved oxygen content was investigated further, because of literature data (5) showing a substantial variation of corrosion potential with dissolved oxygen concentration in the ppb range at a temperature of $\sim 560\text{K}$. Four laboratories performed tests at a frequency of 0.0167 Hz in 561K water containing oxygen concentrations of < 10 ppb, ~ 200 ppb, and ~ 8 ppm. No substantial effect of oxygen was observed. Two of the data sets are shown in Figures 6 and 7. Note that one organization observed the linear type of da/dN versus ΔK behavior (Figure 6) while the other observed the convex upward behavior (Figure 7) irrespective of dissolved oxygen content. Thus it appears possible to conclude that dissolved oxygen content is not a major contributor to the interlaboratory variability shown in Figure 1.

Present Status and Future Plans

At the present time (April 1981), 12 of the 14 round robin participants have completed at least one test in accordance with the Table 3 specification, and the other two hope to complete their first tests shortly. From among the completed tests it is possible to select a group for which most of the potential sources of interlaboratory

variability noted above are either absent or nearly absent. Figure 8 presents the data obtained by six organizations on seven specimens, all of which were tested without significant interruptions in slowly flowing 561K water containing < 100 ppb oxygen, using a 0.0167 Hz sinusoidal waveform giving a constant load range and with the specimen electrically coupled to the autoclave. The agreement is fairly good and indicates that interlaboratory variability can probably be held within acceptable limits through the use of tightly specified test procedures.

Based on this satisfactory result, the Group is at present formulating a plan for a collaborative series of tests at high R. The specification for these tests will incorporate the lessons learned in the present round robin test program and will include much tighter controls, particularly of environmental variables, than those used for the tests performed here. It is also planned to make electrochemical potential measurements during at least some of the tests to check that the test specification is effective in ensuring that the tests are performed under comparable conditions.

CONCLUSIONS

The results of this testing round robin indicate that the test systems and methods used by different organizations to generate cyclic crack growth data for RPV steels in high temperature water differ in many respects and that these differences can lead to wide variations in the data generated by different laboratories (Figure 1). Most of the important differences appear to have to do with environmental aspects of the tests in that the participating organizations obtained consistent data when the test conditions were such that the environmental contribution to crack growth was small (see Figures 2 and 3). Somewhat surprisingly, the dissolved oxygen content of the water was not found to be important (Figures 6 and 7). Tight specification of other environmental variables such as the water chemistry control methods and water flow rate through the autoclave will probably yield data of acceptable consistency (Figure 8) and should be adopted in future collaborative test programs.

ACKNOWLEDGEMENTS

The author is indebted to his colleagues in the ICCGR for the use of their data. Particular thanks are due to Bill Cullen of NRL who was kind enough to plot up da/dN versus ΔK curves from all of the round robin data sheets.

REFERENCES

1. P. M. Scott "An Inter-Laboratory Comparison of Methods for Calculating Crack Growth Rates from Corrosion Fatigue Data", AERE Report, UKAEA Harwell, England (1979)
2. W. L. Server and W. Oldfield, "Nuclear Pressure Vessel Steel Data Base", EPRI Report NP-933, Electric Power Research Institute, Palo Alto, CA, USA (December 1978)
3. "E399 Standard Method of Test for Plane Strain Fracture Toughness of Metallic Materials", American Society for Testing and Materials, Philadelphia, PA, USA
4. K. Torronen, W. Cullen and F. Hanninen, "Mechanisms of Environment Assisted Cyclic Crack Growth of Nuclear Reactor Pressure Vessel and Piping Steels", IEAE Specialists Meeting on Subcritical Crack Growth, Freiburg, W. Germany (May 13-15, 1981).
5. D. Weinstein, "BWR Environmental Cracking Margins for Carbon Steel Piping", Final Report on EPRI Contract RP1248-1, Electric Power Research Institute, Palo Alto, CA, USA (1981)

Table 1

PARTICIPANTS IN THE FIRST TESTING ROUND ROBIN
OF THE ICCGR

<u>Organization</u>	<u>Country</u>
Babcock Power	UK
Babcock and Wilcox	US
Central Electricity Generating Board	UK
Creusot-Loire	France
CISE	Italy
General Electric	US
Japan Atomic Energy Res. Inst.	Japan
Kraftwerk Union	Germany
Naval Research Laboratory	US
Rolls-Royce Associates	UK
Studsvik	France
TRC	Sweden
UK Atomic Energy Authority (Harwell)	UK
UK Atomic Energy Authority (Springfields)	UK

Table 2

TEST MATERIAL

Fabrication History:

- Austenitized at $1172 \pm 14\text{K}$ for 28.8ks
- Water quenched
- Tempered at 944K and air cooled
- Stress relieved at 839K for 7.2ks and at $894 \pm 14\text{K}$ for 180ks

Chemistry (wt%)

<u>C</u>	<u>Mn</u>	<u>P</u>	<u>S</u>	<u>Si</u>	<u>Ni</u>	<u>Cr</u>	<u>Mo</u>	<u>V</u>	<u>Cu</u>
0.19	1.28	0.009	0.013	0.25	0.61	0.04	0.55	0.004	0.10

Mechanical Properties (560K)

<u>Yield Stress</u>	<u>Tensile Strength</u>	<u>Uniform Elongation</u>	<u>Total Elongation</u>	<u>Reduction of Area</u>
386 MPa	569 MPa	12.3%	23.5%	57.9%

Impact Properties

<u>NDTT</u>	<u>RTNDT</u>	<u>Cv Upper Shelf</u>
250K	255K	136 J

Table 3

CONDITIONS FOR ICCGR ROUND ROBIN TESTS

Starting ΔK	27.5 MPa $m^{\frac{1}{2}}$
R	0.2
Frequency	0.0167 Hz
Wave shape	sine
Temperature	561K
Pressure	8.3 MPa
Control mode	load
Water chemistry	high purity water
Cl	<0.1 ppm
F	<0.1 ppm
conductivity	<1.0 $\mu mho/cm$
pH (room temperature)	7.0
O	low as practicable

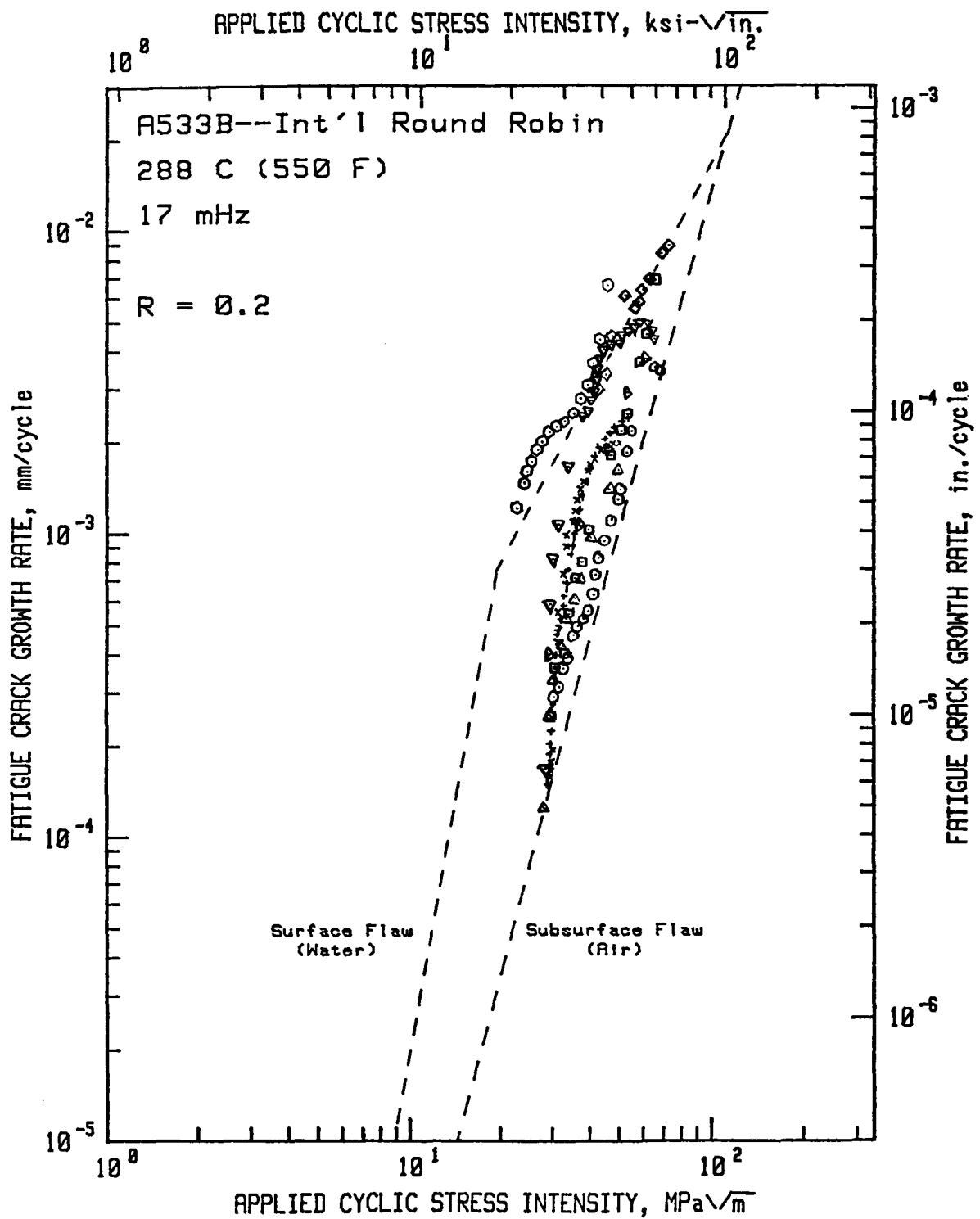


Fig. 1: Results of the first nine round robin tests

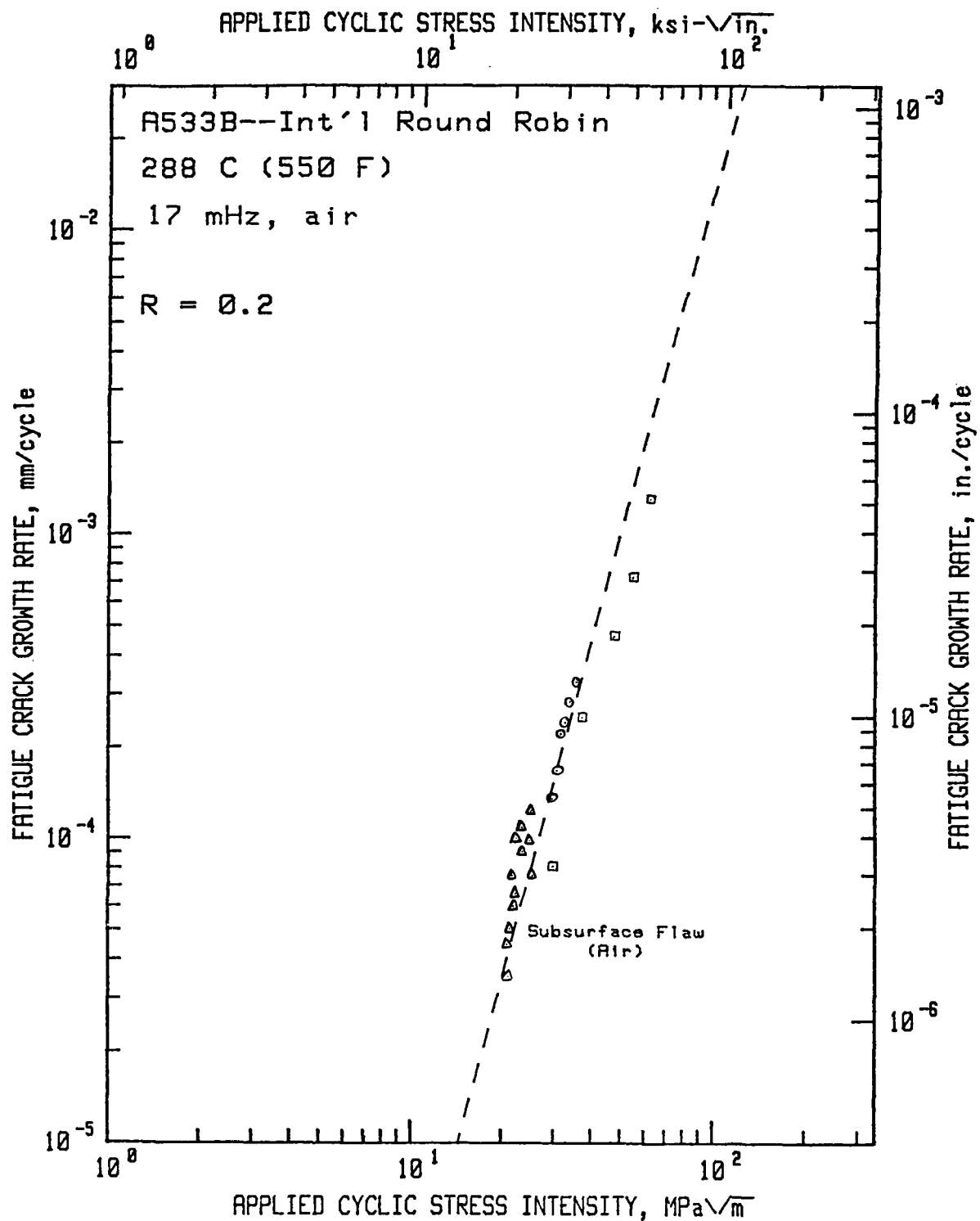


Figure 2: Results of tests by three organizations in 561K air at a frequency of 0.0167 Hz

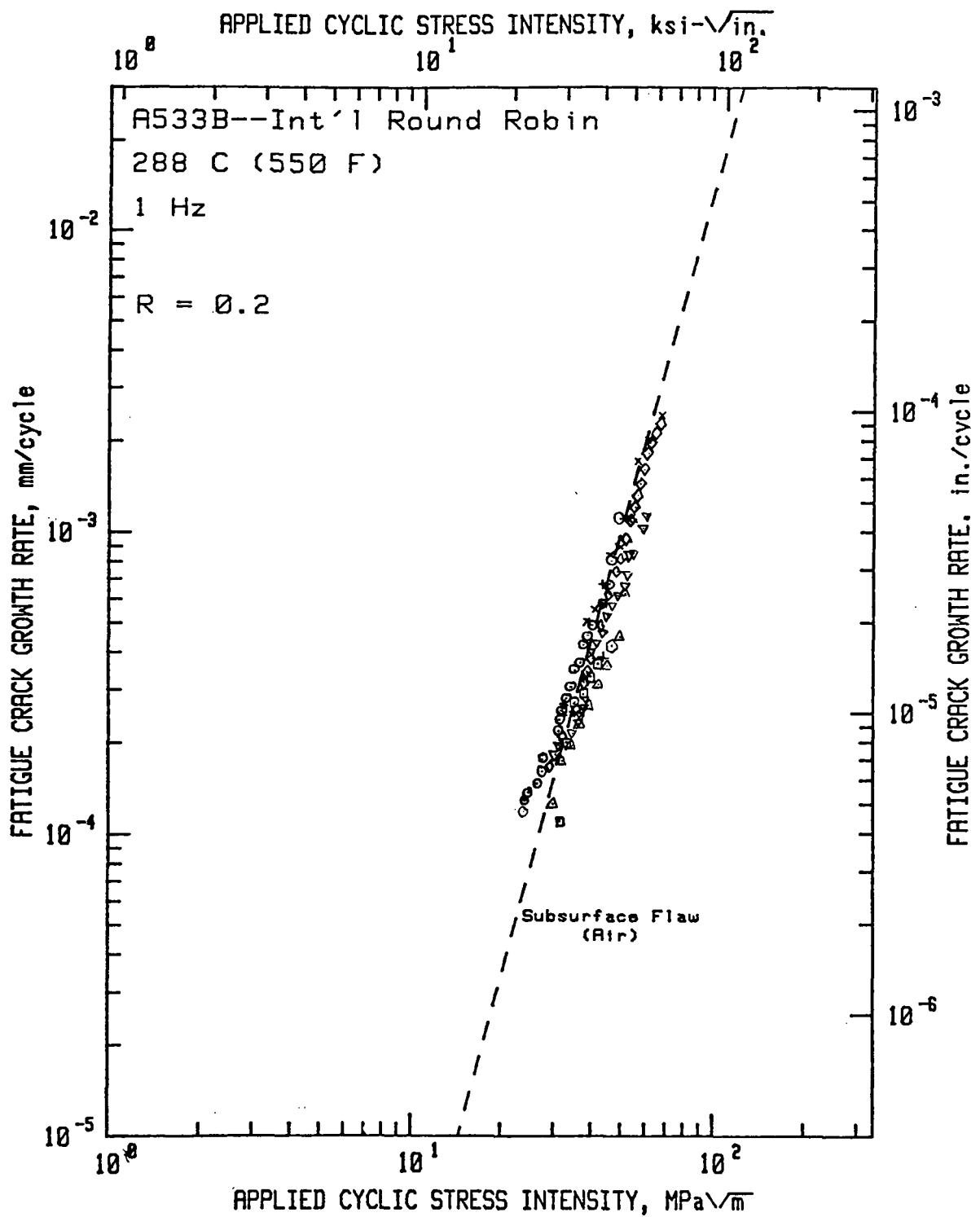


Figure 3: Results of tests by eight organizations in 561K water at a frequency of about 1 Hz

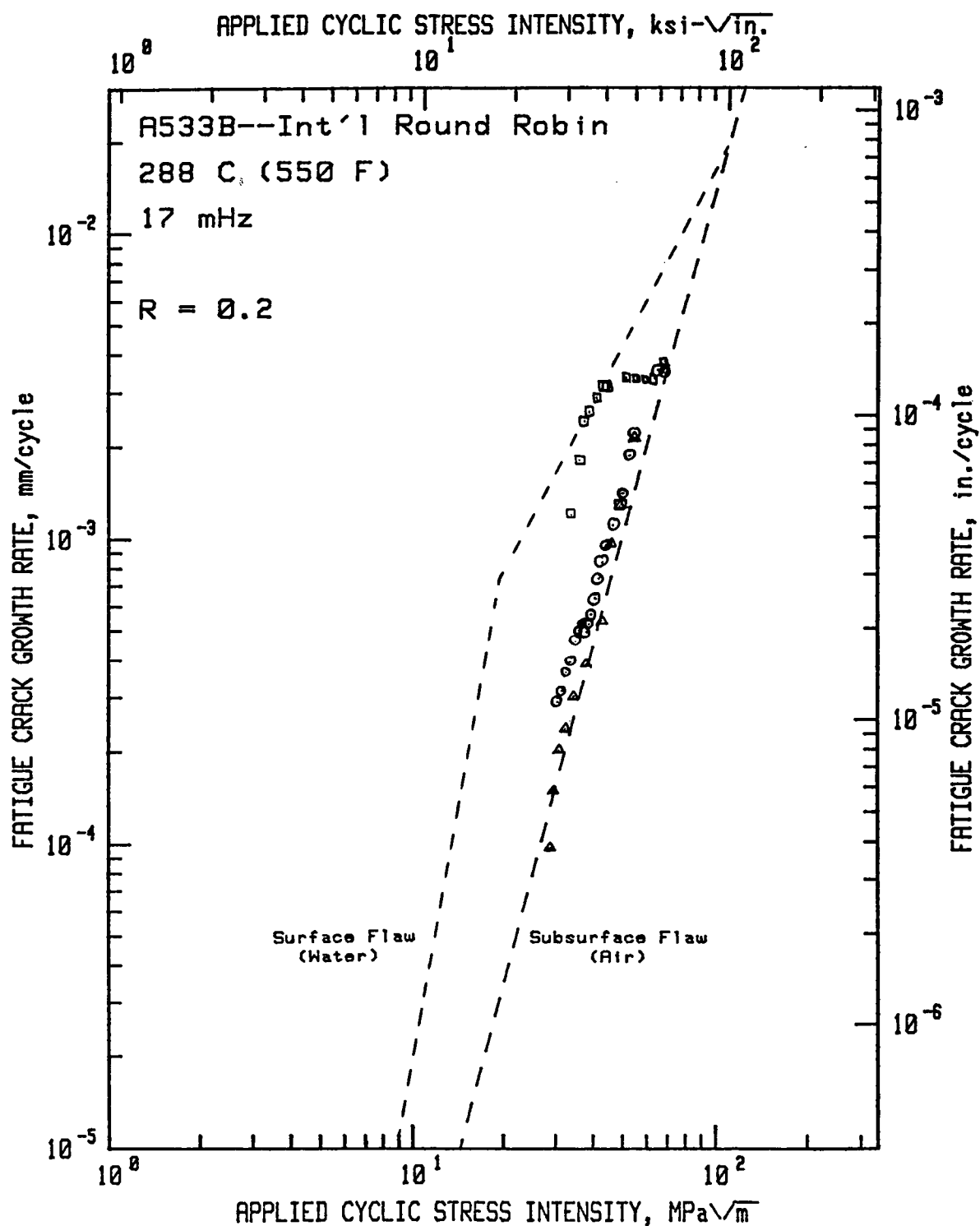


Figure 4: Effect of loading waveform in tests at a frequency of 0.0167 Hz in 561K water. A triangular waveform (circles and triangles) leads to a distinctly different da/dN versus ΔK relationship than a sine wave (squares)

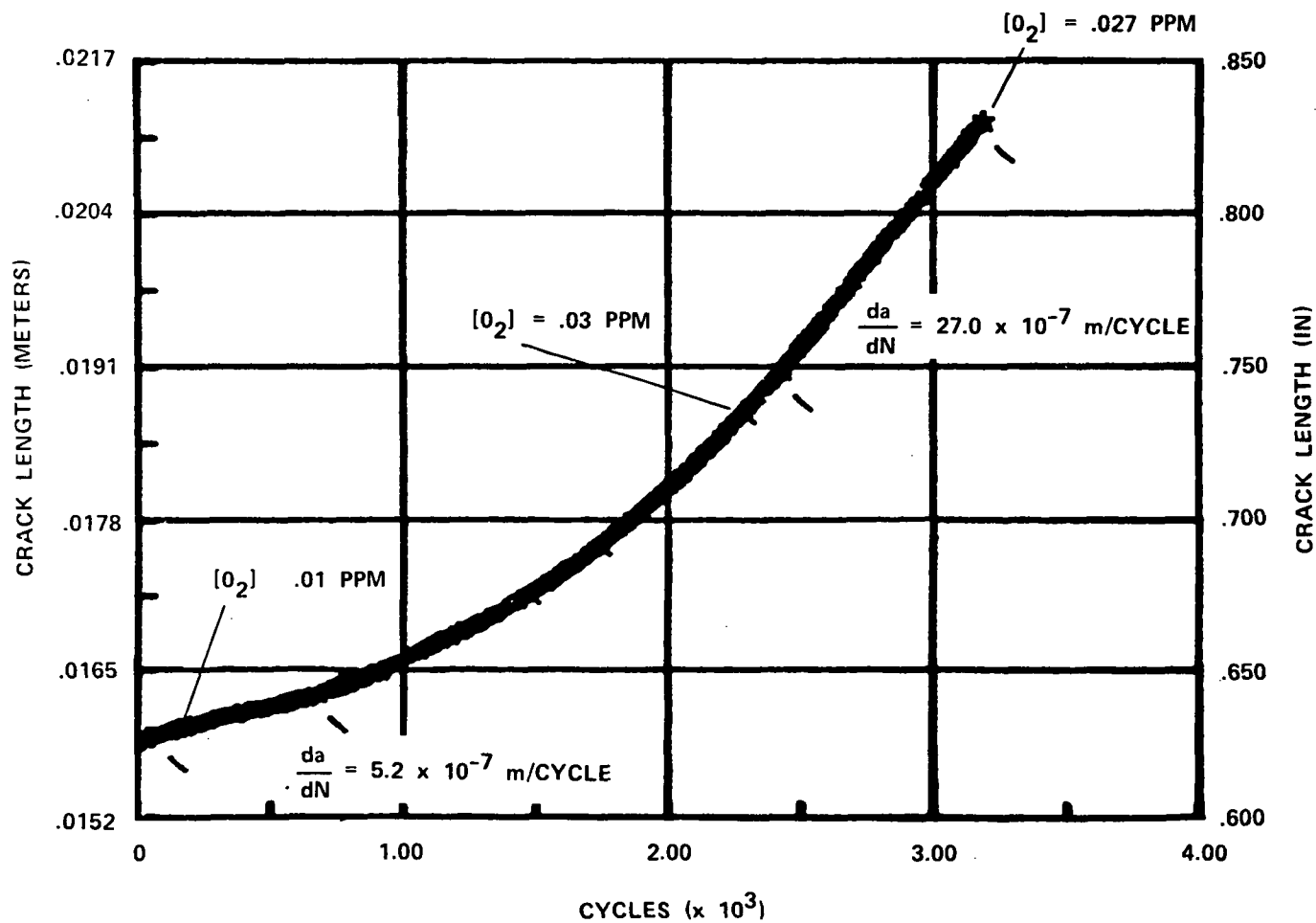


Figure 5: Crack length versus cycles data from the initial portion of a constant ΔK test ($\Delta K = 33 \text{ MPa} \cdot \text{m}^{1/2}$, $R = 0.2$, frequency = 0.167 Hz , temperature = 561K) showing a five fold increase of crack growth rate under nominally constant test conditions.

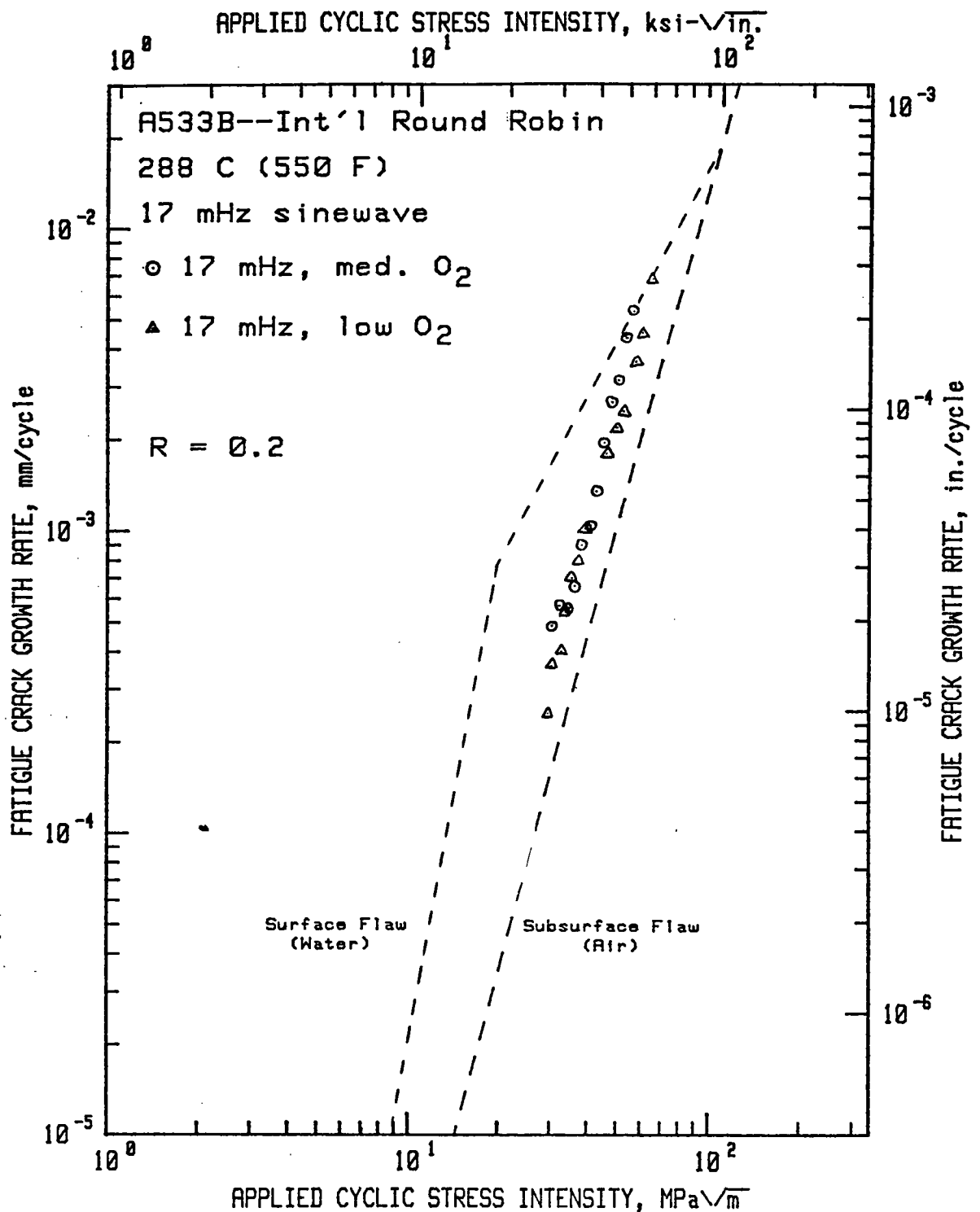


Figure 6: Effect of dissolved oxygen content. Two specimens were tested by one organization at a frequency of 0.0167 Hz in 561K water containing < 10 ppb oxygen in one case and ~200 ppb oxygen in the other

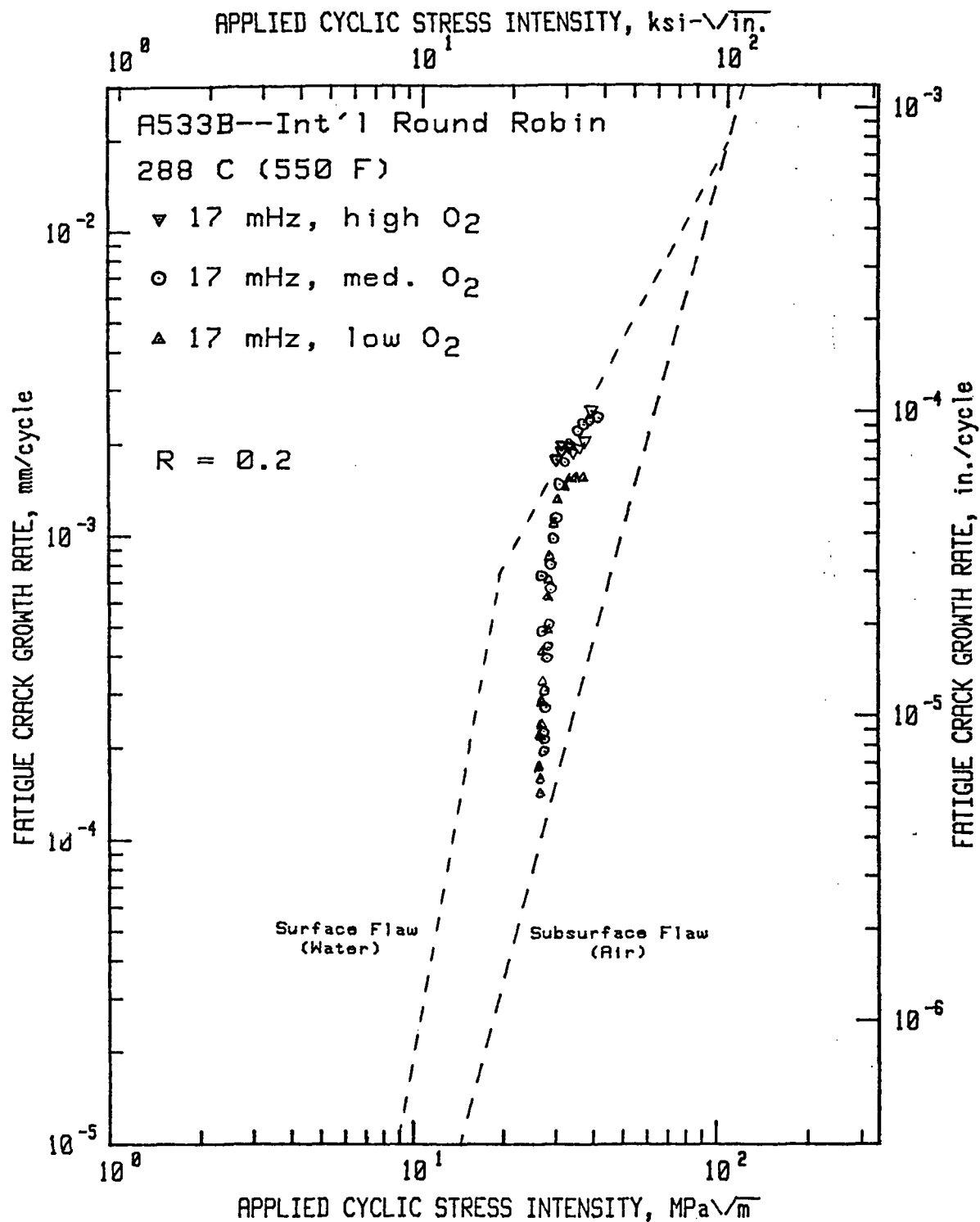


Figure 7: Effect of dissolved oxygen content. A different organization from that involved in Figure 6 tested three specimens at a frequency of 0.0167 Hz in 561K water. One specimen was tested as a dissolved oxygen content of < 10 ppb, one at ~200 ppb, and one at ~8 ppm.

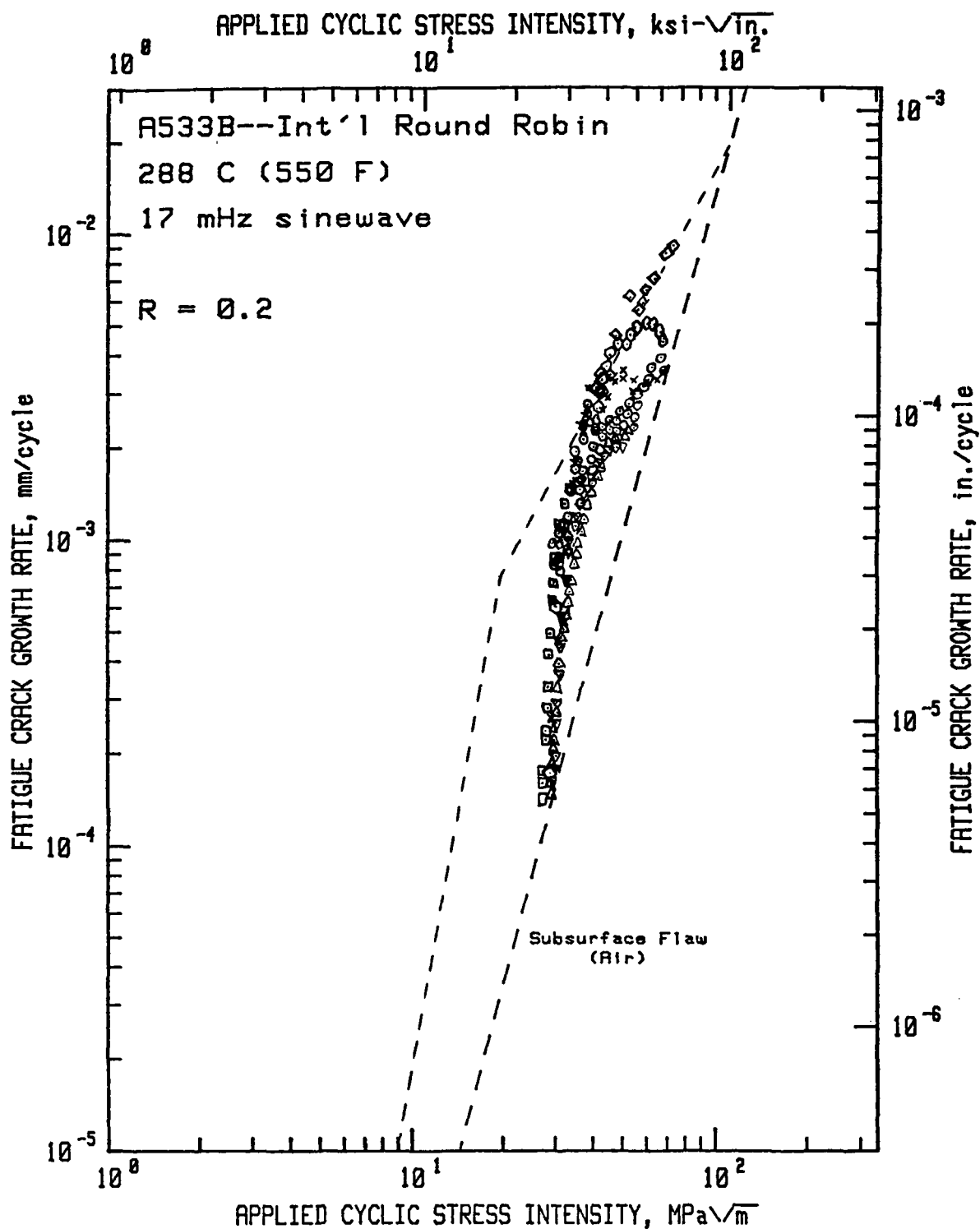


Figure 8: Results of round robin tests on seven specimens conducted by six organizations under similar test conditions

FATIGUE CRACK GROWTH RATES OF IRRADIATED PRESSURE VESSEL STEELS IN SIMULATED NUCLEAR COOLANT ENVIRONMENT

W. H. Cullen

ENSA, Inc.

Buffalo, N.Y., and Washington, D.C.

and

H. E. Watson, R. A. Taylor, F. J. Loss, and H. A. Spencer

Naval Research Laboratory

Washington, DC, USA

ABSTRACT

Fatigue crack growth rates, in a simulated pressurized water reactor primary loop environment, are presented for A508-2, A533-B steels and submerged arc weld metal (Linde 0091 flux) in both the irradiated and unirradiated conditions. The initial results, for specific experimental conditions, constant load amplitude waveforms, and load ratio = 0.2, indicate that irradiation does not enhance fatigue crack growth rates more than the enhancement due to the environment alone. Fractographic examination of the fatigue fracture surfaces showed that the crack propagated by a ductile striation formation mechanism. This article outlines the experimental techniques involved in this testing and describes the results and their possible significance with respect to the existing safety analysis codes.

INTRODUCTION

Fatigue crack growth rate testing of reactor pressure vessel (RPV) and piping steels, in reactor-typical environments has progressed to the point at which several pertinent variables have been and, continue to be, investigated. Among these are waveform and frequency, temperature, material and environmental chemistry and others [1]. For the determination of flaw growth rates for reactor-beltline locations, a potentially important variable

is the amount of radiation damage in the steel. Admittedly, while the detrimental effect of irradiation on fracture properties of RPV steels is well-known, no significant effects of irradiation on fatigue crack growth rates in an air environment have been determined [2]. Nonetheless, testing in an aqueous environment often provides an embrittling effect, or environmental assistance to the fatigue crack growth rates, and the combined effects of irradiation, environment, temperature and fatigue have never been determined.

Fatigue crack growth rates of irradiated and companion unirradiated A533 Grade B, A508 Class 2 and submerged arc weld metal (Linde 0091 flux), in a high-temperature, pressurized, reactor-grade water environment are presented in this article. Tests were conducted for two frequencies (1 Hz, 17 mHz sinusoidal waveforms) and load and environment conditions which attempted to model start-up/shutdown transients in a pressurized-water reactor.

MATERIALS AND TEST CONDITIONS

Compact fracture or wedge opening loaded specimens (1T- or 2T-CT, or 2T-WOL, as defined in ASTM 647-78 [3]) were machined from reactor-typical materials. Chemical analysis and mechanical property studies at room temperature on these materials in the pre-irradiated condition produced the results shown in Table 1. Other irradiation data are found in Ref. 4, but the intent was to provide total irradiation dose and temperature conditions which would simulate end-of-life properties at quarter-thickness of the wall of a pressurized water reactor.

Details of the test procedure, including autoclave description, crack-measurement techniques and data acquisition and processing are found in Refs. 4-6. In order to accurately simulate the pressurized water reactor coolant environment, the water in the test systems was carefully monitored and regulated to yield the specifications shown in Table 2. Water was deoxygenated by continuously bubbling hydrogen gas through the contents of the system's feedwater tanks.

RESULTS

Data for A533-B steel in both the irradiated and unirradiated condition is shown in Figs. 1a and b. Although the materials (codes L83 and HT) are from different heats, and the initial ΔK for the HT-material tests is somewhat higher, the trend of the results is very similar. The 1 Hz tests produce results residing on or near the ASME air default line [7] over the higher portion of the ΔK range which was tested. The 17 mHz results show a substantial increase in growth rate over the 1 Hz results, but since the increase is about the same for both irradiated and unirradiated material, it appears to be a function of the environment and cyclic period, rather than irradiation. Irradiated specimen L83-1 was tested over a ΔK range which began with a value sufficiently low that the classical-three-region behavior of corrosion fatigue crack-growth rates can be seen [8]. The first stage,

called Region I growth, or start-up, occurs at the lowest values of the ΔK range, with crack growth rates rising to a plateau, or Region II growth, characterized by somewhat more ΔK -independent growth rates than for Regions I or III. Lastly, for the higher ΔK values, Region III, the growth resumes a strong ΔK -dependence.

The reader should note that Region I growth behavior should not be construed as an indication of "threshold", or lower limit behavior of these fatigue crack growth rates. The location of Region I for these data sets is simply a function of the initial value of ΔK chosen for these tests; true threshold studies on these materials have only been conducted for air environments, with the results detailed in Ref. [4]. The onset of Region II, the value of the growth rates throughout Region II, and the transition of Region II into Region III growth behavior are established by the test frequency. In this particular case, the 17 mHz test was terminated before the onset of Region III growth had been established. This test was and, in fact, all tests were deliberately terminated well before fracture of the ligament remaining in the specimen(s) so that a final crack length, as inferred from the LVDT displacement gage could be optically confirmed from the specimen(s) fatigue fracture surface.

Figure 2 presents the results of an effort to separate, if present, the effect of irradiation time at temperature from the effects of irradiation damage itself. Specimen L83-19 was conditioned at 288°C for 1225 hr which, combined with residence time in the autoclave prior to and during the test, closely approximates the time for irradiations of the other L83 specimens described above. Specimen L83-18 was tested in the as-received condition. Results of 1 Hz tests in reactor-grade water environment of all three specimens (L83-1, -18, -19) are shown in Fig. 2, allowing the conclusion that the response of the material to fatigue is essentially unaltered by irradiation or by an equivalent time at temperature for these materials as evaluated in this study.

A similar set of tests was conducted on A508-2 material, code Q71. These results are shown in Fig. 3. As for A533-B, there is an easily observable increase in growth rates for the 17 mHz waveform as opposed to the 1 Hz waveform, but this increase is nearly identical to the increase shown in Figs. 1a and b and as before, is due to the influence of the environment during the longer period waveform. Since the test on Q71 was carried out to a longer final crack length, and hence higher ΔK value than L83-6, the onset and extent of Stage II growth is clearly described in this case. Note that the increase in growth rates between the 1 Hz and 17 mHz results is about a factor of twenty, while the increase in cyclic period is about sixty. The relationship is not, therefore, one-to-one, and in fact, if irradiation has little or no effect, we can expect, on the basis of unirradiated results [5,9] that the 17 mHz waveform affords a saturation or maximization of the environmental effect, for PWR environments, and thus, the 17 mHz results of Figs. 1 and 3 represent upper limits of fatigue crack growth for the $R = 0.2$ constant-load-amplitude condition. The comparison

of 1 Hz test results for irradiated and unirradiated, but time-and-temperature-conditioned specimens, also shown in Fig. 3 indicates that the irradiated results are somewhat lower than the unirradiated results, although the difference is not clearly greater than the commonly accepted scatter band (a factor of about two) for similar, intralaboratory fatigue crack growth rate tests.

A second heat of A508-2, code V82 material, showed behavior similar to that of code Q71 material. The results of 17 mHz, sinusoidal waveform tests, shown in Fig. 4, indicate that while this heat of steel appears to be slightly more environmentally susceptible, testing in either the irradiated or unirradiated condition produced nearly identical data.

The fatigue crack growth rate results on irradiated and unirradiated Mn-Mo weld metal, deposited with Linde 0091 flux, shown in Fig. 5, resemble the results described for A533-B and A508-2 and yield a similar conclusion. The 1 Hz results, for both irradiated and unirradiated materials are nearly the same, and reside near the ASME air default line. The 17 mHz results appear to show growth rates lower than the 1 Hz tests at low values of ΔK , but that is likely to be part of the "start-up" character of these tests [10]. The 17 mHz growth rates do crossover and reside above the 1 Hz growth rates over most of the ΔK range examined in this test. The overall growth rate, at 17 mHz, of this weld metal is slightly lower than many of the plate and forging materials described in this report, a fact which is at variance with data relative to sulfur contents of unirradiated pressure vessel steels.

DISCUSSION

The overall results derived from this study, that irradiation does not enhance crack growth rates for simulated reactor coolant environment, is parallel to the earlier results for tests in high and low temperature air environments [2]. In those instances of irradiated specimen results for which the growth rates are depressed (A508, code Q71, 1 Hz tests), this may be due to the increased yield strength of the irradiated specimens. In those cases for which the irradiated results are slightly higher than for comparable tests of similar materials (17 mHz tests - all cases), the increase may be due to a small synergistic effect of the environmental influence on the radiation damaged steel, however, the variability is well within a scatter band defined by previous growth rate evaluations for these materials. In the case of the A508-2 forging, code V82, which seems to be slightly more environmentally susceptible than the code Q71 material, irradiation did not provide any further detrimental effects. It is important to note that for the specific sets of conditions studied (1 Hz and 17 mHz sinusoidal waveform, $R = 0.2$, PWR conditions) none of the present results exceed the existing ASME default lines for aqueous environment fatigue crack growth. It is important to note that these are only a few of the many material, environmental and mechanical test variables which are of importance within an overall study of the effects of irradiation and environment on fatigue crack growth in RPV steels. Other tests to determine the effect of load ratio (R), other materials, especially other welds and heat-affected zones, and transient

conditions involving load, temperature and water chemistry should be conducted and should yield a more complete interpretation of fatigue crack growth.

FRACTOGRAPHY OF IRRADIATED SPECIMENS

The irradiated specimens were examined in an SEM located in a hot cell [11], using cutting and cleaning procedures [12] similar to those described for unirradiated specimens. For the specimens tested at 1 Hz, fatigue crack propagation occurred almost exclusively by a ductile striation mechanism, as is typical in these steels for tests in which the environmental effect is not a factor. For the 17 mHz tests, as shown on the A533-B fatigue fracture surface in Fig. 6a, fatigue crack propagation at lower values of ΔK (27 MPa \sqrt{m}) occurs by a ductile striation formation mechanism, while at higher values of ΔK (Fig. 6b) there is little striation formation, and the rather rough fracture surface indicates that the microstructure and grain morphology heavily influence the crack path. In this sample, relatively little secondary cracking was observed.

Irradiated A508-2 fatigue fracture surfaces, as shown in Figs. 7a and b, are not as dominated by ductile striations, but their formation persists over the entire ΔK range. Extensive secondary cracking is also seen, and as in A533-B, the rough surface indicates that the microstructure strongly influences the crack propagation path.

While there will be continued examination of these and other fracture surfaces, it appears that irradiation of these steels does not noticeably affect the fatigue fracture surface morphology. There appears to be no suggestion of any new fatigue mechanism which might be the result of a material/irradiation/environment interaction. This observation suggests that the essential coincidence of fatigue crack growth rate data for either irradiated or unirradiated, but otherwise comparable steels, is due to the fact that the mechanism for environmentally-assisted fatigue crack growth is essentially unaffected by irradiation.

SUMMARY AND CONCLUSIONS

Postirradiation fatigue crack growth rate tests, in a simulated pressurized water reactor coolant environment, have demonstrated that irradiation does not further increase the growth rates for A508-2 and A533-B steels, or submerged-arc weld metal (Linde 0091 flux), beyond those increases which are due to the environment itself. The reader should note that the results presented here are limited in the scope of the external variables which have been treated, and that to be more complete, other waveforms, temperatures, load ratios and water chemistries should be incorporated into a larger test matrix. However, for simulated pressurized water reactor conditions, and constant-load amplitude tests, $R = 0.2$, the effects of irradiation do not provide any significant changes to the expected fatigue crack growth rates. In particular:

(a) For tests with a 1 Hz sinusoidal waveform, tests of irradiated and unirradiated but temperature-conditioned specimens showed that irradiation had no discernable effect (A533-B and the weld metal) or may tend to slightly decrease the fatigue crack growth rates (A508-2).

(b) For tests with a 17 mHz sinusoidal waveform, the results showed the expected, waveform-dependent increase over the 1 Hz results, but the observed growth rates did not exceed the current ASME Section XI water-environment default line. The irradiated specimen results did not differ significantly from results for unirradiated specimens of similar steels from different heats.

(c) In comparing the results of the different materials, there is little to distinguish them apart, indicating that, at least for conditions of this study, the ASME code will not have to be reformulated with qualifications for the different materials which are in use.

(d) The fractographic examination of the fatigue fracture surfaces of A508-2 and A533-B specimens shows only ductile striation formation and other basically ductile tearing morphologies. There was no clear suggestion of any environmentally or irradiation-embrittled regions, or of any detrimental, synergistic relationship of the high-temperature, aqueous environment with the irradiation damaged steel.

ACKNOWLEDGMENTS

The investigations reported were sponsored by the Reactor Safety Research Branch of the Nuclear Regulatory Commission. The continuing support of this agency is appreciated. The authors also thank J. R. Hawthorne who provided the irradiation capsule design and irradiation logistics.

REFERENCES

1. W. H. Cullen and K. Torronen, "A Review of Fatigue Crack Growth of Pressure Vessel and Piping Steels in High-Temperature, Pressurized Reactor-Grade Water," NRL Memorandum Report 4298, NUREG/CR-1576, Naval Research Laboratory, Washington, D.C., September 1980.
2. L. W. James, "Fatigue Crack Propagation in Neutron-Irradiated Ferritic Pressure-Vessel Steels," Nuclear Safety, Vol. 18, pp. 791-801, 1973.
3. ASTM E647-78, "Test Methods for Constant-Load Amplitude Fatigue Crack Growth Rates Above 10^{-8} m/cycle," ASTM Book of Standards, Part 10, issued annually, American Society for Testing and Materials, Philadelphia, PA, 1910².
4. W. H. Cullen, H. E. Watson, R. E. Taylor, and F. J. Loss, "Fatigue Crack Growth Rates of Irradiated Pressure Vessel Steels in Simulated Nuclear Coolant Environment," J. Nucl. Mater., Vol. 96, pp. 261-268 (1981).

5. W. H. Cullen, et. al, "Fatigue Crack Growth of A508-2 Steel in High-Temperature, Pressurized Reactor-Grade Water," NUREG/CR 0969, NRL Memorandum Report 4063, Naval Research Laboratory, Washington, D.C., September 1979.
6. D. Sturm, F. J. Loss, and W. H. Cullen, "Autoclaves for Testing of Irradiated and Unirradiated Specimens," Materialprüfungsanstalt, Vol. 22, pp. 5-1] (1980).
7. ASME Boiler and Pressure Vessel Code, Section XI, Rules for In-Service Inspection of Nuclear Power Plant Components, ANSI/ASME-BPV-XI, American Society of Mechanical Engineers, New York, NY 10017. Issued annually.
8. R. P. Wei, S.R. Novak, and D. P. Williams, "Some Important Considerations in the Development of Stress-Corrosion Cracking Test Methods," Proceedings, 33rd AGARD Conference on Structures and Materials, Brussels, Belgium, 1971.
9. W. H. Cullen, H. E. Watson, and V. Provenzano, "Results of Cyclic Crack Growth Rates Studies in Pressure Vessel and Piping Steels," in Structural Integrity of Water Reactor Pressure Boundary Components, Annual Report, FY-1979, NRL Memorandum Report 4122, NUREG/CR-1128, December 31, 1979.
10. W. H. Cullen, R. A. Taylor and H. E. Watson, "Result of Cyclic Crack Growth Rate Studies in Pressure Vessel and Piping Steels," in Structural Integrity of Water Reactor Pressure Boundary Components, Quarterly Progress Report, April-June 1980, NRL Memorandum Report 4400, NUREG/CR-1783, Naval Research Laboratory, Washington, D.C., February 1981.
11. J. R. Reed and F. A. Smidt, Jr., "Modification of a SEM for Remote Operation in a Hot Cell," NRL Memorandum Report (to be published).
12. P. M. Yuzawich and C. W. Hughes, "An Improved Technique for Removal of Oxide Scale from Fractured Surfaces of Ferrous Materials," Westinghouse Research Report 76-109-FRTOG-R1, Westinghouse Research Laboratories, Pittsburgh, PA 15235.

FIGURE CAPTIONS

Fig. 1a, b. Fatigue crack growth rates vs applied cyclic stress intensity factor for (a) irradiated and (b) unirradiated A533-B steel in high-temperature, pressurized reactor-grade water. Comparison of these two graphs shows the parallel behavior of the irradiated and unirradiated specimens. Since the unirradiated tests began at a rather high initial value of ΔK , the three-stage behavior, seen clearly in irradiated specimen L83-1, does not manifest itself.

Fig. 2. Fatigue crack growth rates vs applied cyclic stress intensity factor for as-received, unirradiated but conditioned at reactor time and temperature, and irradiated at A533-B steel in high-temperature, pressurized reactor-grade water. These three overlapping data sets indicate that irradiation under conditions of this initial study has an essentially insignificant effect on fatigue crack growth rate.

Fig. 3. Fatigue crack growth rates vs applied cyclic stress intensity factor for irradiated and unirradiated, but reactor time- and temperature-conditioned, A508-2 steel, code Q71. These results are very similar to those for A533-B shown in Figs. 1 and 2. In this case, the irradiated specimen tested at 1 Hz shows a slight, but measurable decrease in crack growth rates.

Fig. 4. Fatigue crack growth rates vs applied cyclic stress intensity factor for irradiated and unirradiated, as received A508-2 steel, code V82, in high-temperature, pressurized reactor-grade water. There is no observable effect of irradiation, although the degree of environmental assistance is slightly greater than for the code Q71 material shown in Fig. 3.

Fig. 5. Fatigue crack growth rates vs applied cyclic stress intensity factor for irradiated and unirradiated, but reactor time- and temperature-conditioned, submerged-arc weld metal, Linde 0091 flux. These results are quite similar to those for the mill products A533-B and A508-2.

Fig. 6. Fatigue fracture surface of A533-B steel from a 17 mHz test at (a) 28 MPa \sqrt{m} (~ 25 ksi $\sqrt{in.}$), and (b) ~ 39 MPa \sqrt{m} (~ 35 ksi $\sqrt{in.}$). The morphology is basically composed of striations and ductile rupture in both cases.

Fig. 7. Fatigue fracture surfaces of A508-2 steel from a 17 mHz test at (a) 28 MPa \sqrt{m} (~ 25 ksi $\sqrt{in.}$), and (b) 60 MPa \sqrt{m} (~ 55 ksi $\sqrt{in.}$). As in Fig. 6, ductile rupture, influenced by the specimen texture and grain morphology, and some striation formation, are apparent.

TABLE 1 - Material Chemistry, Heat Treatment and Mechanical Properties

Material	C	Mn	P	S	Si	Ni	Cr	Mo	Cu	V
A533-B-1 (L83)	.22	1.37	.008	.008	.22	.66	.15	.54	.18	.02
A508-2 (Q71)	.19	.69	.007	.009	.31	.82	.38	.62	.0	.13
A508-2 (V82)	.20	.60	.013	.012	.20	.73	.35	.56	-	-
Submerged-Arc Weld (Q93)	.08	1.49	.047	.017	.60	.58	.03	.39	.24	.01

Primary Heat Treatment

A533-B Class 1 (HSST-01)	Normalized at 870-950°C (1600-1750°F) for 4 hours, air cooled; austenitized at 820-900°C (1500-1650°F) for 4 hours, quenched in agitated water; tempered at 660 ± 14°C (1225 ± 25°F) for 4 hours, furnace cooled).
A508 Class 2 Submerged-Arc Weld	Stress relief annealed at 605°C (1120°F) for 20 hours, furnace cooled.
A508 Class 2 (Forging)	Austenitized 840°C (1550°F) for 9 hours; water quenched; tempered 650°C (1210°F) for 12 hours, air cooled; stress relief annealed 660°C (1225°F) for 20 hours, furnace cooled 30 C/hr max (55°F/hr max).

TABLE 1 -Material Chemistry, Heat Treatment and Mechanical Properties (Continued)

Material	Direction	0.2% Offset Yield Strength MPa (ksi)	Ultimate Tensile Strength MPa (ksi)	Reduction In Area %	Elongation %
A533-B-1 (L83)	TL	472 (68.5)	620 (90.0)*	-	19
A508-2 (Q71)	TL	538 (78.0)	680 (98.6)	-	-
	LT	555 (80.5)	692 (100.4)	-	-
A508-2 (V82)	TL	475 (68.9)	636 (92.2)	59.5	24.9
Submerged-Arc Weld (Q93)		469 (68.1)	579 (84.0)		

TABLE 2 - Water Chemistry Specifications^a

Boron (as boric acid)	1000 ppm
Lithium (as lithium hydroxide)	1 ppm
Chloride ions	.15 ppm
Fluoride ions	.10 ppm
Dissolved oxygen	1 ppb
Dissolved hydrogen (saturation)	30-50 cc/kg water

^aAll other metallic or ionic species should be at about trace levels. Some iron, both in solid and soluble form is the inevitable result of a corroding specimen.

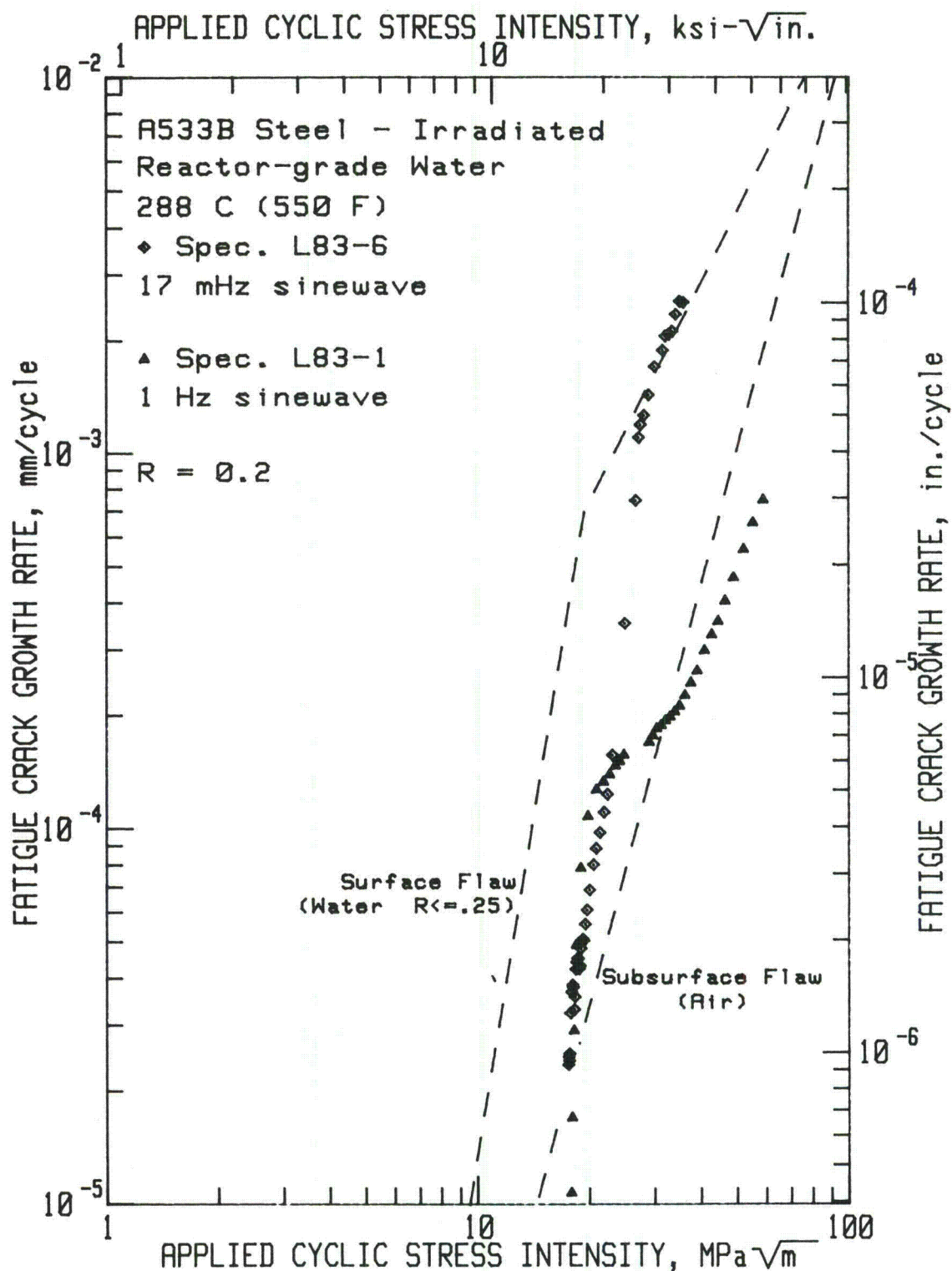


Fig. 1a, b. Fatigue crack growth rates vs applied cyclic stress intensity factor for (a) irradiated and (b) unirradiated A533-B steel in high-temperature, pressurized reactor-grade water. Comparison of these two graphs shows the parallel behavior of the irradiated and unirradiated specimens. Since the unirradiated tests began at a rather high initial value of ΔK , the three-stage behavior, seen clearly in irradiated specimen L83-1, does not manifest itself.

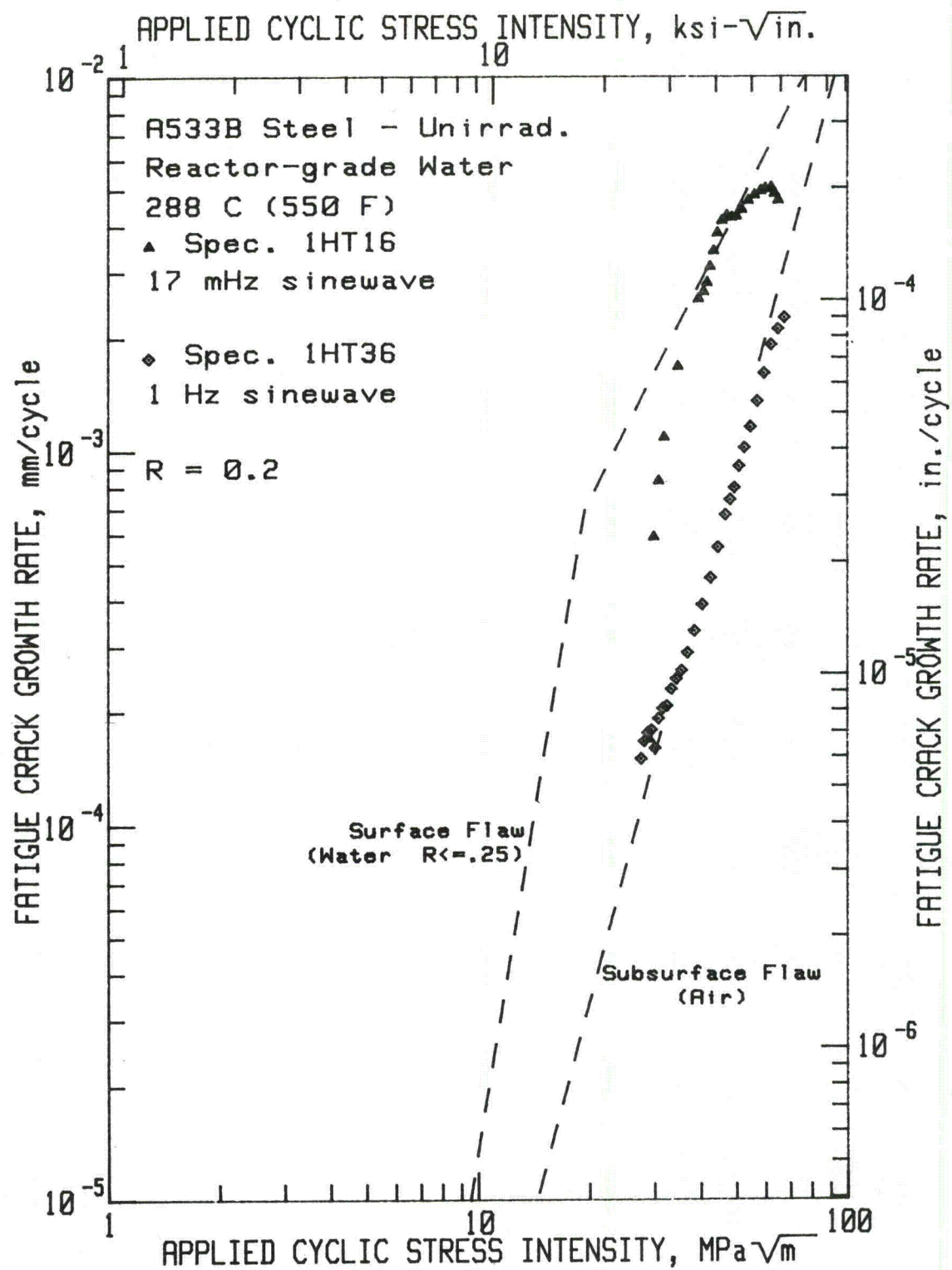


Fig. 1b

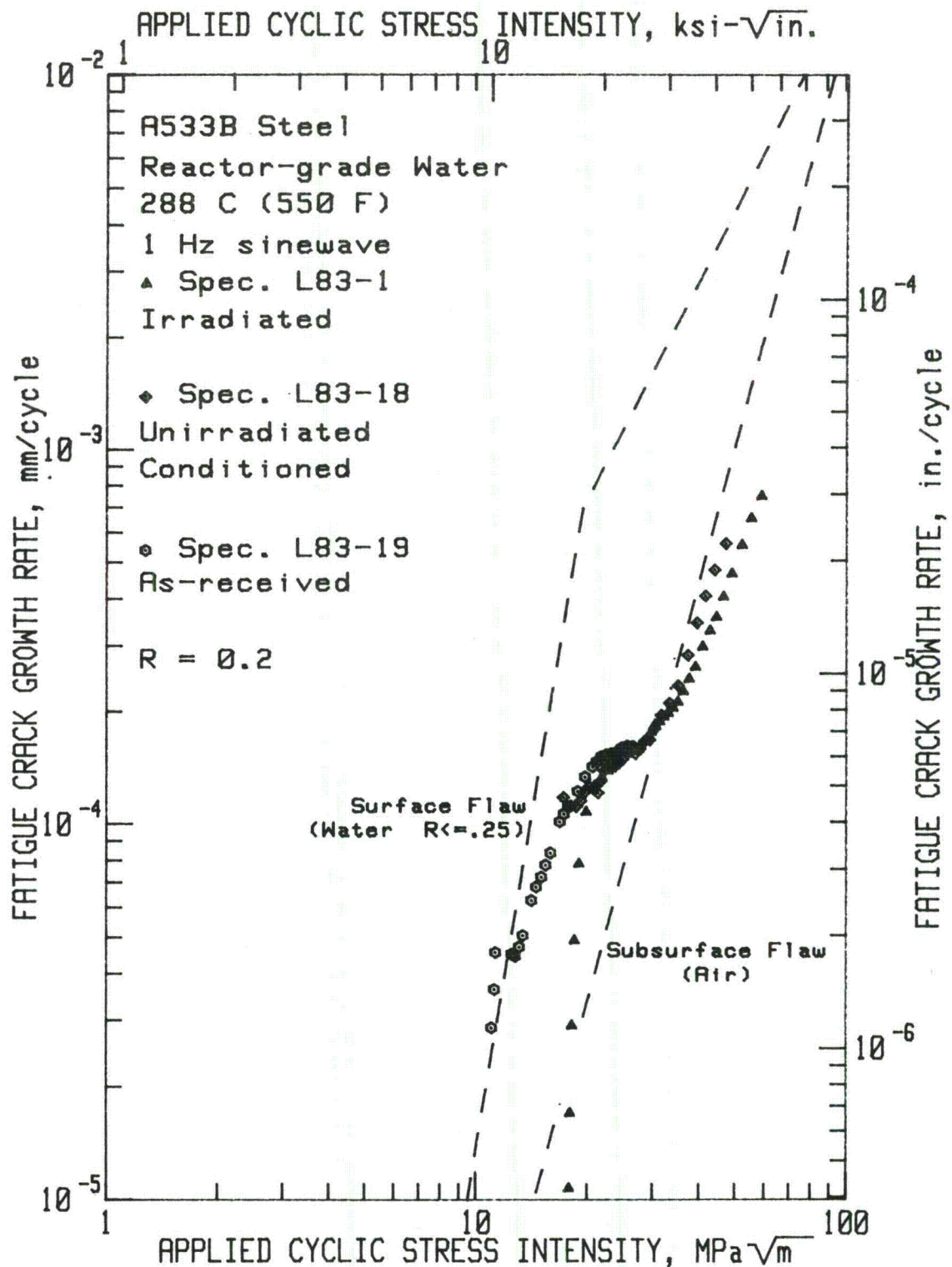


Fig. 2. Fatigue crack growth rates vs applied cyclic stress intensity factor for as-received, unirradiated but conditioned at reactor time and temperature, and irradiated at A533-B steel in high-temperature, pressurized reactor-grade water. These three overlapping data sets indicate that irradiation under conditions of this initial study has an essentially insignificant effect on fatigue crack growth rate.

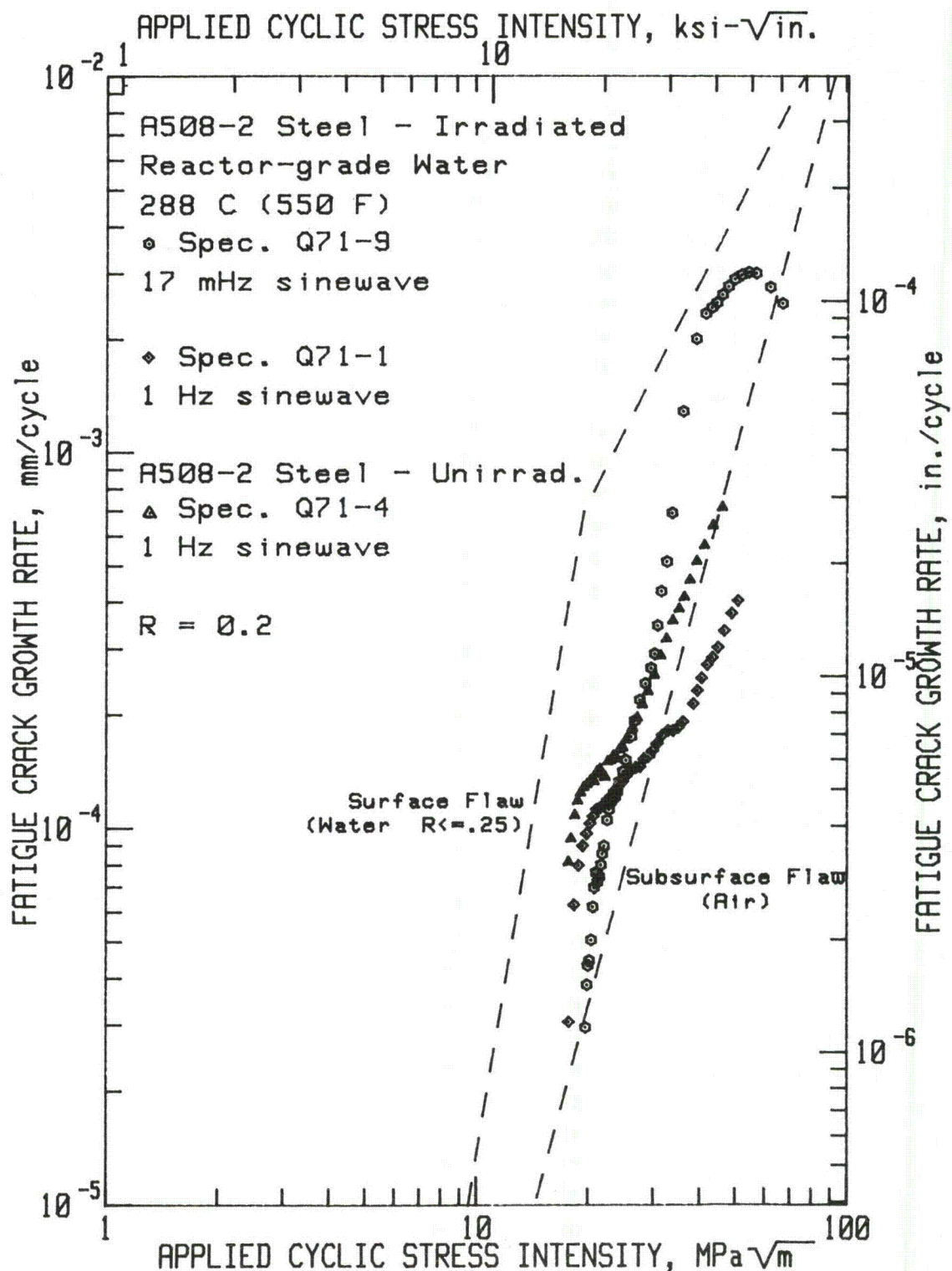


Fig. 3. Fatigue crack growth rates vs applied cyclic stress intensity factor for irradiated and unirradiated, but reactor time- and temperature-conditioned, A508-2 steel, code Q71. These results are very similar to those for A533-B shown in Figs. 1 and 2. In this case, the irradiated specimen tested at 1 Hz shows a slight, but measurable decrease in crack growth rates.

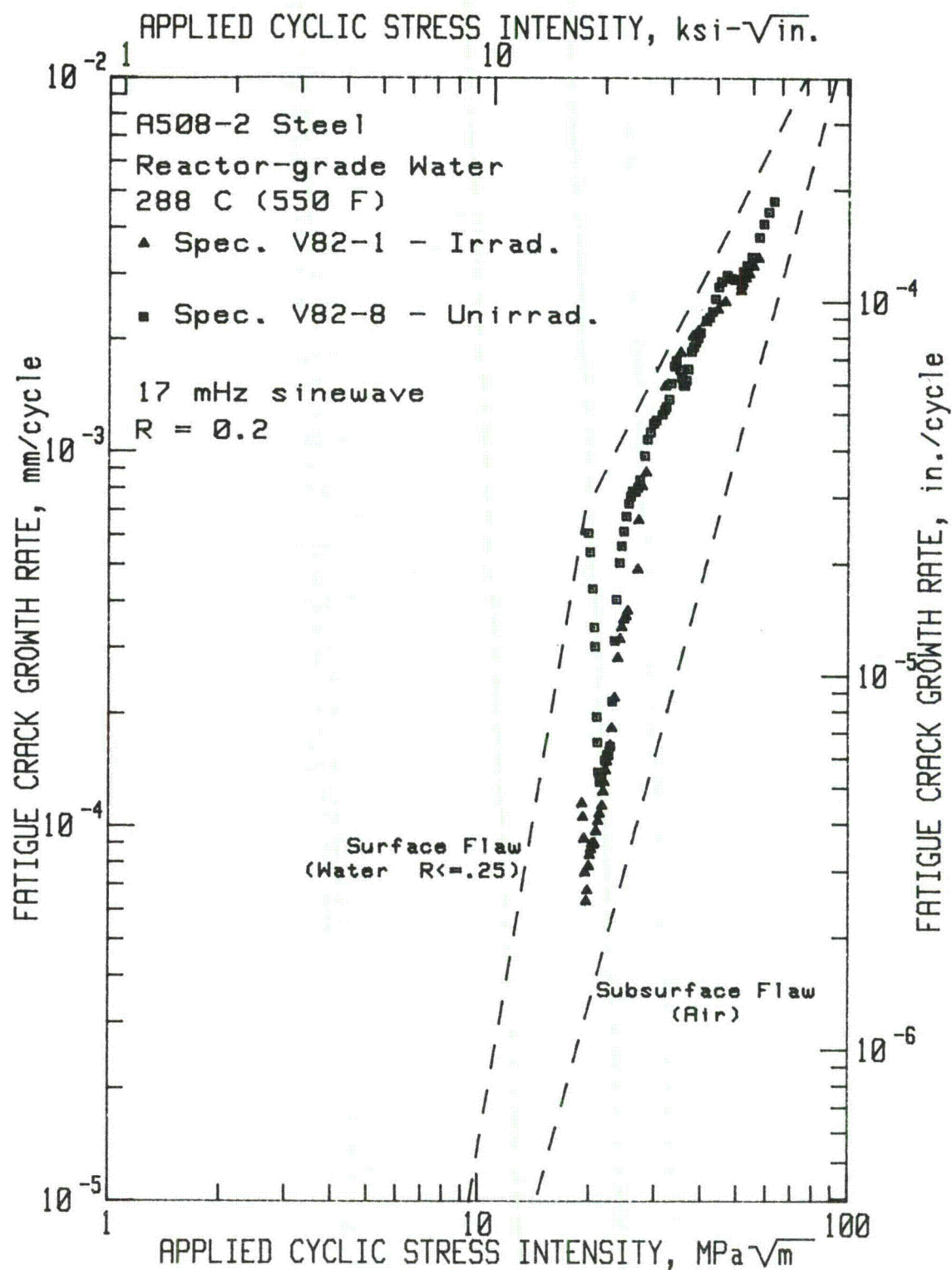


Fig. 4. Fatigue crack growth rates vs applied cyclic stress intensity factor for irradiated and unirradiated, as received A508-2 steel, code V82, in high-temperature, pressurized reactor-grade water. There is no observable effect of irradiation, although the degree of environmental assistance is slightly greater than for the code Q71 material shown in Fig. 3.

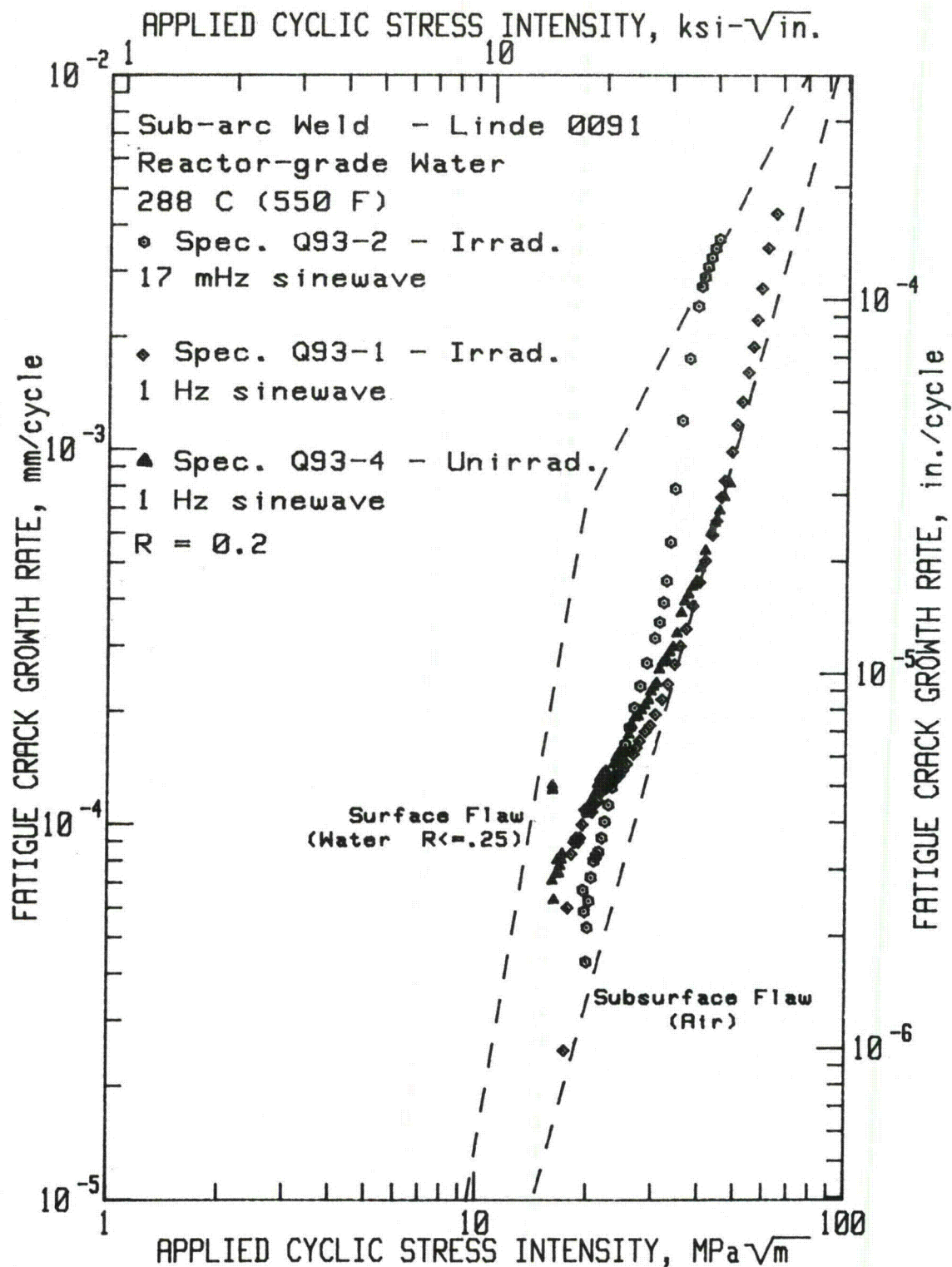
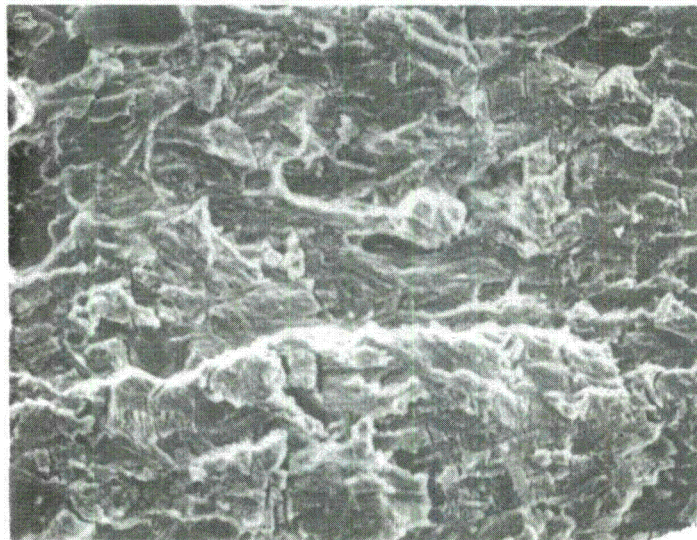
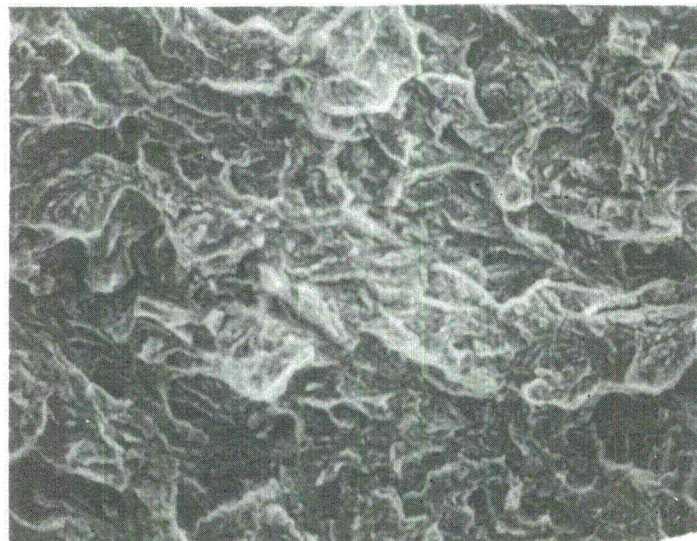


Fig. 5. Fatigue crack growth rates vs applied cyclic stress intensity factor for irradiated and unirradiated, but reactor time- and temperature-conditioned, submerged-arc weld metal, Linde 0091 flux. These results are quite similar to those for the mill products A533-B and A508-2.



A

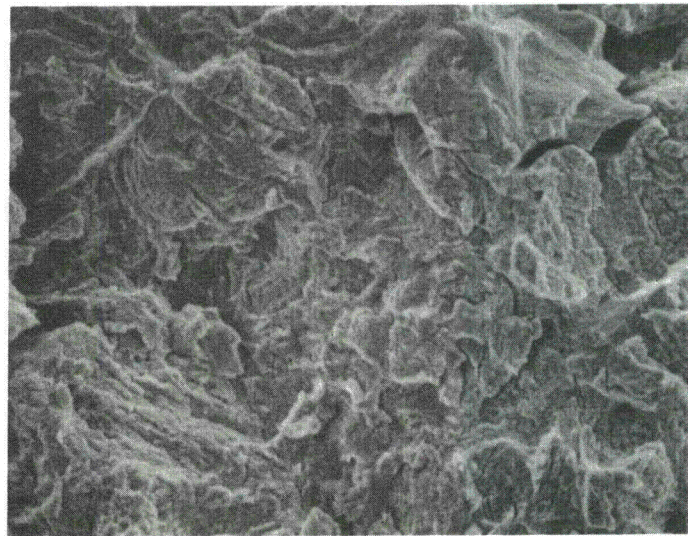
50 μm



B

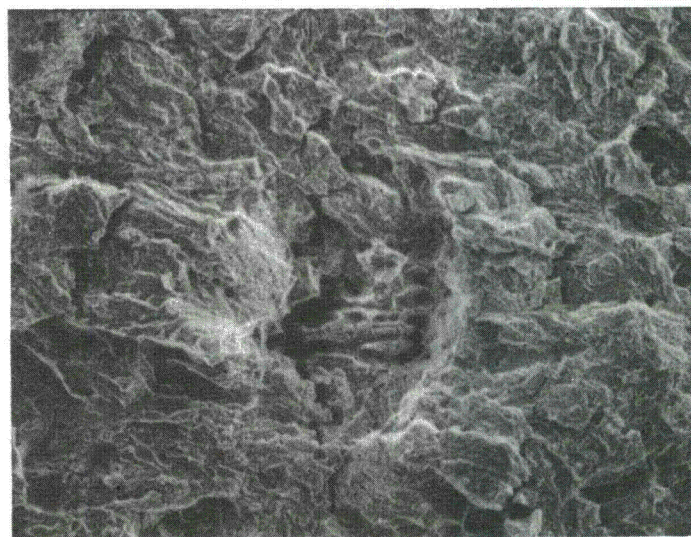
50 μm

Fig. 6. Fatigue fracture surface of A533-B steel from a 17 mHz test at (a) $28 \text{ MPa}\sqrt{\text{m}}$ ($\sim 25 \text{ ksi}\sqrt{\text{in.}}$), and (b) $39 \text{ MPa}\sqrt{\text{m}}$ ($\sim 35 \text{ ksi}\sqrt{\text{in.}}$). The morphology is basically composed of striations and ductile rupture in both cases.



A

50 μm



B

100 μm

Fig. 7. Fatigue fracture surfaces of A508-2 steel from a 17 mHz test at (a) $28 \text{ MPa}\sqrt{\text{m}}$ ($\sim 5 \text{ ksi}\sqrt{\text{in.}}$), and (b) $60 \text{ MPa}\sqrt{\text{m}}$ ($\sim 55 \text{ ksi}\sqrt{\text{in.}}$). As in Fig. 6, ductile rupture, influenced by the specimen texture and grain morphology, and some striation formation, are apparent.

**DESIGN-, OPERATION-, AND INSPECTION-RELEVANT FACTORS OF
FATIGUE CRACK GROWTH RATES FOR PRESSURE VESSEL AND
PIPING STEELS**

W. H. Cullen

ENSA, Inc.

Buffalo, N.Y., and Washington, D.C., USA

and

F. J. Loss and H. E. Watson

Naval Research Laboratory

Washington, D. C. USA

ABSTRACT

Test results which define the influence of waveform, temperature, load ratio and environment on fatigue crack growth rates of reactor pressure vessel steels in simulated reactor primary coolant environments are illustrated and described. The results of two test matrices are included. The first, called the preliminary test matrix was aimed at the determination of crack growth rates for a single material, A508-2, but for a wide variety of waveforms and temperatures. The second, or main matrix for unirradiated materials, was aimed at determining growth rates for a variety of reactor pressure vessel steel plates, forgings and submerged-arc welds, but for two waveforms and two load ratio selections. The results, and their significance for design and in-service inspection related safety analyses, are described in this article. The trends observed in the available data and the areas in need of additional research are identified.

INTRODUCTION

To assure continued safe operation of nuclear reactors used for power generation by the public utilities, a comprehensive and industrious program of inspection and monitoring is carried out. If a flaw indication is found, the reactor owner may proceed in one of two ways: the flaw may be repaired, usually through a weld repair technique, or a fracture mechanics analyses may be carried out resulting in computation of future inspection intervals during which the flaw indication will be carefully monitored to determine whether extension of the flaw has occurred. In addition to knowledge of the stress levels in the neighborhood of the flaw, the fatigue crack growth rates for the material in question must also be known or determined. These fatigue crack growth rates should take into account not only the product form, but also the environment, waveform, temperature and irradiation levels which pertain to the vicinity of the flaw. If satisfactory growth rates are not available, the Appendix A of Section XI of the Boiler and Pressure Vessel Code (1) details a set of default rules, providing crack growth rates which may be used in lieu of actual crack growth rates for the material and conditions which actually pertain.

Typically the transients which occur during operation of a power reactor are the result of brief, temporary shutdowns prompted by an indication of an equipment problem, or more simply, pressure adjustments which are made in response to power demands. Start-ups and shut-downs also account for a few hundred loading cycles in a reactor lifetime. These cycles have periods ranging from a few seconds to several minutes and waveshapes that are basically triangular or sinusoidal. The loads which are realized in the vicinity of a flaw are generally a combination of dead-weight loads of the reactor, its internals and the water, the water pressure, torques and vibrations due to pumping equipment, residual stresses near welds and some stresses induced by thermal gradients. The reactor coolant environment is relatively well-characterized in a pressurized water reactor (PWR) but the lack of buffering solutes and varying dissolved oxygen content of boiling water reactor (BWR) coolants make the latter environment more difficult to typify.

From 1976 through 1978, the Naval Research Laboratory, together with Westinghouse Corporation, carried out a cooperative test plan, sponsored by the Nuclear Regulatory Commission, and termed the "preliminary test matrix." A follow-on program, the "main test matrix" was conducted in 1979 and 1980. The object of the first program was to determine the influence of waveform, temperature, and load ratio on a single pressure vessel steel - A508, Class 2. Then, utilizing the two most illustrative, reactor-typical, waveform conditions, as determined by the preliminary matrix, the main test matrix was directed at determination of fatigue crack growth rates for a wide variety of reactor pressure vessel steels, welds and heat-affected zones (HAZ). Testing of a limited variety of irradiated steels is also within the scope of the main test matrix.

APPROACH

The approach to this research, as embodied in the concept of the preliminary test matrix, was to determine fatigue crack growth rates for a variety of test waveforms consisting of ramp and hold components of varying lengths. As examples, one second, and one, five and thirty minute ramp times were combined with one, three, thirty and sixty minute hold times. To avoid confusing results, tests were conducted from start to finish with a single waveform selection, composed of one ramp time component and one hold time component from the above list. As adjuncts to the set of preliminary matrix tests, other waveforms were selected for additional tests, with the rationale for these choices explained in the following section.

In order to provide the most germane data, the testing is conducted using simulated pressurized water reactor primary loop coolant. Crack growth rates are determined in autoclaves, or small pressure vessels using the water chemistry given in Table 1. The environment is monitored very carefully, with continuous on-line sampling of dissolved oxygen contents, specific conductance, and pH. Batch samples for more complete elemental analysis by classical wet chemistry methods are taken once each week, or more often, depending on test schedules and progress. Temperature is held constant to within two centigrade degrees, and the water circulates to prevent stagnation.

Table 1 - Typical pressurized water reactor coolant chemistry^a

Boron (as boric acid)	1000 ppm
Lithium (as lithium hydroxide)	1 ppm
Dissolved oxygen	1 ppb
Dissolved hydrogen	30-50 cc/kg (H ₂ O)
Chloride	0.10 ppm
Fluorine	0.10 ppm

^a All other elements should be held to trace levels; a small amount of iron, both solid and soluble, will be detected, and is the inevitable result of corroding specimens.

Tests were conducted at both 93°C (200°F) at essentially atmospheric pressure, and 288°C (550°F), with constant amplitude loads at a load ratio of 0.1 to 0.2. Each specimen was instrumented with a displacement gage, which measured crack mouth opening (δ). Since the ratio of δ to load (P) is proportional to the crack length, this provided a method to determine the latter without visual observation. The empirical relationship derived for this purpose accounted for gage position, temperature, and specimen geometry. Over the three-year duration of this test series, steadily improved methods of data acquisition were employed, culminating in a fully-automated computer-controlled data acquisition and processing system. The details of autoclave hardware, specimen instrumentation and data acquisition methods may be found in Refs. 2-4.

A508-Class 2 forging steel was selected as the one material to be investigated in this test matrix. Specimens were cut from the nozzle drop-outs by first removing about 40 mm of the outer surfaces, including the inside cladding, and blanking out specimens from the remaining material. All specimens were oriented so that the tensile stress at the crack tip was parallel to the hoop stress direction of the drop-out.

The samples were either 25.4 mm thick (1T) compact specimens, or 50.8 mm thick (2T) WOL specimens. In the case of the compacts, the machined notch extended to an a/W of 0.25 and these were precracked to an a/W of 0.30. The WOL specimens had a machined notch 25.4 mm ($a/W = 0.19$) and were precracked an additional 6 to 50 mm (0.3 to 2 in.) depending on the initial ΔK level desired. The maximum stress intensity applied during precracking was less than or equal to the initial stress-intensity levels for the test. All precracking was performed at room temperature in an air environment. During the latter phases of testing, additional precracking in the test environment was performed. This was done in an attempt to promote environmental equilibrium at the crack tip before initiating the actual test.

RESULTS

In the following presentation of the data, the first four figures are paired, for certain similar, or identical, characteristics of the waveform, with the lower temperature results on the left, and the higher temperature results on the right. There appear to be three factors which strongly influence the crack growth rates of A508-2 in the reactor-grade water environment: ramp time, hold time, and temperature. An interrelationship among the three determines the particular crack growth rate; it is impossible to isolate the effects of one variable without fixing the other two.

Figure 1 shows test results for waveforms with a one second ramp time component, coupled with substantially longer hold times. At either temperature, this produced essentially identical data, located on, or very near the ASME air default line, which is included (together with the 1972 water default line) on all the plots in this article. For these short ramp time components, during which the environment has an insufficient opportunity to attack the crack tip enclave, there appears to be no environmental assistance.

Figure 2 shows test results for waveforms with longer ramp times (from one to thirty minutes), coupled with one to three minute hold times. In this case, the lower temperature results reside midway between the ASME air and water default lines, which represent a substantial increase over the results shown in Fig. 1a. However, for the higher temperature, the test results, as in Fig. 1b, reside on or near the ASME air default line. Thus, a substantial ramp time component, together with a low temperature, produces environmentally assisted crack growth rates.

To determine whether the hold time component was influencing the results, tests involving only ramp components were conducted, and the

results are shown in Figs. 3 and 4. The ramp time only tests at low temperature produced environmentally accelerated data, shown in Fig. 3 for a 60 sec ramp time, while the high temperature results remain located near the air default line, showing no environmental assistance. Figure 4 shows results of a similar test, but with a 22 sec. ramp time component. Even with the shorter ramp time, the results are similar -- higher growth rates for the lower temperature, and no clear cut environmental assistance for the higher temperature test. For both of these cases (Figs. 3 and 4), it should be noted that the results are nearly identical to those of Fig. 2, for the respective temperatures, indicating that the presence or absence of a hold time component does not affect the degree of environmental assistance.

About midway through the series of tests represented by the data in the previous four figures, it was realized that a 17 mHz sinusoidal waveform, together with a high temperature (288°C) produced crack growth rates which were significantly higher than any of the ramp/hold, or ramp/reset combinations which had been tested at the 288°C temperature. Figure 5 shows results of one test which bears out this fact. Attempts were made to reproduce this data using a ramp/hold combination (22 sec ramp, 4 sec hold) which is the trapezoidal approximation to the positive slope of a sinusoidal waveform. The results of two tests (both shown in Fig. 5) fail to reside as high as the 17 mHz sinewave test. Consideration of similar tests conducted at other facilities (5) indicates that sinusoidal waveforms with periods ranging from 0.2 to 2 minutes may all produce crack growth rates which reside midway between the ASME air and water default lines. In short, for 288°C temperatures, there are no ramp only, or ramp/hold waveforms which yield environmentally-assisted fatigue crack growth rates, but a substantial range of sinusoidal waveforms do result in enhanced growth rates. The environmental mechanism which produces this result is not understood at the present time. It is possible that the constantly varying ramp rate resulting from the sinusoidal waveform may alter the potentio-kinetic processes at the crack tip in a way that is substantially different from that for fixed ramp rate waveform. Another speculation is that the decreasing load portion of the sinusoidal waveform, or the dwell time around the minimum load may enhance the environmental assistance.

During the initial phases of this research, when test systems were being implemented and improved, and outages and other failures were frequent, common test practice was to choose an initial value of applied cyclic stress intensity such that relatively easily measureable crack extensions would occur over rather short times. Typically, for $R = 0.2$ and waveforms of about 60 sec periods, a ΔK value of 25 MPa \sqrt{m} was selected. While the research carried out under this proviso produced the desired amount of scoping data on various materials (5) and enabled the understanding of the temperature and waveform effects described above, the measurement of fatigue crack growth rates for lower stress intensity factor ranges (10-25 MPa \sqrt{m} for $R = 0.2$) has not been carried out. Now that the reliability of test and data acquisition systems has substantially improved, recent research has extended our understanding of fatigue crack growth rates into the lower ΔK ranges.

On the basis of these recent tests, it is becoming evident that fatigue crack growth rates for these reactor pressure vessel materials, at least for sinusoidal waveforms and low load ratios, follow the conventional three-region behavior which has been amply discussed in the classical presentation of stress-corrosion cracking (6) and corrosion-fatigue crack growth (7). This is shown schematically in Fig 6a, which has been adapted, in a simplified way, to these results. In terms of K , the exact onset of the transition from Region I to Region II behavior is generally a function of the material and the environment. In terms of crack growth rate, the level of Region II is primarily a function of test frequency, all other things being equal. The reader should note that Region I growth behavior should not be construed as an indication of "threshold," or lower limit behavior of these fatigue crack growth rates. The location of Region I for these data sets is simply a function of the initial value of K chosen for these tests; true threshold studies on these materials have only been conducted for air environments, with the results detailed in Ref. 7. The onset of Region II, the value of the growth rates throughout Region II, and the transition of Region II into Region III are established by the test frequency.

In illustration of this conclusion, fatigue crack growth rates for A508-2 steel are shown in Fig. 6b, together with the trend lines shown in the accompanying figure. At the present time, this data describes the limits of the research completed on the extension of data into the lower ΔK regime. While this set of trend lines adequately describes the behavior of this material, there remain some aspects of this description for which additional research would be helpful. The exact position of the trend lines for lower values of ΔK , especially for longer period waveforms, is not well established. At the Naval Research Laboratory, efforts are now underway to measure fatigue crack growth rates of 17 mHz (or comparable frequency) waveforms on tests for which the initial stress intensity factor was about 15 MPa \sqrt{m} . Similar efforts, in constant ΔK tests, with $\Delta K = 16.5$ MPa \sqrt{m} , are underway at Babcock and Wilcox Research Laboratories, Alliance, Ohio. The data resulting from the above two efforts should assist in a more complete definition of the actual trends.

At the time this contribution was written, testing of the main matrix program was essentially complete, and the results were essentially as expected. Figure 7 shows two shaded regions, for $R \sim 0.7$ and $R \sim 0.2$, which for the most part, encompass the data generated for the respective conditions. Also shown are the new surface flaw default lines as contained in the 1980 edition of the ASME Code. Much of the justification for the bilinear shape and positioning of these lines may be found in a reference by Bamford (8). Briefly, a regression method was employed to determine a 95 percent confidence level on upper limits for fatigue crack growth rates for two sets of load ratio conditions, $R \gtrsim 0.2$ and $R \gtrsim 0.7$. At the present time, this choice of code default lines seems to represent a conservative estimate of the upper bound of the available data.

It seems likely, however, that the rather high growth rates described by these default lines, especially for lower ΔK values, may lead to calculations of unrealistically short inspection intervals, or reactor lifetimes. In these cases, many utilities may choose, as the code indicates they may, to determine crack growth rates for the particular product form equivalent to that in which the suspected flaw resides. In some cases, the data may be available; in other cases, it may have to be generated—either case may prove to be an alternative less expensive than a costly repair job, or a nearly continuous inservice inspection procedure.

An incorporation of the Section XI computational methodology in Section III of the ASME Code (9) is also under consideration by the code writing committees of the ASME. This makes the selection of and rules for application of default crack growth rate laws even more critical, since flaws which are discovered during the construction phase of a reactor pressure vessel will face an entire reactor lifetime of applied stress cycles, irradiation and environmental attack.

With this preliminary matrix data as a background, a main test matrix was subsequently configured. The object of the main test matrix was to determine crack growth rates under simulated pressurized water reactor conditions for a wide variety of reactor pressure vessel steels, submerged arc welds, and the associated heat-affected zones, but for a limited selection of two waveforms and two load ratios. A 60 sec ramp/reset and 17 mHz sinusoidal waveform were selected as being both reactor-typical, and from the preliminary matrix results, should provide a valuable indication of the range of crack growth rate behavior for reactor-typical materials and test conditions. At this same time, a smaller, but otherwise similar, matrix was constructed to define a series of tests of irradiated materials.

There are several conclusions drawn from this main matrix data, which is presented in its entirety in Ref. 10. These conclusions are detailed in the reference, but are summarized below:

(a) There are no significant categorical differences in fatigue crack growth rates between any of the RPV materials tested, which included submerged-arc welds deposited with three different fluxes (Linde 80, Linde 124, Linde 0091), heat-affected zones associated with each of the above, A508-2 forging steel and A533B plate steel.

(b) The 1980 version of the Section XI default lines is a generally conservative estimate to all of these various materials, even though the equations for the lines were derived only for A508 and A533 data.

(c) There are three strong, external influences on the data:

(1) Load ratio effect - for a given value of ΔK , decreasing the load ratio, R , increases the crack growth rate. This effect has been well-documented for many alloy-environment systems and this evidence confirms that pressure vessel steels behave similarly.

(2) Waveform effect - while changes in crack growth rate are known to stem from changes in the waveform, RPV steels in the reactor-typical environment have a rather unique dependence on waveform, as outlined in a preceding section of this paper.

(3) Effect of sulfur content - while a significant collection of data only exists for several heats of A533B, it appears that increasing sulfur content leads to higher corrosion fatigue crack growth rates. Crack growth rates for steels with .014 to .021 percent sulfur were grouped distinctly above growth rates for steels with lower (.008 to .012 percent) sulfur contents.

CONCLUSIONS

Based on the above data, the following conclusions have been drawn.

1. For lower temperatures (93°C , 200°F) and low load ratios, ($R = 0.1, 0.2$), waveforms containing a ramp time component of greater than one second duration yield crack growth rates residing midway between the 1972 versions of the air and water environment default lines, or just under the 1980 version of the low load ratio ($R \leq 0.25$) surface flaw default line.

2. For high temperature and low load ratios, all ramp and hold waveforms tested produced crack growth rates residing on or near the subsurface flaw (air environment) default line. Additionally, all low temperature and low load ratio tests with a one second ramp time fell on or near the air default line. This places all such data significantly below the ASME default line, and where such waveforms pertain, use of the default line growth rate formula, rather than the actual data, will produce overly conservative computations of reactor lifetime or require inspection intervals. However, for high temperatures and low load ratios, 17 mHz sinusoidal waveforms produce significantly higher crack growth rates, residing about midway between the 1972 ASME air and water default lines.

3. For higher load ratios, there is more variance in the available data (5) and a general conclusion is not possible. There are apparently some product forms and compositions for which crack growth rates are substantially lower than the default line for high load ratio controlled growth rate.

4. When tested over a ΔK range which begins with a sufficiently low value ($\sim 15 \text{ MPa} \sqrt{\text{m}}$ for $R = 0.2$) and which extends over a sufficiently large range (15 to $\text{MPa} \sqrt{\text{m}}$ or more) the classical three-region behavior of corrosion fatigue crack growth rates can be described.

CONSIDERATIONS FOR FUTURE RESEARCH

The above results were developed for a pressurized water reactor environment. Boiling water reactor (BWR) environments are most notably different in that during normal operation, the coolant contains 200 to 300 ppb dissolved oxygen, as opposed to the negligibly small (<1 ppb) level in a

PWR. Consideration of the available data relevant to BWR environments (11,12) indicates that the data points fall in the same two zones as the PWR-type data (Fig. 6), however, the trends of the data, as functions of waveform and temperature, are not as clearly established as in the above description for A508-2 in a PWR environment.

Fatigue crack growth rate research for reactor safety use is far from a completed task, for there are many areas which have not been explored, or in which only slight progress has been made. A look at the data in this report, or in review papers (5,13) shows that there is no data in the near-threshold, or very low growth rate regime ($\sim 10^{-7}$ to 10^{-8} m/cycle). It is in this area that flaw extension will require millions of cycles in order to produce measurable extensions. Thermal cycling and pump vibrations do, however, provide alternating stresses at frequencies high enough to result in millions of cycles. Thus, it is important to gain a better understanding of this topic. The current ASME default rules do not provide a threshold, or lower stress-intensity factor limit, below which fatigue crack growth will not occur. Thus, in calculations using the code default lines, any flaw will grow, regardless of its size or the stress level, if the requisite number of cycles are fed into the calculations.

Another important consideration in the application of this data is that reactor-typical waveforms involve cycles of a variety of amplitudes and periods, while the available crack growth data pertains only to constant amplitude, constant frequency testing. Furthermore, there is no indication of any predictive method which adequately enables computation of variable amplitude crack growth rates from constant amplitude test results. Variable amplitude testing of these materials in simulated nuclear coolant environments is in its infant states (14).

Another closely related topic, which must be more thoroughly investigated, is stress-corrosion cracking (SCC), both as a mechanism by itself and in tandem with fatigue cycling involving hold times. Recent evidence indicates that these materials, formerly believed to be resistant to SCC, do show signs of cracking, albeit at rather high levels of applied stress-intensity factor (10,15).

ACKNOWLEDGMENT

The investigations reported were sponsored by the Reactor Safety Research Division of the U. S. Nuclear Regulatory Commission. The continuing support of this agency is appreciated. The innovative experimental design and overall technical assistance of R. E. Taylor contributed to the success of this research. The assistance of J. R. Hawthorne, who handled the irradiation logistics, is also appreciated.

REFERENCES

1. "Rules for Inservice Inspection of Nuclear Power Plant Components," Section XI of the ASME Boiler and Pressure Vessel Code, ANSI-BPV-XI-1, issued annually, American Society of Mechanical Engineers, 345 East 47th St., New York City, NY 10017.
2. W. H. Cullen, et al., "Fatigue Crack Growth of A508 Steel in High-Temperature, Pressurized Reactor-Grade Water," NUREG/CR 0969, NRL Memorandum Report 4063, Naval Research Laboratory, Washington, DC 20375.
3. W. H. Cullen, et al., "Operation of a High-Temperature, Pressurized Water Fatigue Crack Growth Facility," Closed Loop, MTS Corporation, Minneapolis, MN, October 1980.
4. W. H. Cullen, et al., "A Computerized Data Acquisition System for a High-Temperature Pressurized Water Fatigue Test Facility," in Computer Automation of Materials Testing, ASTM STP 10, pp. 127-140, American Society for Testing and Materials, Philadelphia, PA 19103.
5. W. H. Cullen and K. Torronen, "A Review of Fatigue Crack Growth of Pressure Vessel and Piping Steels in High-Temperature, Pressurized, Reactor Grade Water," NUREG/CR-1576, NRL Memorandum Report 4298, Naval Research Laboratory, Washington, DC 20375.
6. R. P. Wei, S. R. Novak, D. P. Williams, "Some Important Consideration in the Development of Stress-Corrosion Cracking Test Methods," Proceedings 33rd AGARD Conference on Structures and Materials, Brussels, Belgium, 1971.
7. P. C. Paris, R. J. Bucci, E. T. Wessel, W. G. Clark and T. R. Mager, "An Extensive Study on Low Fatigue Crack Growth Rates in A533 and A508 Steels," in Stress Analysis and Growth of Cracks, ASTM STP 513, American Society for Testing and Materials, Philadelphia, PA, 1972, pp. 141-176.
8. W. H. Bamford, "Application of Corrosion Fatigue Crack Growth Rate Data to Integrity Analyses of Nuclear Reactor Vessels," Third ASME Congress on Pressure Vessels and Piping, San Francisco, CA, June 1979.
9. "Nuclear Power Plant Components: General Requirements," Section III of the ASME Boiler and Pressure Vessel Code, ANSI-BPV-III-1, issued annually, American Society of Mechanical Engineers, 345 East 47th St., New York City, NY 10017.

10. W. H. Bamford, W. H. Cullen, L. J. Ceschini, R. E. Taylor, and H. E. Watson, "Environmentally-Assisted Subcritical Crack Growth in LWR Materials," in Structural Integrity of Water Pressure Boundary Components, Annual Report, Fiscal Year 1980, NRL Memorandum Report, Naval Research Laboratory, Washington, DC 20375 (in publication).
11. D. A. Hale, et al., "Task K-Effect of BWR Environment" in Reactor Primary Coolant System Pipe Rupture Study Progress Reports GEAP-10207-32 through GEAP-10207-40, General Electric Co., Nuclear Systems Division, 175 Curtner Ave., San Jose, CA, 1974-1978.
12. D. A. Hale, J. Yuen and T. Gerber, "Fatigue Crack Growth in Piping and RPV Steels in Simulated BWR Water Environment," GEAP 24098, General Electric Co., Nuclear Systems Division, 175 Curtner Ave., San Jose, CA.
13. L. A. James, "Fatigue Crack Propagation in Neutron-Irradiated Ferritic Pressure Vessel Steels," Nuclear Safety, 18, pp. 791-801 (1977).
14. W. H. Cullen, H. E. Watson, V. Provenzano, "Results of Cyclic Crack Growth Rate Studies in Pressure Vessel and Piping Steels," in Structural Integrity of Water Reactor Pressure Boundary Components, Annual Report, Fiscal Year, 1979, F. J. Loss, (Ed), NUREG/CR-1128, NRL Memorandum Report 4122, Naval Research Laboratory, Washington, DC 20375.
15. W. H. Bamford, D. M. Moon and L. J. Ceschini, "Cyclic Crack Growth Rate Studies Conducted by Westinghouse Nuclear Energy Systems Under NRL Contract," in Structural Integrity of Water Reactor Pressure Boundary Components, Quarterly Progress Report, October-December, 1979, NUREG/CR-1240, NRL Memorandum Report 4124, Naval Research Laboratory, Washington, DC 20375.

FIGURE CAPTIONS

Fig. 1. Fatigue crack growth rate data vs applied cyclic stress-intensity factor for all the tests with a very short (1 sec) rise time. In this and the following figures, the lower temperature test results are on the left. Both these temperatures yield growth rates close to the ASME Section XI air default line.

Fig. 2. Fatigue crack growth rate data vs applied cyclic stress-intensity factor for all tests with both significant ramp times and hold times (1 min or greater for each). In the left-hand data sets, the effect of the increase in crack growth rates due to the lower temperature is clearly seen.

Fig. 3. Fatigue crack growth rate data vs applied cyclic stress-intensity factor for tests with a one minute ramp, but no hold time. As in Fig. 2, the lower temperature tests resulted in the higher fatigue crack growth rates.

Fig. 4. Fatigue crack growth rate data vs applied cyclic stress intensity for tests with a 22 second ramp and no hold time. The results are very similar to those shown in Fig. 3.

Fig. 5. Fatigue crack growth rate data vs applied cyclic stress-intensity factor for a test with a 17 mHz sinusoidal waveform. Also shown are the results of two tests with a 22 second ramp, 4 second hold time, which is the trapezoidal equivalent of the positive slope of a sinusoidal waveform.

Fig. 6. Illustration of the three-region behavior of fatigue crack growth rates in the reactor-typical environments (a) the trend lines for 1 Hz and 17 mHz data in 288°C reactor-grade water, and for baseline, air environment data (b) actual fatigue crack growth data superposed on the trend lines of (a).

Fig. 7. A summary plot of the available data for fatigue crack growth rate tests in high-temperature, pressurized, reactor-grade water, for both high (0.7) and low (0.1-0.2) load ratios. The 1980 versions of the ASME air and water default lines are also shown.

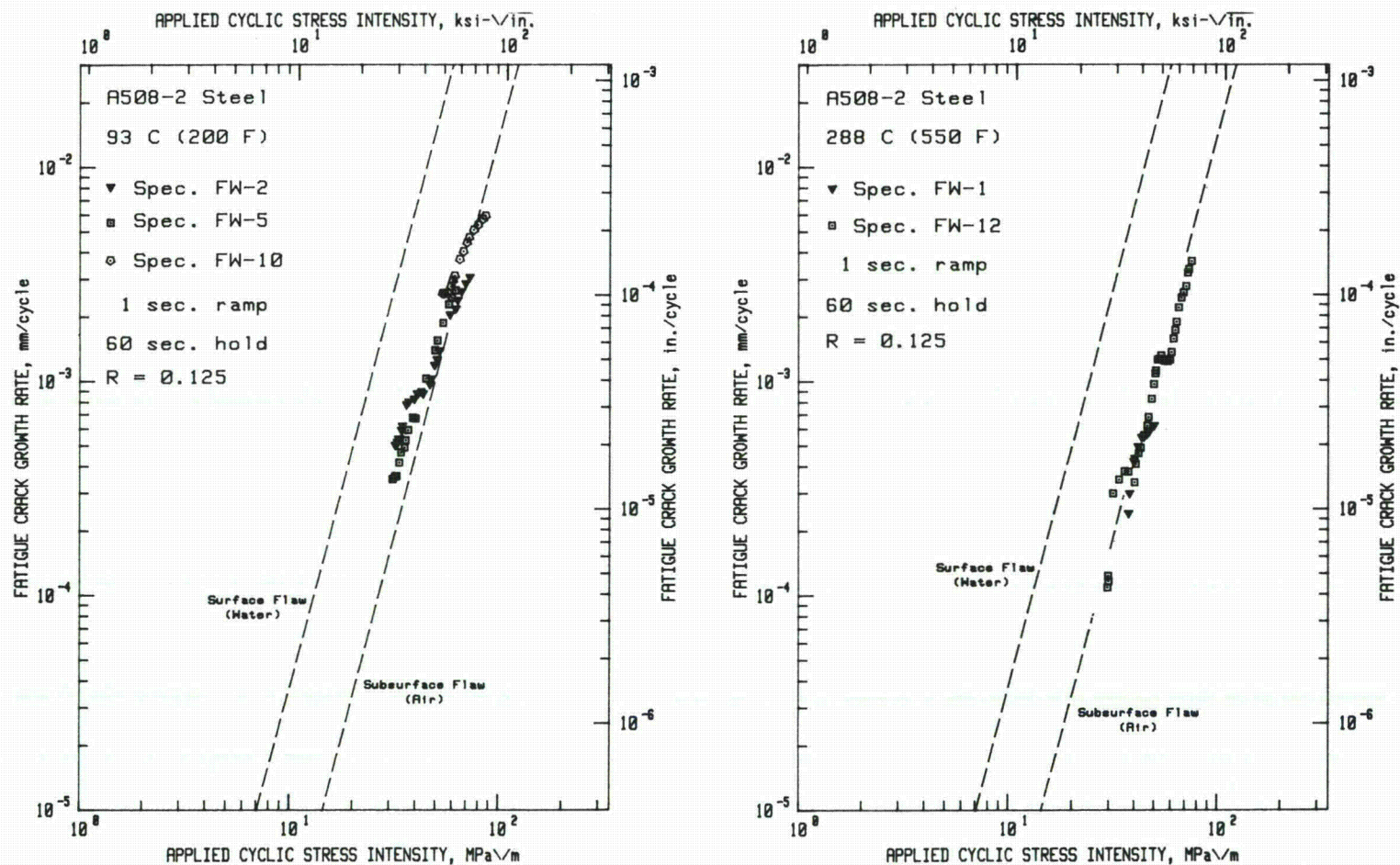


Fig. 1. Fatigue crack growth rate data vs applied cyclic stress-intensity factor for all the tests with a very short (1 sec) rise time. In this and the following figures, the lower temperature test results are on the left. Both these temperatures yield growth rates close to the ASME Section XI air default line.

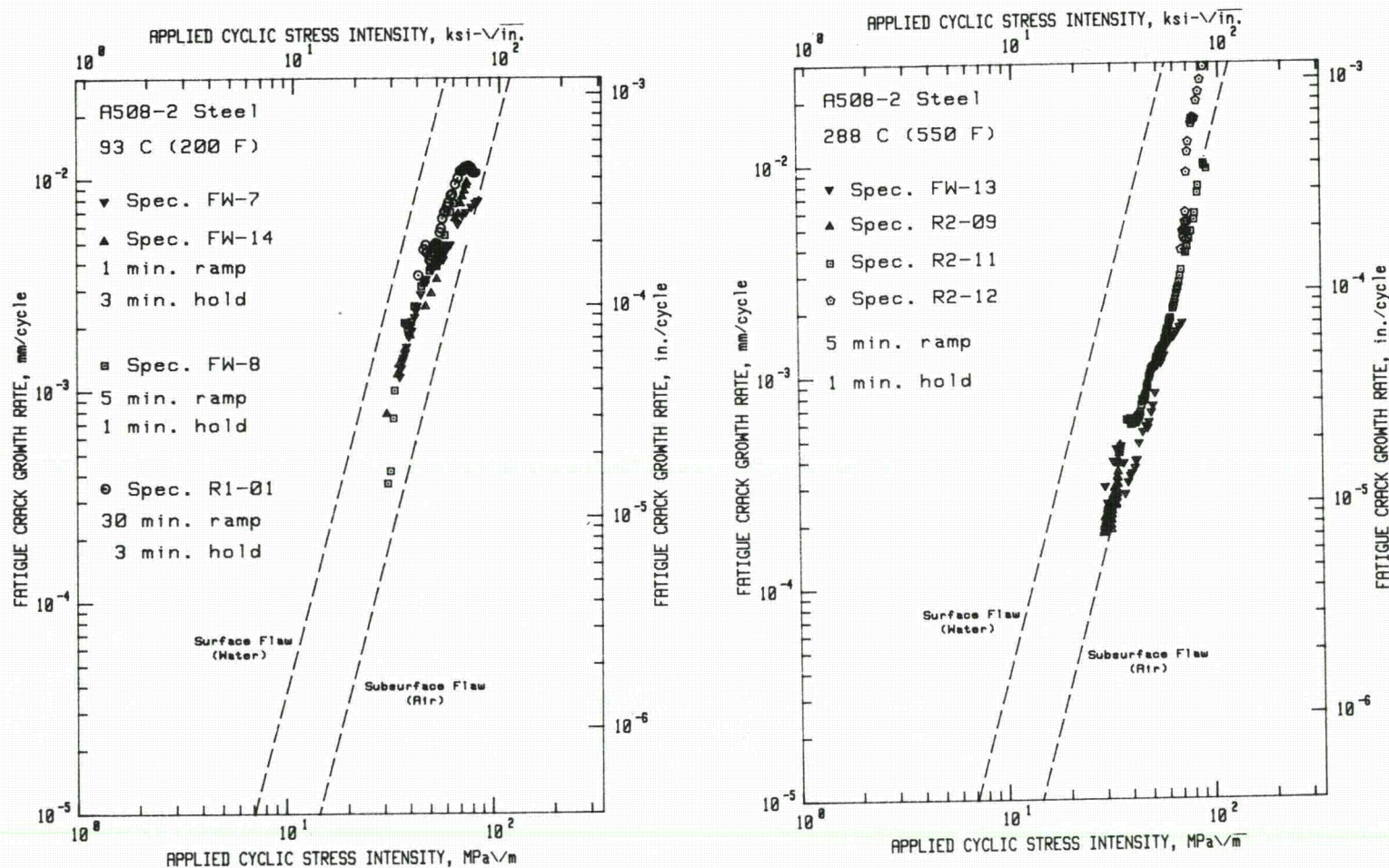


Fig. 2. Fatigue crack growth rate data vs applied cyclic stress-intensity factor for all tests with both significant ramp times and hold times (1 min or greater for each). In the left-hand data sets, the effect of the increase in crack growth rates due to the lower temperature is clearly seen.

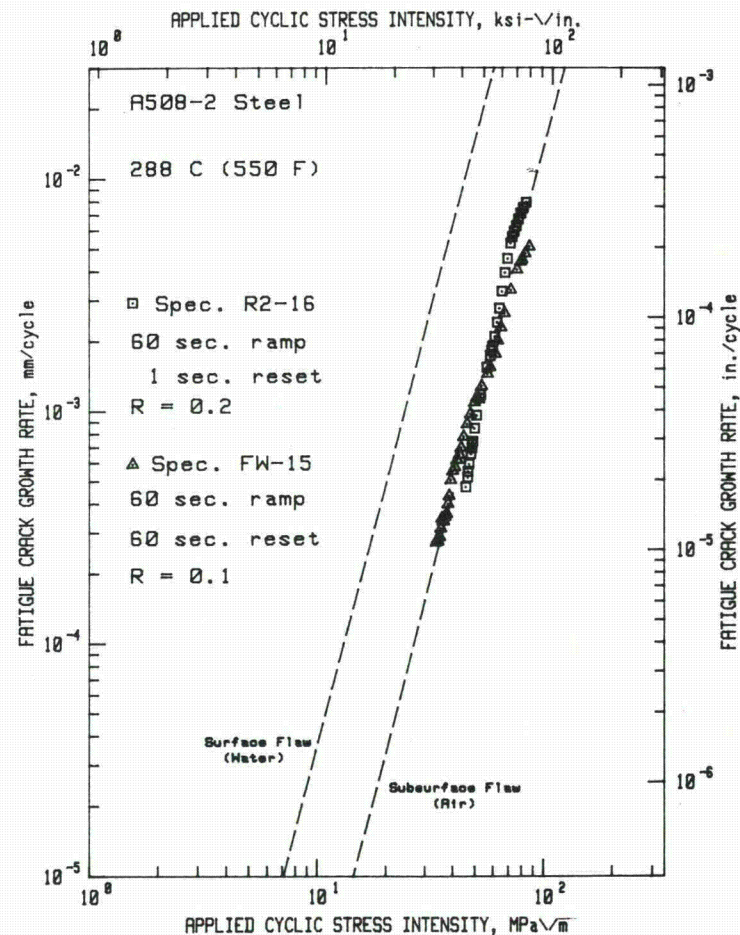
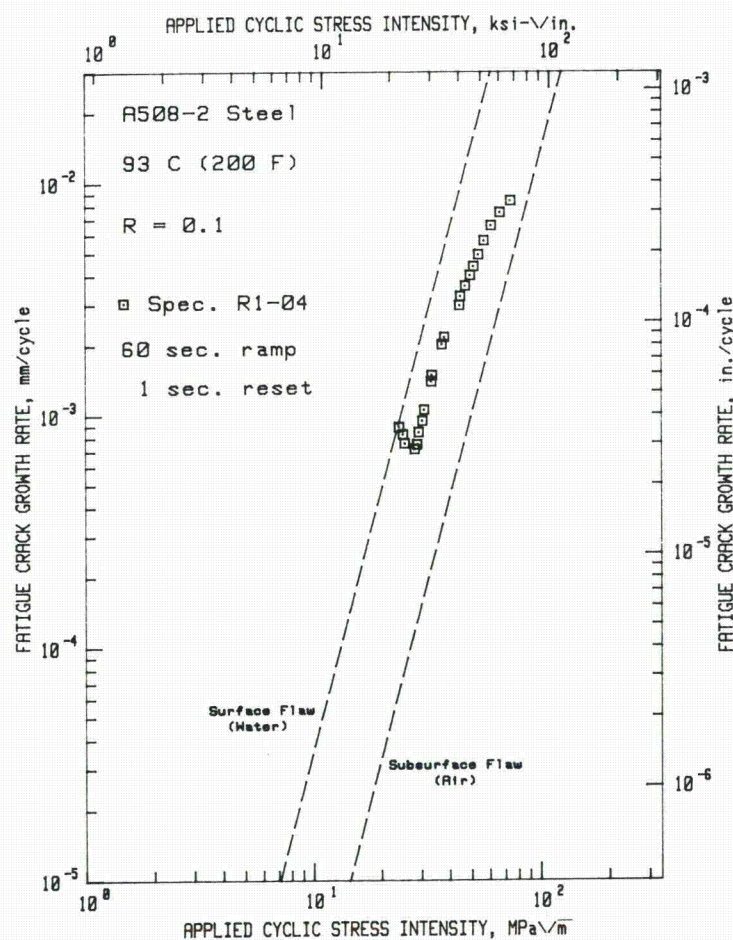


Fig. 3. Fatigue crack growth rate data vs applied cyclic stress-intensity factor for tests with a one minute ramp, but no hold time. As in Fig. 2, the lower temperature tests resulted in the higher fatigue crack growth rates.

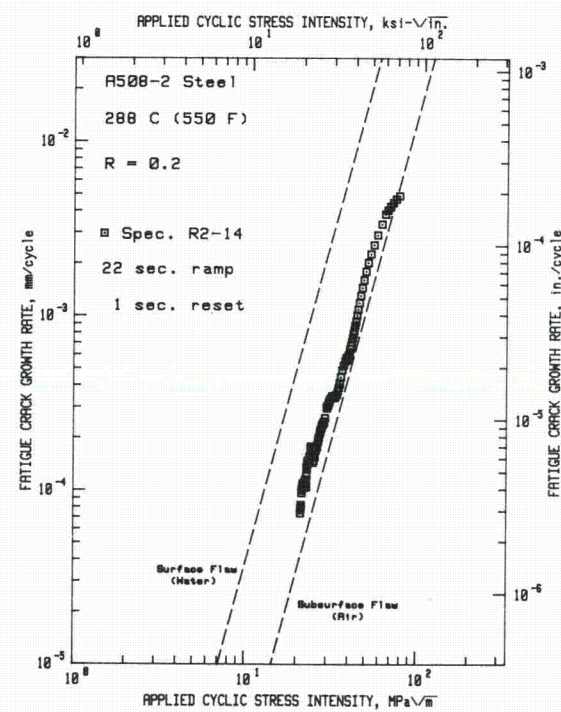
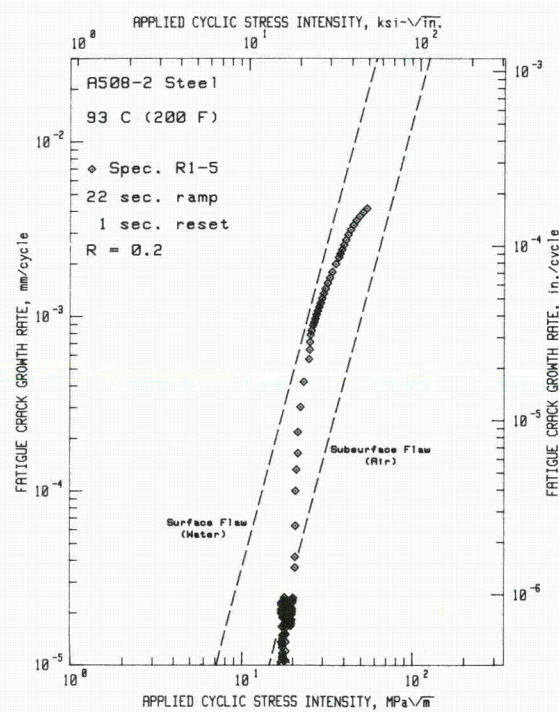


Fig. 4. Fatigue crack growth rate data vs applied cyclic stress intensity for tests with a 22 second ramp and no hold time. The results are very similar to those shown in Fig. 3.

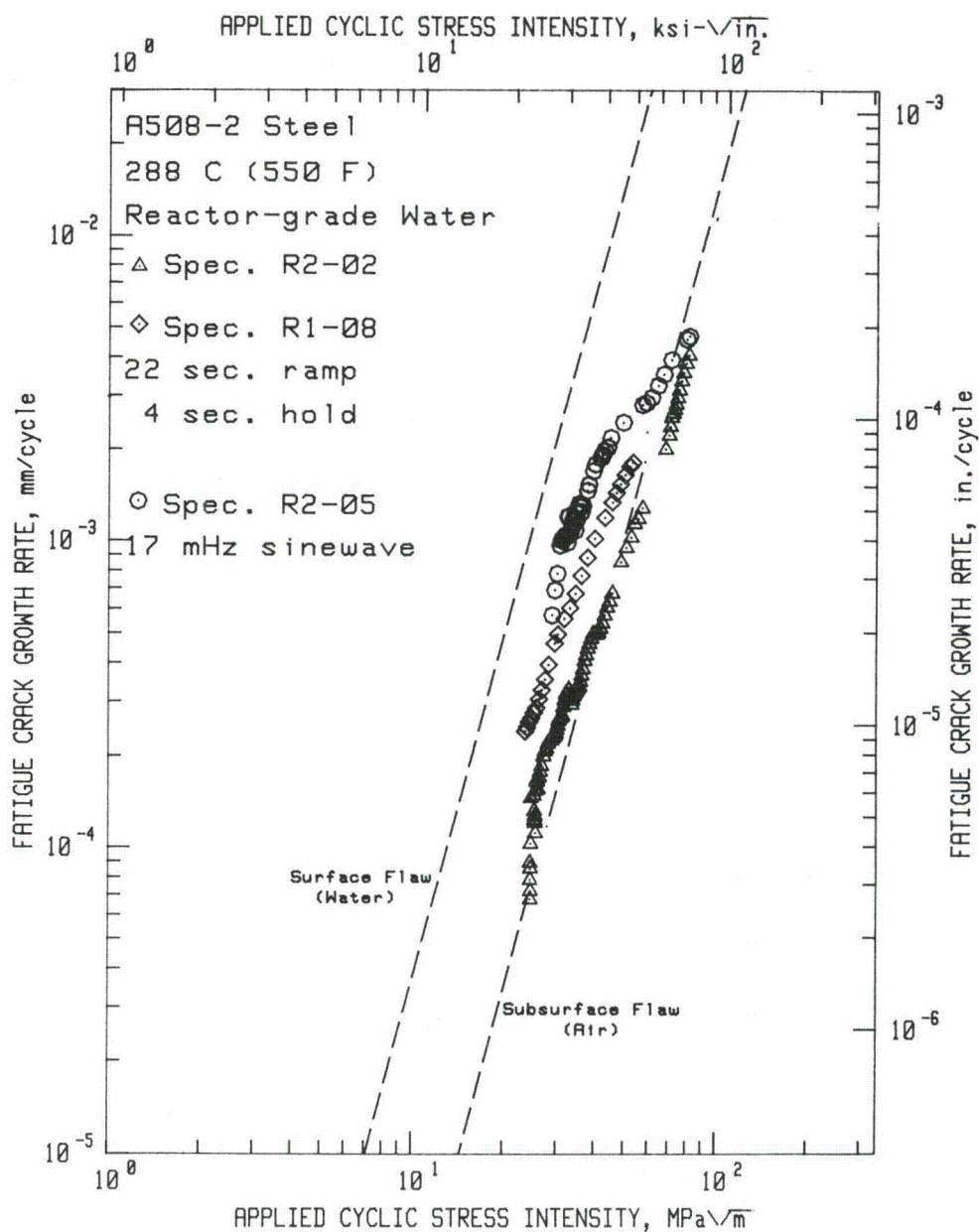


Fig. 5. Fatigue crack growth rate data vs applied cyclic stress-intensity factor for a test with a 17 mHz sinusoidal waveform. Also shown are the results of two tests with a 22 second ramp, 4 second hold time, which is the trapezoidal equivalent of the positive slope of a sinusoidal waveform.

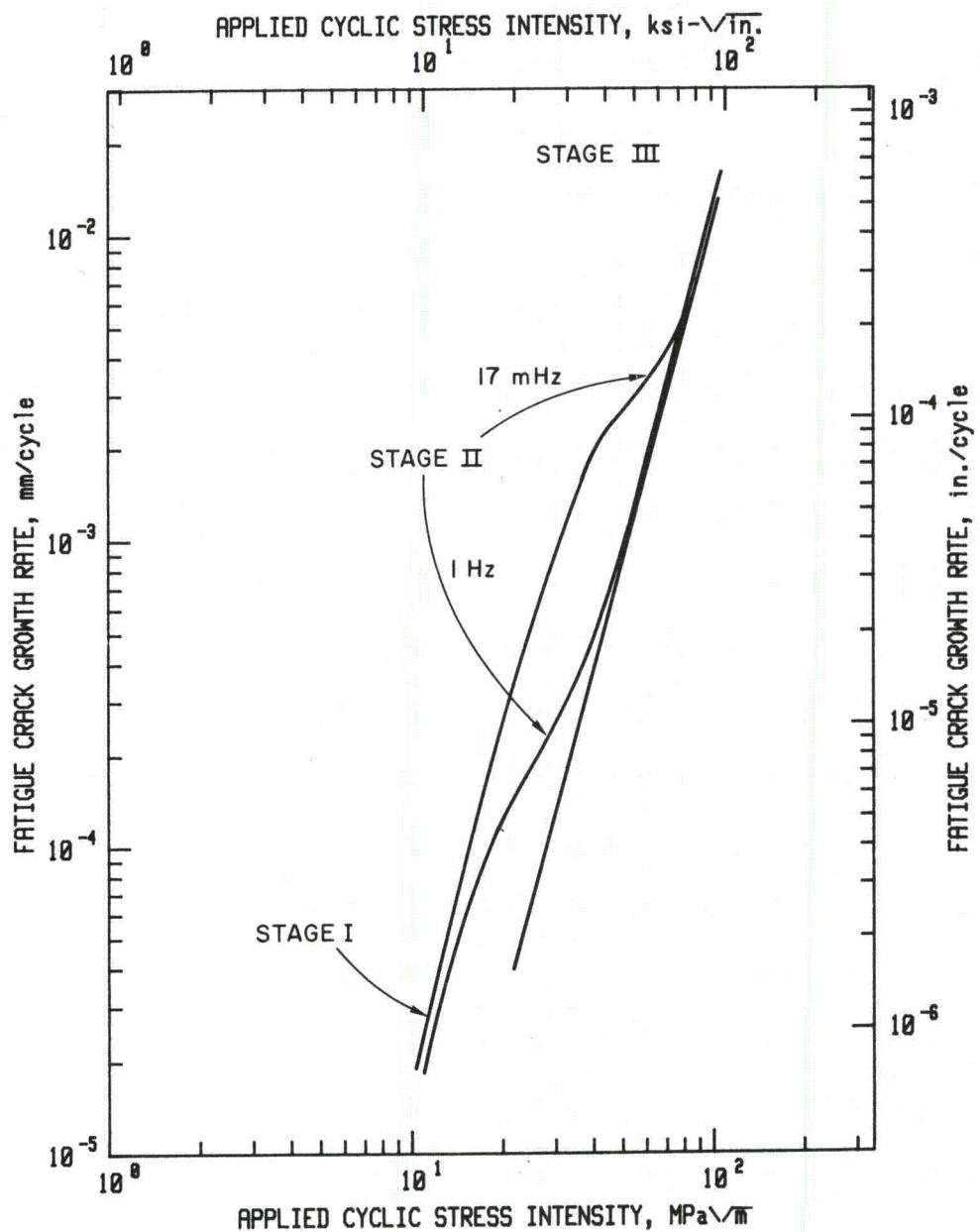


Fig. 6. Illustration of the three-region behavior of fatigue crack growth rates in the reactor-typical environments (a) the trend lines for 1 Hz and 17 mHz data in 288°C reactor-grade water, and for baseline, air environment data (b) actual fatigue crack growth data superposed on the trend lines of (a).

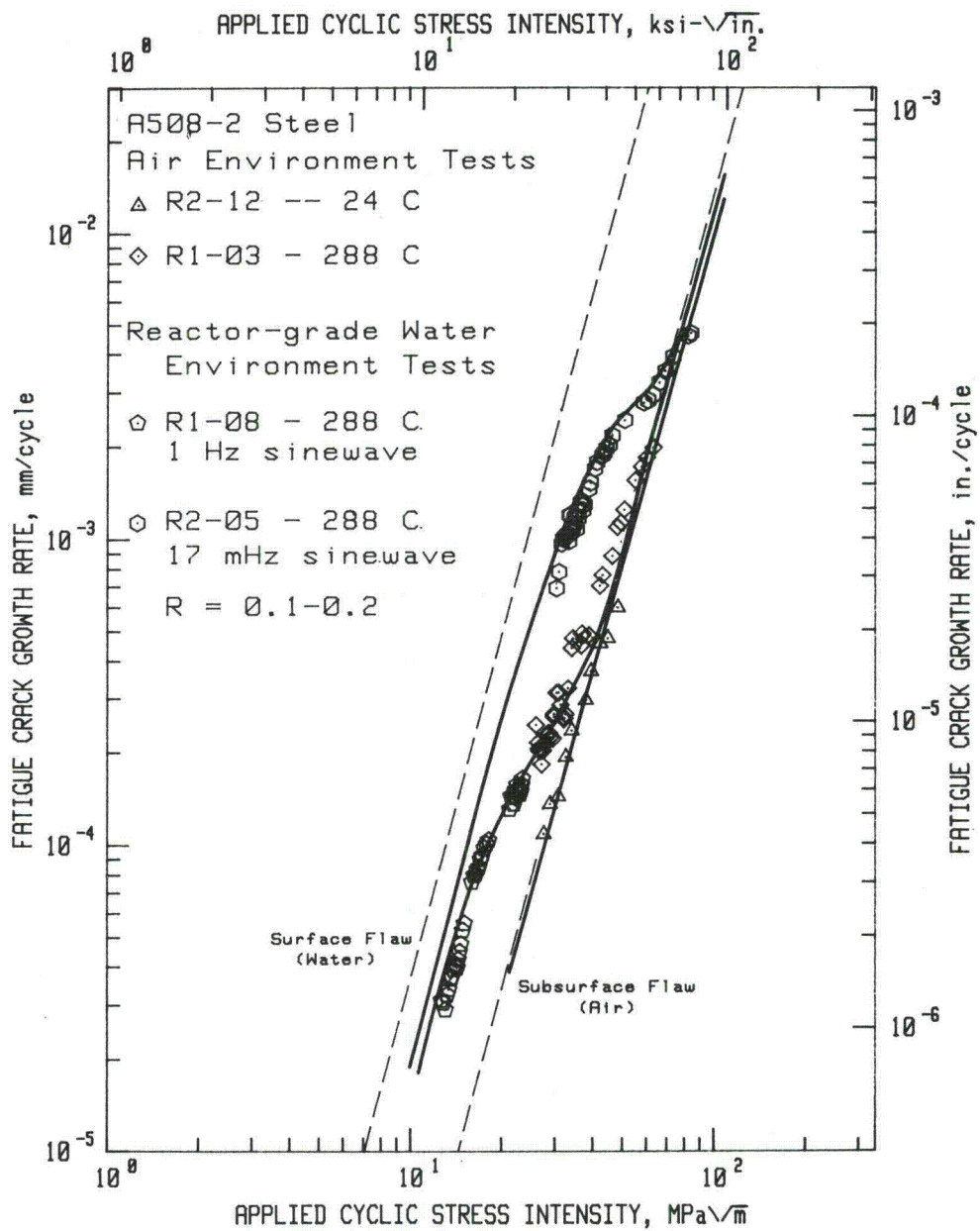


Fig. 6b

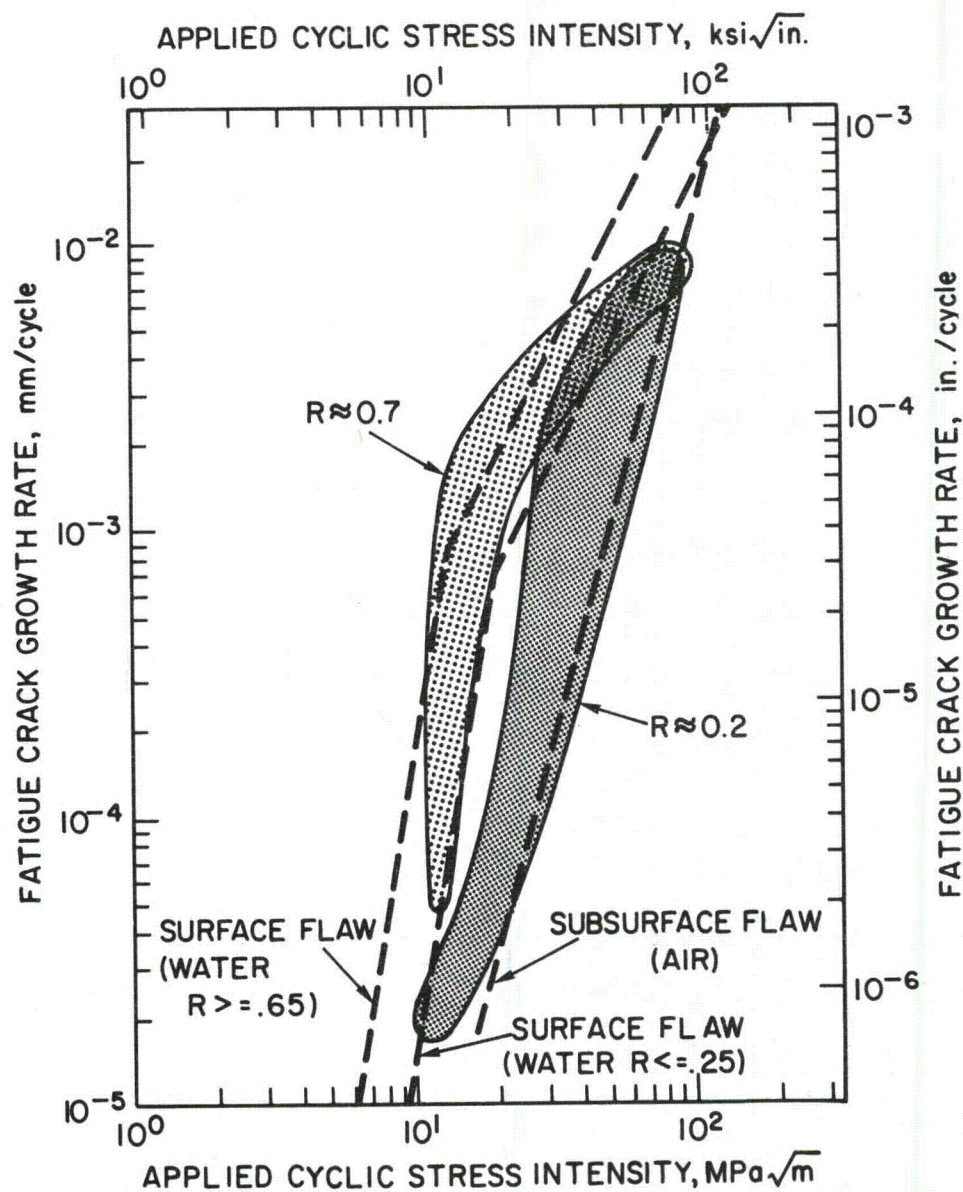


Fig. 7. A summary plot of the available data for fatigue crack growth rate tests in high-temperature, pressurized, reactor-grade water, for both high (0.7) and low (0.1-0.2) load ratios. The 1980 versions of the ASME air and water default lines are also shown.

Experience with an autoclave-refreshing system for crack growth measurements under PWR- and BWR-environmental conditions.

A. Gerscha, E. Klausnitzer and N. Wieling

Approximately 20 years ago KWU began investigating the materials behaviour under medium conditions. First experiments were carried out in static autoclaves and PWR-conditions. At that time those experiments mainly included Zr-alloys, low alloy steels and high alloy CrNi-steels.

4 years ago the first investigations under BWR-conditions were planned, for which a refreshing system had to be constructed that would allow adjusting the proper water chemistry.

After long time experience with static autoclaves KWU started with cyclic investigations under PWR-conditions in a small autoclave (Fig. 1), having a volume of 1,5 l. Inside this autoclave primarily force-controlled fatigue experiments in the tension range were carried out on high alloy CrNi-steels and Inconel.

This autoclave was equipped with a device that permitted measurement of force also inside the autoclave itself. For detecting crack initiation a LVDT (Linear Variable Differential Transducer) was mounted outside the autoclave.

Having completed this work the inner structure of the autoclave was changed in such a way that crack growth experiments on CT 25 specimens could be carried out. The internal force measuring device, however, had to be abandoned for lack of space. This did not create any problem because the fatigue experiments had shown that friction forces inside the bearing are smaller than 1 % and nearly time independent.

For calculating the crack length via compliance the external length measuring device was available, the application of which proved somewhat problematic because changes of temperature of the autoclave and/or the loading piston would cause changes in

length, unless precautions have been taken. To avoid these problems right from the beginning, a length measuring device on strain-gage basis was designed and built that was attached directly to the sample, similar to a clip-gage. This length measuring device proved useful in several tests each running a couple of month.

Since our own crack growth experiments and experiments of other institutions have shown that, among other factors, the oxygen content will affect crack growth rate and since defects with BWR-plants were submitted for investigation, a refreshing system serving several cyclicly operated autoclaves was built, taking into account the experience gained with operation of the static autoclaves.

In the present design the refreshing system can provide three autoclaves with the same water chemistry. Extension of the system is possible, if necessary.

A flow chart of the system is shown in Fig. 2. Firstly the demineralized water is degassed at 90 °C with N₂ then cooled down again to 20 °C. Past the storage tank, additives, if necessary, are put in and fed into the feed water tank. From there the feed-water enters the externally heated autoclave via a high pressure pump variable in a wide range (5 to 60 liters/hour) and a pre-heating section. The water leaving the autoclave is cooled back and drained.

O₂-concentration is checked continuously, that is by a membrane electrode according to the Clark-methode-(Make WTW, range of measurement 0 - 5 and 0 - 15 ppm).

As mentioned at the beginning, operational experience with a cyclicly operated small autoclave has been gained since approximately 1975. This served as basis for design and construction of a 75 liter autoclave making possible to carry out crack growth experiments even with large samples up to CT 75 respectively WOL-100X in the range of higher K-values.

For designing the autoclave the following conditions were fixed:

Maximum temperature of operation	300 °C
Maximum pressure of operation	160 bar
Capacity	75 liters
Material	13 CrMo 44 (A182-61T)

On the basis of those conditions the shop drawing as well as the calculations for the design had to be approved by the TÜV.

Also during the pressure test the responsible TÜV was present and after successful completion he gave the permission for operation.

The design should be such that several small specimens (CT 50) could be placed in series or that one center-cracked panel could be installed. By using an electron beam welded compound specimen the latter specimen type makes possible (Fig. 3) the simultaneous testing of several cracks located in different materials or material ranges.

A schematic drawing of the autoclave is given in Fig. 4. With this design the cover, usually located on top, is at the bottom, having the advantage of simplifying the operations of putting in and taking out the sample or inspection of the sample(s), since to do this only a simple lift of the shell is necessary. Furthermore, opening or closing the autoclave can be done in normal working position. Besides this there is the advantage that the measuring leads (temperature, load and length) leaving the cover are moved as little as possible.

If the autoclave is not operated together with the refreshing system, the feedwater tank for filling the autoclave has to be placed beside the machine and a separate pump has to be used for pumping the water into the autoclave.

As to be seen also, the autoclave has two ports having the advantage that it can be placed on the machine base for accurate mechanical alignment and that it will not move upon loading the sample as it happens with autoclaves having one port only.

As an example Fig. 4 shows two mounted CT - 50 specimens, to be provided with a displacement measurement device as shown in Fig. 5. It is screwed tightly with both legs to the front face. On a smaller scale this design proved most satisfactorily within the 1,5 liter autoclave during a period of approx. 2 years. As to the temperature field inside the autoclave it should be mentioned that a gradient exists in the lower part. In the part containing the samples, however, temperature differences are small as shown in Fig. 6. Extension of the isothermal zone is not planned, since this range accomodates the force measuring device (Fig. 4) which is insensitive to temperature.

For closing the autoclave the same principles as with RPV-screws have been applied, i.e. the screws are strained elastically by a hydraulic straining apparatus at 4 positions simultaneously and then the nuts are turned on. For sealing the cover a comb profile seal ring with flange tightenings on both sides is used, allowing to close the cover several times (3 - 5) and it is exchangeable without any problems. For the piston-rod-ports water cooled teflon-graphite seals are used which, being adjustable, allow operation for several years without need for exchange.

Fig. 7 shows the autoclave mounted into a ± 900 kN servo hydraulic testing machine. For reasons of space and access a double spindle machine with hydraulic gripping device in the cross head is used for the mechanically adjustable cross head. It can be operated statically and dynamically using 40 to 160 liters oil/min supplied by 1 - 4 hydraulic high pressure pumps. The piston is guided by a hydrostatic bearing which can support side forces as well.

The autoclave is closed, but it can be lifted upwards by a lifting device integrated into the testing machine. The refreshing system can not be seen, since it has been placed underneath the machine. Righth behind the machine there is the preheating section for having the pipes as short as possible and so to minimize heat losses of the feedwater.

At first the servohydraulic system was tested during a period of 5 months with a sample at 280 °C in air under the same conditions and the same instrumentation as later on inside the autoclave.

No problems showed up, so the autoclave was installed, the next sample was mounted and the experiment under medium conditions was started. After a couple of days (weekend) of operation it was noticed that the O₂-content of the water in the feedwater tank was too high, 0,5 instead of 0,01 ppm. This caused an increase of the crack growth rate by a factor of ten. The defect was a leaking screw which was repaired.

Since one month the system operates without any problems and it is not to be expected that further serious problems will show up, since the "trouble spots" (seals, force and length measurement, refreshing system) operate satisfactorily since years.

Fig.1: Versuchsautoklav eingebaut in einen 200 kN-Pulsator
1,5 Liter Autoclave mounted in a 200 kN-Pulsator

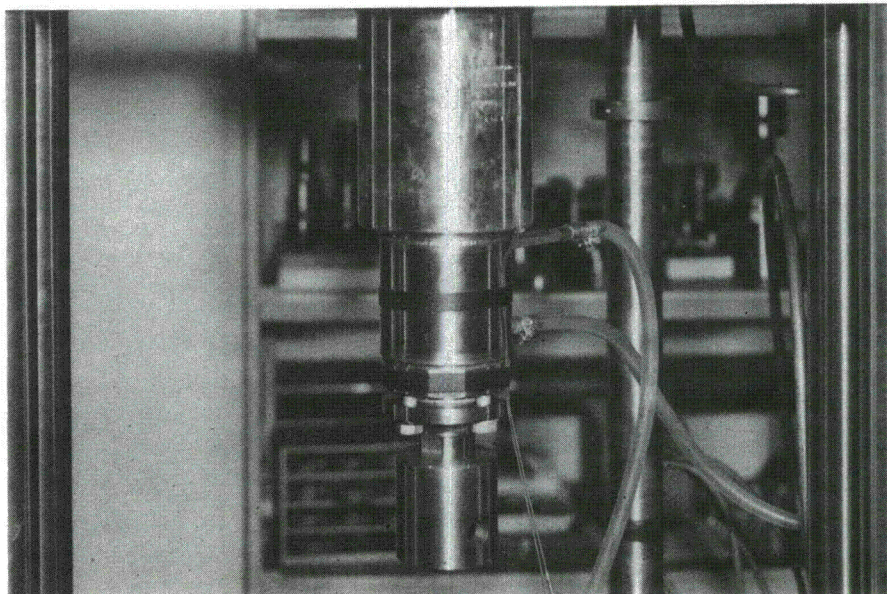
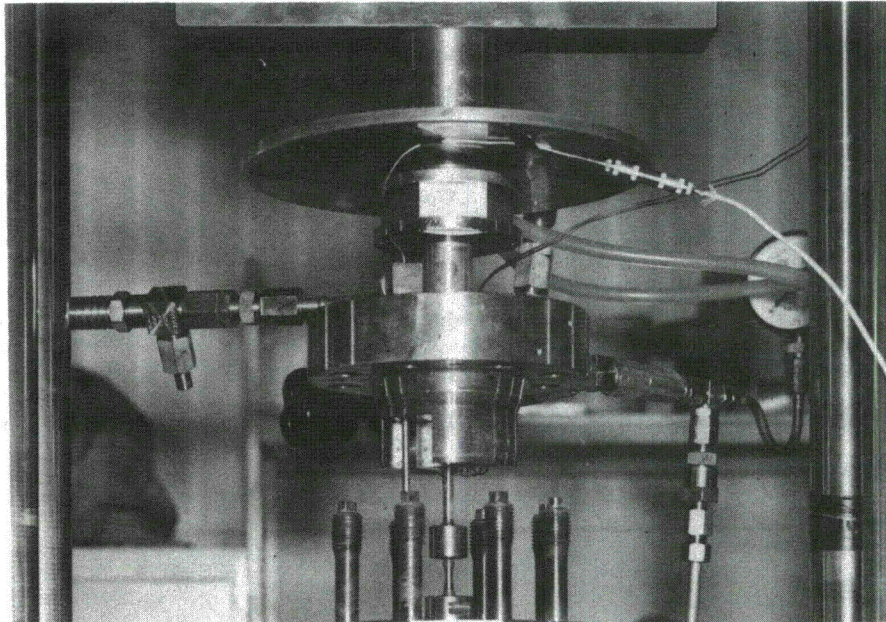
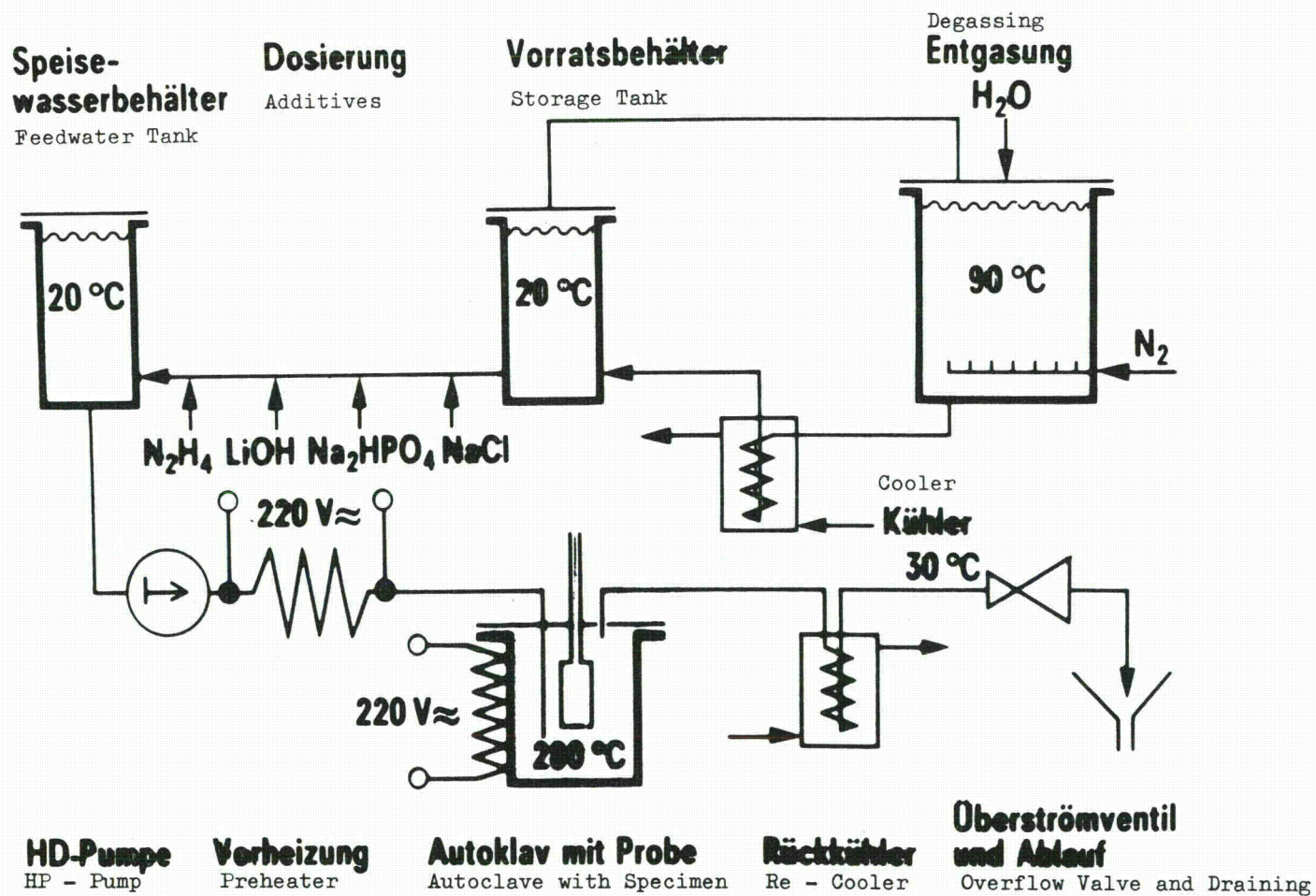


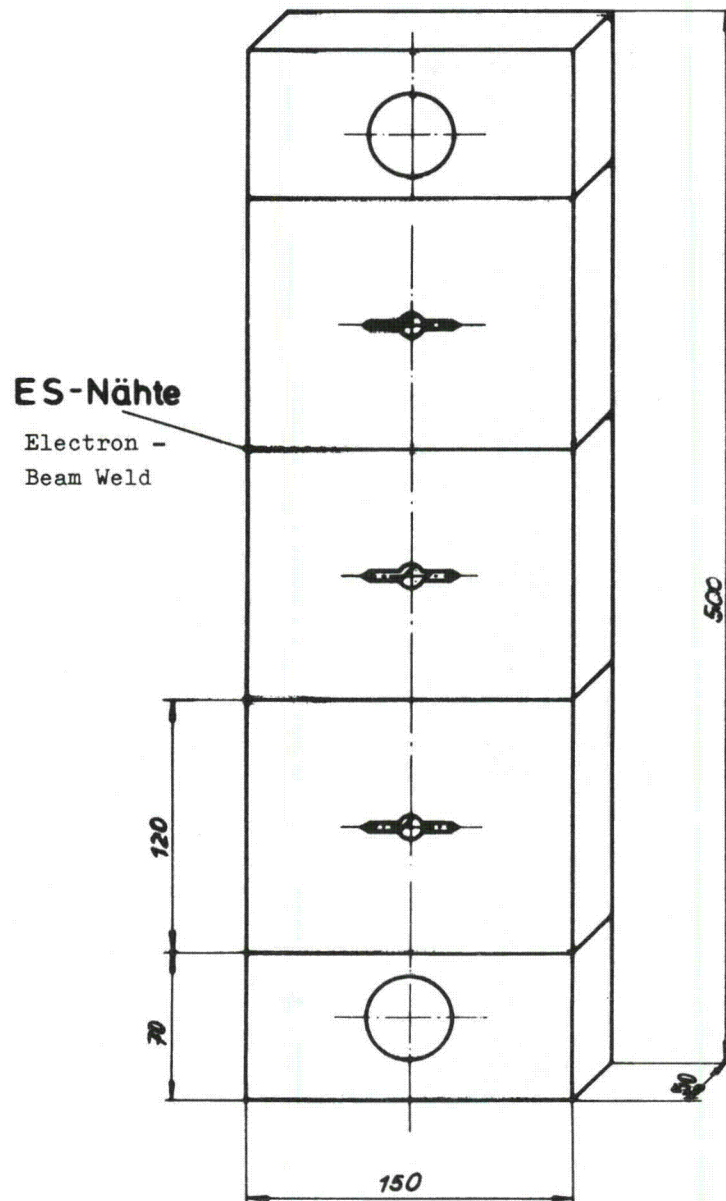
Fig.2 Refreshing - Autoklavenanlage (Flußschema)
Autoclave with Refreshing System (Flow Diagram)



Mehrfach-Verbundprobe für Rißwachstumsversuche

Fig.3

Multi - Compound - Specimen for Crack Growth Tests



Schematische Darstellung des 75 Liter Autoklaven
Schematic Diagram of 75 Liter Autoclave



Fig.5 Dehnmeßsystem montiert auf eine CT - 25 - Probe
Strain gage system mounted on a CT - 25 - specimen

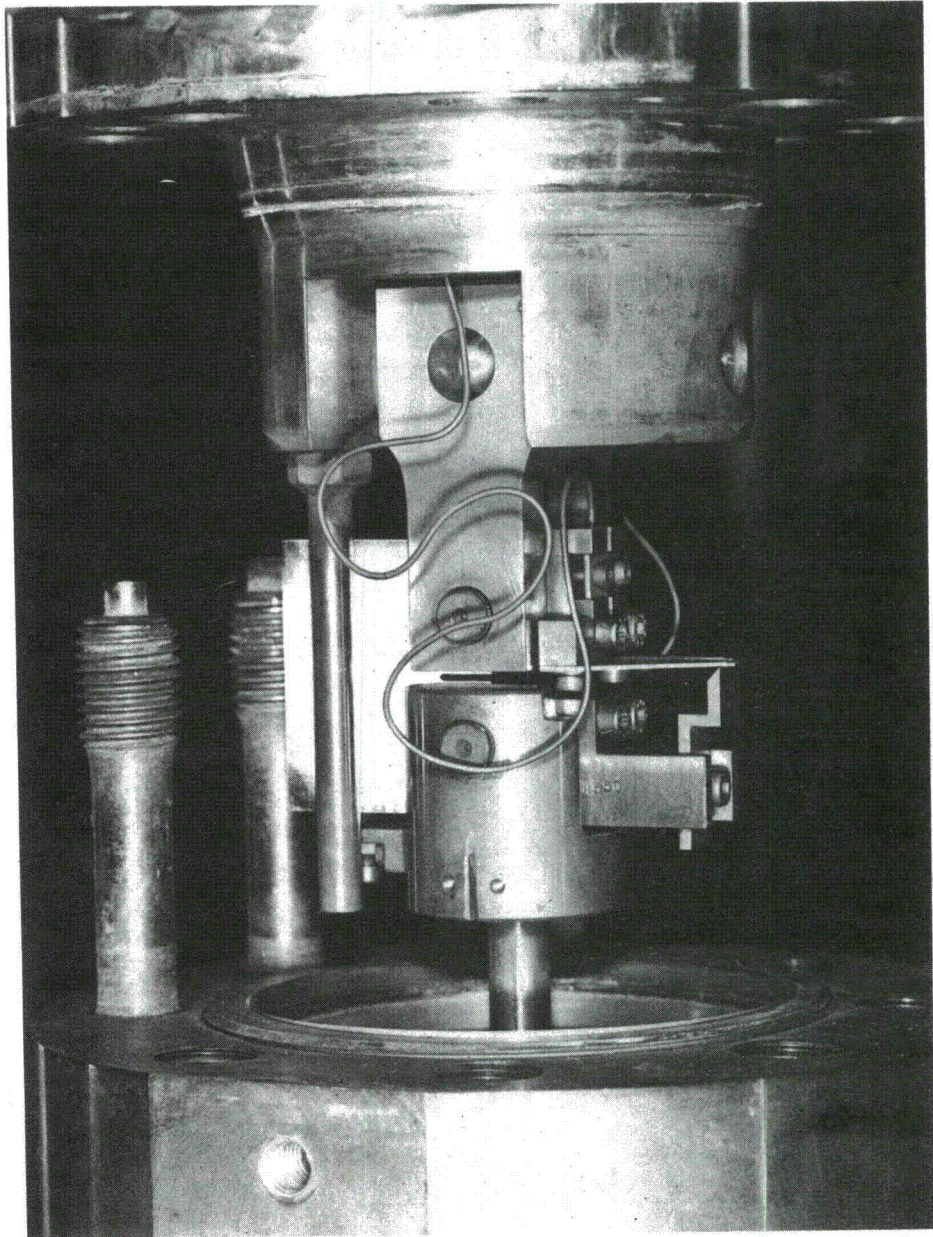
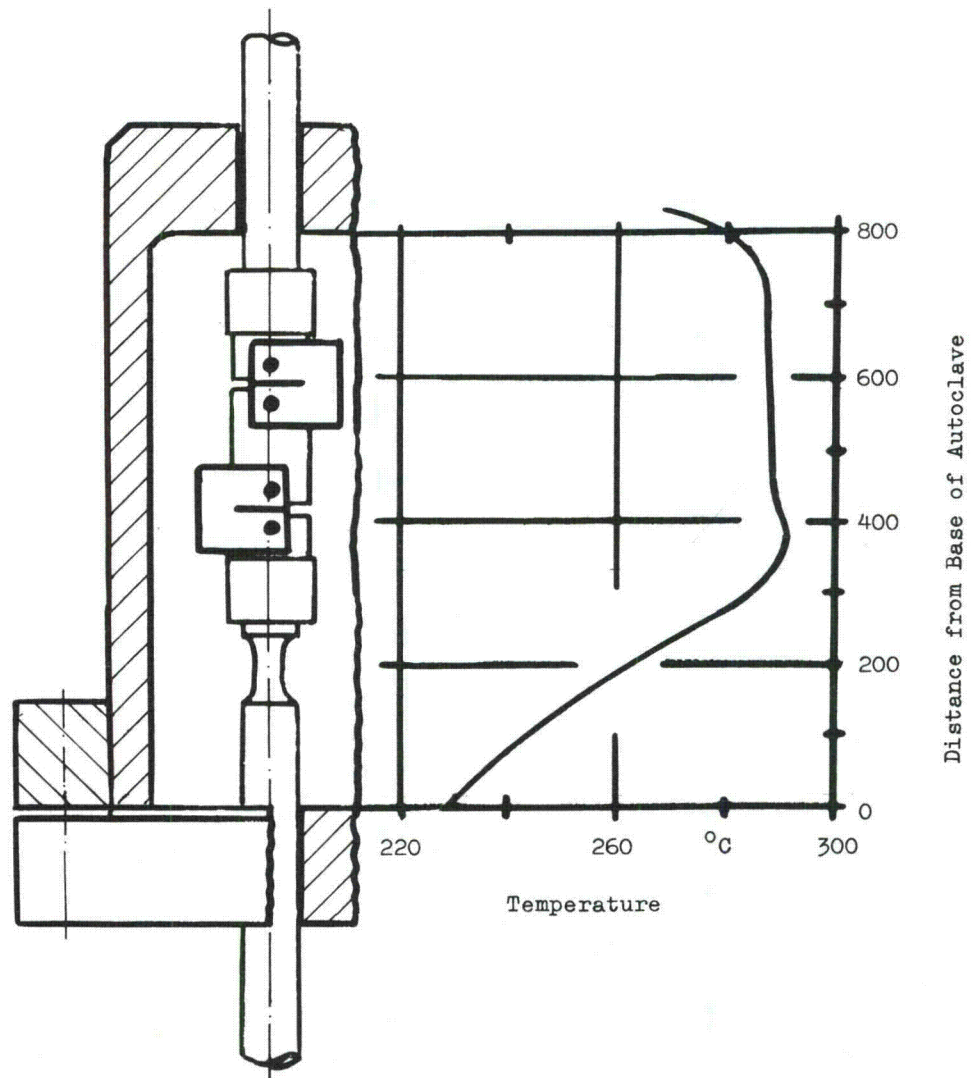


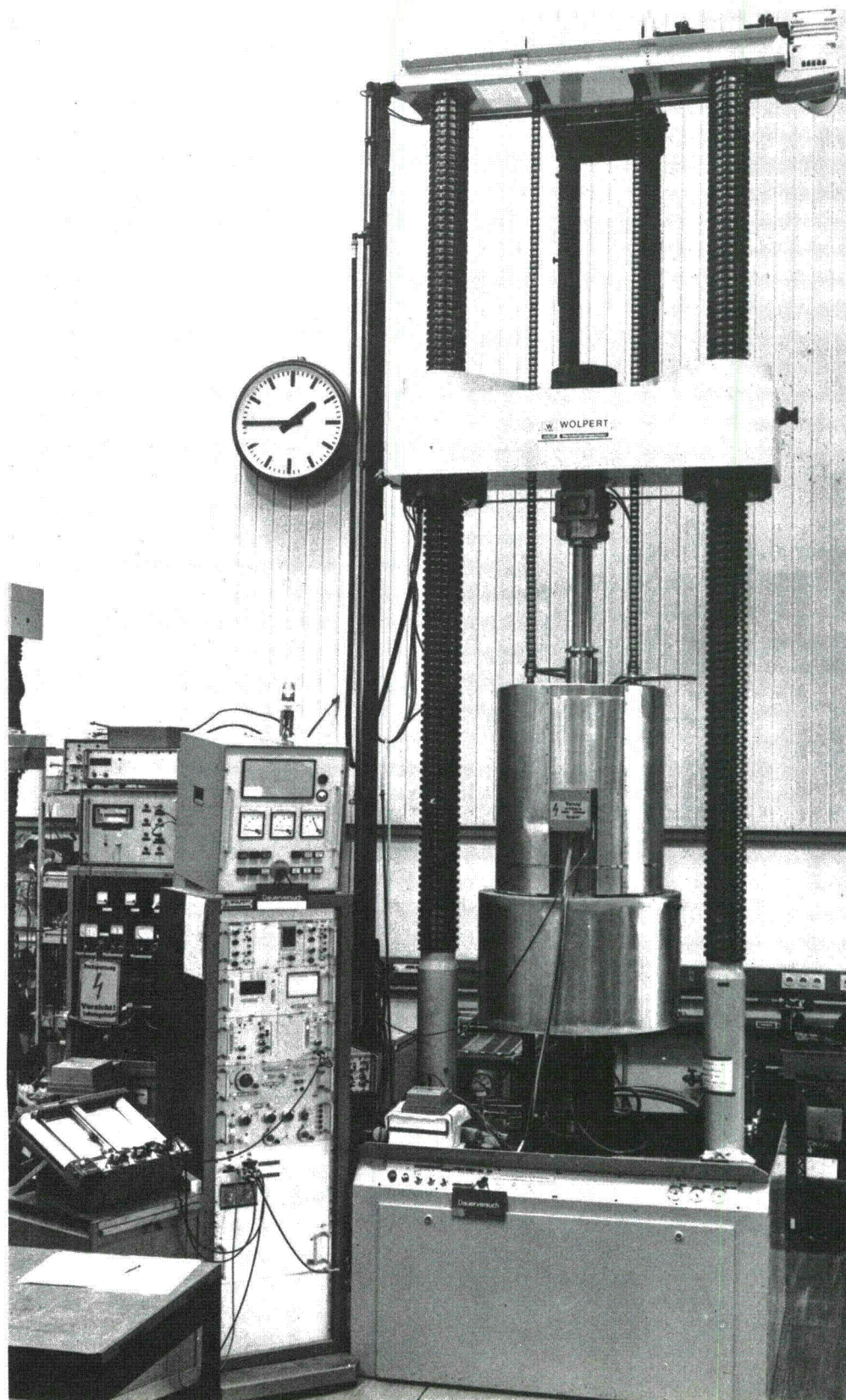
Fig.6 Temperaturgradient in einem 75 Liter Autoklaven
 Temperaturegradient in a 75 Liter Autoclave



Gesamtansicht des 75 Liter Autoklaven eingebaut in eine
900 kN Servo-Hydraulik

Fig.7

General view of 75 Liter Autoclave mounted in a 900 kN
servo-hydraulic



CRACK GROWTH RESISTANCE OF LOW ALLOY STEEL
IN HIGH TEMPERATURE OXYGENATED WATER

DA Hale, CH Lange, and JN Kass

Crack growth rates for Low Alloy Steel in high temperature, high purity oxygenated water were studied under cyclic loading conditions. Both fracture mechanics and simulated reactor pressure vessel nozzle test specimens were utilized. Cycle frequency, mean stress, and coolant oxygen content were studied. The role of crack face oxidation in mitigating crack growth rates was identified. The overall data band is similar to that reported in the literature for Pressurized Water Reactor conditions. The overall impact of the study is that disposition of indications potentially found by future in-service inspections can be made with improved confidence since the resistance to crack extension is quite high.

INTRODUCTION

Types A533 and A508 low alloy steel are used in pressure vessel applications. The ASME Boiler and Pressure Vessel Code Section III is the primary tool for design by analysis of this and other pressure retaining components. The present design philosophy is one of preventing crack initiation by use of special rules that account for geometric discontinuities and are focused towards precluding overload fracture and low cycle fatigue cracking. The excellent service history which these components have achieved to date is testimony to the success of this design procedure.

Several years ago the ASME Code added the concept that an analysis method is needed to provide disposition of potential flaws or indications found by in-service inspection. This approach is based upon linear elastic fracture mechanics techniques and the specific method of analysis is contained in Section XI of the Code. One of the key elements in this approach is accounting for potential crack extension due to fatigue loading. Laboratory studies conducted by Mager¹, Kondo², Gerber³, and Hale⁴ were used to define the fatigue crack growth response.

In Reference 1, crack growth behavior in Pressurized Water Reactor (PWR) coolant was studied with efforts focused on assessment of moderate loading, some mean stress effects, and an initial assessment of loading waveshape effects.

References 2, 3, and 4 consisted of studies in high temperature, high purity, oxygenated water environments. The influence of the same parameters studied in Reference 1 was assessed. These studies, along

with some work conducted at the U.S. Naval Research Laboratory by W. Cullen were used to define a "Design Curve" for fatigue crack growth in Appendix A of Section XI of the Code.

This Design Curve was represented by a Paris Law expression:

$$\frac{da}{dn} = A\Delta K^B$$

where $\frac{da}{dn}$ = crack growth rate

ΔK = cyclic stress intensity

A and B = constants

Following this initial effort, laboratory studies focused on the roles of waveshape, cycle frequency, mean stress, and high stress intensity values (Bamford⁵, Hale⁶, Cullen⁷). The principal results of these studies were that more rapid crack growth rates were found at slow frequencies and high mean stresses. Moreover, the single sloped Paris Law was found to greatly overpredict crack growth rates at high values of K_I . In Reference 7, a fractographic study was performed on specimens tested in PWR coolant and hydrogen embrittlement was postulated as the major cracking mechanism.

Other significant parameters were identified as being important to allow definition of crack growth behavior in high temperature, high purity, oxygenated water coolants. These included an assessment of coolant oxygen effects and further study of the observed tendency for decrease

in crack growth rates due to apparent blunting or blockage of the crack tip by formation of corrosion product. This effect was first noted by Kondo² and later by Hale⁶. Moreover, it was deemed important to assess the effect of very slow cycle frequency and define a means to account for mean stress effects. Finally, a comparison of weld metal to base metal behavior was needed.

The data summarized in this report represent results of an extensive program to address the items listed above.

TEST DESCRIPTION

Test Facilities

The high pressure/temperature water environment used for this program was provided by a high flow test loop (Environmental Fatigue Loop 1) in General Electric's Experimental Mechanics Laboratory (San Jose, California). A schematic drawing of this loop is shown in Figure 1.

The loop includes a canned rotor pump which provides sufficient flow (~12 gallon/minute) to ensure that all specimens tested in the loop are subjected to a highly refreshed environment. Bypass demineralizer beds are provided to maintain the conductivity and pH of the demineralized water environment (Table 1). The levels of dissolved oxygen, conductivity, and pH of the loop water are continuously monitored. Dissolved oxygen level is controlled by a gas control system that continuously purges a gas mixture through the makeup tank at a rate needed to establish the desired dissolved oxygen level in the makeup water which is being continuously added to the loop. The oxygen concentration is controlled by constantly purging the makeup water supply with varying amounts of nitrogen gas and air. As less air and more nitrogen is bubbled through the water, the ratio of dissolved nitrogen to dissolved oxygen increases, thus reducing the dissolved oxygen concentration. By using no air at all in the process, the oxygen concentration can be reduced to essentially zero.

Specimen loading was accomplished using a closed loop, electrohydraulic test machine that applies a cyclic load to a group of up to six specimens arranged in a series chain inside a pressure vessel. A computer is available for use with this facility to acquire and analyze the data. A schematic drawing of this system is shown in Figure 2.

Test Specimen/Techniques

Both Wedge Open Loading (WOL) and Compact Tension (CT) crack growth test specimens were used for these tests. Both are standard fracture mechanics specimen geometries. They are shown in Figure 3. Although the WOL and CT specimens are very similar, the CT is shorter and has a more rapid increase in applied stress intensity (K) for given increase in crack length.

Two techniques were used to monitor progress of the fatigue crack. The primary technique utilized a high temperature/pressure linear variable differential transformer (LVDT) to measure the specimen crack opening displacement (COD) which accompanied specimen loading. The resultant load/COD data (i.e., compliance) was used to calculate crack lengths.

The back-up technique for monitoring crack lengths, which was used only on the six initial test specimens and has not been used for the last two years, consisted of a series of 0.028-inch diameter holes drilled on 0.100-inch centers normal to the plane of fatigue crack growth. These holes were connected to external pressure switches with capillary tubing. This hole/capillary tube/switch system was evacuated and backfilled with

an inert gas to a pressure slightly below the operating pressure in the test vessel. As the fatigue crack front intersected each hole, a pressure pulse was applied to an external pressure switch stopping an individual cyclic load counter. The resultant data is incremental crack growth information representing the cycles required to extend the fatigue crack in 0.100-inch increments. Figure 4 shows a standard WOL specimen with capillary holes and a LVDT mounted on the front face.

Extensive post-test fractography was performed on all specimens to obtain information on fracture modes and fatigue crack front geometries. A special 10x traversing microscope with x and y axis micrometer measuring capability was used to measure the crack length associated with each capillary hole and, more importantly, locate and define the shape of any beachmarks present on the fracture surface and initial and final crack lengths.

Test Matrix

A total of seventeen (17) low alloy steel specimens were tested. Of these, eleven (11) were made from A508 Class II plate material, four (4) from A533B plate material, and two (2) from welds.

One weld specimen was fabricated from A508 plate material such that the plane of the fatigue crack growth was oriented in the weld heat affected zone (HAZ). The other was made from A533B alloy material with the fatigue crack plane oriented in the weld filler metal.

The physical and mechanical properties of all the materials included in this study are listed in Table 2. The specimens were machined from the plate material such that the plane of fatigue crack growth was normal to the rolling plane and parallel to the primary rolling direction.

Several multispecimen tests were run. The pertinent parameters for these tests are listed in Table 3. The test frequencies chosen cover a wide range. They include a very fast frequency of 300 cph, where little environmental effect was expected, and slower frequencies of 75, 60, 18, and 7.5 cph where the environmental effects observed become more significant. In order to investigate the behavior of very slow frequencies, a test containing four (4) specimens was run at 0.741 cph.

A symmetric sawtooth loading waveshape was used for the first test, specimen 04-3Q. A skewed sawtooth, which emphasized time spent under rising load, was used for all subsequent tests except the last three (3) which used a haversine loading waveshape. Holdtime effects were not considered during this study.

Four values of mean load (i.e., R^* ratio) were included: 0.78, 0.6, 0.2, and 0.05. These mean stress values and frequencies represent a broad range of conditions that might be expected in actual service.

* $R^* \triangleq$ Minimum Load \div Maximum Load

TEST RESULTS

The end-of-test fracture surface for the A533 weld filler metal specimen is shown in Figure 5. The pronounced crack front curvature visible in the picture is typical of all the low alloy test specimens. Only one half of the test specimen is shown because the other half was used for conventional metallography.

Crack length vs. cycles data for all specimens tested are presented in Figures A-1 through A-9 in Appendix A. (Specimen C-35 showed no growth, therefore, no data are presented.) Note that the abscissae for each of the curves are different and that the tests represent different loading conditions.

Generally, the crack growth behaviors observed fall into three categories as illustrated in Figure 6. Type I behavior is representative of data that obey the Paris Law - that of increasing growth rate with increasing crack length (and ΔK). Type II behavior consists of constant or decreasing growth rates with increasing crack length (and ΔK). Type III behavior was also observed, with no growth at first followed by combinations of Types I and II. In most cases, the deviations from Type I behavior were found for specimens where testing was interrupted by test autoclave depressurization/cooldown events in which the specimens were exposed to air or air saturated water. However, this effect was also noted in a few specimens tested without interruptions.

DISCUSSION

In order to see more clearly the effects of frequency and mean stress, crack growth data are plotted as time-based crack growth rate, da/dt^* vs. effective stress intensity factor. This use of time-based crack growth rate da/dt and effective stress intensity, $(K_{eff} = K_{max}(1-R)^{1/2})$ allows normalization of all of the test data.

Figure 7 is a plot of da/dt vs. K_{eff} for Specimens 04-3Q, C-33, C-9, CS-15, CS-19, CS-34, and 1HT-19. The frequency, R ratio, and specimen number are identified for easy reference. These data represent a broad range of frequency and mean stress values, 300 to 0.74 cph, and $R = 0.05$ to 0.78 , respectively. Other test specimens in the matrix were not included because results were compromised by test interruptions.

Inspection of Figure 7 shows that the crack growth data from these seven specimens follow a very definite pattern. All exhibit an initially very steep slope at relatively low K followed by a region of decreasing slope, at higher K , with a possible tendency for saturation at a plateau value of da/dt (slope of zero). There is also a tendency for stratification with increasing plateau values observed at higher cycle frequencies. Finally, the crack growth rates appear to decrease below 10^{-6} inch/hour (2.5×10^{-5} mm/hr) for K values of 18-20 $\text{ksi}\sqrt{\text{in}}$ (20-22 $\text{MPa}\sqrt{\text{m}}$).

* da/dt (inch/hour) $\triangleq da/dN$ (inch/cycle) $\times f$ (cycle/hour)

To investigate the effects of oxygen on crack growth rates, specimens 1H-T19, 1H-T37, and 1H-T39 were tested in water with different oxygen concentrations. Figure 8 is a superposition of the crack length/cycles data for these three specimens. From Figure 8, it is clear that increasing oxygen level accelerates crack growth. To examine more closely these differences in cracking behavior, the crack growth rates derived from Figure 8 are plotted in Figure 9 as a function of ΔK . Also shown in Figure 9 are the ASME Section XI design lines for air and water environment.

The crack growth rates of the zero and 0.2 ppm O_2 specimens are identical up to a ΔK of $33 \text{ ksi}\sqrt{\text{in}}$ ($36 \text{ MPa}\sqrt{\text{m}}$). Above this value of ΔK the zero O_2 specimen exhibits a plateau in growth rates which falls below the 0.2 ppm O_2 specimen. The 8 ppm O_2 specimen exhibits higher initial growth rates for ΔK below $33 \text{ ksi}\sqrt{\text{in}}$ ($36 \text{ MPa}\sqrt{\text{m}}$). However, at higher ΔK values, where the data were obtained from relatively deep cracks (a few tenths of an inch), growth rates for the 8 ppm O_2 specimen are similar to those observed for the 0.2 ppm O_2 specimen.

The data in Figures 7 and 9 show that after an initial period of increasing crack growth rate, it is not uncommon for a crack to slow down or stall. Slower growth rates are found for deeper cracks and test interruptions. This behavior is attributed to the build up of oxides in the crack tip region early in the test.

In order to provide data to help understand this mechanism, a special test condition was run. Three specimens (CS-16, -19, and -20) were fabricated from the same material (A508-2 plate), with the same nominal initial total crack length. Specimen CS-16 was given a standard length

fatigue precrack { ~ 0.1 " (2mm) }. However, specimens CS-19 and -20 were given extra long fatigue precracks { ~ 0.3 " (8mm) }. This crack depth was selected based upon previous experience which showed that the aforementioned decreasing crack growth rate behavior was observed after 0.1" to 0.3" (2-8 mm) of crack growth. In addition, specimen CS-20 was given a special presoak cycle which consisted of exposure to the 0.2 ppm, 550⁰F water environment for a 43 hour period while being held under a constant load equal to the maximum load planned for the cyclic portion of testing. This was done to allow oxides to build up in the crack tip prior to the start of cyclic testing.

Figure 10 is a plot of crack length vs. cycles for specimens CS-20, CS-19, and CS-16. Note that the curves were normalized to have the same initial crack length, a_0 , and that the displacement in data for CS-20 resulting from LVDT shift has been corrected. Inspection of Figure 10 shows that both CS-16 and CS-19 have similar growth rates early in the test while CS-20, the presoaked specimen, exhibits no growth for the first 2500 cycles. Subsequently, CS-20 exhibited growth rates similar to the other two specimens. These results, therefore, support the belief that oxide crack blockage retards crack growth.

Some observations can be made about crack growth behavior by inspecting the fracture surfaces at high magnification. Figure 11 is a 500x photo of the crack tip of specimen CS-34. Considerable oxide buildup can be seen in the crack, especially near the crack tip. Notice also the splits away from the main crack as it grows through the material. Figure 12 is

a 1000x Scanning Electron Microscope (SEM) photo of the fracture surface from this same specimen (CS-34) which clearly shows a heavy oxide layer. Finally, Figure 13 is a low magnification SEM photo (50x) of the fracture surface. Note the differences between the fracture surface obtained when the specimen was pulled apart in room temperature air and the flat featureless surface found in the environmental fracture (on left). The latter surface condition is attributed to heavy surface oxidation.

A comparison of the data plotted in Figure 7 with similar PWR and air data is made in Figure 14. These data illustrate the effect of oxygen at cycle frequencies where environmental effects are maximized. In Figure 14, the data are plotted as time-based growth rate, da/dt , vs. K_{max} with the low alloy data discussed in this report identified as oxygenated water data. As can be seen from Figure 14, the oxygenated water data are very similar to the PWR data with both sets of data lying to the left of air data.

The plateau da/dt value for oxygenated water data is slightly higher than that for the PWR environment. More important, however, the K_{max} values, below which the growth rates are less than 10^{-6} in/hr (2.5×10^{-5} mm/hr) are slightly higher in the oxygenated water case. This is very encouraging because the lowest frequency studied in the PWR case is a factor of 10 faster than the oxygenated water case. This further suggests that the 0.2 ppm oxygenated water environment is similar to a "zero" oxygen (i.e., PWR) environment.

The results from Specimens C-15 and CS-34 allow comparisons to be made for the weld material. Specimen C-15 was made from the A508 material with the fatigue crack plane oriented in the weld heat affected zone. CS-34 was fabricated from A533B material with the fatigue crack plane oriented in the weld filler material.

In order to compare the crack growth behavior of the weld material to the base material, data from Specimens C-15, CS-34, C-10, and CS-19 are plotted in terms of crack growth rate vs. effective stress intensity factor in Figure 15. Specimen C-10, made from A508 plate material, is compared to C-15. CS-19, made from A533B, is compared to CS-34. The pairing is based on common cycle frequency. Figure 15 shows that the curves of CS-19 and CS-34 as well as those of C-10 and C-15 are very similar.

CONCLUSIONS

For the ranges of stress intensity levels, frequency, and mean load covered by the present tests, low alloy steel displays a complex interaction with a high temperature, oxygenated water environment.

Typically, the growth rates observed for short cracks are significantly moderated at deeper (i.e., ~0.2-0.3", 5-8 mm) crack lengths. This effect appears to be related to the formation of large amounts of oxide within the fatigue crack and on crack faces. The corrosion fatigue behavior of the two welded specimens tested was not significantly different than that of the base material.

The effects of cycle frequency and mean stress can be represented by plotting the data as da/dt vs. K_{eff} . There appears to be a characteristic "plateau" value of growth rate for given cycle frequencies and high mean stress tends to result in relatively higher crack growth rates. Below a value of $K_{maximum}$ equal to 28-32 $\text{ksi}\sqrt{\text{in}}$ (31-35 $\text{MPa}\sqrt{\text{m}}$), growth rates are quite slow ($<10^{-6}$ inch/hr (2.5×10^{-5})).

Over a broad range of test conditions, the data collected in 0.2 ppm oxygenated water are similar to that for PWR conditions.

REFERENCES

1. Mager, T., "Fatigue Crack Growth Characteristics of A533 B Class 1 Plate in an Environment of High Temperature Primary Grade Nuclear Reactor Water," Trans ASME Journal of Pressure Vessel Technology, June 1976.
2. Kondo, T. et al., "Fatigue Crack Propagation Behavior of ASTM A533 B and A302B Steels in High Temperature Aqueous Environment," Paper 6, HSST Program Sixth Annual Meeting, Oak Ridge National Laboratories, April 1972.
3. Gerber, R., et al., "Fatigue Crack Growth in SA508 C12 Steel in High Temperature High Purity Water Environment," Trans ASME Journal of Engineering Materials and Technology, October 1974.
4. Hale, D. A., "Fatigue Crack Growth of Low Alloy Steel in a High Temperature High Purity Oxygenated Water Environment," presented at March 1979, Annual Meeting of National Association of Corrosion Engineers, Atlanta, Ga., to be published in Corrosion.
5. Bamford, W., et al., "Some Mechanical Observations on the Crack Growth Characteristics of Pressure Vessel and Piping Steels in PWR Environment," presented at March 1979 Annual Meeting National Association of Corrosion Engineers, Atlanta, Georgia, to be published in Corrosion.
6. Hale, D. A., Yuen, J. L., and Gerber, T. L., "Fatigue Crack Growth in Piping and RPV Steels in Simulated BWR Water Environment," NUREG/CR-0390, GEAP-24098, R-5, U. S. Nuclear Regulatory Commission January 1978.
7. Cullen, W. H., "A Review of Fatigue Crack Growth of Pressure Vessel and Piping Steels in High-Temperature, Pressurized Reactor-Grade Water," NUREG/CR-1576, NRL Memorandum Report, Nuclear Regulatory Commission, September 1980.

TABLE 1

High Temperature/Pressure Oxygenated Water Environment

Temperature	550 ⁰ F (288 ⁰ C)
Pressure	1230 psig (8.48 MPa)
Conductivity	0.5±0.2 μmho/cm at 25 ⁰ C
Dissolved Oxygen Content	100 to 300 ppb
pH	6.0±0.5 at 25 ⁰ C
Chloride	<0.1 ppm
Fluoride	<0.1 ppm

Table 2

SPECIMEN PLATE MATERIAL - CHEMICAL ANALYSES

Material Specification	Chemical Composition				ASTM Requirements	Vendor Test Results ^b psi (MPa)	GE Check Results ^b psi (MPa)	GE Check Results ^c psi (MPa)
	ASTM Requirements ^a (%)	Certified Analysis (%)	Check Analysis (%)					
ASTM A508C12	C - 0.027 maximum	C 0.20	0.23	Minimum Tensile				
	Mn - 0.50 to 0.90	Mn 0.68	0.68	Strength				
	P - 0.025 maximum	P 0.007	0.011	75,000 psi	97,000	96,100	90,000	
	S - 0.025 maximum	S 0.009	0.011	(517 MPa)	(669)	(663)	(621)	
	Si - 0.15 to 0.35	Si 0.027	0.29	Minimum Yield				
	Ni - 0.50 to 0.90	Ni 0.88	0.80	Strength				
	Cr - 0.25 to 0.45	Cr 0.35	0.37	50,000 psi	77,500	74,2000	67,700	
	Mo - 0.55 to 0.70	Mo 0.65	0.70	(345 MPa)	(534)	(512)	(467)	
	V - 0.05 maximum	V Not Analyzed	0.004					
ASTM A533-73 ^d (SAE336-1)	C - 0.25 maximum	C 0.190		Minimum Tensile				
	Mn - 1.10 to 1.55	Mn 1.280		Strength				
	P - 0.035 maximum	P 0.009		80,000 psi				
	S - 0.040 maximum	S 0.013		(552 MPa)				
	Si - 0.13 to 0.32	Si 0.250		Minimum Yield				
	Mo - 0.41 to 0.64	Mo 0.550		Strength				
	Ni - 0.37 to 0.73	Ni 0.610		50,000 psi				
ASTM A533-73 ^e (SAE336-1) (For Weld HAZ CS-34 only)	C - 0.25 maximum	C 0.18		Minimum Tensile				
	Mn - 1.10 to 1.55	Mn 1.36		Strength				
	P - 0.035 maximum	P 0.009		88,500 psi				
	S - 0.040 maximum	S 0.010		(611 MPa)				
	Si - 0.13 to 0.32	Si 0.250		Minimum Yield				
	Mo - 0.41 to 0.64	Mo 0.560		Strength				
	Ni - 0.37 to 0.73	Ni 0.650	69	69,900 psi				
				(482 MPa)				

^aMaterial Code:

C = Carbon
 Si = Silicon
 P = Phosphorus
 Cr = Chromium
 Mo = Molybdenum
 Ni = Nickel
 S = Sulfur
 Mn = Manganese
 Fe = Iron

^bRoom Temperature^c500°F

^dAustenitized at 899 ± 14 Deg. C for 8 hours and water quenched; tempered at 671 Deg. C and air cooled; stress relieved at 566 Deg. C for 2 hours and 621 ± 14 deg. C for 50 hours.

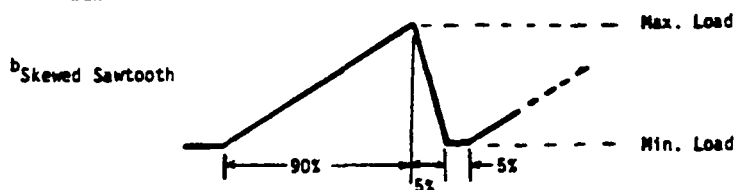
^ePlate and tests heated 1630-1660°F, held 4 hours and 25 minutes and water quenched, then tempered 1290-1300°F, held 4 hours and 8 minutes and water quenched.

Table 3

FATIGUE CRACK GROWTH TESTS

Specimen Number	Material	Specimen Type	Frequency (cycles/hr)	Waveshape	R ^a	K _{max} Initial/ ΔK Initial ksi/in (MPa/m)	K _{max} Final/ ΔK Final ksi/in (MPa/m)	Total Crack Growth in. (mm)	Measurement COD	Capillary	
04-30	A533	WOL	300	Sawtooth	0.78	45/10 (49/11)	82/18 (90/20)	0.7 (18)	No	Yes	
C-33	A508	WOL	300	Skewed ^b Sawtooth	0.05	21/20 (23/22)	35/33 (38/36)	0.53 (13)	Yes	Yes	
C-9	A508	WOL	75	↓	0.6	43/18 (47/20)	62/25 (68/27)	0.38 (10)	Yes	Yes	
C-34	A508	WOL	18		0.05	20/19 (22/21)	23/22 (25/24)	0.13 (3)	Yes	Yes	
C-10	A508	WOL	↓		0.6	35/14 (38/15)	53/21 (58/23)	0.44 (11)	No	Yes	
C-11	A508	WOL				35/14 (38/15)	47/19 (52/21)	0.35 (9)	No	Yes	
C-12	A508	WOL				35/14 (38/15)	45/18 (49/20)	0.3 (8)	No	No ^c	
C-15	A508 Weld HAZ	WOL				35/14 (38/15)	53/21 (58/23)	0.46 (12)	Yes	Yes	
C-35	A508	WOL	7.5			22/9 (24/10)	22/9 (24/10)	None	Yes	No	
CS-15	A508	CT	7.5			30/12 (33/13)	58/23 (64/25)	0.36 (9)	Yes	No	
CS-16	A508	CT	0.741 ^d				34/13 (37/19)	38/15 (42/16)	0.08 (2)	Yes	No
CS-19 ^e	A508	CT	0.741 ^d				29/12 (32/13)	36/14 (39/15)	0.14 (3)	Yes	No
CS-20	A508	CT	0.741 ^d				30/12 (32/13)	32/13 (35/14)	0.05 (1)	Yes	No
CS-34	A533 Weld Filler Metal	CT	0.741 ^d	↓	↓	32/13 (35/14)	47/19 (52/21)	0.25 (6)	Yes	No	
1H-T19 ^e	A533	CT	60	Haversine	0.2	32/26 (35/28)	52/41 (57/45)	0.37 (10)	Yes	No	
1H-T37 ^f	A533	CT	60	↓	↓	32/26 (35/28)	48/38 (53/42)	0.32 (9)	Yes	No	
1H-T39 ^g	A533	CT	60	↓	↓	32/26 (35/28)	49/39 (53/42)	0.35 (9)	Yes	No	

$$R = \frac{K_{min}}{K_{max}}$$



^cCrack length measurements based on beginning and end points and, where present, fracture surface artifacts.

^dDual frequency test. Frequency increase by a factor of ten (7.407 cph) during the middle of testing

^eTest environment, 550°F (288°C)/1250 psi (8.6x MPa) pressure, high purity oxygenated water (0.2 ppm O₂)

^fSame test environment except O₂ content of water = 0.0 ppm

^gSame test environment except O₂ content of water = 8 ppm

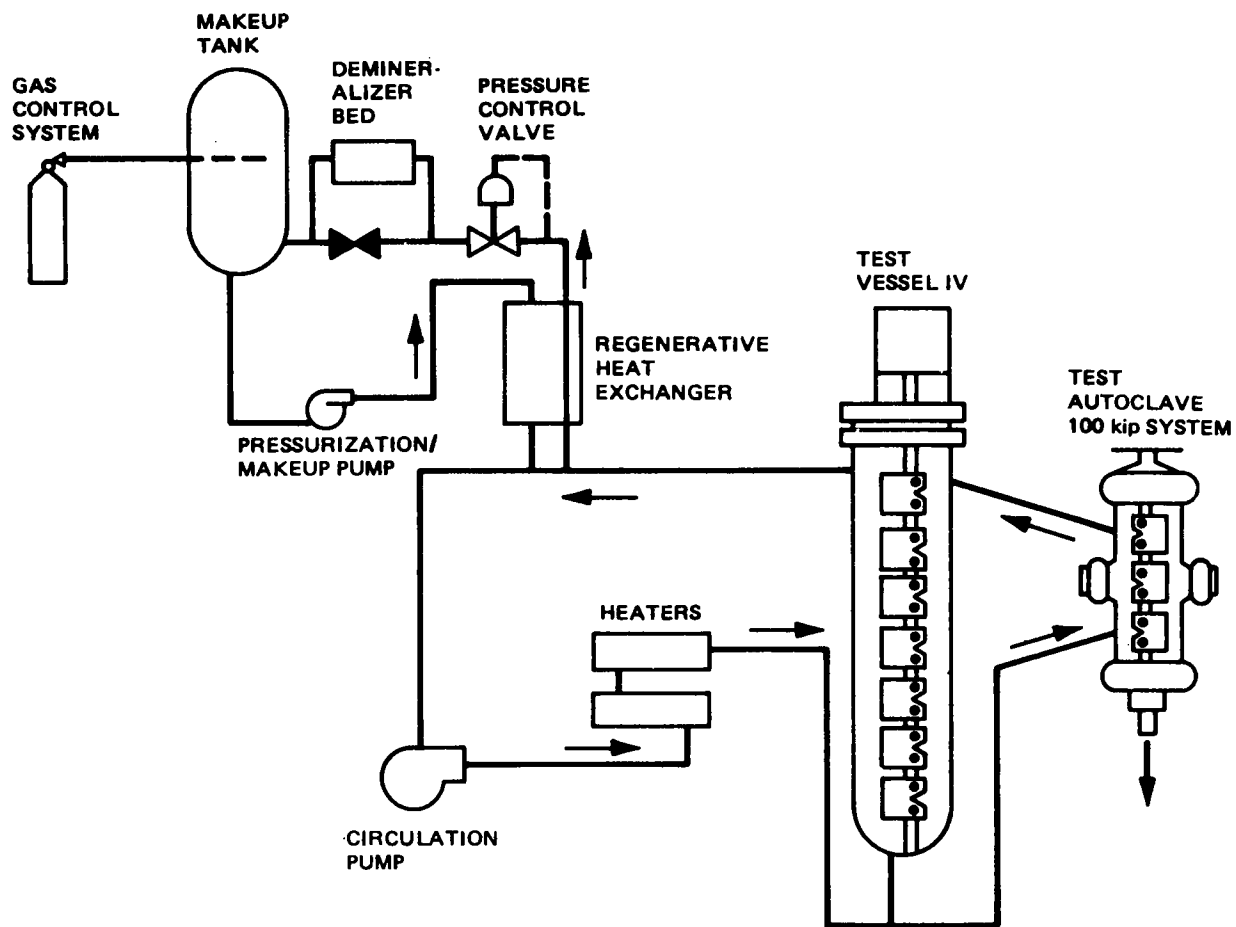


Figure 1. Simulated BWR Water Test Loop

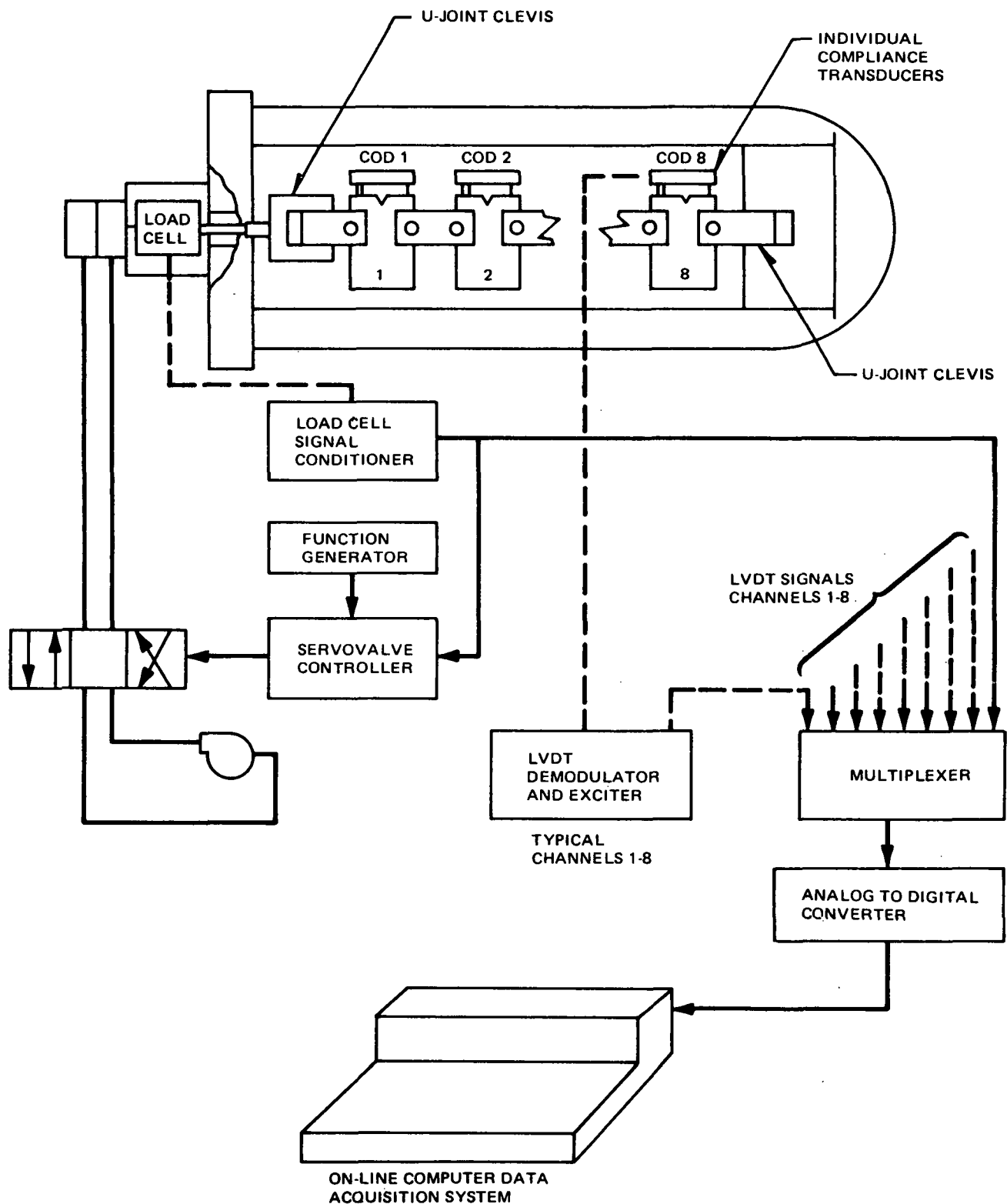
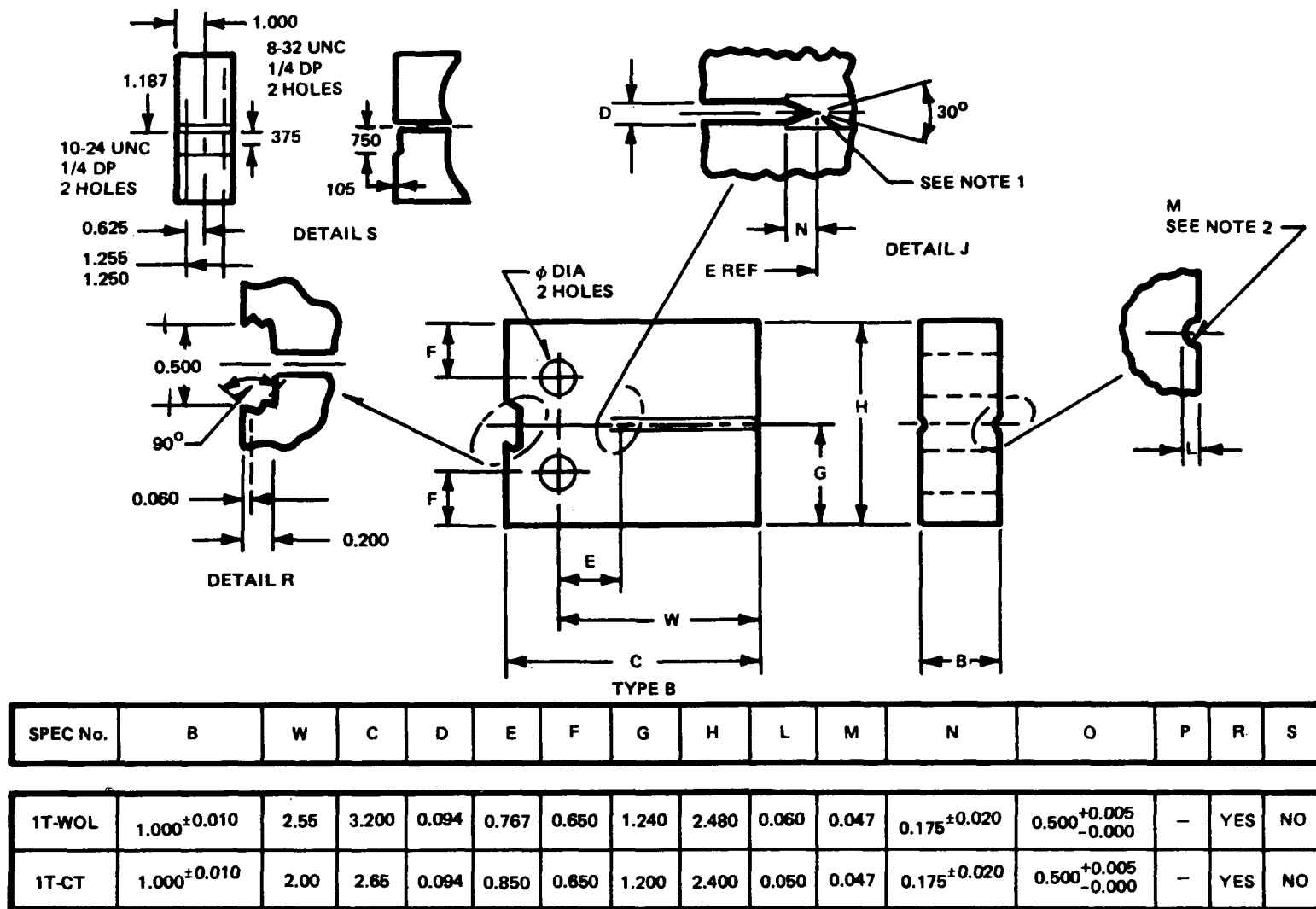


Figure 2. Test Vessel VI, Multispecimen Environmental Test Facility



NOTES:

1. 0.007 in. MAXIMUM RADIUS (EDM)
2. LAY MARKS TO FALL PARALLEL TO AXIS OF RADIUS SURFACE
FINISH TO BE 32

Figure 3. WOL or Compact Tension Specimen for Crack Growth Rate Study
(All Dimensions in Inches)

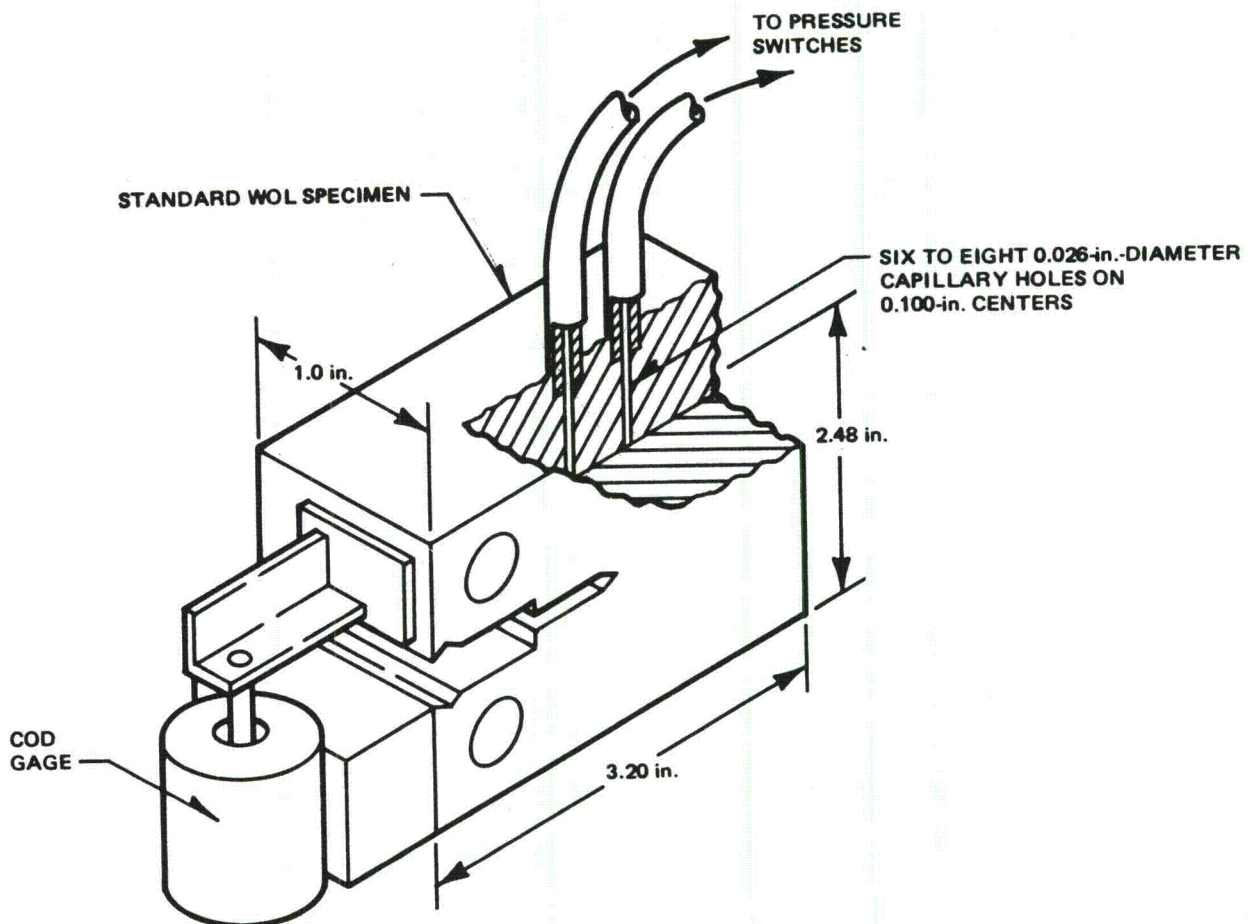


Figure 4. Specimen Modifications for Remote Crack Length Measurement Capability

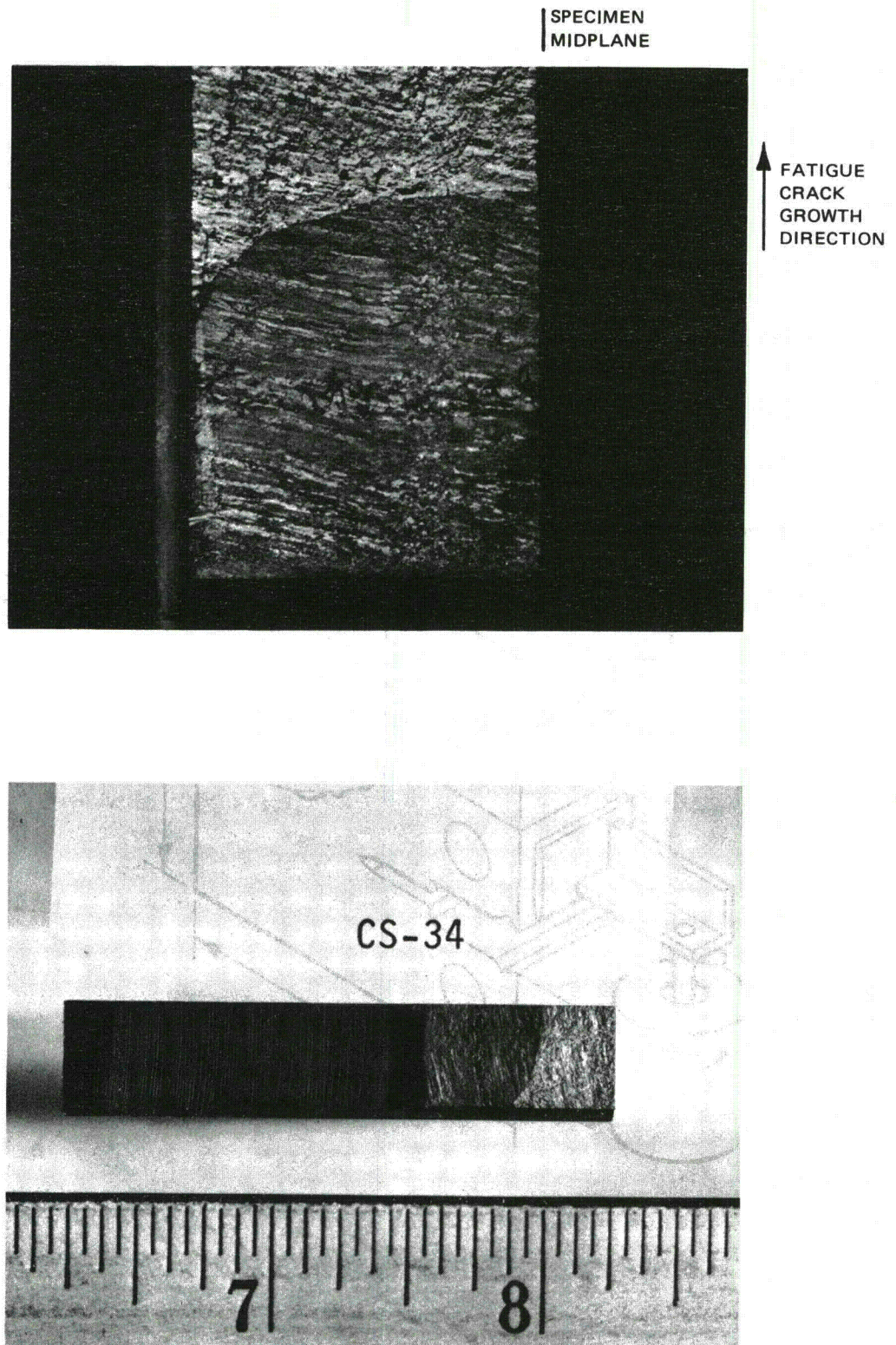
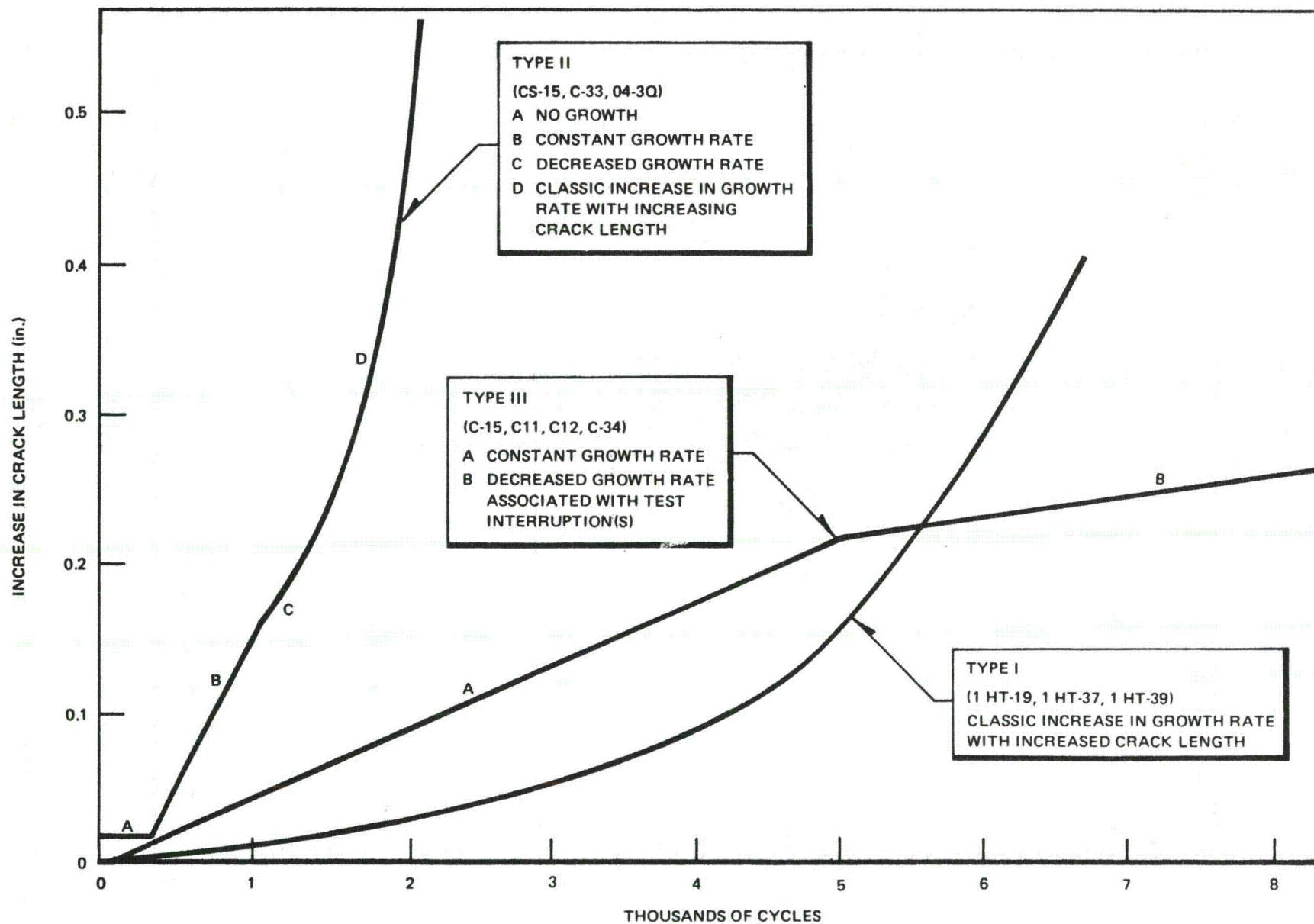
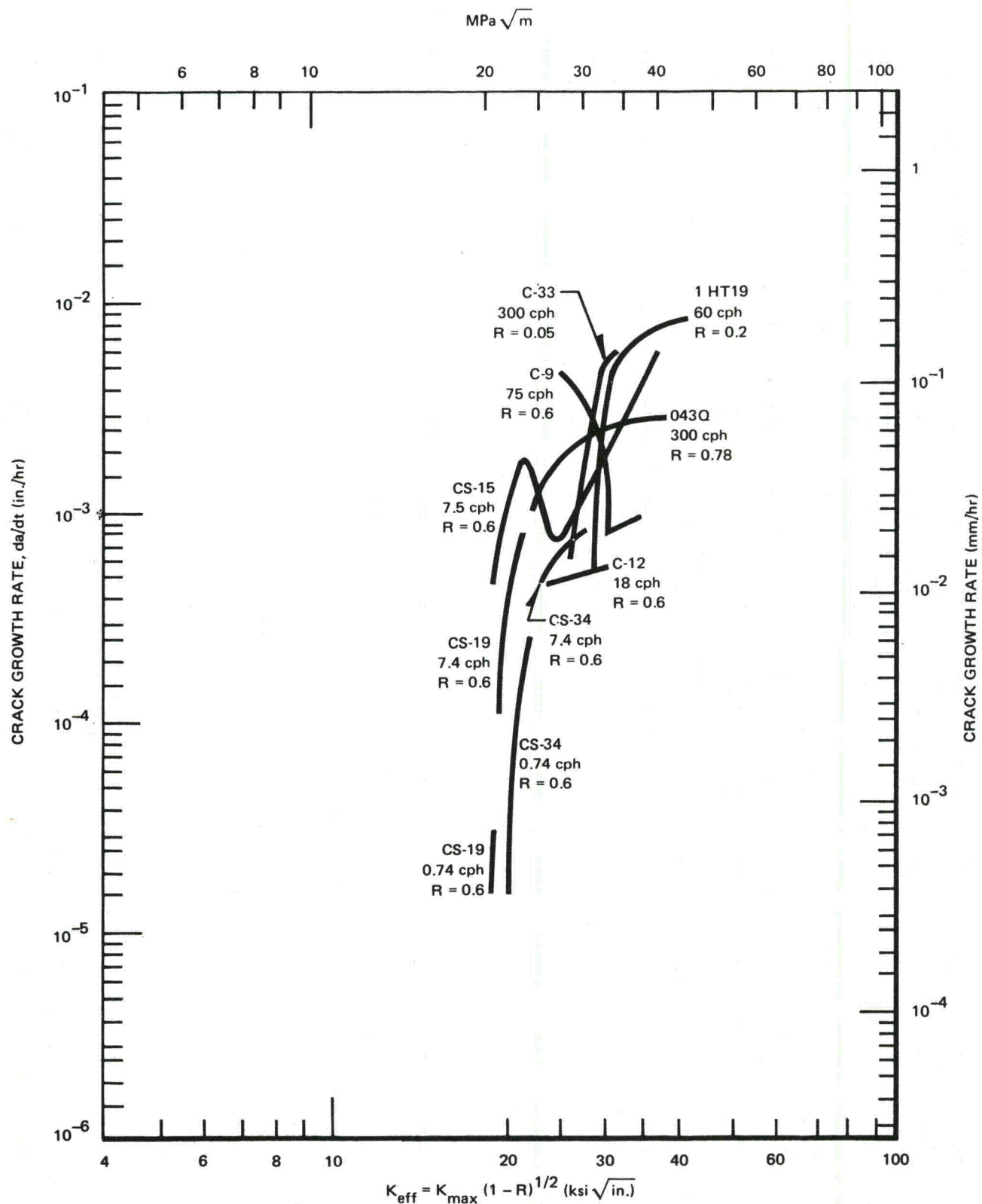


Figure 5. Final Fracture Surface, Specimen CS-34 (One Half Slice)



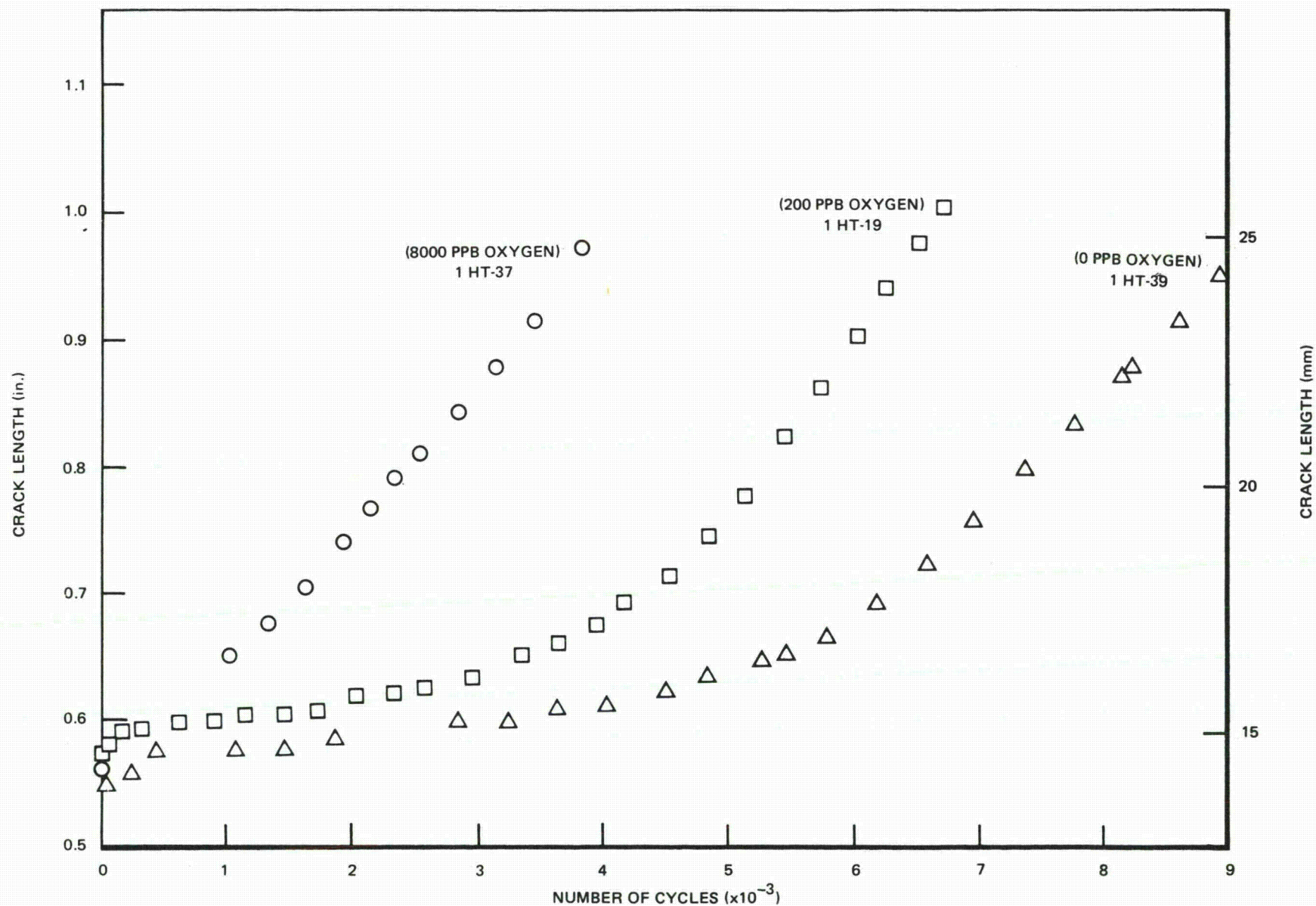
11291-07

Figure 6. Types of A vs. N Plots



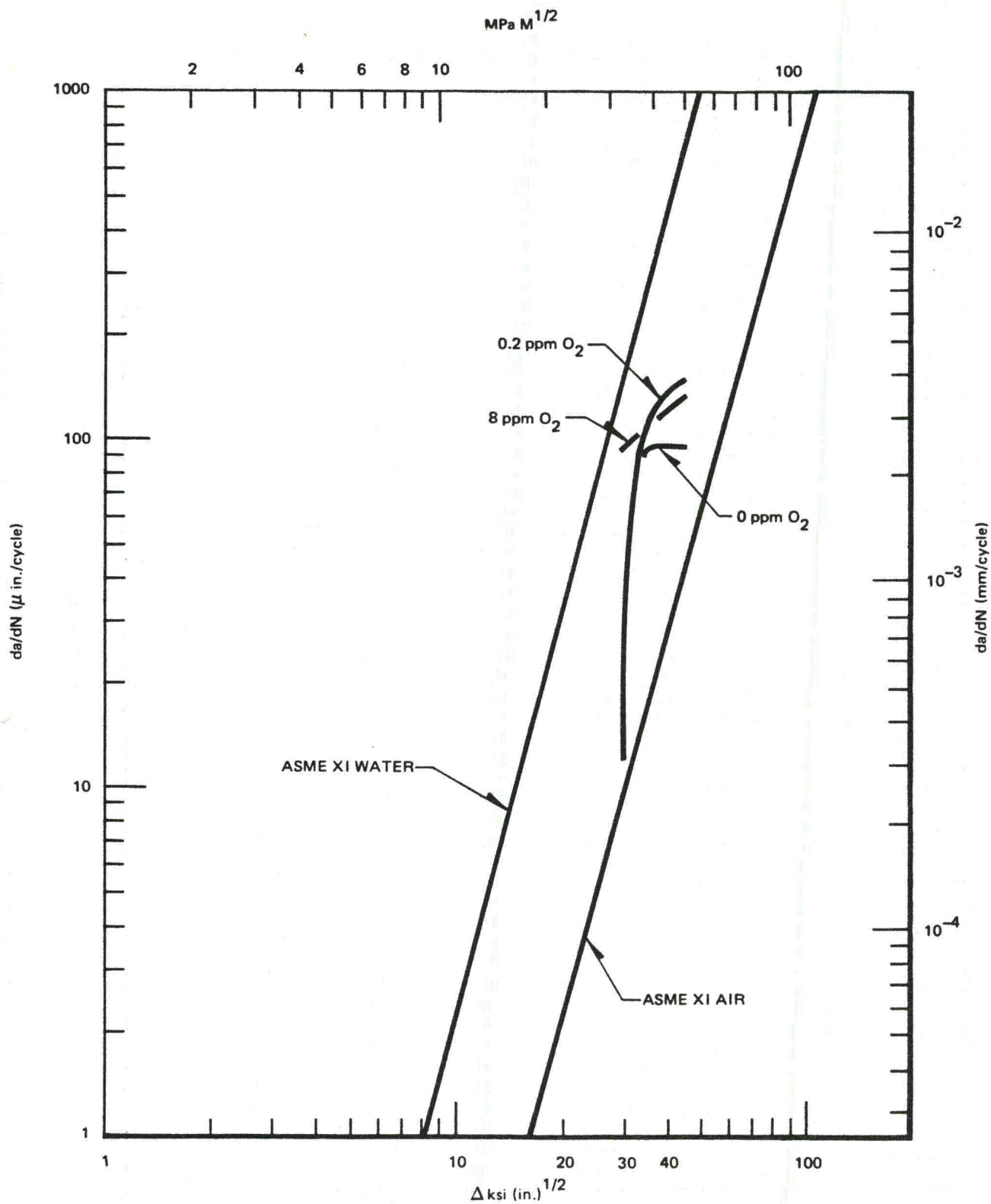
11291-03

Figure 7. Effect of Frequency and Mean Stress, 0.2 ppm 550°F Water Environment



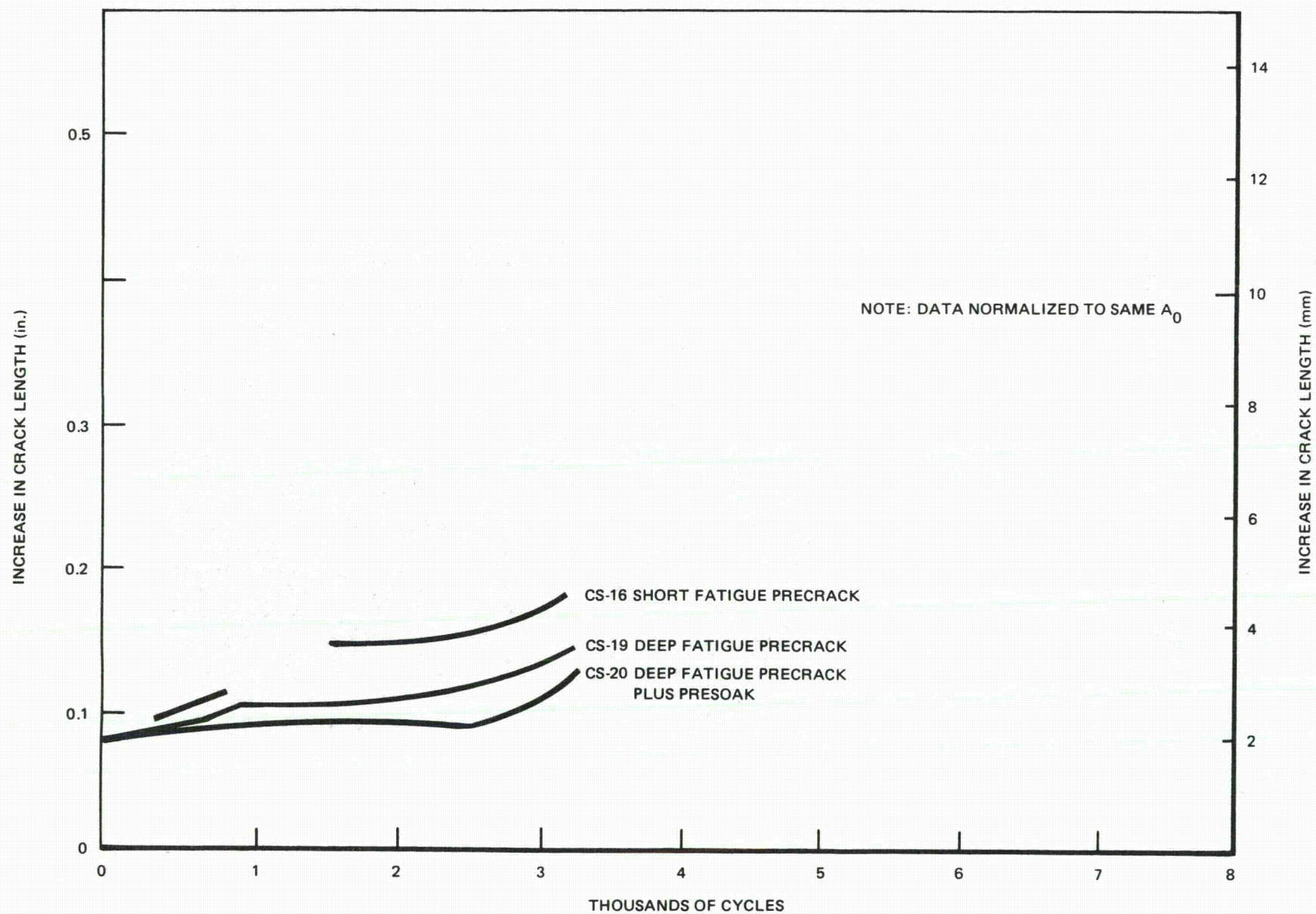
11291-04

Figure 8. Crack Length vs. Cycles Data at 600 Cycles per Hour



11291-06

Figure 9. Effect of O_2 on Crack Growth Rate



11291-05

Figure 10. Oxide Crack Blockage Effect

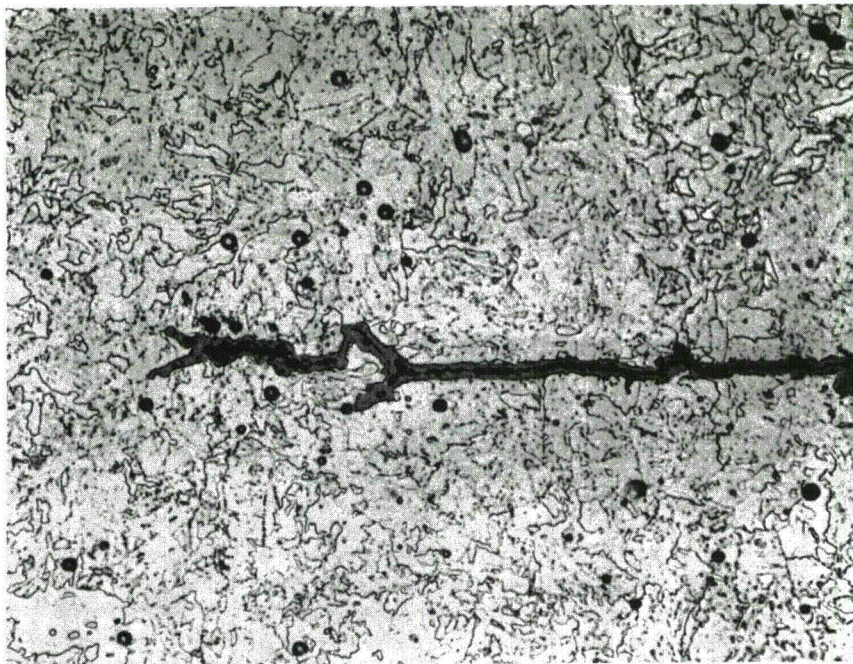


Figure 11. Specimen CS-34, Crack Tip Region 500X

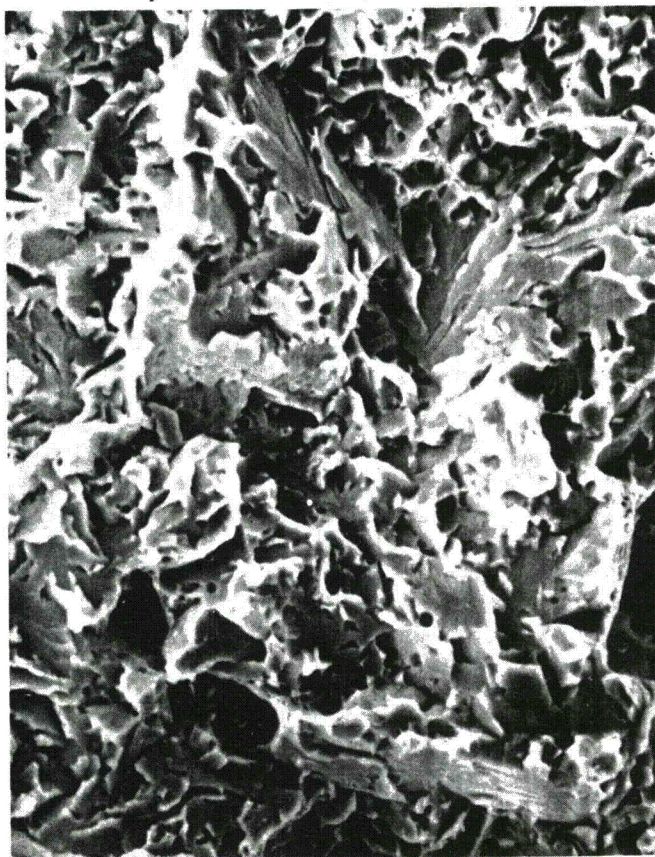
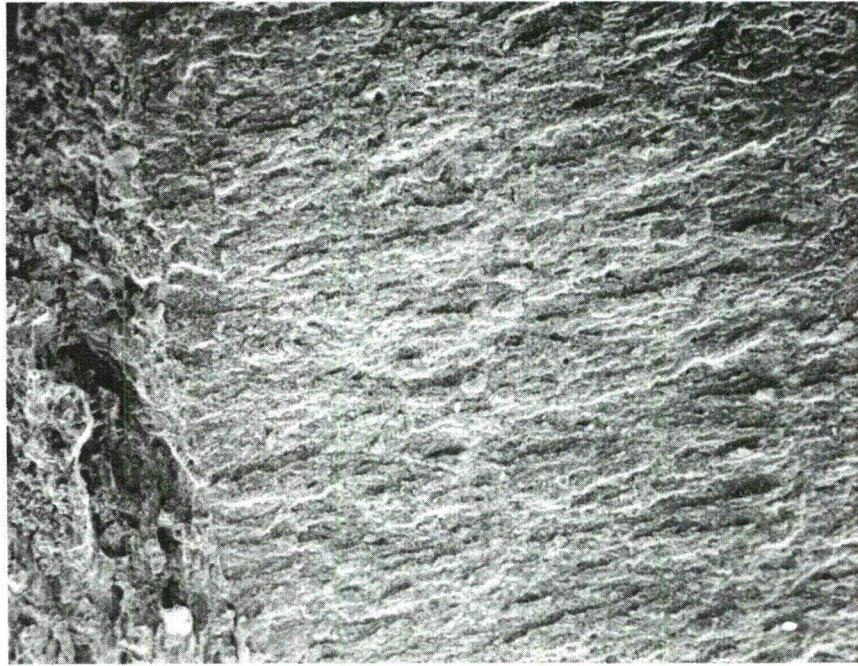
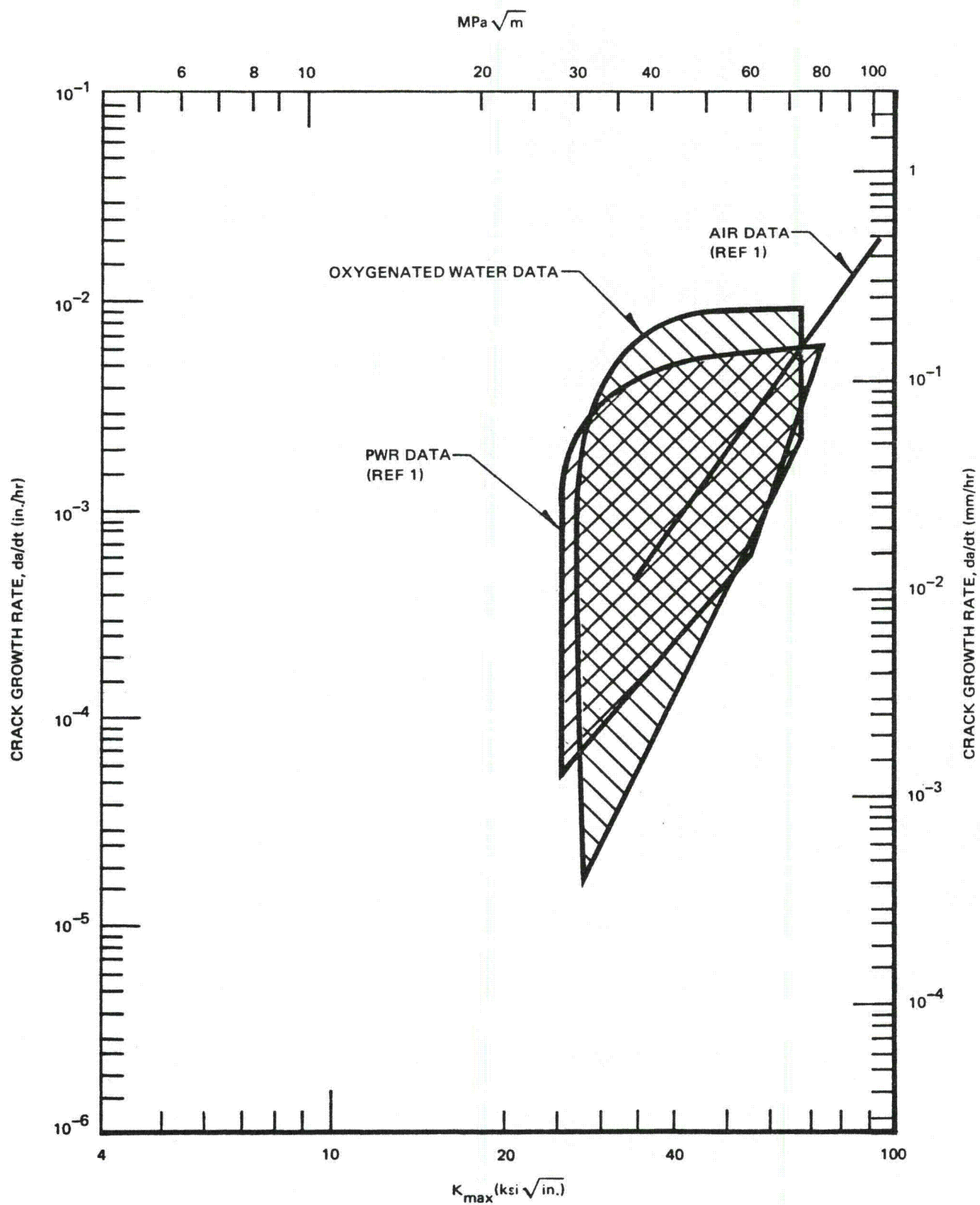


Figure 12. Specimen CS-34, Fracture Surface at 1000X



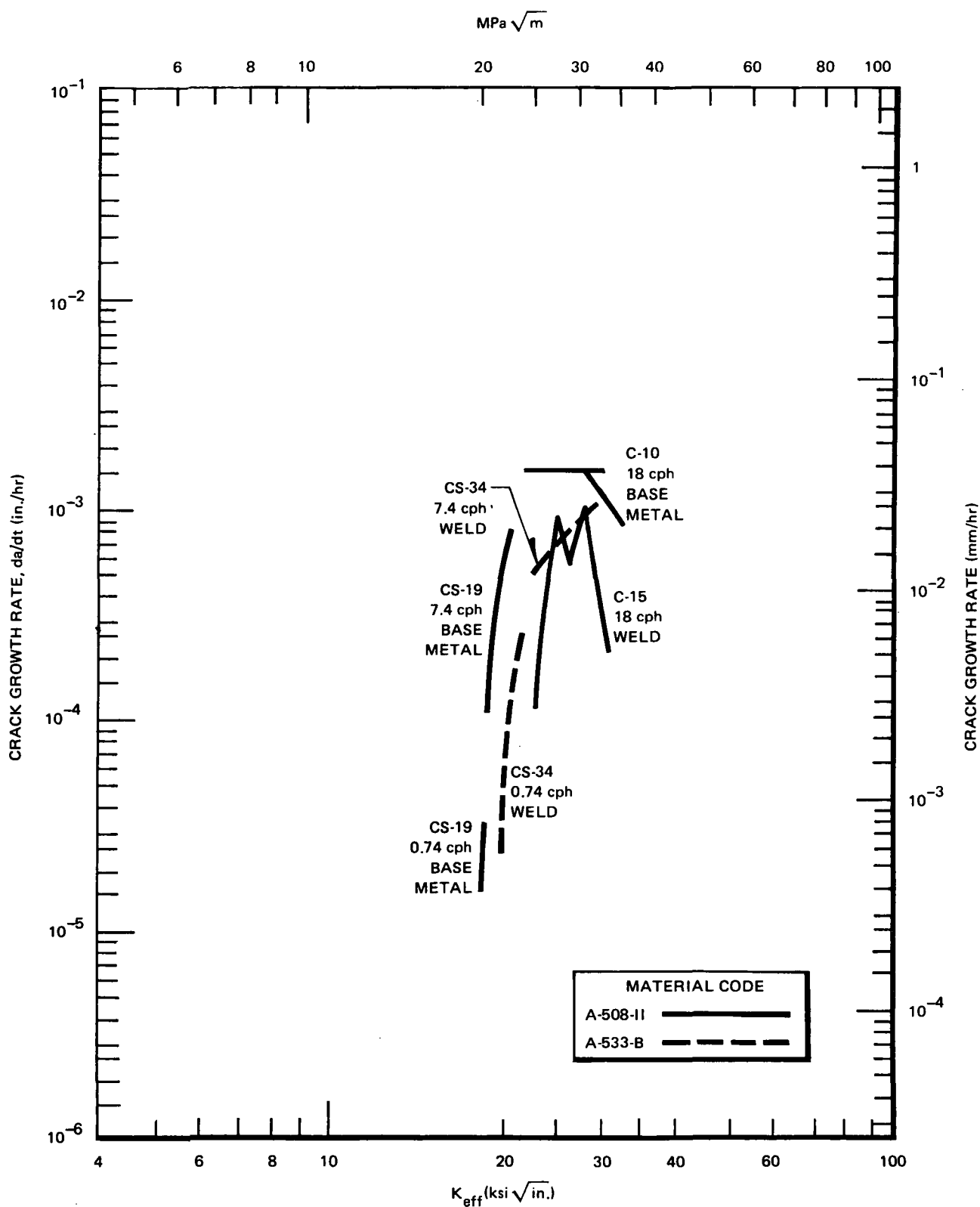
ENVIRONMENT ← → AIR

Figure 13. Specimen CS-34, Fracture Surface at 50X



11291-01

Figure 14. BWR, PWR, and Air Data Comparison



11291-02

Figure 15. Welds vs. Base Metal

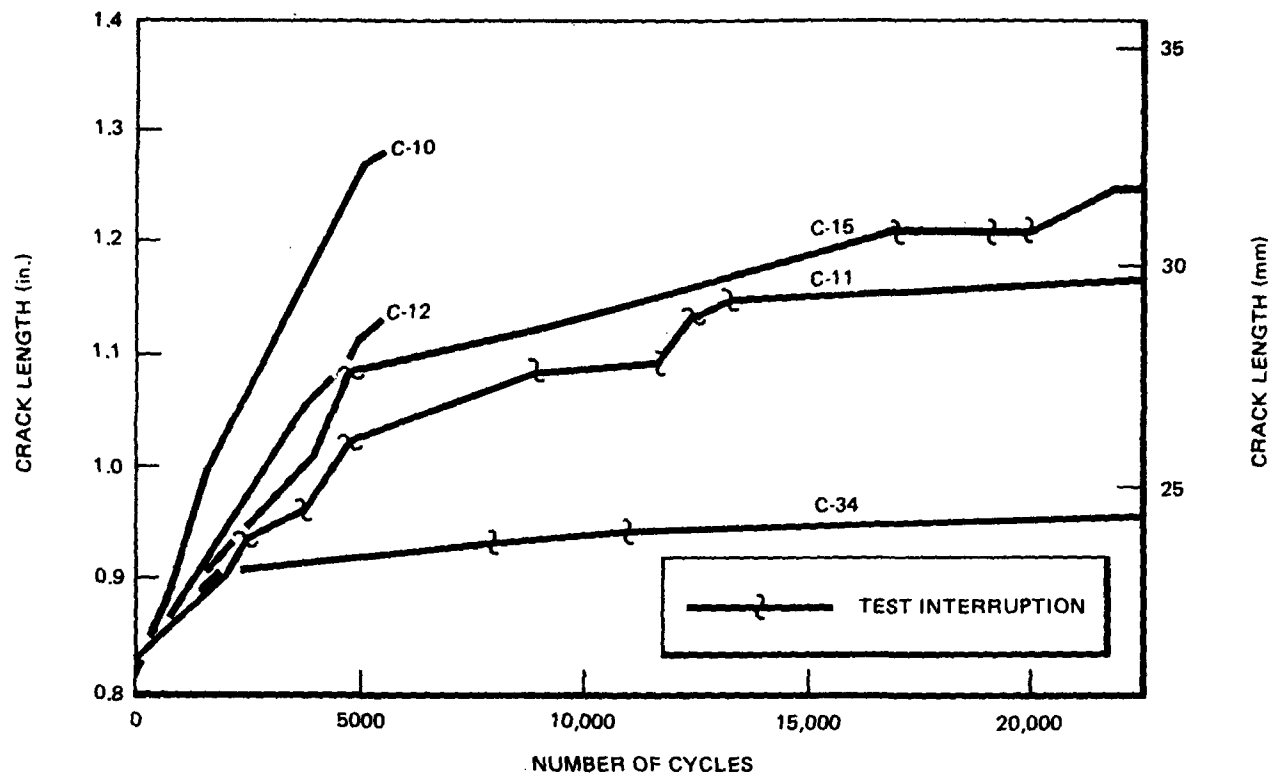


Figure A-1. Crack Length vs. Cycles Data at 18 Cycles per Hour

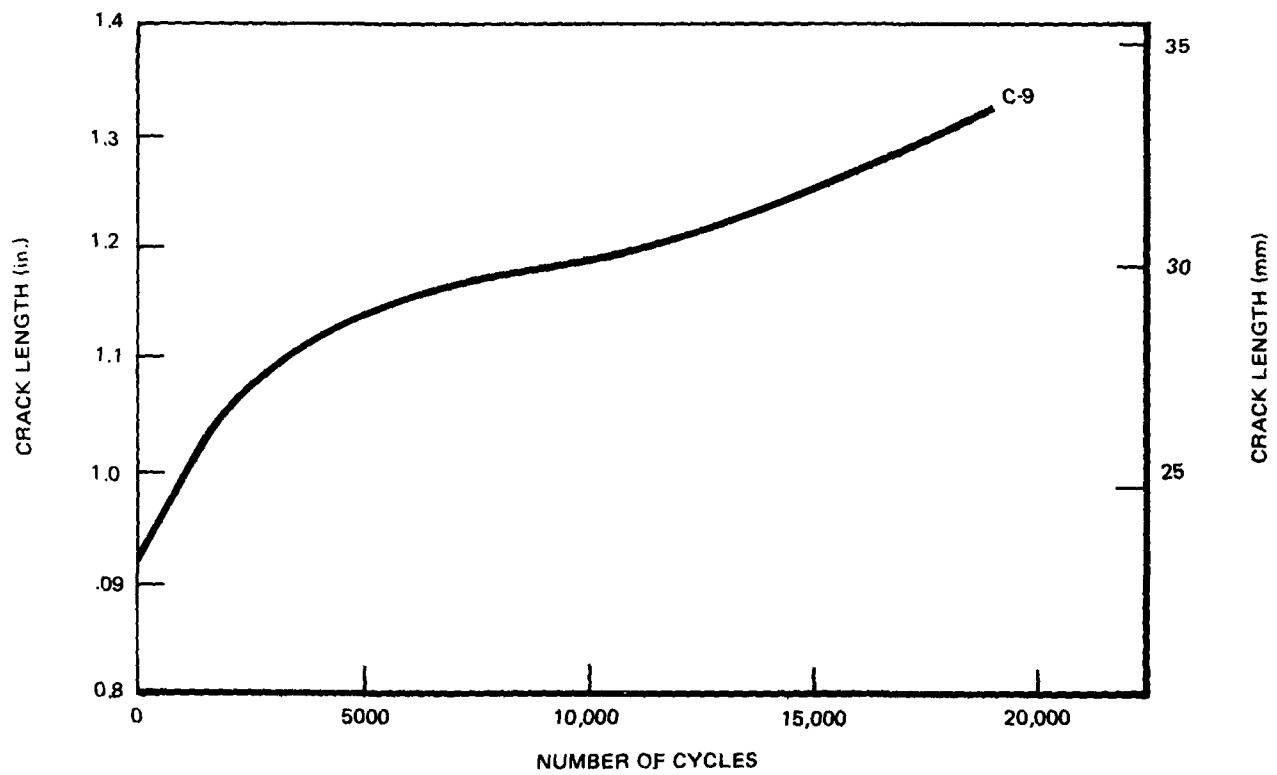


Figure A-2. Crack Length vs. Cycles Data at 75 Cycles per Hour

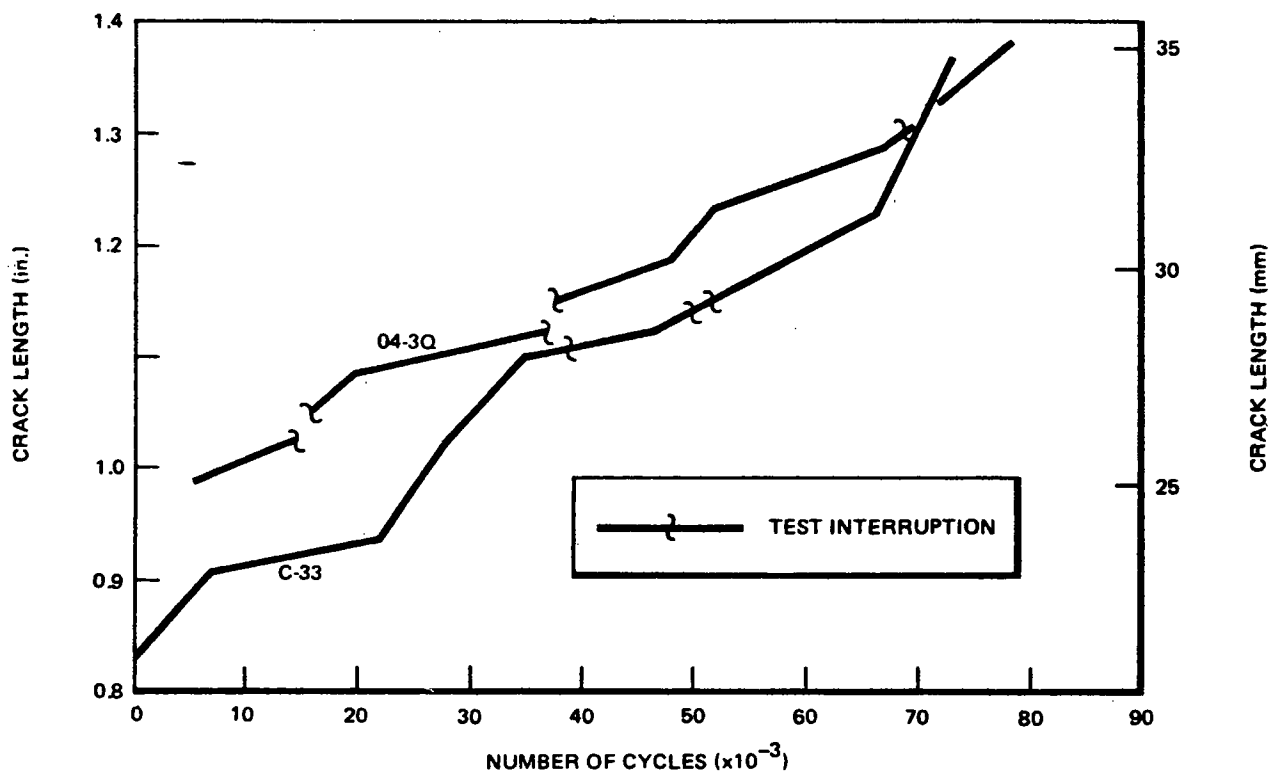


Figure A-3. Crack Length vs. Cycles Data at 300 Cycles per Hour

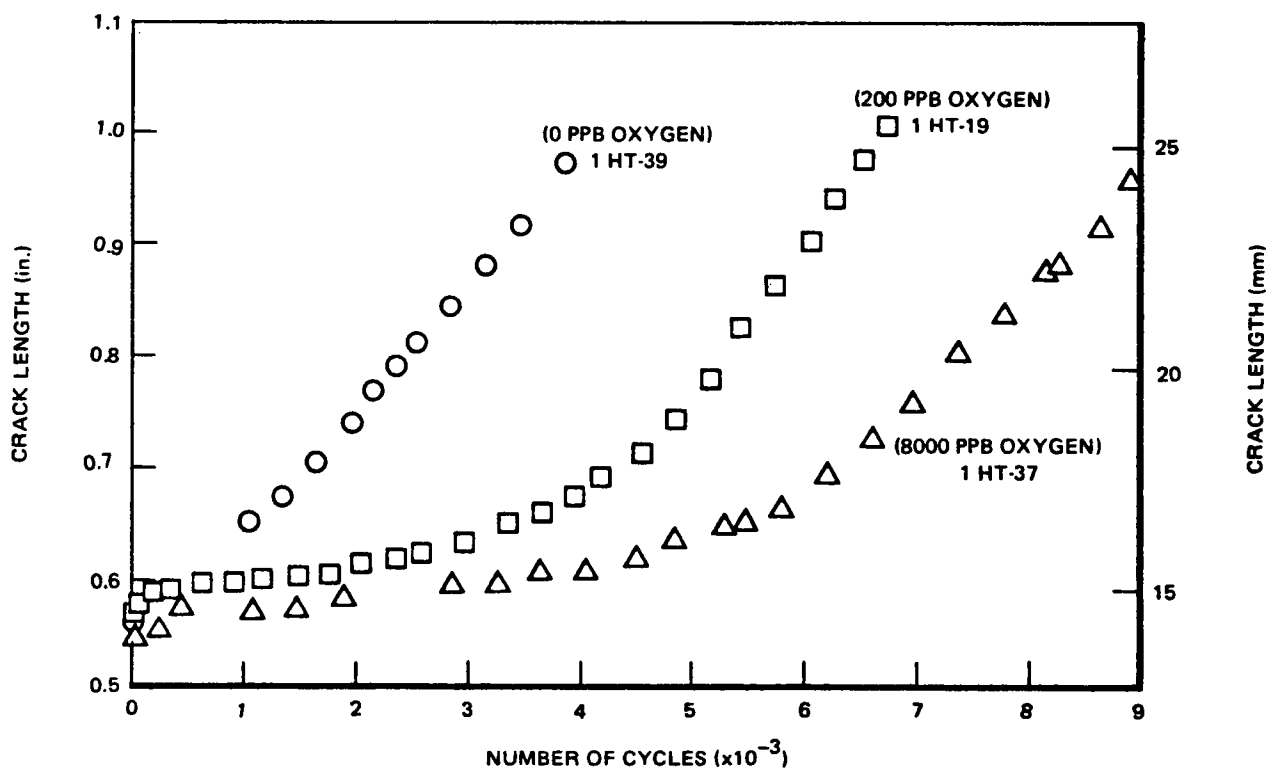


Figure A-4. Crack Length vs. Cycles Data at 600 Cycles per Hour

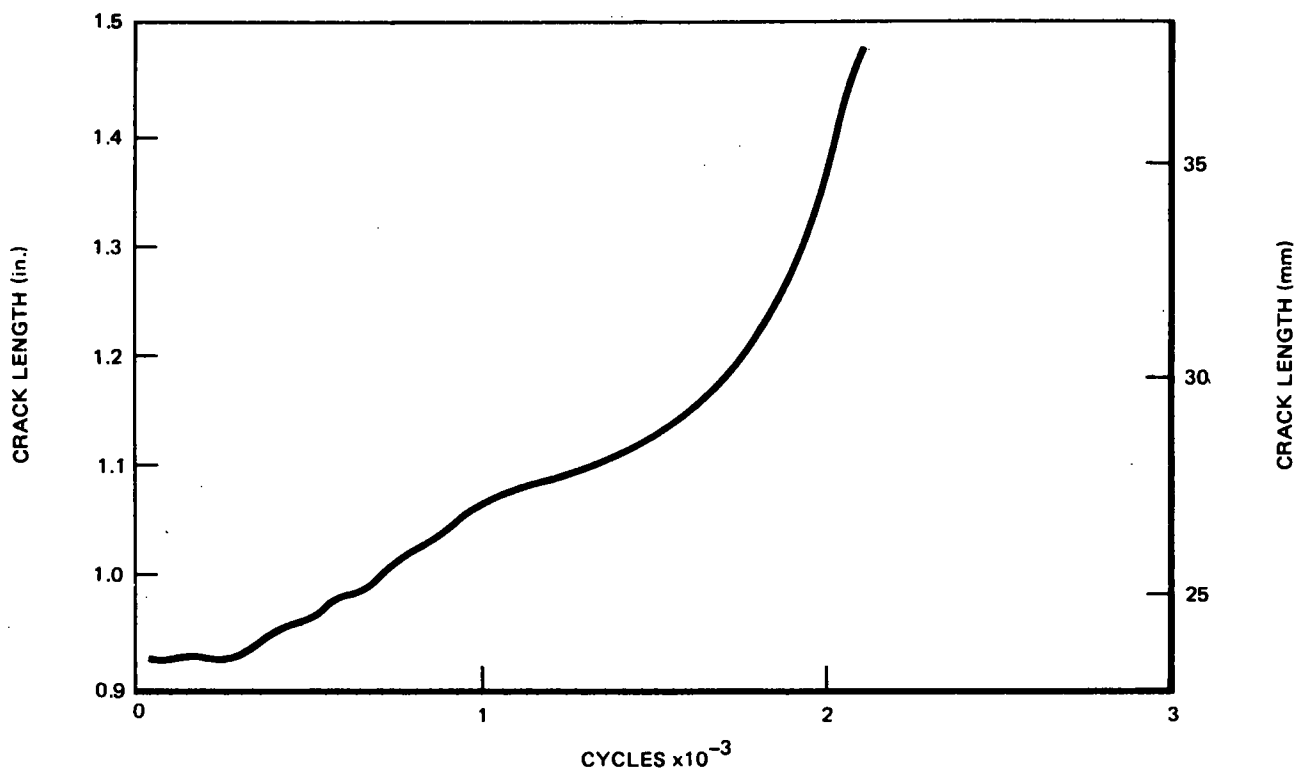


Figure A-5. Fatigue Crack Growth a vs. N at 7.5 Cycles per Hour, Specimen CS-15

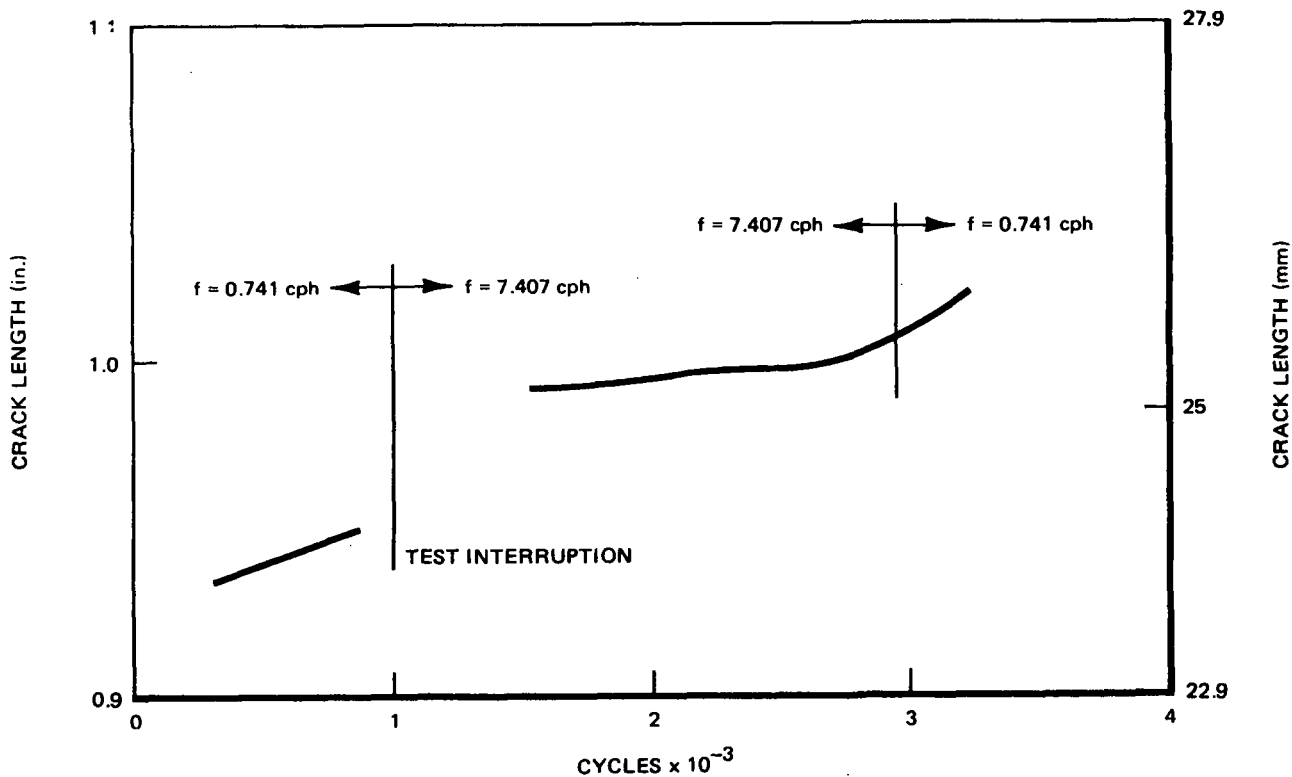


Figure A-6. Fatigue Crack Growth a vs. N , Smoothed Data, Specimen CS-16

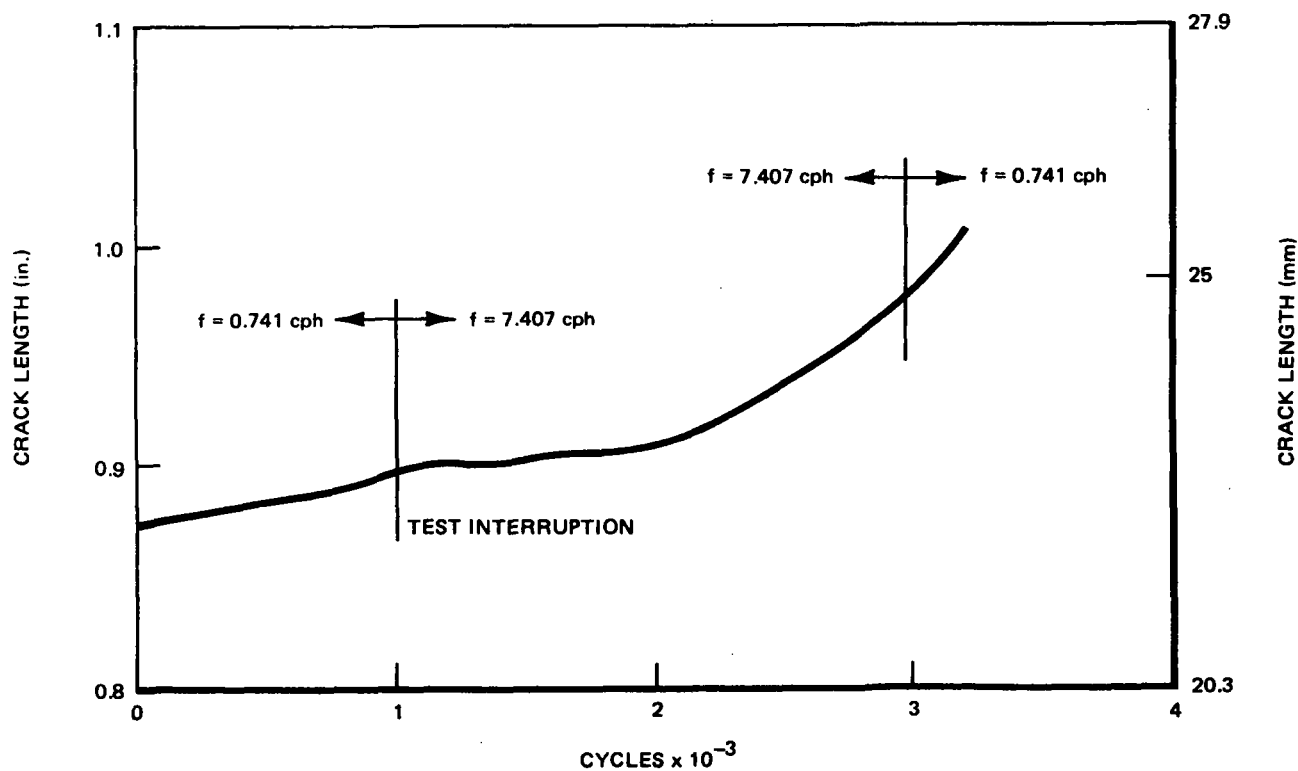


Figure A-7. Fatigue Crack Growth a vs. N , Smoothed Data, Specimen CS-19

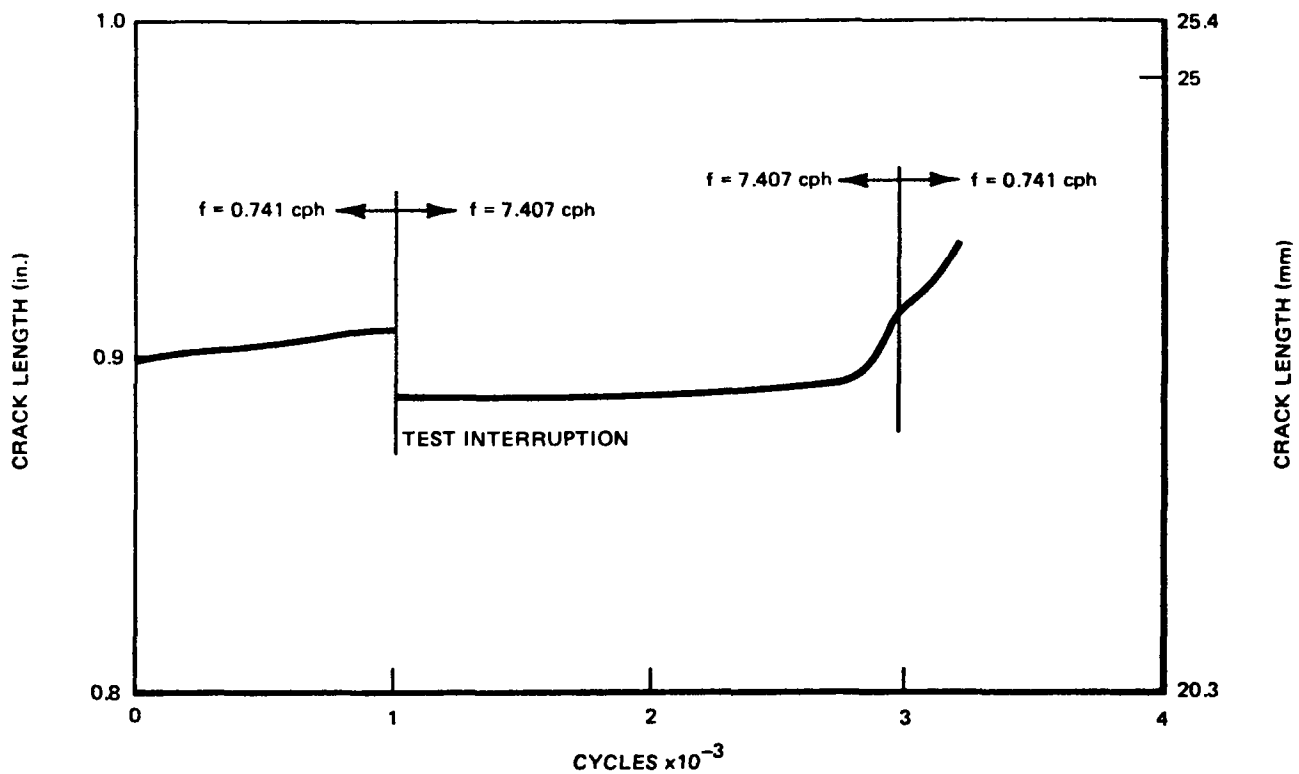


Figure A-8. Fatigue Crack Growth a vs. N, Smooth Data, Specimen CS-20

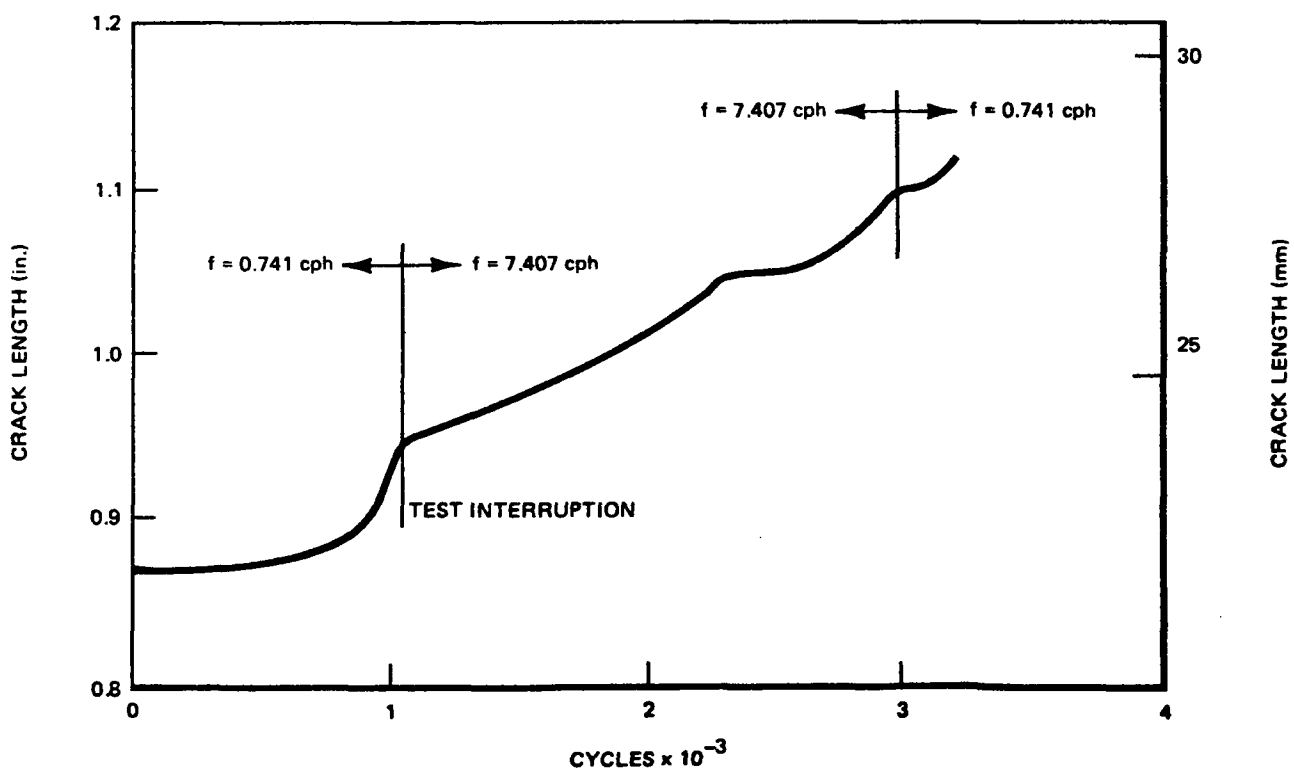


Figure A-9. Fatigue Crack Growth a vs. N, Smoothed Data, Specimen CS-34

Fatigue Crack Growth Through Typical Weld HAZ Microstructures of SA 533 Gr. B Steel in BWR Water Environment

T. Kondo*, H. Nakajima*, H. Takahashi**, and T. Shoji**

* Japan Atomic Energy Research Institute

** Tohoku University

Abstract

Cyclic crack growth behaviour of SA 533 Gr.B steel specimens with microstructures of simulated weld heat-affected zone was examined by testing the materials having a common origin but different thermal history in a typical BWR type water environment. The variation of the heat treatment employed was provided by reproducing the three typical microstructures; ie. (i) Base metal—air quenched and tempered, (ii) Fine grained bainitic portions at HAZ—oil quenched and tempered and (iii) Coarse grained martensitic portions at HAZ, each of which was to simulate the local microstructural constituent appearing along the fusion lines periodically. In order to be consistent with the previous work on the actual HAZ specimens in the methodological bases crack growth rate measurements were made using constant ΔK type contoured double cantilever beam (CDCB) specimens of 30 mm thickness. The test environment used was 288°C water containing 100 ± 50 ppb oxygen, which was prepared by distilling and deionizing processes, and was fed to the test section at the continuous refreshing rate of 1000 ml/min.. No essential difference in the behaviour was noted among all types of materials in the test conditions employed when tests were made in ambient air. In the tests with the BWR type environment all the materials showed some accelerated crack growth relative to the corresponding air results. It was specially noted that the degrees of the acceleration were dependent on the microstructure as had been observed on the actual weld-HAZ only when higher stress(load)ratio, ie. $R = 0.5$ was given, while no notable difference was noted with $R = 0.1$. The highest susceptibility to the environment-enhanced cracking was shown by the hardest (martensitic) material. Based on the measurements of the residual tensile stresses around the weld HAZ portions, an interpretation was made as that the residual stress acted to increase the stress ratio in the specimens taken from the HAZ.

1. Introduction

Structural portions with discontinuities like weld lines and their heat affected zones (HAZ) have been recognized to have some higher probability of containing pre-existing flaws than other portions. It may be also reasonable to suspect that such lines or plates of inhomogeneity would provide a sort of preferred paths for the growth of subcritical flaws in the event of either mechanical or mechano-chemical failure. Evaluation of the response of welded objects to fatigue crack growth in corrosive environments has dual incentives on the above noted aspect in the sense that the local peculiarity at the welded portions consists of mechanical and metallurgical natures, which could have different interactions with the environment. Studies of such aspect on the nuclear pressure vessel steels in simulated coolant environment have been limited in only some exploratory type works^{(1),(2)}. In this study special attention was paid to examine the sensitivity, if any, of the weld HAZ materials of SA533 gr.B steel to the environment-enhanced cracking under cyclic loading. The method employed at this time is to confirm more quantitatively the previously observed phenomenon⁽¹⁾. In the previous work a section of actual weldment was used in a constant K type fracture mechanical specimen. While, in this work, entire blocks of the material were heat treated to provide a bulk body of material that simulated each microportion with respect to their specific metallurgical features.

2. Previous works.

Typical weld HAZ of a SA533 gr.B steel vessel is accompanied by alternately appearing microstructures as shown in Fig.1. Using a contoured double cantilever beam (CDCB) type specimen as shown in Fig.2, the rates of cyclic crack growth was observed during the passage of a crack through weld HAZ. The rate da/dN observed under constant ΔK conditions varied as passing through the tempered martensite and sorbite structures in alternated fashion. Those micro regions responded to the loading in the simulated BWR environment rather differently relative to the crack growth behavior of the same material in air environment. Hard martensite portions generally showed lower crack growth rates than those for the softer fine grained sorbite regions in non-corrosive environments. In the high temperature water and with comparatively high ΔK cycles, the martensitic portions showed substantially accelerated cracking relative to the sorbitic portions. Those results are summarized in Fig.3 and 4. In regard of the fatal limitation of such measurement about the small local portions of the weldment, a confirmative work has been attempted in the present work under mechanically more defined conditions.

3. Experimental

The material used in this investigation was SA533 grade B steel of the chemical composition shown in Table 1. This material, 165 mm thick plate, is from the common heat with the welded material used in the previous study.

In order to cross-check the previous results; which were focused on the sensitivity of the material to the environment-enhanced cracking in the direction along the weld HAZ fusion line⁽¹⁾, some sections of the plate were heat-treated before machining. By the treatment contrastive

difference in microstructure was given to each block without changing the chemical composition among those alternatives and the base metal. Three types of microstructures finally selected were such that (1) the martensite of the highest hardness which was obtained by oil quenching the material, (2) the tempered martensite of intermediate strength obtained by oil quenching and the subsequent tempering and (3) the original base metal with tempered bainite. The heat treatment and its mechanical properties are given in Table 2. The microstructure corresponding to each heat treatment is shown in Fig. 5. From the measured hardness the actual strength level of the coarse grained, tempered martensite which appeared along the weld HAZ was estimated as to amount of between the martensite and the tempered martensite prepared in the present study.

The geometry of the CDCB type specimen employed in this study is shown in Fig. 6. Those specimens were machined from the plates in the "L-S" direction according to the nomenclature of ASTM specification, E399-74⁽³⁾.

Stress intensity factor (k) for this specimen can be calculated by the following equation;⁽⁴⁾

$$K = \sqrt{\frac{4P^2 \times \alpha}{Bn \times B}}$$

where

K: stress intensity factor (MPa \sqrt{m})

P: applied load (MN)

B: overall specimen thickness (m)

Bn: specimen thickness measured between roots of side groove (m)

α : 313 (1/m)

The specimen design taken here has been confirmed to provide a reasonably constant stress intensity factor ranges, ΔK , under cyclic loading of fixed amplitudes during a certain known segment of crack extension⁽⁵⁾. It was also confirmed by the authors that the testing with the CDCB specimens of the present design provides the statistical accuracy of the measurements substantially greater than the standard CT specimens. The quantization of the crack growth rate data was achieved essentially based on the total crack extension divided by the number of cycles producing that increment in each loading condition.

Prior to the onset of testing in water, the specimens were given cyclic loading for the purpose of precracking with the stress intensity factors below 25 MPa \sqrt{m} .

The corrosion fatigue tests were performed with an electro-hydraulic fatigue testing machine of ± 10 ton capacity incorporated with the high temperature and pressure recirculating autoclave system. Distilled and deionized water was continuously fed at the rate of 1000 ml/min through the test section. The details of the apparatus construction and specifications have been reported elsewhere⁽⁶⁾.

The water chemistry condition for the tests in this investigation was as follows:

temperature	288 \pm 2 °C
pressure	8.4 MPa
refreshing rate	1000 ml/min
conductivity	1 > $\mu\text{mho} \cdot \text{cm}^{-1}$
dissolved oxygen	100 \pm 50 ppb

Water quality was continuously monitored at the outlet of the test section as well as at the

inlet to the pressurizing pump.

The wave form and loading frequency employed were triangular and 1 C/min respectively with stress ratios of 0.1 and 0.5.

The fatigue crack growth rate for high temperature water environment was measured by the two independent parallel means, i.e. compliance measurements by means of direct immersion type LVDT attached to the specimen shoulder and the beach marks appeared in the fracture surfaces.

After each run of test, the fracture surfaces were examined with respect to the direction and straightness of the crack extension during the test under measurements. No tendency of either extensive branching or crack tunneling was found on the fracture surface of all the specimens tested. The length of crack allowed to grow for each single loading condition was 1.5 to 2 mm, which was sufficient length to evaluate directly the cyclic crack growth rate da/dN in the form of $\Delta a/\Delta N$.

Fractographic observation was made by SEM before and after removal of corrosion products by an electrochemical technique⁽¹¹⁾.

4. Results

Crack growth rate

The experimentally determined relationships between the crack growth rates (da/dN) and the stress intensity factor range (ΔK) are shown in Fig.7 and 8. The results involve a number of variables; microstructure, test environment and stress ratio. In those results, the following interpretations have been drawn;

- (1) In the ambient air environment, fatigue crack growth rates of the materials of the present study fell around the lower part of the crack growth rate line for surface flaws in the ASME Code, Section XI, regardless of the given variability of microstructure and stress ratio. It is, therefore, judged that the effects of microstructure and stress ratio⁽⁷⁾ on the fatigue crack growth are negligible in the air environment within the range tested.
- (2) The crack growth rates were accelerated in the BWR type water environment relative to those in the ambient air^{(6),(8),(9)}. The increased growth rate acceleration under higher stress ratio conditions reported in literature⁽⁸⁾ was confirmed also in this study. Unlike the results⁽⁸⁾ referred above, the absolute values of the measured growth rate were still below the level of surface crack growth rate (wet) of the ASME Code, Section XI.

To review the observed effect of the increased stress ratio on fatigue crack growth behavior more exactly, the results in Fig.7 and Fig.8 were replotted on the graph with crack growth rate in the water environment ($[da/dN]_{\text{water}}$) versus the crack growth rate in the ambient air ($[da/dN]_{\text{air}}$) for the stress ratios of 0.1 and 0.5 as shown in Fig.9 and Fig.10 respectively. The diagonal solid line of 45° slope in each graph is the line where no net influence of environment exists. Similarly any deviation of the datapoint to either side corresponds to either acceleration or deceleration of the growth rate in the water environment.

Comparing the two graphs, it can be interpreted that the sensitivity of the hardened material to the environment-enhanced cracking becomes apparent only with increased stress ratio.

Figure 11 shows another version of the results, in which an acceleration factor was defined as $[da/dN]_{\text{water}}/[da/dN]_{\text{air}}$, and plotting was made against the stress intensity factor range.

Here, again, unity of the acceleration factor indicates the neutrality of the environment to the crack growth acceleration in the aqueous environment. The obtained large degree of acceleration occurring in the material with hard martensite is to be recognized as the effect specific to the combination of the metallurgical state of the material and the aqueous environment.

Fractography

Examination of all the fracture surfaces after removal of surface films yielded only ductile striations that are generally seen in the SA533 gr. 8 specimens cyclically cracked in the BWR type water environment. The representative microfractographs for the three types of materials, cracked in water with stress ratio of 0.5, are compared in Fig. 12. As shown in Fig. 13, the stress intensity factor level applied is reflected in the feature of the fracture surface, where trend of sub-crack formation is seen to be increased either by increasing ΔK or stress ratio.

5. Discussion

The results of the present work agreed in the respect that the stronger martensitic micro-structure has some sort of susceptibility to the cracking when cyclically loaded in the high temperature aqueous environment containing oxygen of nearly equal concentration to that in BWR. The existence of the dissolved oxygen of such levels, however, is not known to be an essential prerequisite to the observed kind of crack enhancement. In the previous work on the weld HAZ, environmentally-accelerated crack growth at the martensitic portion was observed in the tests of low stress ratio ($R=0.2$). In contrast, the results of the present work indicated that the similar acceleration phenomenon could occur only when the stress ratio was high. This apparent discrepancy is explained by the existence of tensile residual stress at the HAZ considered here.

The residual stresses in the weldment used in the previous work can be estimated by referring to the early work⁽¹²⁾ on the measurement of residual stresses in the weldment of the same lot. The measurements were made along the X and Y directions by applying strain gauges at the spots indicated in Fig. 14, and the specimen was cut to follow the resultant relief of internal stresses. The results of the measurements are shown in Fig. 15. At least about 10 - 20 MPa (1 - 2 kg/mm²) of tensile stresses seem to remain in the HAZ. In the actual case perhaps somewhat higher levels could have existed in certain local portions in view of the non uniformity seen in the measured results.

In order to see approximately if such levels of residual stress can contribute to shift the practical stress ratio acting on the growing crack tip, a rough estimation is made by using a simplified model. Assuming that tensile residual stress in the direction parallel to the loading axis of a 1T-CT specimen under cyclic loading remains to act together with the externally loaded stress, the values of the resultant K at the crack tip is figured out as a simple sum of the two elements. The results of the estimation are drawn in Fig. 16. The possible levels of effective stress ratio under given external loading may, then, be expressed as in Fig. 17.

The crack growth rate tests carried out using welded specimens with the tensile residual stress were, therefore, recognized as the test with stress ratio higher than the nominal test conditions by certain extent depending on the level of the tensile stress remained.

The requisite of higher stress ratio for the enhanced cracking of the martensite structure to occur, as observed in this work, seems to suggest that there would be some critical K level, above which the process comes into operation. Such a speculation is schematically illustrated

References

1. Suzuki, M., Takahashi, H., Shoji, T., Kondo, T. and Nakajima, H., "The Environment Enhanced Crack Growth Effects in Structural Steels for Water Cooled Nuclear Reactors", in The Influence of Environment on Fatigue, Inst. Mech. Engrs., London, 1977, p. 161 - 169.
2. Mager, T.R. and McLoughlin, V.J., "Effect of an Environment of High Temperature Primary Grade Nuclear Reactor Water on the Fatigue Crack Growth Characteristics of A533 Grade B Class 1 Plate and Weldment Materials", WCAP-7760(HSSTP-TR-16), October 1971.
3. ASTM Standard E399-74, "Standard Method of Test for Plane-Strain Fracture Toughness of Metallic Materials", 1974.
4. Mostovoy, S., Crosley, B.P. and Ripling, E.J., "Use of Crack-Line Specimens Measuring Plane-Strain Fracture Toughness", J. Material, vol. 2, No. 3, 1967, p. 661 - 681.
5. Nakajima, H., Shoji, T., Kikuchi, M., Niitsuma, H. and Shindo, M., "Detecting Acoustic Emission During Cyclic Crack Growth in Simulated BWR Environment", in Fatigue Crack Growth Measurement and Data Analysis, ASTM STP 738, to be published in 1981.
6. Kondo, T., Kikuyama, T., Nakajima, H., Shindo, M. and Nagasaki, R., "Fatigue of A302 Grade B Steel in High Temperature Simulated Nuclear Reactor Environment", Proc. 1st Int. Conf. on Corrosion Fatigue, NACE and AIME, 1972, p. 539 - 556.
7. Paris, P.C., Bucci, R.J., Clark, W.G. and Mager, T.R., "Extensive Study of Low Fatigue Crack Growth Rates in A533 and A508 Steels", in Stress Analysis and Growth of Cracks, ASTM STP 513 part 1, 1972, p. 141 - 176.
8. Bamford, W.H., "Application of Corrosion Fatigue Crack Growth Rate Data to Integrity Analysis of Nuclear Reactor Vessels", ASME Publication 79-PVP-116, ASME, 1979.
9. Cullen, W.H. and Torronen, K., "A Review of Fatigue Crack Growth of Pressure Vessel and Piping Steels in High-Temperature, Pressurized Reactor-Grade Water", NUREG/CR-1576, NRL Memorandum Report 4298, September 1980.
10. Bamford, W.H., "The Effect of Pressurized Water Reactor Environment on Fatigue Crack Propagation of Pressure Vessel Steels", in The Influence of Environment on Fatigue, Inst. Mech. Engrs., London, 1977, p. 51 - 56.
11. Yuzawich, P.M. and Hughes, C.W., "An Improved Technique for Removal of Oxide Scale from Fractured Surfaces of Ferrous Materials", Practical Metallography, vol. 15, 1978, p. 184 - 195.
12. Suzuki, M., Komura, I. and Takahashi, H., "Nondestructive Estimation of Residual Stress in Welded Pressure Vessel Steel by means of Remanent Magnetization Measurement", Int. J. Pres. Ves. & Piping, vol. 6, No. 1, 1978, p. 87 - 112.
13. Brown, W.F., Jr and Srawley, J.E., "Plane Strain Crack Toughness Testing of High Strength Metallic Materials", ASTM STP 410, 1967, p. 12.

in Fig. 18, where the observed phenomenon is given a tentative nomenclature of "stress corrosion cracking" although no positive evidence to define the phenomenon has been provided yet. To the moment such a speculation made here may subject to a criticism in regard of the lack of any peculiarity in the fractography of the materials cracked in the fashion of the present interest. Further studies are being extended to the examination of the cracking behaviours of various structural steels with wide variety of strength.

5. Conclusions

Using specimens heat treated to represent the weld-induced microstructure, cyclic crack growth tests were conducted with special emphasis placed on the effect of high temperature water environment on the crack growth rate. Based on the test results, The following conclusions were drawn;

- (1) The material with martensitic microstructure prepared from SA 533 gr. B steel by oil quenching showed higher susceptibility to the environment-enhanced cyclic crack growth when tested in BWR type water at 288°C.
- (2) The effect was apparent under the condition of higher stress ratio($R=0.5$) but was not appreciable with lower stress ratio($R=0.1$).
- (3) The results were considered as qualitatively consistent with the observed cyclic crack growth behavior along the HAZ of a weldment.

Table 1 Chemical composition of material(wt%)

C	Si	Mn	P	S	Ni	Cr	Mo	Cu	V	Sb	As	Sn
0.17	0.02	1.48	0.011	0.006	0.58	0.16	0.52	0.13	0.003	0.0041	0.015	0.008

Table 2 Heat treatment and room temperature tensile properties of specimen materials

Heat Treatment	Tensile Properties		
	Yield Strength MPa	Ultimate Tensile Strength MPa	Total Elongation %
890°Cx3.5hr A.C. → 660°Cx3.5hr F.C. → 600°Cx40.5hr F.C.	480	608	27.0
1000°Cx30min O.Q.	1103	1128	19.3
1000°Cx30min O.Q. → 620°Cx40.5hr F.C.	499	629	30.0

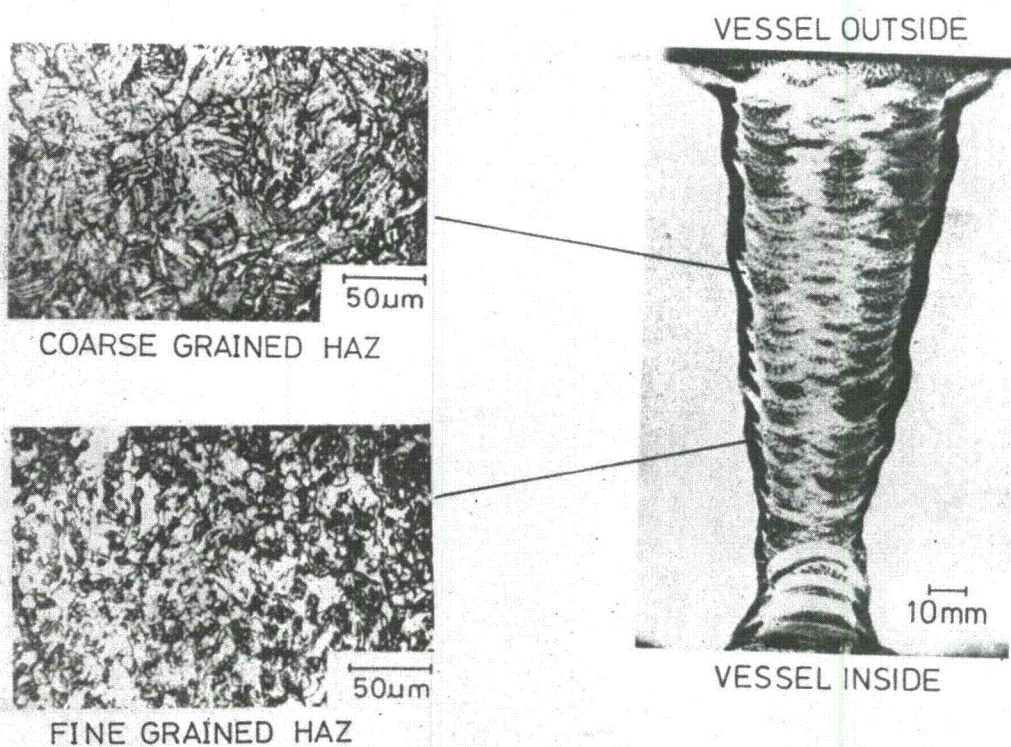


Fig. 1 A macro-etch photograph of multi-pass submerged-arc weldment and typical weld HAZ microstructures.

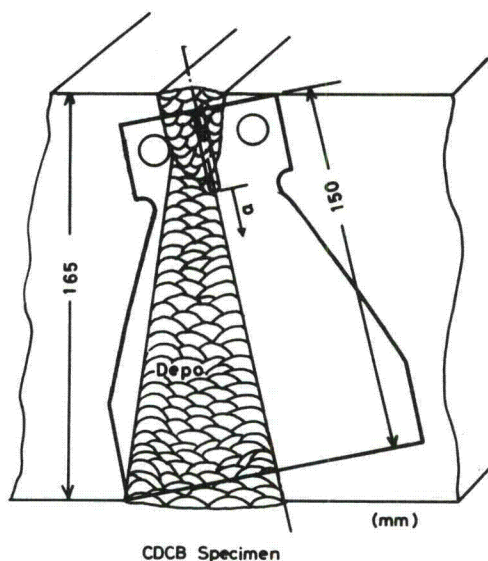


Fig. 2

Specimen extraction method from the original plate.

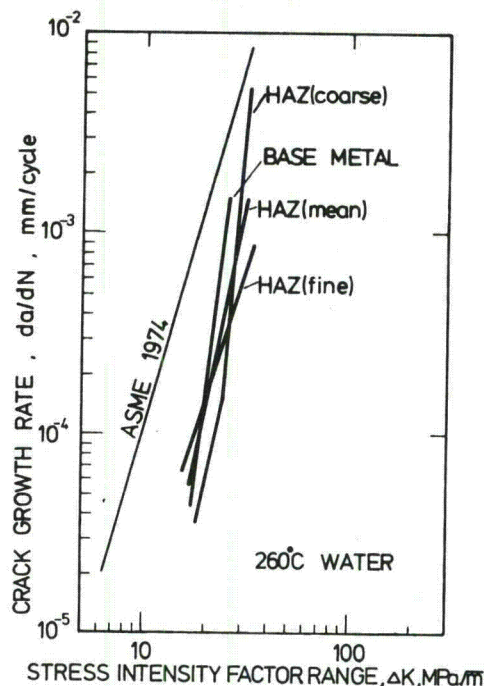


Fig. 3

Fatigue crack growth rate of weld HAZ (coarse grained tempered martensite and fine grained sorbite) in high temperature aqueous environment.

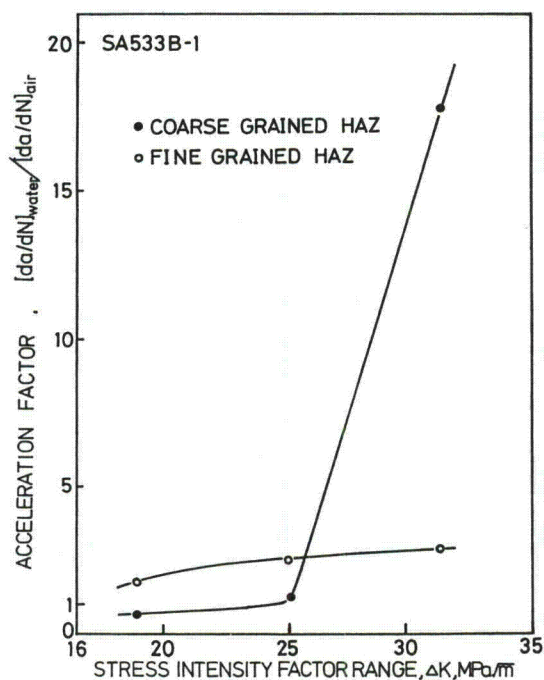
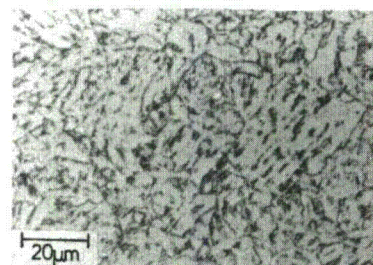
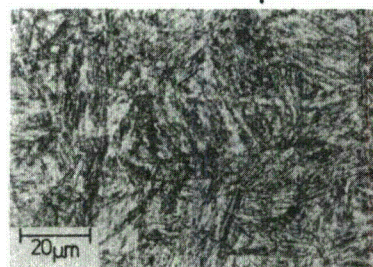


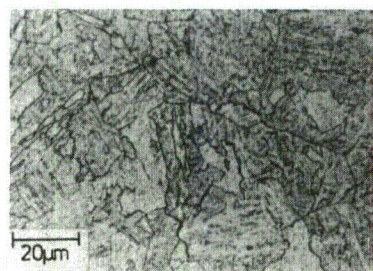
Fig. 4 Relationship between fatigue crack acceleration factor vs stress intensity factor range.



Air Quench-Tempered



Oil Quenched



Oil Quench-Tempered

Fig. 5 Three types of microstructures which were obtained by the various heat treatments.

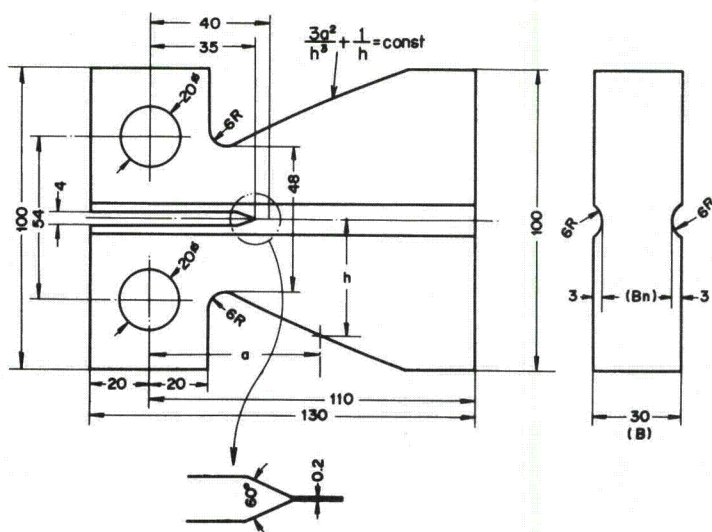


Fig. 6 Geometry of contoured double-cantilever beam type specimen.

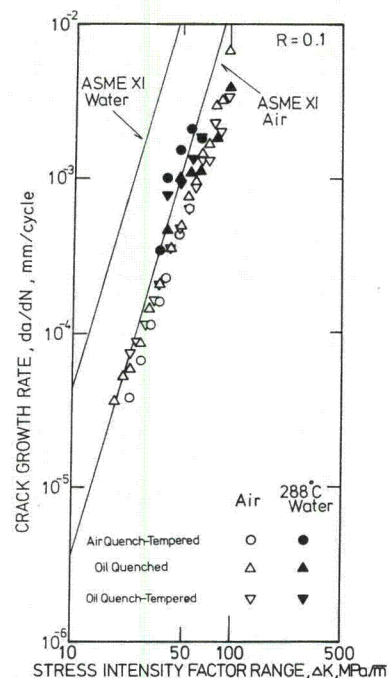


Fig. 7

Relationship between crack growth rate vs stress intensity factor range under stress ratio of 0.1 in ambient air and simulated BWR environments.

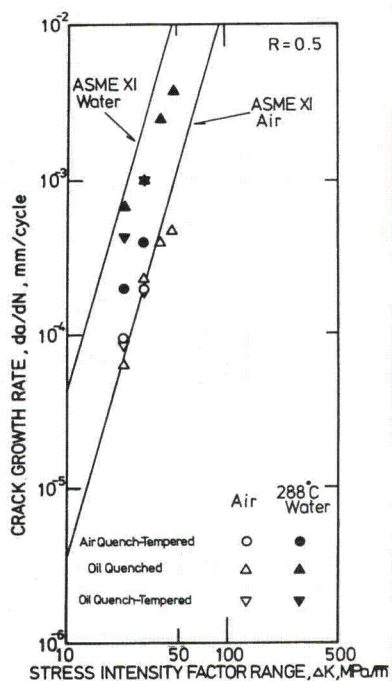


Fig. 8

Relationship between crack growth rate vs stress intensity factor range under stress ratio of 0.5 in ambient air and simulated BWR environments.

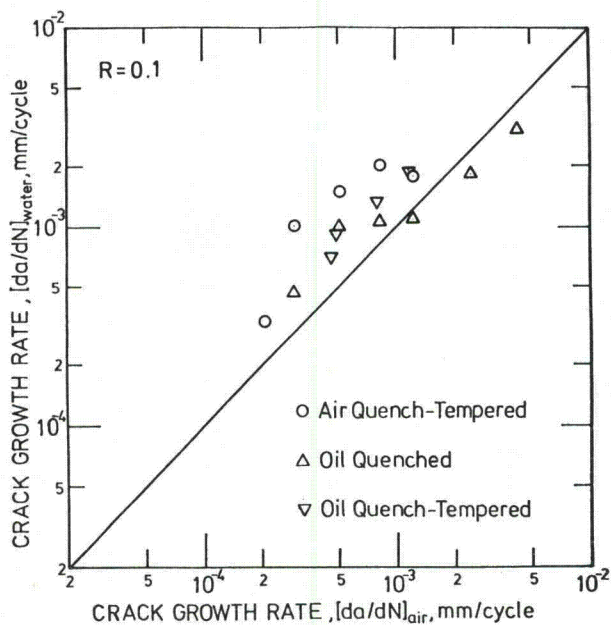


Fig. 9 Relationship between $[da/dN]_{\text{water}}$ vs $[da/dN]_{\text{air}}$ under stress ratio of 0.1.

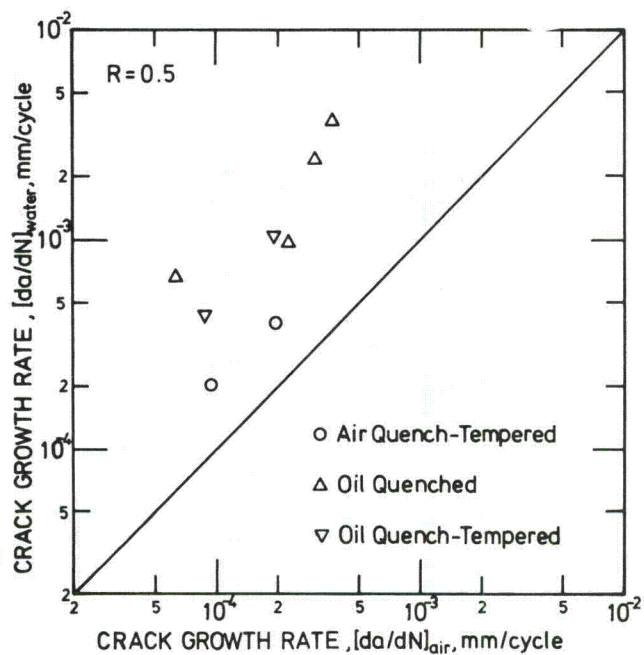


Fig. 10

Relationship between $[da/dN]_{\text{water}}$ vs $[da/dN]_{\text{air}}$ under stress ratio of 0.5.

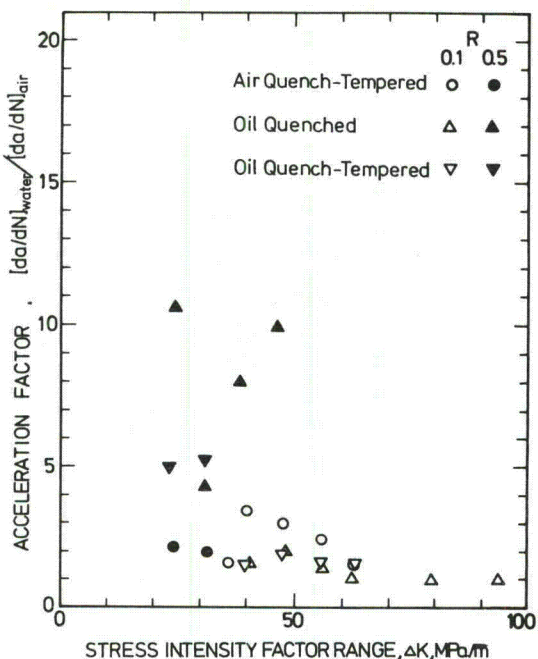


Fig. 11

Relationship between fatigue crack acceleration factor vs stress intensity factor range.

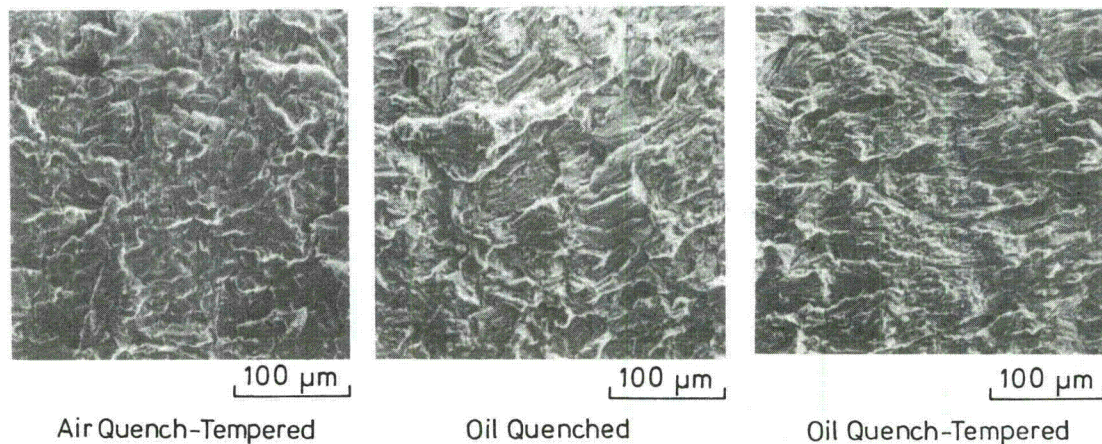


Fig. 12 Scanning electron micrographs of typical fracture surfaces for three different microstructures fatigue tested in simulated BWR environment.



$\Delta K = 31 \text{ MPa}/\sqrt{\text{m}}$

100 μm



$\Delta K = 46 \text{ MPa}/\sqrt{\text{m}}$

Oil Quenched

$R = 0.5$

CRACK PROPAGATION DIRECTION

Fig. 13 Effect of stress intensity factor range on fractographic feature of material with martensite.

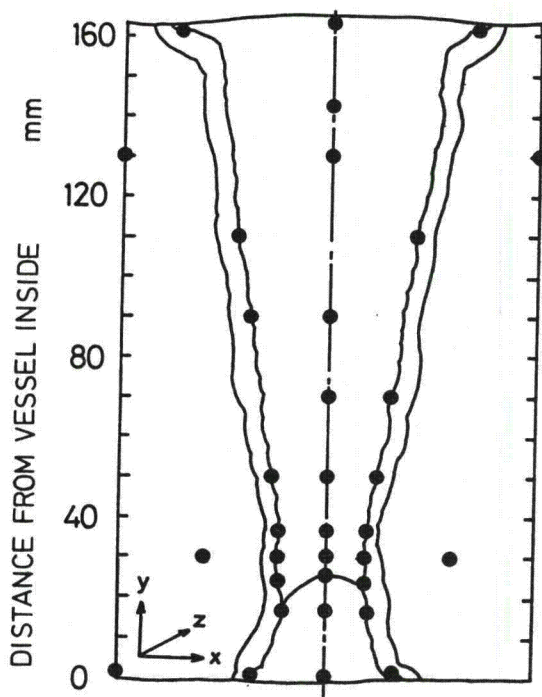


Fig. 14 Measuring points of residual stress.

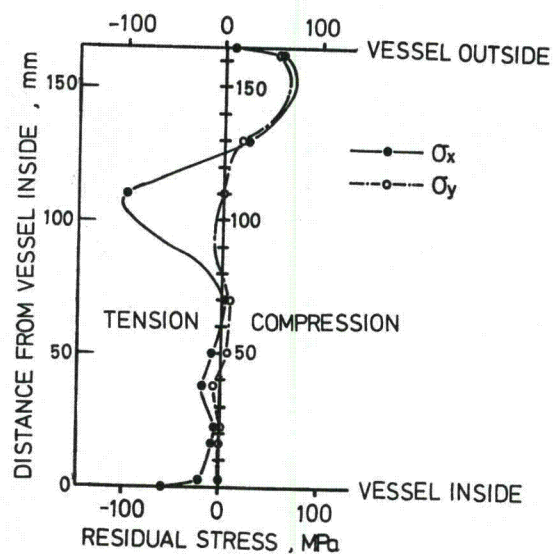
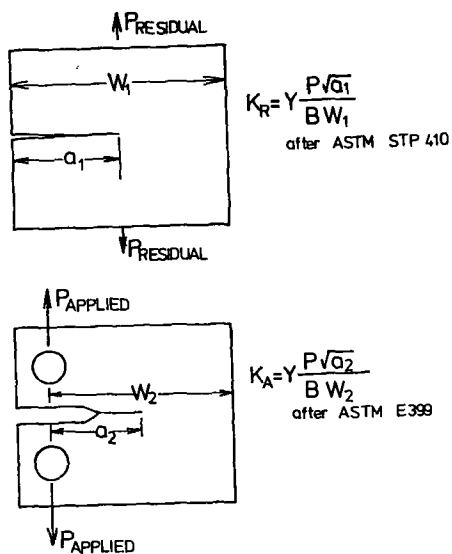


Fig. 15 Distribution of residual stress along the fusion line after stress relief treatment at 600°C for 40 hr.



$$K_{ACTUAL} = K_{RESIDUAL} + K_{APPLIED}$$

Fig. 16 K calculation method for both single-edge-cracked specimen in tension and compact tension specimen.

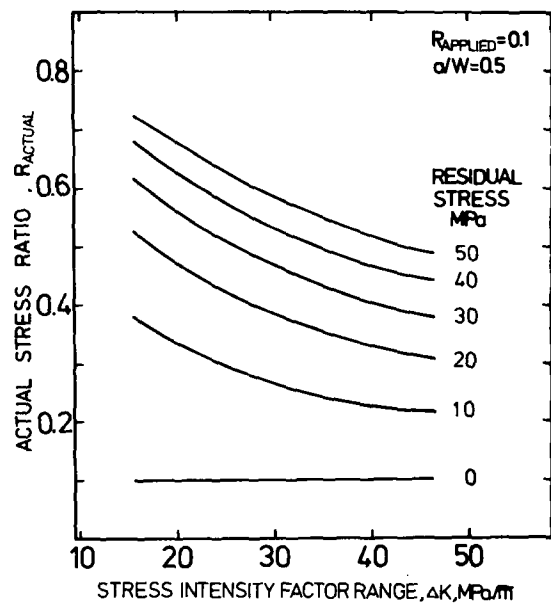


Fig. 17 Relationship between actual stress ratio vs stress intensity factor range in consideration of the effect of residual stress.

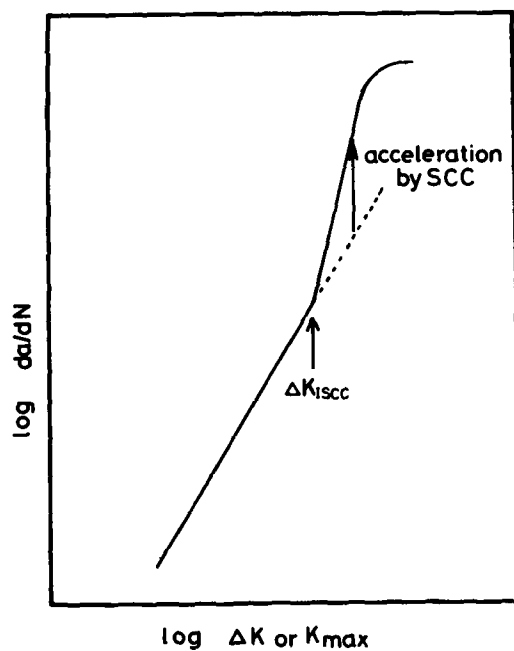


Fig. 18 Schematic diagram for time-dependent crack growth behavior.

CRACK GROWTH BEHAVIOR OF SENSITIZED STAINLESS STEEL IN HIGH TEMPERATURE, HIGH PURITY OXYGENATED WATER

RM Horn, DA Hale, CW Jewett, CH Lange, and JN Kass

Crack growth rates for sensitized Type-304 stainless steel in high temperature, high purity oxygenated water were studied under both cyclic and non-cyclic loading conditions. Fracture mechanics test specimens were utilized to develop the laboratory data in stainless steel with various degrees of sensitization. Cyclic crack growth tests were performed to evaluate the roles of cyclic frequency and degree of sensitization in oxygenated water. Crack growth rates were measured and the conditions resulting in IGSCC were identified. Non-cyclic constant load tests under varying coolant oxygen conditions and varying degrees of sensitization were also performed successfully to develop crack growth rate data. Evaluation of all growth data as a function of coolant oxygen, sensitization level, and loading mode were made. The significance of these data is discussed in terms of formulating potential in-service inspection plans.

INTRODUCTION

The stress corrosion cracking behavior of Type 304 stainless steel in oxygenated high temperature water has been extensively studied. Excellent overviews have been provided by Cowan, Gordon, and Tedmon^{1, 2}. The well known chromium depletion model³ has been successfully used to explain the observation that intergranular stress corrosion cracking will occur if the material is sensitized by thermal treatment and then exposed to high stress in the presence of oxygenated water. Most of the studies⁴⁻⁷ have involved the use of test specimens designed to assess crack initiation under constant load or constant extension rate using small tensile specimens, although recently, studies involving welded pipes have been conducted. The fracture behavior has been found to depend on coolant oxygen, degree of sensitization, and load or loading rate.

There is also a need to assess the crack propagation resistance of this material using a fracture mechanics approach under various types of loading to assess the usefulness and examination frequency of in-service inspection programs that may potentially be implemented. As in any fracture mechanics study, information is needed on material properties, stress, and stress intensity factors in the component to be evaluated. This paper provides an assessment of the crack propagation materials properties.

Some previous work in both high temperature and low temperature water has already been conducted⁹⁻¹². Most of this work has been studies of

fatigue crack growth. In Reference 8, Kawakubo et al provided a comprehensive study of cycle frequency load waveshape and coolant oxygen effects on heavily sensitized material. Slow cycle frequency and high coolant oxygen were found to enhance growth rates. In Reference 9, Ford studied heavily sensitized material at 93°C/1.5 ppm oxygen. His studies were focused on an assessment of cycle frequency and mean stress. The influence of these parameters on the threshold stress intensity factor for cracking and on crack growth rates was amply discussed. However, only a very limited amount of test data has been generated to assess behavior under sustained load^{6, 9}.

The purpose of this study was to assess the crack growth behavior of Type 304 stainless steel under both cyclic and constant loads and to determine the variation in behavior as a function of the main variables that influence crack initiation behavior, degree of sensitization, and coolant oxygen. By performing this study, a methodology to predict the behavior of stainless steel components with ASME code procedures for ferrite steels is being developed. This would allow the continued use of T-304 stainless steel components instead of their removal and replacement with IGSCC resistant stainless steel developed for current boiling water reactor applications, thus sparing utilities costly and untimely outages for repair.

EXPERIMENTAL PROCEDURES

A. Test Facilities

The high pressure/temperature water environment used for this program was provided by a high flow test loop (Environmental Fatigue Loop 1) in General Electric's Experimental Mechanics Laboratory.

A schematic drawing of this loop is shown in Figure 1. The loop included a canned rotor pump which provided sufficient flow (~12 gallon/minute) to ensure that all specimens tested in the loop were subjected to a refreshed environment. Bypass demineralizer beds were provided to maintain the conductivity and pH of the demineralized water environment. The level of dissolved oxygen, conductivity and pH of the loop water was continuously monitored during testing. Dissolved oxygen level was controlled by a gas control system that continuously purged a gas mixture through the makeup tank at a rate needed to establish the desired dissolved oxygen level in the makeup water which was added continuously to the loop.

Cyclic specimen loading was accomplished using a closed loop electrohydraulic test machine that applied a cyclic load to a group of up to six specimens arranged in a series chain inside a pressure vessel. Constant load tests were performed under dead weight loading or using a servohydraulic machine. A computer was available for use with the servohydraulic test machines to acquire and analyze the data.

B. Test Specimen/Techniques

Cyclic and constant load tests were run as part of this program. Compact Tension (CT)-type crack growth test specimens containing side grooves were used for the cyclic tests¹⁰. The primary technique used to monitor crack growth utilized a high temperature/high pressure linear variable differential transformer (LVDT) to measure the specimen crack opening displacement (COD) which accompanied specimen loading. The resultant load/COD data (i.e., compliance) was used to calculate crack lengths using standard relationships.¹¹

The majority of constant load crack growth tests were performed under constant load using tapered double cantilever beam (TDCB) specimens. The specimen is displayed in Figure 2. The TDCB specimen was used to produce a stress intensity field that was only a function of the applied load and specimen thickness, and therefore, independent of crack length. This specimen design has been used before by VanderSly and others¹²⁻¹⁴. The other constant load tests were conducted using CT specimens. As in the cyclic tests, LVDTs were used to measure in-situ compliance. In addition, room temperature clip gage compliance measurements were used to supplement LVDT measurements; in the TDCB specimens, these measurements were used to evaluate crack growth rates. The use of an on-line computer greatly facilitated data acquisition for the CT specimens. Accurate and repeatable compliance data could be obtained by averaging many load displacement pairs from three unload-load cycles for any single compliance data point.

C. Material Condition

The material for testing was taken from two heats of Type 304 stainless steel. The compositions are listed in Table I. The material was received in the solution annealed condition. The room temperature and 288°C (550°F) tensile properties are listed in Table I. Prior to testing, the material received a heat treatment to sensitize the material to various desired levels. To select the heat treatment to impart this sensitization, a study was performed on each heat to evaluate isothermal heat treatments. Using the results of Clarke to guide heat treatment parameters¹⁵, an isothermal study at 621°C (1150°F) was performed to select the proper isothermal holding time. Electrochemical Potentiokinetic Reactivation (EPR)¹⁶ response of the heats was used to evaluate the heat treatment. Figure 3 shows this response for the two heats used. Using Clarke's data that showed that an EPR value of $\sim 15 \text{ C/cm}^2$ was typical of many weld heat affected zones, the 621°C, 2 hour treatment was chosen to represent the weld sensitization treatment. A 621°C, 24 hour treatment was selected to represent furnace sensitization, an extremely sensitized material condition.

D. Test Matrices

Two separate testing efforts have been carried out. The test program, cyclic crack growth evaluation, and constant load crack growth evaluation, will be detailed separately.

1. Cyclic Crack Growth

Six specimens were tested as this part of a complete study at the General Electric Nuclear Energy Division^{17, 18}. These tests were conducted at two frequencies, 7.5 cph and 0.74 using a skewed sawtooth waveform. The tests were conducted at one oxygen level, 0.2 ppm O₂. Three sensitization levels were investigated with emphasis on the weld sensitization and furnace sensitization treatments. The test matrix is given in Table II. All of these tests were conducted at an R-ratio, K_{max}/K_{min} , of 0.6. A prior study also included sensitized and non-sensitized material with testing performed at higher frequencies with different R-ratios where environmental effects were limited¹⁸.

2. Constant Load Crack Growth

As part of this study, six tests were performed under constant load conditions. These tests were directed toward gathering crack growth data under in-service environment, load and/or sensitization conditions. These tests were conducted to supplement

other unpublished data gathered at General Electric by Clarke and Wang. Two tests were run in furnace sensitized material in 8 ppm O_2 to supplement existing data. Tests of ~1000 hours duration were conducted under constant load rising stress intensity conditions. In addition, four tests were performed using the TDCB specimens, under constant stress intensity conditions. These specimens were weld sensitized and were tested in 0.2 ppm O_2 high temperature water. These tests were conducted for ~6600 hours. Table III lists all the tests and the test parameters.

CYCLIC LOAD RESULTS

Plots of crack length as a function of cycles were generated for each of the specimens tested. These data are summarized in Figure 4. Crack growth on the order of 0.150" over ~1500 hours occurred in each specimen tested. Each point represents the average of several in-situ measurements. The high R-ratio led to low K-ranges and slow changes in the crack growth driving force. The emphasis of this study was to evaluate the influence of sensitization on cyclic crack growth at the very low frequencies (≤ 7.5 cph). Earlier work at higher frequencies on materials both sensitized and non-sensitized showed that the 0.2 ppm O_2 288°C water did not enhance crack growth rates significantly¹⁸.

The first group of three specimens tested in this phase (7.5 cph, $R=0.6$), SS-10, SS-11, and SS-12, represented different degrees of sensitization. Table II shows that these specimens had EPR values ranging from 10.5 C/cm^2 (SS-11) to 27 C/cm^2 (SS-10). The points have been plotted as crack growth rate (in/hr) versus maximum stress intensity factor (K_{max}) in Figure 4. Notice that all the points plot in the same vicinity, indicating that the three degree of sensitizations exhibited similar environmental crack growth rates at this frequency. This effect was also exhibited by specimens SS-7 and SS-21, both tested at 0.74 cph and $R=0.6$. These specimens covered the same range of sensitization; SS-7 having an EPR value of 13 C/cm^2 and SS-21 having a value of 27 C/cm^2 . As seen in Figure 4, these points also plot in the same location again showing no differences in crack growth rates over the sensitization range. Figure 5

shows this data compared to higher frequency data from the earlier studies. On a time basis, the rates are consistent with the previous data.

There were, however, differences in fracture morphology related both to the differences in DOS among Specimens SS-10, -11, and -12, and to the change in load level for a given specimen. All the previous tests at higher frequencies produced pure transgranular fractures. Specimen SS-10 exhibited considerable areas of mixed mode (intergranular (IG) + transgranular) morphology corresponding to the first phase of testing when low loads were used. Corresponding areas on Specimen SS-11 were predominantly transgranular with a slight indication of IG. The corresponding areas on Specimen SS-12 were totally transgranular in nature. Specimen SS-10 (high DOS) also exhibited small patches of IG morphology near both sides, immediately behind the fatigue precrack. No purely IG cracking was observed anywhere in Specimens SS-11 (medium DOS) or SS-12 (low DOS).

On the other hand, all three specimens (SS-10, -11, and -12) experienced transgranular cracking when much higher loads were used. This same effect of DOS on fracture morphology was observed in the 0.75 cph specimens (SS-7 with medium DOS, and SS-21 with high DOS). Specimen SS-7 displayed behavior very similar to SS-11; i.e., transgranular cracking with slight indications of IG. Specimen SS-21 was totally intergranular. Much more IG was noted in Specimen SS-21 than SS-10, which was expected since SS-21 was run at a slower frequency. Figure 6 compares the fracture surfaces of SS-7 and SS-21. Thus, slower frequencies and/or higher DOS promoted intergranular cracking.

DOS does not dramatically affect macroscopic crack growth rates on a time basis, even though it completely changes fracture morphology.

Specimen SS-21 did show the highest crack growth rates, however. The effects of frequency and oxygen concentration on crack growth rates and the mode of fracture of sensitized stainless steel were also investigated by Kawakubo⁸. These data showed that frequency and oxygen concentration affect the fracture mode only at slower frequencies and higher oxygen concentrations, promoting intergranular cracking, particularly in 8 ppm O₂.

Figure 7 compares the General Electric highly sensitized data of Figure 4 with the 0.2 ppm oxygen concentration data of Kawakubo.⁸ The Kawakubo data were obtained at low mean stress levels while the GE sensitized data were obtained at high mean stress levels. In order to make the comparison meaningful, the crack growth rates were plotted versus effective stress intensity factor to normalize the mean stress effects. At the three higher frequencies, 300 cph, 18 cph, and 7.5 cph, the GE sensitized data agree reasonably well with the data from Kawakubo. However, the data for the slowest frequency specimen (SS-21) do not compare as favorably. This lack of agreement is due to the high mean stress which promoted IGSCC in the General Electric low frequency data, leading to accelerated crack growth. This is better shown in Figure 8 which displays crack growth rates on a per cycle basis against frequency. It can be seen that only at the slow frequencies are the crack growth rates higher. At the slowest frequency, ~.7 cph for both sets of data, the GE 0.2 ppm O₂ data at high R and the Kawakubo 8 ppm O₂ data show the extreme enhancement in crack growth per cycle. Figure 9 summarizes the role of frequency

and sensitization on crack growth mode. Only at frequencies below 10 cph is any intergranular cracking experienced. IGSCC then only occurs in high DOS under cyclic loading, whether in 8 ppm O_2 or 0.2 ppm O_2 high temperature water. Note that at the relatively high cycle frequencies where non-intergranular cracking occurs there is little difference between behavior in 0.2 and 8 ppm oxygenated water. At the slowest frequencies where intergranular cracking occurs, more rapid growth rates were found in 8 ppm than in 0.2 ppm oxygenated water by Kawakubo. However, our study showed little difference under these conditions when the material was highly sensitized. This could be due to the higher mean stress.

CONSTANT LOAD RESULTS

The data from the six tests performed under constant load are displayed in Figure 10. This figure shows additionally the unpublished data previously generated by Wang and Clarke in furnace sensitized material exposed to 8 ppm O_2 . The data generated in furnace sensitized material exposed in 8 ppm O_2 which was totally IG in character fits well with data already generated. The crack growth rates continuously increase as the stress intensity increases over the range of $10 \text{ ksi}\sqrt{\text{in}}$ to $34 \text{ ksi}\sqrt{\text{in}}$. Although only one point was plotted for each test, several hundred hours of exposure were used to evaluate crack growth with in-situ compliance measurements. The data from the weld sensitized specimens exposed to 0.2 ppm O_2 high temperature water are significantly different. These tests, performed for several thousand hours resulted in small but meaningful amounts of IGSCC. Figure 11 shows the fracture appearance of the Specimen 4904 SS-1. The room temperature compliance measurements and the actual crack length measurements agreed well. These measurements as well as visual side measurements identified when crack initiation had taken place. The rates derived from these measurements were an order of magnitude slower than those measured in the furnace sensitized specimens.

The characteristics of the crack growth are somewhat different than the classic three stage stress corrosion behavior where a plateau region is exhibited.¹⁹ The furnace sensitized data does show similarities to other data generated by Ford on stainless steel in 1.5 ppm O_2 , 93°C high purity water.⁹ It also is similar in rate to the cyclic crack

growth data generated by this study and by Kawakubo⁸. The data does show a very high dependence on the stress intensity which is characteristic of stress corrosion in a variety of systems²⁰⁻²³.

The weld sensitized data is more sparse. The growth rates at stress intensity levels of 20 and 24 ksi/ $\sqrt{\text{in}}$ are similar to one another. The specimens exposed at higher stress intensity levels exhibited some non-uniform cracking at the sides, increasing the average crack advancement and, in turn, the average crack growth rate. All this data could only support a simple linear crack growth dependence on K. The data, however, does supply evidence that coolant oxygen content and/or sensitization level has a very important influence on the magnitude of the growth rate. The growth rates for the lower coolant oxygen and weld sensitization level are much lower than that for the high oxygen and high degree of sensitization condition.

It was important then to determine the extent to which coolant oxygen and degree of sensitization, as separate variables, influence results. Two additional CT specimens were prepared with high sensitization (621°C/24 hours) and weld sensitization (621°C/2 hours) in a 0.2 ppm oxygenated water. These specimens were tested between 22 and 33 ksi/ $\sqrt{\text{in}}$. Initial results are showing that the high sensitization sample has a growth rate much higher than the weld sensitization samples, but still a factor of two lower than the highly sensitized specimens in 8 ppm oxygenated water at $K > 27$ ksi/ $\sqrt{\text{in}}$. Thus, both degree of sensitization and coolant oxygen content appear to be important in the determination of the crack growth rates for static load conditions.

CRACK GROWTH DISCUSSION

Ford²⁴ has recently applied the slip-dissolution model of crack propagation to quantitatively predict observed crack growth rates in sensitized stainless steel tested in 1.5 ppm 100°C oxygenated water. The slip dissolution model is basically an electrochemical mechanism that considers the time period for formation of oxide at the crack tip and fracture of this oxide by mechanical loading. The crack velocity is expressed as:

$$V = \frac{M}{\rho FN} \cdot \frac{Q_f}{t_f} \quad (\text{Reference 25})$$

where V = crack growth rate

M, ρ = atomic weight and density of metal

N = valence change during oxidation process

F = Faraday's constant

t_f = periodicity of oxide rupture rate

Q_f = oxidation charge density passed in t_f after the oxide rupture event.

It is possible to qualitatively explain the principal observations of this study in terms of the above model.

For fatigue crack growth, transgranular cracking is observed at rapid frequencies because there is insufficient time during the loading cycle for the crack to penetrate into the chromium depleted region

adjacent to the base metal. Since the cracking mode is not intergranular at these higher frequencies, then there is no effect of degree of sensitization since that parameter is essentially a measure of grain boundary effects.

At the slow frequencies or static loads where intergranular cracking is observed, there is sufficient time during the loading event for penetration into the grain boundary and oxide reformation. For this case, one would expect the observed effect of sensitization and coolant oxygen content in terms of the t_f and Q_f parameters described above. The periodicity of oxide rupture depends on the crack tip strain rate and the fracture strain of the oxide. The crack tip strain rate must be sufficiently slow that significant grain boundary penetration occurs before the significant fracture of the oxide is obtained. Constant extension rate tests conducted by Solomon²⁶ have shown that at slow extension rates, intergranular fracture morphology was promoted at high sensitization levels and that lower fracture strains were observed as the degree of sensitization increased. Hence, as the degree of sensitization increases, one would expect the periodicity of oxide rupture would decrease as sensitization increases and the crack growth rate should increase as is observed. In a morphological sense, the continuous carbides and deep chromium depletion consistent with high sensitization would allow deeper intergranular penetration at each rupture event than the more discontinuous carbides associated with weld sensitization. The role of the coolant oxygen content is a little more complex because the crack tip is located in a crevice. The bulk water chemistry reflects only the extent of the

potential gradient down the crevice. A steeper potential gradient would be expected to occur for 8 ppm oxygen than 0.2 ppm oxygen. With this in mind, more rapid growth rates would be expected in the 8 ppm oxygenated water solution since the corrosion potential is higher (more positive) than the 0.2 ppm oxygen case. Ford²⁴ has observed increased corrosion potentials with increased oxygen contents and consequent increase in crack growth rates at 288°C for sensitized stainless steel.

DISCUSSION OF IMPACT OF CRACK GROWTH ON PIPING

Crack growth data is only useful if the information can be applied to field situations. The laboratory data must be used to predict the size of stress corrosion cracks as a function of time. By knowing the initial size of a crack in a component, one can use the crack size predictions to structure inspection schedules to assure that the crack does not reach a critical size for net section collapse^{17, 27}. This critical size is only a function of material, geometry, and loading. The environment does not influence the basic elastic-plastic behavior of the material once the crack is unstable. The methodology that one must use to predict the crack growth behavior has two parts. The first is the evaluation of the crack driving force in the piping. The second is the crack growth rates as a function of that driving force. The overall output of the prediction methodology is crack depth as a function of time.

The first task is to define the approximate crack driving force in the component of interest. This is a function of the stress state of the component. For a pipe, which is sensitized due to the girth welding process, the axial stresses are the ones of interest. Axial stresses result from pressure, weight, thermal gradients, and welding residual stresses. The crack tip stress intensity, K , which "drives" the intergranular stress crack is a function of this stress state.

Buchalet and Bamford²⁸, using two-dimensional finite element methods determined the stress intensity factor for circumferential flaws in the pipe geometry from linear elastic methods. Assuming that in pipes of

interest, linear elastic behavior is applicable, stress intensity as a function of depth can be defined for a specific pipe. Using representative stresses in piping, a typical K_I vs. depth profile can be determined for the pipe size of interest.²⁷

The second step is the determination of crack depth using this stress intensity information with the load history of the piping. By knowing the load history, one can evaluate the contribution of cyclic and constant load crack growth. For most piping, cyclic crack growth contributions are small, and constant load history governs crack growth. Integration of the constant load crack growth rate curve using the pipe stress intensity function leads to a typical crack depth vs. time plot for a particular starting flaw size. One could use this information in the development of inspection plans to monitor crack growth without any risk of the component failing to perform its function.

CONCLUSIONS

It is apparent from the foregoing results and discussion that the crack growth rates and fracture morphologies are a complex function of the type of loading, stress intensity factor, mean stress, degree of sensitization, and coolant oxygen content. The principal conclusions are as follows:

- Decreasing cyclic frequency for fatigue crack growth results in increased growth rates per cycle (decreasing rates per unit time). Intergranular cracking is only observed at the slowest frequencies.
- There is little effect of degree of sensitization on fatigue crack growth rates unless the cycle frequency is slow enough to produce intergranular cracking. In that case, more rapid growth rates are produced with higher degree of sensitization.
- The presence of mean stress during fatigue cycling promotes intergranular behavior and more rapid crack growth rates. The mean stress effect can be accounted for by use of the K_{eff} parameter.
- Higher fatigue crack growth rates are obtained with higher stress intensity factors.
- For static load conditions, higher crack growth rates are obtained at higher stress intensity factors.

- Both increased sensitization and coolant oxygen content promote higher crack growth rates.
- The crack growth data generated can be used to predict crack depth as a function of time. For piping components, the constant load data is most useful in making this prediction.

ACKNOWLEDGEMENT

A large portion of this work was performed as part of a research program funded primarily by the Electric Power Research Institute. We acknowledge this support and in particular, the helpful discussions with Dr. R. Jones and Dr. D. M. Norris, Jr. at the Institute. We would also like to acknowledge help from our colleagues, M. Bensch, T. Caine and J. Heald in performing the crack growth testing.

REFERENCES

1. R. L. Cowan, II, and D. S. Tedmon, Jr., "Intergranular Corrosion of Iron-Nickel-Chromium Alloys," Advances in Corrosion Science and Technology, Vol. 3, Ed. M. G. Fontana and R. W. Staehle, 1973.
2. R. L. Cowan, II, and G. M. Gordon, "Intergranular Stress Corrosion Cracking and Grain Boundary Composition of Fe-Ni-Cr Alloys," NEDO-12399, 1973, General Electric Co., San Jose, California.
3. H. H. Klepfer, et al., "Cause of Cracking in Austenitic Stainless Steel Piping," NEDO-2100, 1975, General Electric, San Jose, Calif.
4. W. Berry, Corrosion, Vol. 29, No. 12, 1973.
5. D. Vermilyea, Corrosion, Vol. 29, No. 1, 1973.
6. W. Clarke, Corrosion, Vol. 29, No. 1, 1973.
7. J. N. Kass, Corrosion, Vol. 36, No. 6, 1980.
8. T. Kawakubo, Corrosion, Vol. 35, No. 6, 1979.
9. F. P. Ford, Corrosion, Vol. 36, No. 11, 1980.
10. ASTM Specification E399.
11. S. J. Hudak, Jr., et al., "Development of Standard Methods of Testing and Analyzing Fatigue Crack Growth Rate Data, Third Semi-Annual Report, Air Force Contract F33615-75-C-5064," 1977.
12. S. Mostovoy, P. B. Crosley, and E. J. Ripling, "Use of Crack Line Loaded Specimens for Measuring Plant Strain Fracture Toughness," Journal of Materials, Vol. 2, 1977.
13. W. A. VanDerSlys, "Engineering Fracture Mechanics," Vol. 1, 1969.
14. P. B. Crosley, and E. J. Ripling, "Nuclear Engineering Design," Vol. 17, 1971.
15. W. Clarke, "The EPR Method for the Detection of Sensitization in Stainless Steel," GEAT 24888, February 1981.
16. W. Clarke, "Comparative Methods for Measuring Degree of Sensitization in Stainless Steel ASTM STP 656 Intergranular Corrosion of Stainless Alloys," R. Stergerwald (ed.), 1978.
17. R. M. Horn, et al., "The Stability and Growth of SCC in Large Diameter BWR Piping," Third Semi-Annual Report, December, 1980.

18. D. A. Hale, ASME Journal of Engineering Materials and Technology, June 1978.
19. M. O. Speidel, M. J. Blackburn, T. R. Beck, and J. A. Feeney, Corrosion Fatigue: Chemistry, Mechanics and Microstructure, National Association of Corrosion Engineers, 1972, pp. 324-345, (NACE-2).
20. M. O. Speidel, Hydrogen Embrittlement and SCC of Iron-Base Alloys, Firmany, France, 1973.
21. M. Speidel, Met. Trans., Vol. 6A, 1975, pp. 631-51.
22. A. Russell, Met. Trans., Vol. 10A, No. 9, 1979.
23. M. Landkof, Corrosion, Vol. 36, No. 5, 1980.
24. F. P. Ford, "Mechanism of Environmentally Controlled Crack Growth of Fractured Steels in High Temperature Water," IAEA Meeting on Environmental Cracking, Freiburg, West Germany, May 11-15, 1981.
25. R. Parkins, Metal. Sci., Vol. 465, August 1977.
26. J. Alexander, "Alternate Pipe Alloy for BWR Pipe Applications," Sixth Semi-Annual Report, NEDO-23750-6, September 1980, General Electric, San Jose, California.
27. R. M. Horn, et al., "The Growth and Stability of SCC in Large Diameter BWR Piping, " Second Semi-Annual Report, June, 1980.
28. C. B. Buchalet and W. H. Bamford, "Stress Intensity Factors - Solutions for Continuous Surface Flaws in Reactor Pressure Vessels," Mechanics of Crack Growth, ASTM STP 590, ASTM, 1976.

FIGURE CAPTIONS

- Figure 1: Simulated BWR Water Test Loop
- Figure 2: Tapered Double Cantilever Beam Specimen for Constant Load Crack Growth Tests
- Figure 3: Electrochemical Potentiokinetic Reactivation (EPR) Readings as a Function of Isothermal Holding Time at 1150°F for Heats 03580, 04904
- Figure 4: Effect of Degree of Sensitization on Fatigue Crack Growth Rates of T-304 Stainless Steel in 0.2 ppm O₂ 288°C High Purity Water
- Figure 5: Fatigue Crack Propagation Rates of Highly Sensitized T-304 Stainless Steel Tested in 0.2 ppm O₂, 288°C High Purity Water.
- Figure 6a: Fracture Surface of Specimen SS-7 Showing Transgranular Environmental Cracking.
6b: Fracture Surface of Specimen SS-21 Showing Intergranular Cracking.
- Figure 7: Comparison of Fatigue Crack Propagation Rates with Data from Reference 8 for Sensitized T-304 Stainless Steel Tested in 0.2 ppm O₂, 288°C, High Purity Water
- Figure 8: Fatigue Propagation Rates vs. Frequency at $K_{eff}=20 \text{ ksi}\sqrt{\text{in}}$ for Sensitized T-304 Stainless Steel in 0.2 ppm O₂, 288°C Water.
- Figure 9: Effects of Frequency and Degree of Sensitization on Fracture Mode Under Cyclic Loading in High Temperature, High Purity Water
- Figure 10: Constant Load Crack Growth Rates as a Function of Stress Intensity Level, Environment, and Sensitization Level in T-304 Stainless Steel
- Figure 11: Fracture Surface of Specimen 4904 SS-1 Exposed to Constant Load in 0.2 ppm O₂, 288°C, High Purity Water

TABLE I

COMPOSITION OF TYPE-304 STAINLESS STEEL MATERIAL

Heat No.	C	Mn	Cr	Ni	Percent Alloy Addition		S	Si
					Mo	P		
03580 ^a (ladle)	0.068	1.78	18.45	8.16	0.39	0.029	0.022	0.39
(check)	0.066	1.84	18.54	8.16	0.38	0.029	0.025	0.40
(04904 ^b (ladle)	0.067	0.94	18.67	8.09	0.44	0.022	0.022	0.37
(check)	0.071	0.97	18.65	8.15	0.41	0.023	0.026	0.37

MECHANICAL PROPERTIES OF TYPE-304 STAINLESS STEEL MATERIAL

(a) Heat 03580

Test Temperature	0.2% Yield Strength (ksi)	Ultimate Tensile Strength (ksi)	Elongation (%)	Reduction in Area (%)
Room Temperature ^a	42.6	85.3	67	63.0
550°F ^a	27.8	64.7	42	51.6

(b) Heat 04904

Test Temperature	0.2% Yield Strength (ksi)	Ultimate Tensile Strength (ksi)	Elongation (%)	Reduction in Area (%)
Room Temperature ^b	37.1	89.0	73	67.2
550°F ^b	20.9	65.7	46	57.2

^a Average of three specimens^b Average of two specimens

TABLE II

FATIGUE CRACK GROWTH TESTS^j

Specimen Number	Material	Frequency (cycles/hr)	Wave shape	R ^a	K _{max} Initial/ ΔK Initial	K _{max} Final/ ΔK Final	Total Crack Growth in. (mm)	Measurement	
					ksi/√in (MPa√m)	ksi/√in (MPa√m)		CSO	Capillary
SS-10	Type 304 High DOS	7.5	Skewed ^b Sawtooth	0.6	24/95 (27/10.5)	33/13 ^d (36/14)	0.134 (3.4)	Yes	No
SS-11	Type 304 Medium DOS	↓			23/9.4 (26/14)	34/14 ^d (37/15)	0.185 (4.7)	Yes	No
SS-12	Type 304 Low DOS				23/9.4 (26/10.4)	34/14 ^d (37/15)	0.178 (4.5)	Yes	No
SS-6	Type 304 Medium DOS	↓			36/19 (39/15)	49/20 ^d (54/22)	0.102 (2.6)	Yes	No
SS-7	Type 304 Medium DOS	0.74			28/10 (29/11)	29/11 (32/12)	0.070 (1.8)	Yes	No
SS-21	Type 304 High DOS	0.74	↓	↓	26/10 ⁱ (29/11)	29/11 ⁱ (32/12)	0.070 ⁱ (1.8)	Yes	No

$$R = \frac{K_{min}}{K_{max}}$$

^bSkewed Sawtooth^dLoad levels increased at 12,500 cyclesⁱPreliminary results only^jEnvironment for all specimens except SS-1A is 0.2 ppm O₂, 150°F water

TABLE III - CONSTANT LOAD TEST

<u>Specimen ID</u>	<u>Type</u>	<u>Environment</u>	<u>Heat Treatment</u>	<u>EPR (C/cm²)</u>	<u>K-level (ksi/\sqrt{in})</u>	<u>Testing Time (hour)</u>
TC-3	CT	8 ppm O ₂	621 ⁰ C, 24 hr.	35	32-34	250
SS-21	CT			30	21-23	1200
4904 SS-1	TDCB	0.2 ppm O ₂	621 ⁰ C, 2 hr.	15	19-20	6630
4904 SS-2	"	"	"	"	24-25	6630
4904 SS-3	"	"	"	"	27-29	6630
4904 SS-4	"	"	"	"	31	2940

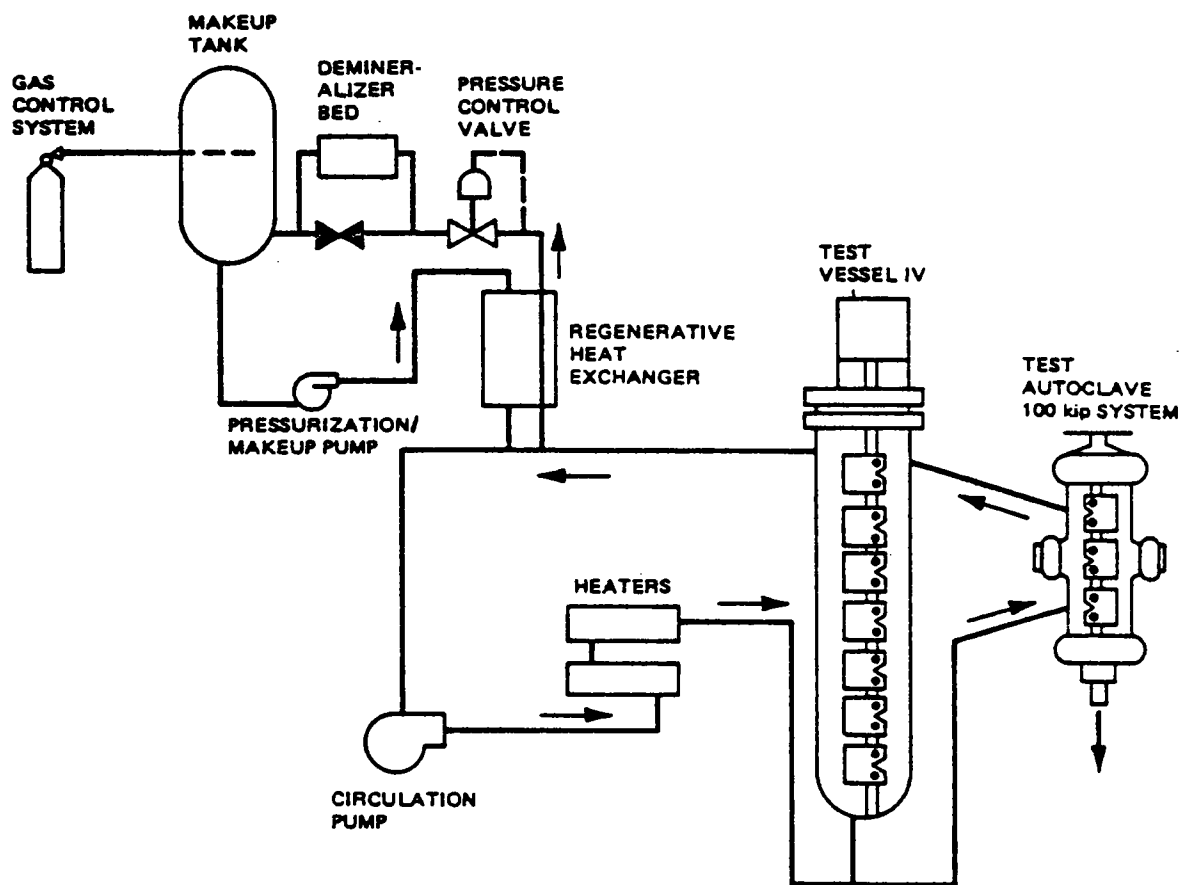


Figure 1.

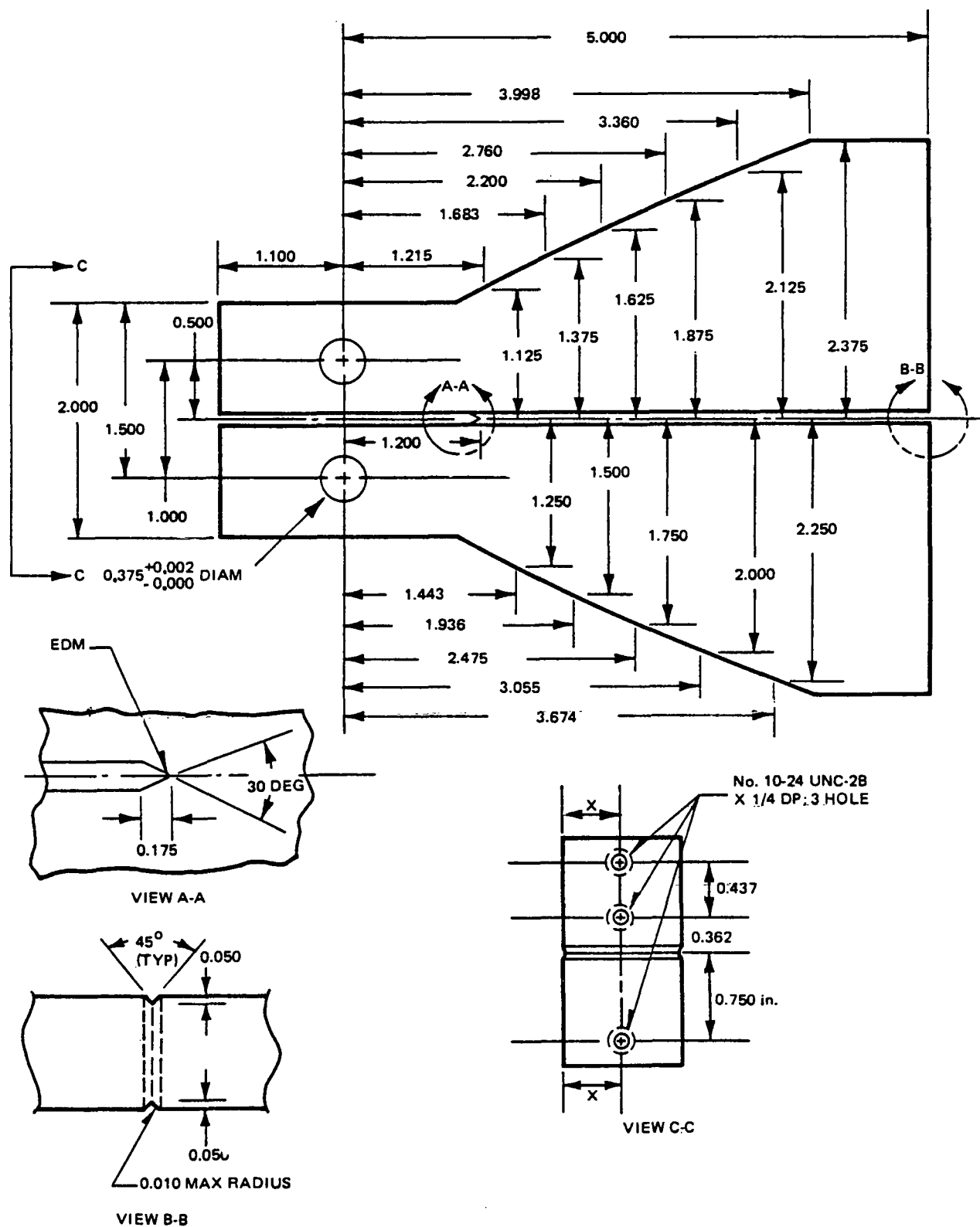


Figure 2.

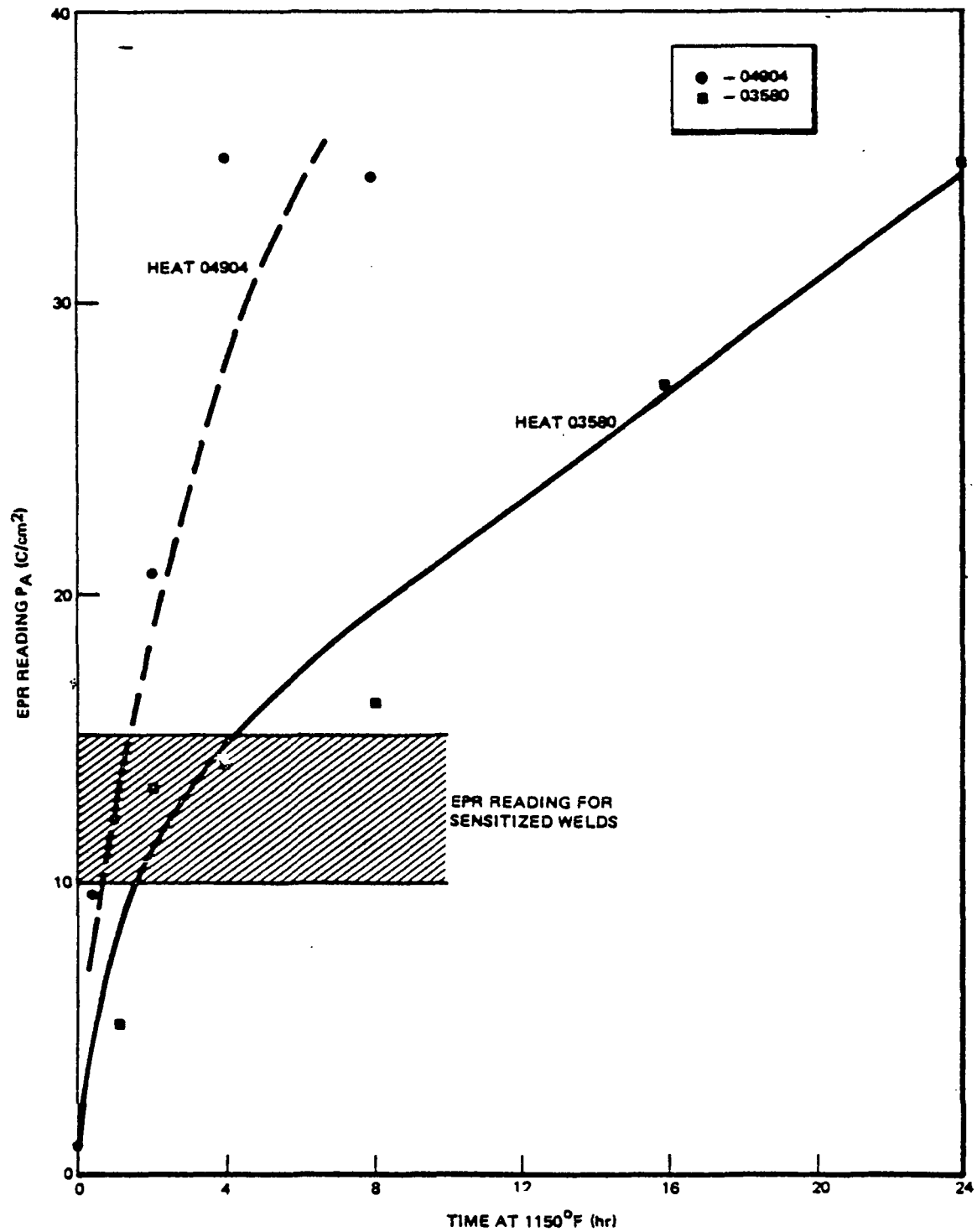


Figure 3.

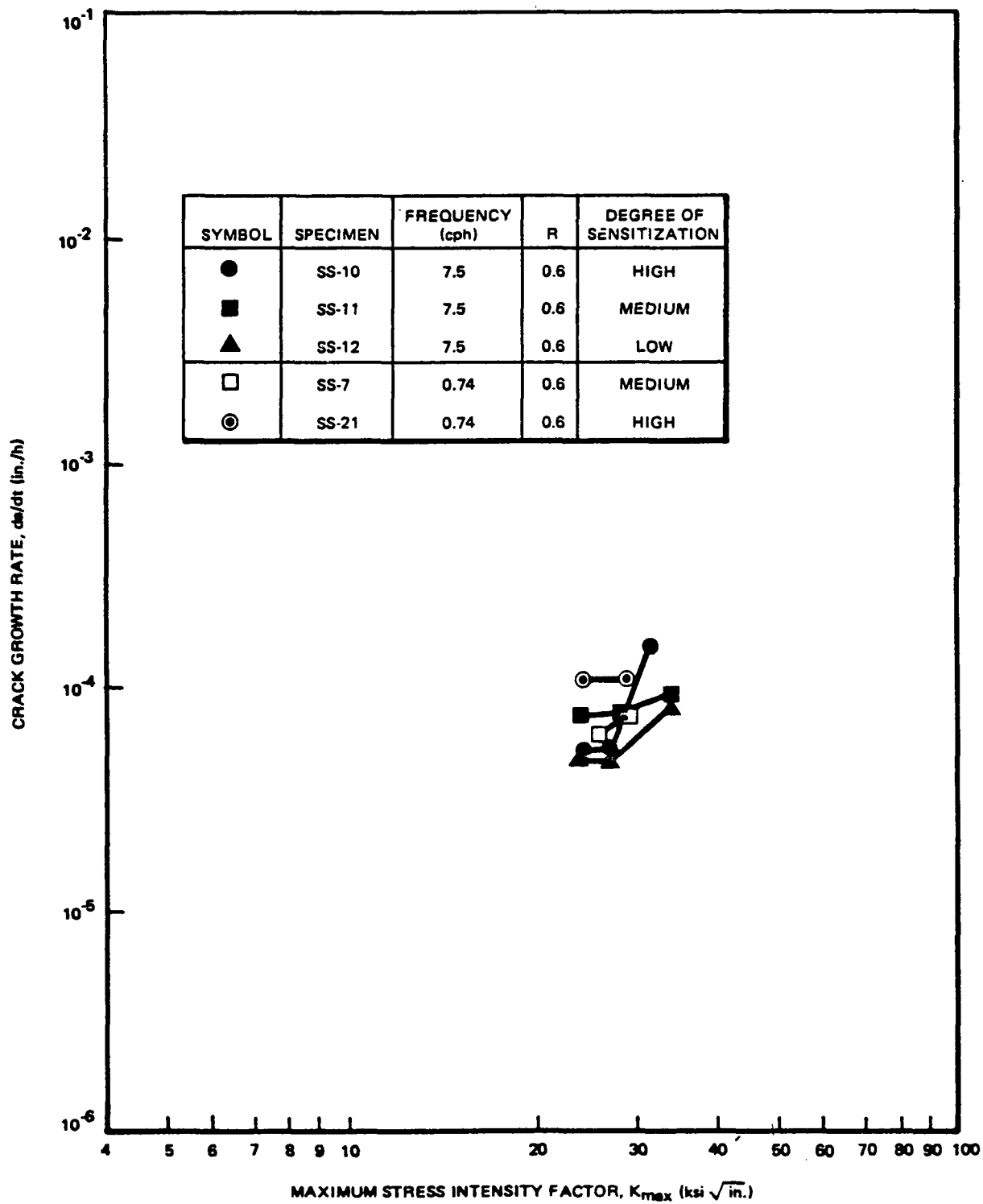


Figure 4.

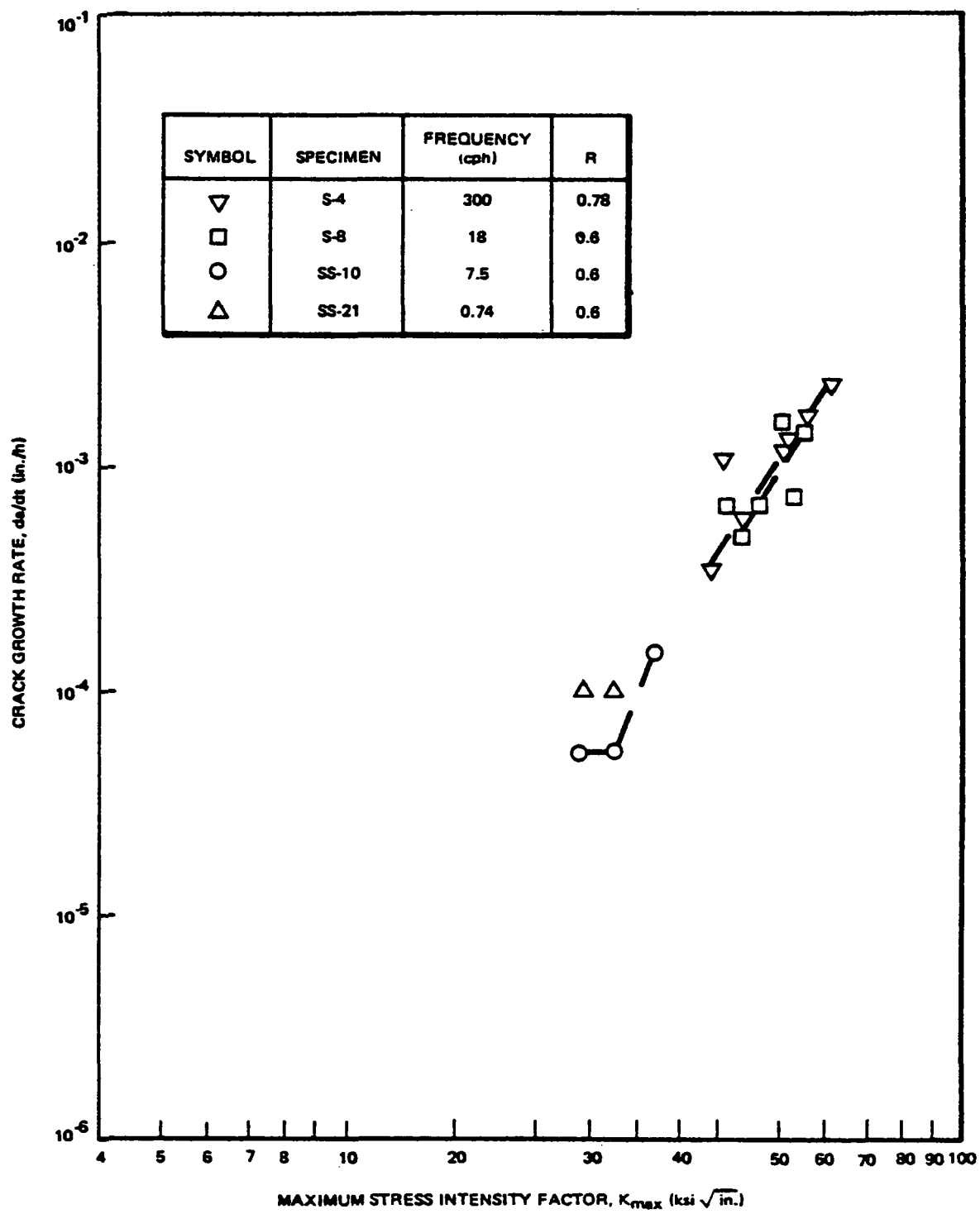
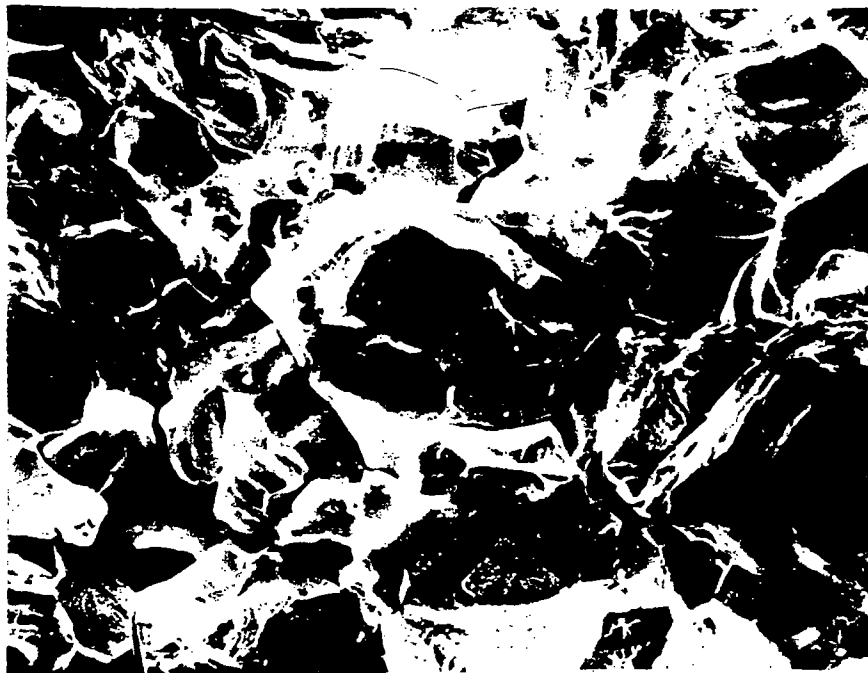


Figure 5.



(a)



(b)

Figure 6.

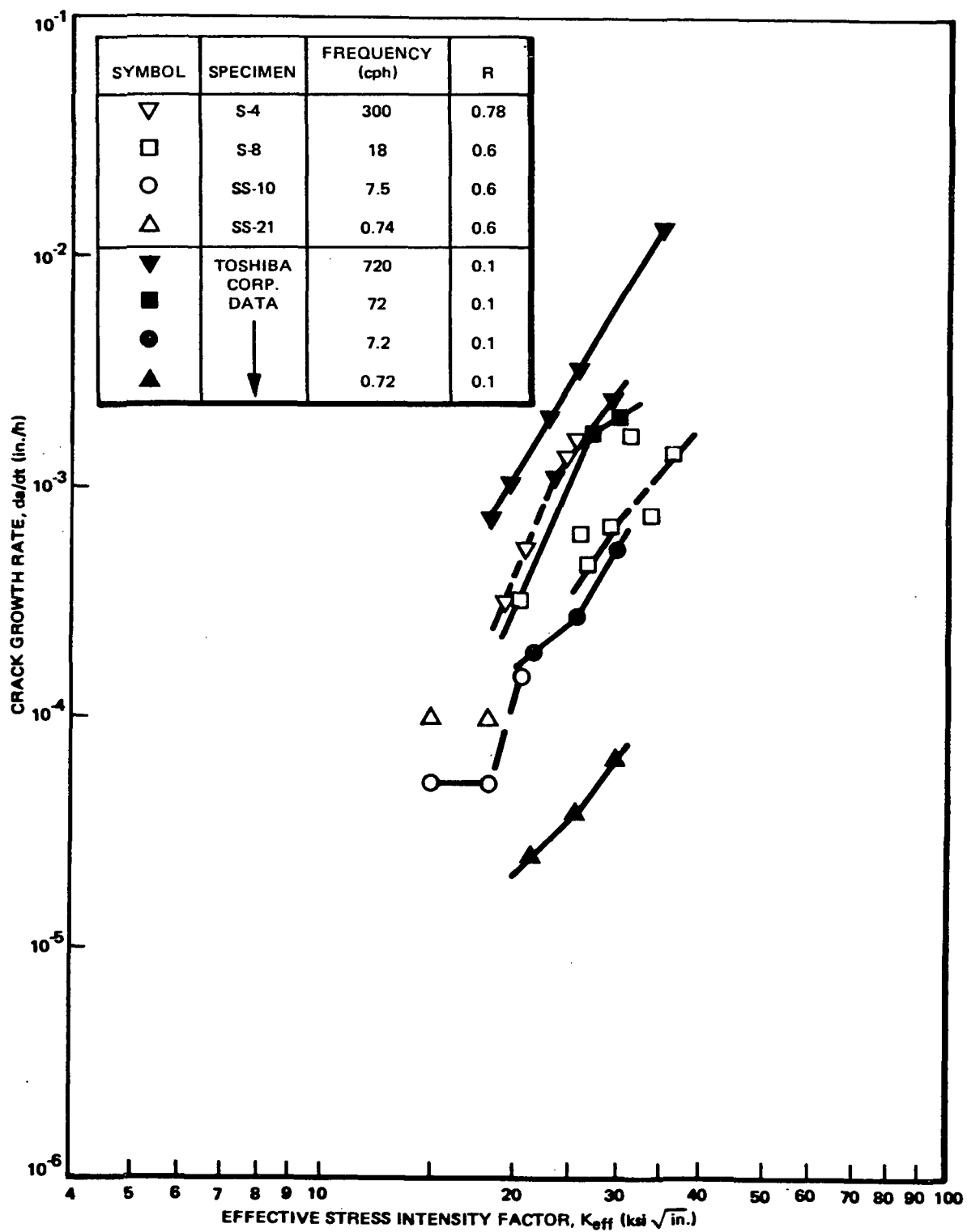
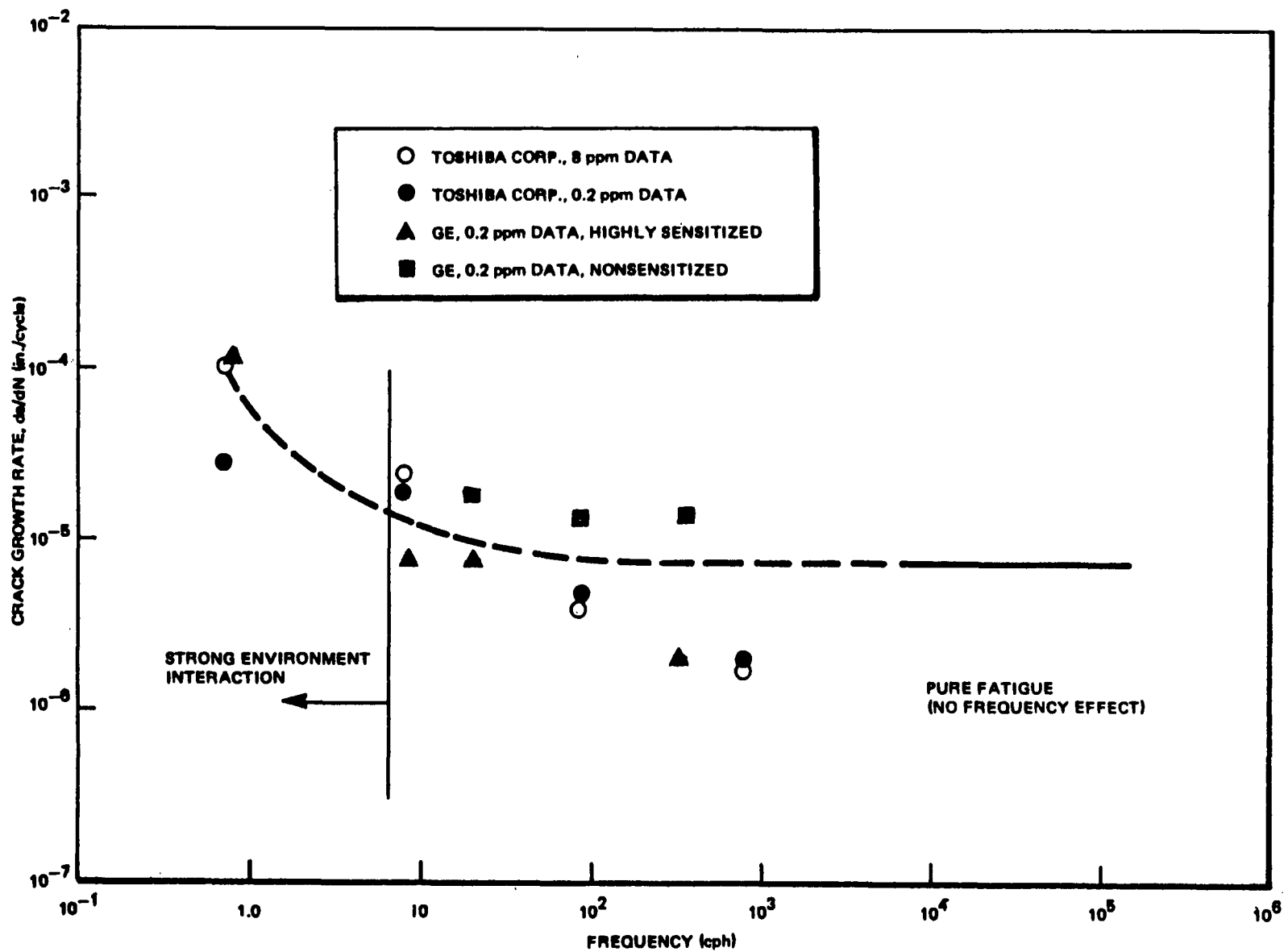


Figure 7.

Figure 8.



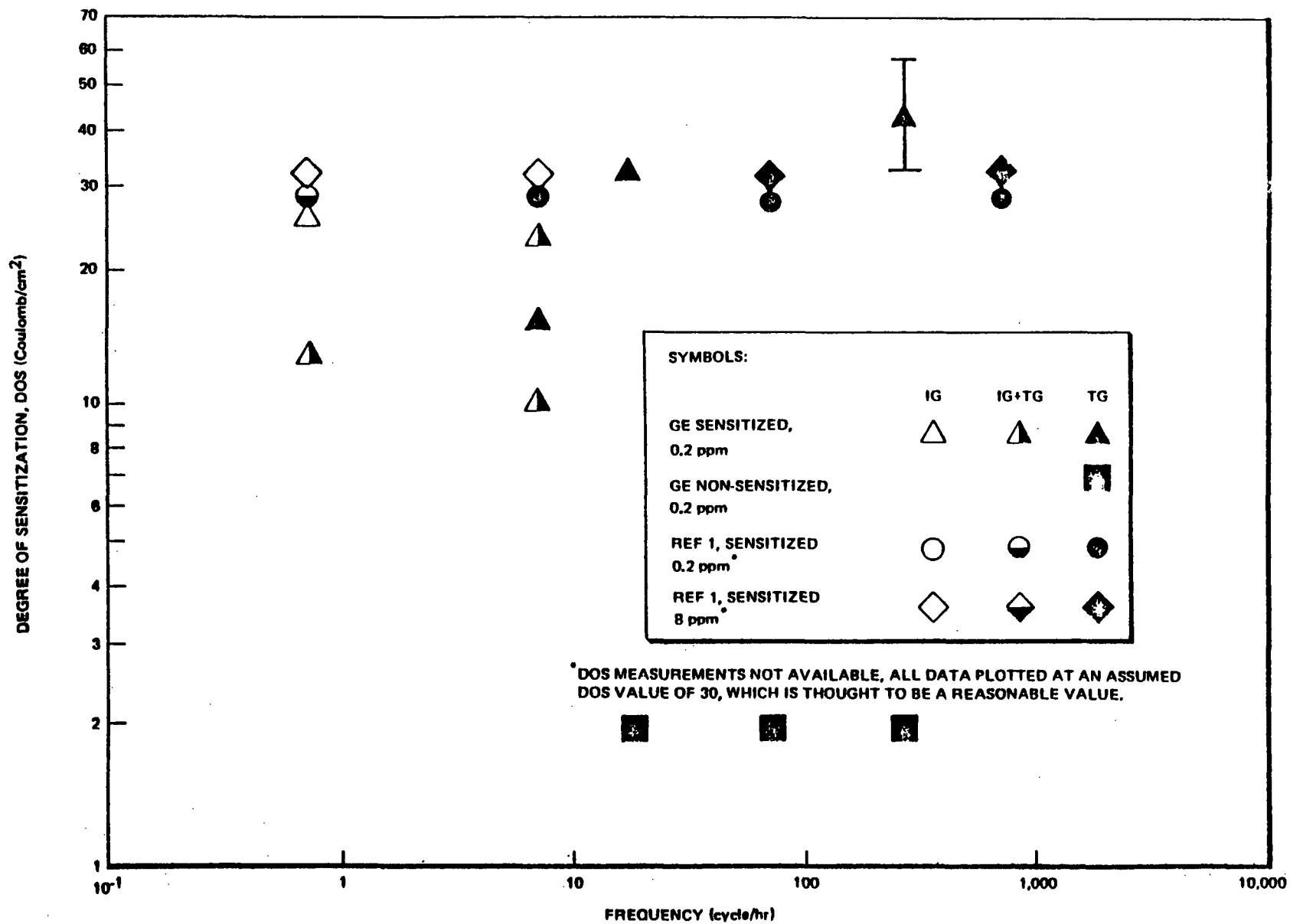


Figure 9.

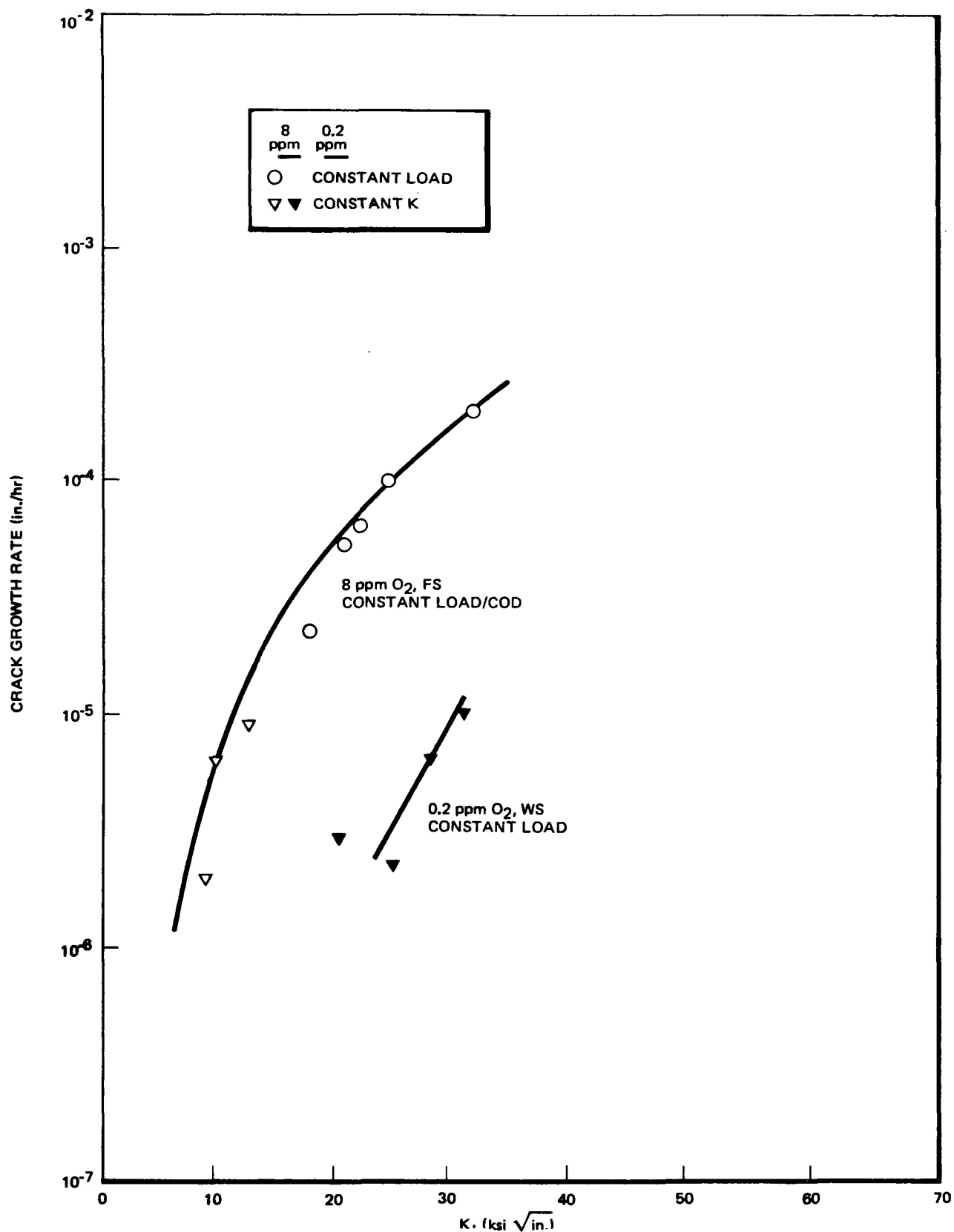


Figure 10, CRACK GROWTH RATE VS. K, SENSITIZED STAINLESS STEEL

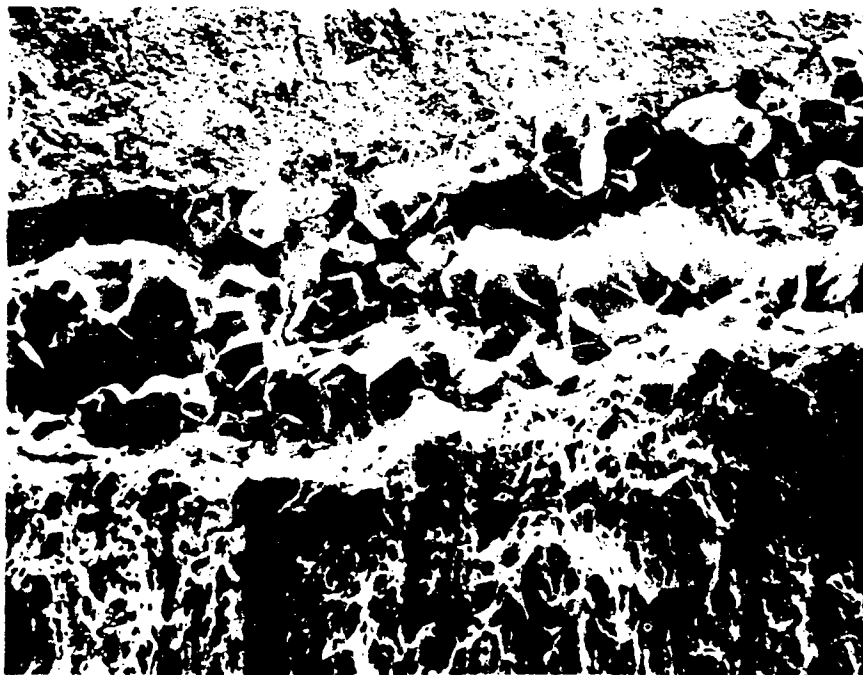


Figure 11.

LOW TEMPERATURE SENSITIZATION OF WELD HEAT-
AFFECTED ZONES IN TYPE 304 STAINLESS STEEL

by

R. D. Caligiuri, L. E. Eiselstein,
and M. J. Fox

Presented at the
International Atomic Energy Agency Meeting
Freiburg, Germany, 13 to 15 May 1981

R. D. CALIGIURI and L. E. EISELSTEIN are Materials Scientists at SRI International, 333 Ravenswood Avenue, Menlo Park, California 94025, and M. J. FOX is Project Manager, Electric Power Research Institute, Nuclear Power Division, 3412 Hillview Avenue, Palo Alto, California 94303, USA.

ABSTRACT

The effects of low temperature sensitization (LTS) on the initiation and growth of the intergranular stress corrosion cracks in Type 304 stainless steel weld heat-affected zones (HAZs) were investigated. Constant extension rate test data indicate that LTS heat treatments as low as 400°C can facilitate the initiation of intergranular stress corrosion cracking (IGSCC) in the HAZs in 288°C, 0.2 ppm O₂, high purity water after only a few days at the sensitizing temperature. Extrapolation of these data using an Arrhenius temperature dependence to a 288°C sensitizing temperature predicts that, along with appropriate environmental and stress conditions, IGSCC can initiate in the HAZs in as little as one month. Crack growth experiments on compact tension specimens given the same heat treatments suggest that once initiated, the cracks grow slowly, at a rate ranging from 10⁻⁸ to 10⁻⁷ mm/s, depending on the environment. The corresponding threshold stress intensities, K_{ISCC}, defined as the stress intensity below which growth stops, range from 15 to 25 MPa√m, also depending on environment. The K_{ISCC} are similar, but the growth rates are about an order of magnitude lower than the growth rates reported for Type 304 stainless steel sensitized at temperatures above 600°C.

INTRODUCTION

A major corrosion problem in boiling water reactors (BWRs) is the intergranular stress corrosion cracking (IGSCC) of stainless steel pipe in the recirculation system. There appear to be three prerequisites for stress corrosion: a sensitized microstructure, a critical level of stress (or stress intensity), and a critical environmental condition.

A sensitized microstructure is obtained in Type 304 stainless steel if it is held in a critical temperature range long enough to allow the grain boundary precipitation of metal carbides. During any welding operation, a zone adjacent to the weld heat-affected zone experiences temperatures in the critical range, but welding procedures usually can be chosen so that the time and temperature will be insufficient to cause significant sensitization.

However, it has been shown^{1,2} that Type 304 stainless steel may be sensitized at relatively low temperatures (less than 500°C) if $M_{23}C_6$ nuclei are first formed in the critical temperature range for carbide nucleation. The chromium depletion accompanying the formation of the nuclei is not sufficient to cause severe sensitization, but once formed, the nuclei are able to grow at temperatures below the normal sensitization range and increase the degree of sensitization. The combination of the nucleating heat treatment and the subsequent prolonged low temperature heat treatment is called low temperature sensitization (LTS).

This paper reports results of research aimed at determining the extent of LTS at reactor temperatures and the subsequent effects of LTS on the propagation of IGSCC in Type 304 stainless steel pipe.

EXPERIMENTAL METHODS

Material

All experiments were conducted on specimens taken from a length of 60-cm-dia. (24-in.), Schedule 80, Type 304 stainless steel solution-annealed pipe that had been cut into 61-cm sections and welded back together by Bechtel National, Inc. The base composition of the pipe is shown in Table I. Machine Gas Tungsten Arc Welding was used for all passes, including the root fusion pass. Details on the welding procedures and parameters used have been previously reported.^{3,4}

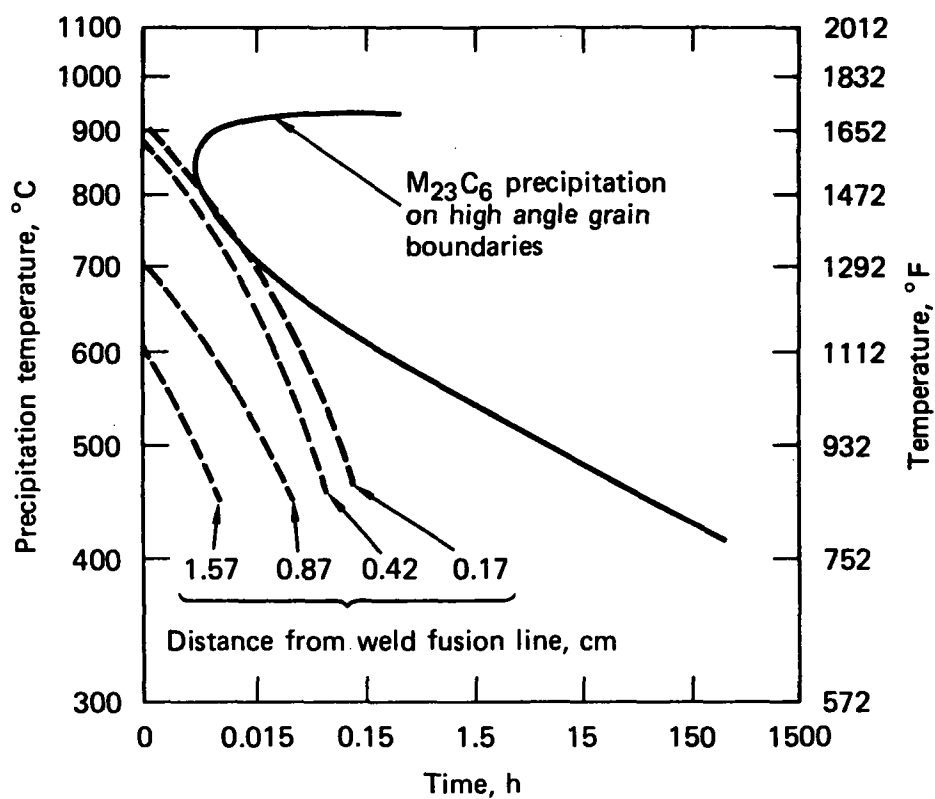
During welding, the temperature-time profiles were monitored at various distances from the weld fusion line on both the inside and the outside walls of the pipe. The resulting profiles were analyzed to determine the total time spent above a given temperature for each location in the weld heat-affected zone (HAZ) integrated for all passes. These data are shown superimposed on a time-temperature-precipitation diagram $M_{23}C_6$ in Type 304 stainless steel containing 0.05 wt% C in Fig. 1. The dashed lines are the cooling curves determined from the thermocouple measurements made during welding; the solid curve is the precipitation data of Cihal.⁵ Only cooling curves at locations within about 0.4 cm of the weld fusion line intersect the nose of the precipitation curve, and then only by a small amount. Therefore, little carbide precipitation is expected as a result of the thermal exposure during welding. This was later confirmed by detailed optical³ and transmission electron microscopy.⁴

Specimen Fabrication

Smooth, round bar tension specimens for the constant extension rate tests (CERTs) were machined from the welded pipe sections so that the specimen axis was oriented parallel to the pipe axis. The specimens were located such that the center of the gage length corresponded to the centerline of the weld. The geometry of the specimens were in accordance with

Table 1
CHEMICAL COMPOSITION OF 61-cm (24-in.)-DIAMETER
SCHEDULE 80 PIPE

<u>Element</u>	<u>wt%</u>
C	0.068
Mn	1.52
P	0.013
S	0.027
Si	0.92
Cr	18.62
Ni	8.43
Mo	0.20
Cu	0.31
Co	0.17
Fe	Bal



MA-8603-72

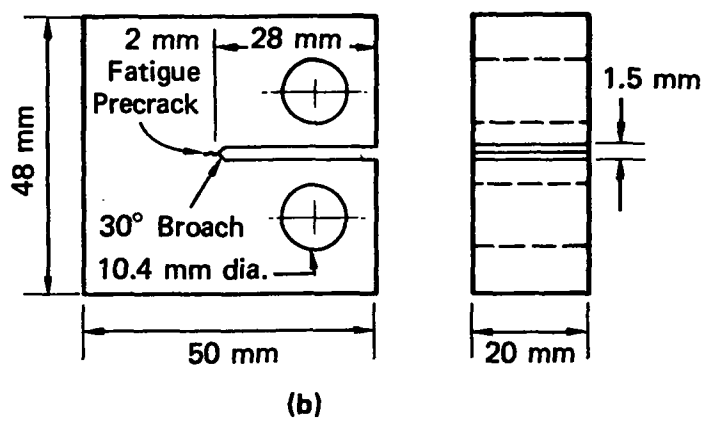
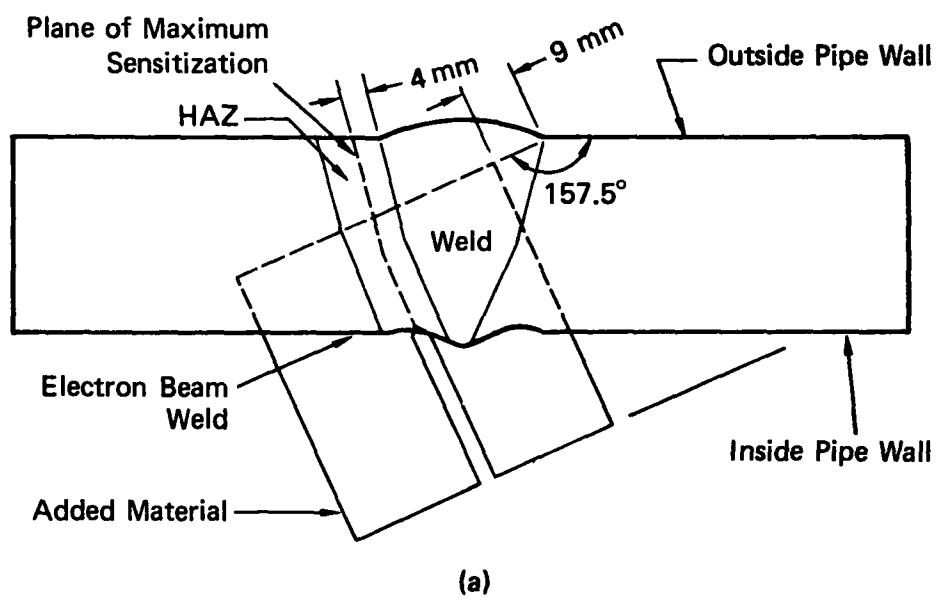
Figure 1. Thermal histories in HAZ during welding as a function of distance from the fusion line superimposed on the time-temperature-precipitation curve for $M_{23}C_6$ in Type 304 stainless steel.

ASTM specification E8-69,⁶ except for an extra long gage length (6.35 cm). This extended gage length allowed us to reach strain rates of about 10^{-6} s⁻¹ during the CERTs.

Compact tension (CT) specimens for crack growth experiments were prepared from the welded pipe sections. These specimens were fabricated by first grinding and cleaning the inside wall of the welded pipe, and then electron-beam welding a block of the pipe base material onto this surface. A CT specimen was then machined from this welded block, as shown in Fig. 2. The notch of the specimen was aligned parallel to the plane of maximum sensitization in the HAZ (about 3 mm from the weld fusion line) which was determined from optical and transmission electron microscopy.^{3,4} The machined specimens were then fatigue-precracked to place a sharp crack tip in the HAZ away from the electron-beam weld plane. The geometry and fatigue precracking of the specimens were in accordance with ASTM specification E399-78.⁷

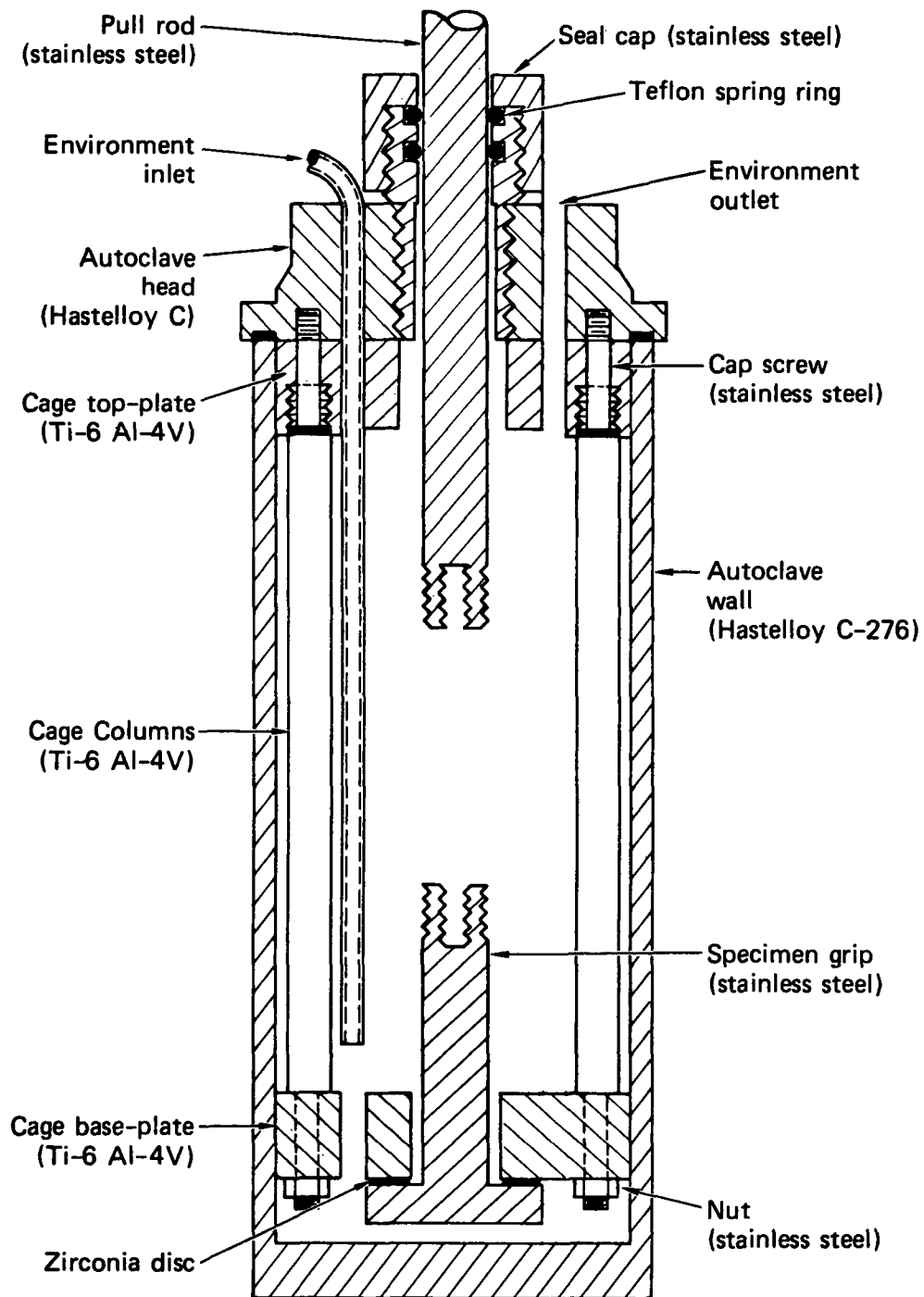
Testing Environment

A tension cage and a frictionless seal were designed and constructed to fit a 2-liter autoclave for conducting the CERTs and the CT tests in a simulated BWR environment. The autoclave assembly is shown in Fig. 3. Note from Fig. 3 that the specimens were electrically insulated from the autoclave to prevent polarization of the specimen. A recirculating system was designed and fabricated to supply to the autoclave high purity (10^{-6} S conductivity) water pressurized to 2.6 MPa and containing various levels of dissolved oxygen. The autoclave was refreshed at a rate of about 2 ml/minute. The water in the autoclave was heated by an external resistance furnace, and the temperature was controlled by a thermocouple immersed in the autoclave. Periodically during each test, the oxygen content in the water both upstream and downstream of the autoclave was measured using Winkler titration. The oxygen content was invariably within 2% of the desired value, indicating minimal oxygen consumption during the test.



SA-8603-38

Figure 2. Compact tension specimens for crack growth rate studies.



SA-8603-8R

Figure 3. Detailed drawing of tension cage assembled inside the autoclave. This cage is used for both the CERT and the compact tension experiments.

Constant Extension Rate Tests (CERTs)

CERTs were performed to evaluate the effects of LTS heat treatments on the minimum time required to initiate IGSCC in the weld HAZs. The autoclave assembly shown in Fig. 3 was mounted onto a screw-driven Instron machine specially modified to yield a crosshead speed of 6.35×10^{-5} mm/s.³ The specimens were threaded into the grips, and the water temperature and chemistry were stabilized. The specimens were preloaded to 28 MPa, then pulled at the above crosshead speed to failure. The initial strain rate was 1×10^{-6} s⁻¹. Load, time, water pressure, and water temperature were monitored, and the results were stored on magnetic tape using a computerized data acquisition system. After fracture, the specimens were removed and subjected to posttest optical and scanning electron microscopy. The stored data were plotted in the form of true-stress/true-strain curves.

Compact Tension (CT) Experiments

The CT experiments were performed to evaluate the effects of LTS heat treatments on the growth of intergranular cracks through the weld HAZs. The same autoclave assembly used for the CERTs was used for the CT experiments except that it was mounted on a System 810 MTS servo-hydraulic testing machine. In these experiments, crack opening displacement (COD) was controlled by an MTS Model 610.32 water immersible clip gage. The total crack length at any given time during the test was determined using the compliance method. The normalized compliance/crack-length relationship used for our specimens was as follows:⁸

$$a = w \left[C_0 + C_1(U_x) + C_2(U_x)^2 + C_3(U_x)^3 + C_4(U_x)^4 + C_5(U_x)^5 \right] \quad [1]$$

where:

$$U_x = \left[\left(\frac{BEV_x}{P} \right)^{1/2} + 1 \right]^{-1}$$

w = Specimen length
 a = Crack length
 E = Elastic modulus
 V_x = Crack opening displacement at $-0.345w$ from load line

P = Applied load

$\frac{BEV}{P}x$ = Normalized compliance

B = Specimen width

and

$C_0 = 1.0012$

$C_2 = 23.057$

$C_4 = 1798.3$

$C_1 = 4.9165$

$C_3 = 323.91$

$C_5 = 3513.2$

This relationship was established for our specimens and our test environments by measuring the compliance of specimens with different known crack lengths in the environments of interest. Once the instantaneous crack length is known, the instantaneous stress intensity can then be calculated for our specimen geometry using the appropriate relationships given in ASTM specification E399-78.⁷ During each CT test, the load, time, COD, water pressure, and water temperature were monitored, and the results were stored using a computerized data acquisition system. On completion of the test, the specimen was broken open and the final crack length was measured. This measurement, coupled with the stored data, was used to plot a crack-growth-rate/stress-intensity curve for the given LTS treatment and environment. Finally, the fracture surface of each specimen was subjected to detailed optical and scanning electron microscopy.

Previous work^{4,9-12} has established that the measured growth rates in CT experiments are influenced by the specimen loading method. In all our experiments, we used static COD control. The CT testing procedure devised and used in this program was as follows:

- Load the specimen to an initial stress intensity of about $38 \text{ MPa}\sqrt{\text{m}}$ and fix the crack opening displacement (COD).
- Wait for crack initiation to occur.
- Allow the crack to grow sufficiently to establish a reasonable growth rate at that stress intensity.
- Decrease the stress intensity slightly by relaxing the COD and establish the growth rate characteristic of this stress intensity value.
- Continue this procedure until the crack stops growing. The stress intensity below which no growth is detected is the threshold value (K_{ISCC}).

This technique allowed us to generate an entire growth-rate/stress-intensity curve in a single test. The stress intensity increments were small enough so that the cracks did not have to be reinitiated at each stress intensity level. Total time required to complete a test was about one month.

RESULTS AND DISCUSSION

Constant Extension Rate Tests

The results of the CERTs are summarized in Table II. The environment for each experiment was 288°C, 0.2 ppm O₂. This environment is characteristic of steady-state BWR operation.¹² The first four experiments were performed on material given an LTS treatment of 400°C for various times. The corresponding true-stress/true-strain curves are shown in Fig. 4. The serrations in the curves are due to slight variations in water pressure. The second four experiments were performed on material given an LTS treatment of 500°C for various times. The corresponding true-stress/true-strain curves for the 500°C specimens were similar to those shown in Fig. 4, but with different elongations to failure and ultimate tensile strengths.

It is evident from the data in Table II that susceptibility to IGSCC can be established in these weld HAZs between 48 and 96 hours after exposure at 400°C, and between 10 and 30 hours after exposure at 500°C. Furthermore, a high degree of susceptibility (greater than one-third IGSCC on the fracture surface) was reached at 500°C after 30 hours and at 400°C after 384 hours.

These apparent incubation periods represent the time required to initiate stress corrosion cracks for the given LTS heat treatment. Since the environment, surface condition, and strain rate are constant for all the experiments, these periods really represent the time required to develop sufficient carbide precipitation on the grain boundaries for the initiation of a sharp intergranular crack. Furthermore, since the growth of carbide particles is diffusion-controlled, there should be an Arrhenius-type relationship between the incubation time, t_o , and temperature, T :

$$\frac{1}{t_o} = A \exp \left(\frac{-Q}{RT} \right) \quad [2]$$

Table 2
SUMMARY OF CONSTANT EXTENSION RATE TESTS ON WELDED TYPE 304 STAINLESS STEEL
IN 288°C, 0.2 ppm O₂ HIGH PURITY WATER

Specimen No.	Specimen Condition	Y.S., ^a MPa(ksi)	UTS, ^b MPa(ksi)	e, ^c %	R.A., ^d %	IGSCC, ^e %
8603-7	Welded plus 400°C, 48 h	153 (22.2)	469 (67.9)	25.4	66.8	0
8603-8	Welded plus 400°C, 96 h	167 (24.2)	466 (67.5)	20.7	29.4	25
8603-9	Welded plus 400°C, 192 h	159 (23.0)	452 (65.5)	20.9	29.4	25
8603-10	Welded plus 400°C, 384 h	141 (20.4)	451 (65.4)	15.7	20.0	35
8603-11	Welded plus 500°C, 10 h	156 (22.6)	452 (65.0)	25.5	75.0	0
8603-12	Welded plus 500°C, 30 h	152 (22.0)	308 (44.7)	20.0	23.0	50
8603-13	Welded plus 500°C, 100 h	155 (22.5)	186 (26.9)	10.0	N.M. ⁺	80
8603-14	Welded plus 500°C, 150 h	152 (22.0)	162 (23.5)	5.0	N.M. ⁺	80

^aY.S.: Yield strength, 0.2% offset.

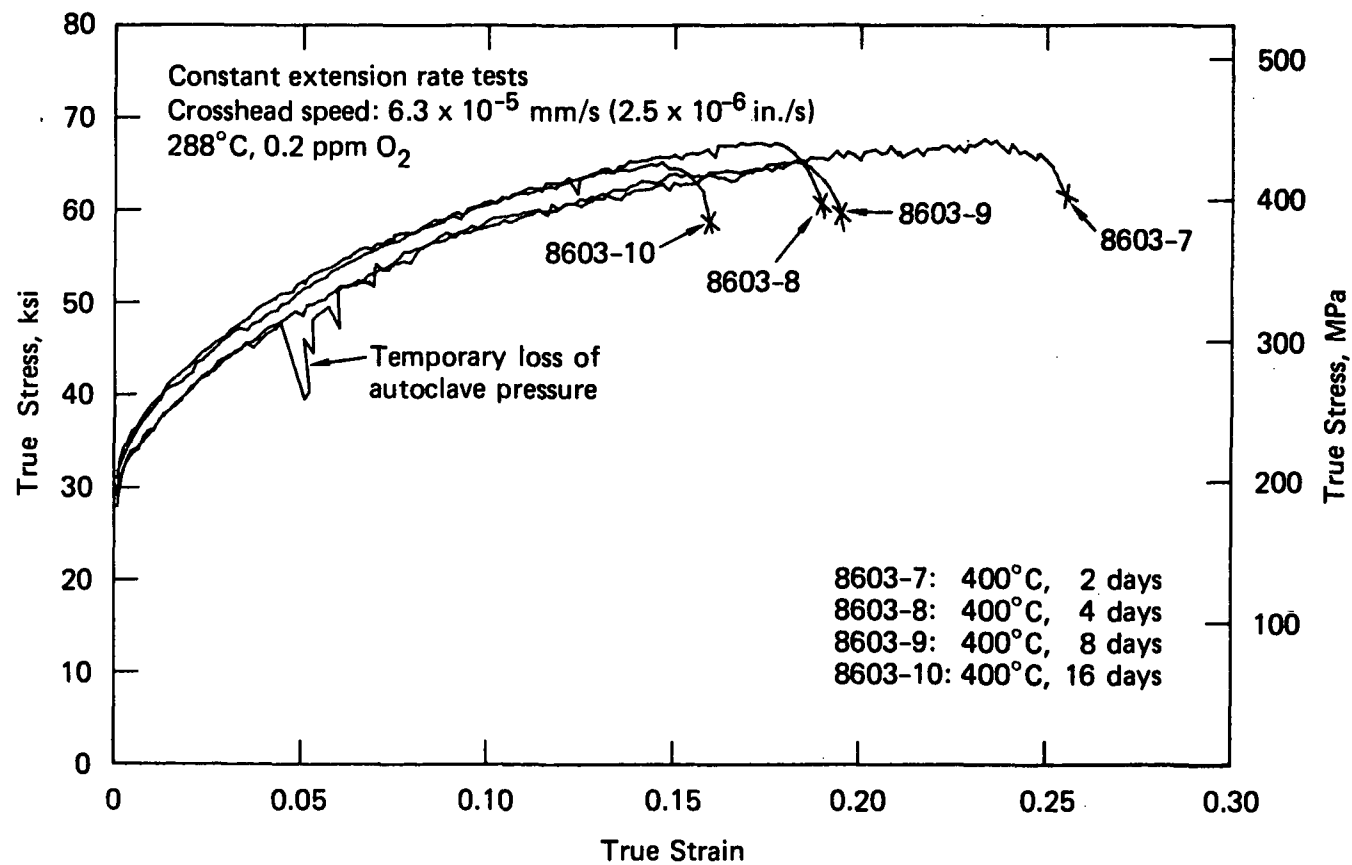
^bUTS: Ultimate tensile strength.

^ce: Elongation to failure, 6.35 cm (2.5 in.) gage length.

^dR.A.: Reduction in area at neck.

^eIGSCC: Percentage of fracture surface exhibiting intergranular stress corrosion cracking.

+ N.M.: Not measurable.



MA-8603-58

Figure 4. True-stress/true-strain curves for CERT Specimens 8603-7, 8603-8, 8603-9, and 8603-10. All were taken from the inside pipe wall location. The nominal strain rate was $1.0 \times 10^{-6} \text{ s}^{-1}$

where A depends on such factors as grain size, strain rate, surface condition, and environment but is a constant for these experiments, and Q is the activation energy of the process or processes controlling the growth of carbide precipitates at these temperatures. We can use the data from Table II to calculate this activation energy. The incubation period at 500°C is between 10 and 24 hours. The incubation period at 400°C is between 48 and 96 hours. Using the minimum values, the activation energy is:

$$Q = -R \left[\frac{\ln(\frac{1}{10}) - \ln(\frac{1}{48})}{\frac{1}{773} - \frac{1}{673}} \right] = 67 \frac{\text{kJ}}{\text{mole}}$$

Correspondingly, using the maximum values, the activation energy is:

$$Q = -R \left[\frac{\ln(\frac{1}{24}) - \ln(\frac{1}{96})}{\frac{1}{773} - \frac{1}{673}} \right] = 59 \frac{\text{kJ}}{\text{mole}}$$

Therefore, the activation energy for the sensitization of Type 304 stainless steel weld HAZs over the temperature of 500° to 400°C is 63 ± 4 kJ/mole, as determined from the limited CERT data.

Using this activation energy and the incubation times at 500° and 400°C, we can calculate a value for the pre-exponential factor, A, in Eq. [2]. The value is between 300 and 3000 hours⁻¹ depending on whether the maximum or minimum incubation times are used. Using the calculated values for Q and A, we can estimate the incubation time at 288°C using Eq. [2]. The estimated value is 647 ± 125 hours. Therefore, based on these limited data, it appears that sufficient sensitization for the initiation of IGSCC can develop in a weld HAZ in as little as one month under steady-state BWR operating conditions.

Povich and Rao,² from their CERT experiments on LTS-treated Type 304 stainless steel weld HAZs, measured an activation energy for sensitization between 500° and 350°C of about 160 kJ/mole. This value is considerably higher than the value deduced from the above incubation time data and leads

to an estimate of the time required to initiate IGSCC of 10 years at 288°C. This difference might be due to the fact that our estimates are based on only two data points. It may also be due to the fact that Povich and Rao used strain-to-failure as their measure of IGSCC, and strain-to-failure in CERT depends on both initiation and growth of intergranular cracks. Growth of intergranular cracks can depend on other parameters besides degree of sensitization (such as crack tip chemistry), and therefore they may have been measuring an activation energy for growth of intergranular cracks through sensitized Type 304 stainless steel rather than the activation energy for the sensitization process itself. Clearly, more incubation time data are needed to obtain a more accurate estimation of the time required to develop sufficient sensitization for the initiation of IGSCC under LTS heat-treatment conditions.

Compact Tension Experiments

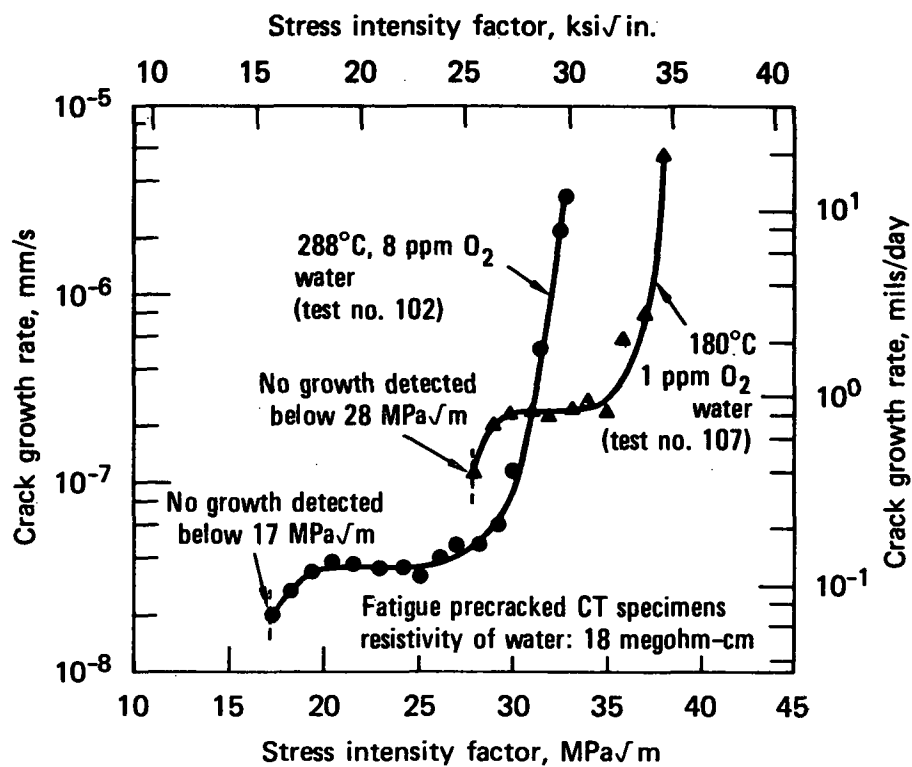
The seven CT tests performed in this program are summarized in Table III. The LTS heat treatment was the same in all cases: 500°C for 24 hours. As can be seen, cracking was observed in only two specimens, both of which were given this LTS heat treatment. We were unable to initiate cracking in as-welded specimens under our static loading conditions, irrespective of the environment. We were also unable to initiate cracking in LTS-treated specimens in environments containing less than 1 ppm O₂. Other workers^{9,10} have found similar difficulties in inducing cracking in low oxygen (<1.0 ppm O₂) environments, even under cyclic loading.

Crack-growth-rate/stress-intensity curves were successfully generated for those experiments in which cracking was initiated. These curves are shown in Fig. 5. The individual data points were calculated from the crack opening displacement, load, and time data as described earlier. The curves are best fits through these data. The crack opening displacement and load data were sufficiently consistent throughout the experiments that the stress intensity data are accurate to within $\pm 1 \text{ MPa}\sqrt{\text{m}}$ and the crack growth rate data are accurate to within $\pm 2 \times 10^{-8} \text{ mm/s}$.

Table 3
SUMMARY OF CRACK GROWTH-STRESS INTENSITY SCREENING EXPERIMENTS

<u>Test</u>	<u>Test Temp. (°C)</u>	<u>O₂ (ppm)</u>	<u>Specimen Condition</u>	<u>Time of Test (hr)</u>	<u>Max. K_I (MPa√m)</u>	<u>IGSCC</u>
8603-101	288	7.7	As-welded	120	66	No
8603-102	288	7.7	As-welded plus LTS	834	33	Yes
8603-103	288	7.7	As-welded	509	38	No
8603-104	288	0.2	As-welded plus LTS	507	38	No
8603-105	288	0.2	As-welded	512	38	No
8603-106	288	1.9	As-welded plus LTS	508	38	No
8603-107	180	1.0	As-welded plus LTS	643	38	Yes

LTS: 500°C, 24 hours, furnace cool.



MA-8603-50

Figure 5. Crack growth rate as a function of stress intensity factor for welded and low temperature sensitized Type 304 stainless steel in high purity water. For both specimens, the LTS treatment was 500°C for 24 hours.

The data in Fig. 5 are indicative of a strong environmental effect on crack growth rate. Dropping the test temperature 100°C increased the Stage II propagation rate an order of magnitude even though the dissolved oxygen content was lowered from 8 ppm O₂ to 1 ppm O₂. This is consistent with the CERT data of Ford,¹¹ which show a peak in growth rate at 180°C. It also appears that the threshold stress intensity (K_{ISCC}) increases with decreasing test temperature. However, this may be due to the crack stop-ping because there are no sensitized grain boundaries available at the crack tip. The environment of 180°C, 1 ppm O₂ is observed during BWR startups,¹² whereas the combination of 288°C and 8 ppm O₂ is rarely observed.¹²

The data in Fig. 5 also exhibit a stress-independent (Stage II) region that exists between 20 and 27 MPa√m for the 288°C, 8 ppm O₂ experiment, and between 30 and 35 MPa√m for the 180°C, 1 ppm O₂ experiment. The flatness of the curves in these regions suggests that the crack advance mechanism in LTS-treated material is electrochemically controlled rather than stress- (or strain-) controlled in these regions. These Stage II crack growth rates are also almost an order of magnitude lower at similar stress intensities than growth rates reported on material sensitized at temperatures above 600°C. Horn et al.¹⁰ have conducted experiments on Type 304 stainless steel specimens sensitized at 620°C and tested in 288°C, 8 ppm O₂ high purity water. They report growth rates of about 10⁻⁷ mm/s at stress intensities between 15 and 25 MPa√m. Park and Shack⁹ at Argonne National Laboratory report measuring growth rates of about 8 x 10⁻⁸ mm/s in the same environment on Type 304 stainless steel furnace sensitized at 600°C over the same stress intensity range. Indeed, they have not observed any definite stress-independent region. Neglecting any effects caused by differences in loading method or material chemistry, these results further suggest that the electrochemical process driving Stage II crack advance in LTS material is different from the mechanism (which may be stress-controlled) driving crack advance in furnace-sensitized material.

Note from Fig. 5 that, above 27 MPa√m for the 288°C, 8 ppm O₂ experiment and above 35 MPa√m for the 180°C, 1 ppm O₂ experiment, the growth rates are strongly dependent on stress intensity (Stage III).

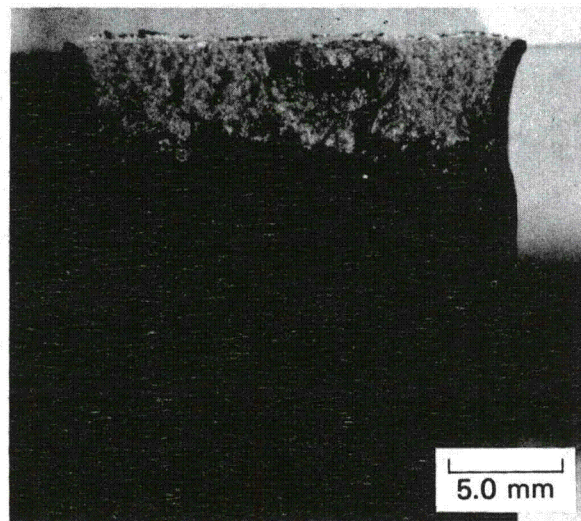
The data available suggest an exponential dependence of crack growth rate on stress intensity for both experiments. This strong dependence on stress intensity suggests that in this region the crack advance mechanism is stress- (or strain-) controlled rather than electrochemically controlled, and the stress intensity at which the transition from electrochemical to stress control is made depends on the environment. Therefore, while crack advance in material sensitized within the normal $M_{23}C_6$ precipitation range (i.e., above 600°C) is always controlled by crack tip stress, crack advance in LTS-treated material is controlled by crack tip stress above a certain environmentally controlled stress intensity level.

Finally, note from Fig. 5 that the threshold stress intensity for crack propagation (K_{ISCC}) is about 17 MPa \sqrt{m} for the 288°C environment and is about 28 MPa \sqrt{m} for the 180°C environment, and therefore appears to depend on the test environment. This effect can be understood at least qualitatively in terms of crack opening displacement. The smaller the crack opening, the smaller the amount of fresh water that can reach the crack tip in a given time to replenish the oxygen and to remove any corrosion products. For a given oxygen content, there is a critical crack opening (hence stress intensity) below which insufficient fresh water can reach the crack tip to drive the electrochemical process(es) controlling crack advance. Furthermore, the higher the oxygen content in the water, the smaller the amount of fresh water required at the crack tip in a given time to permit crack growth. Therefore, it is to be expected that higher oxygen content environments will exhibit lower threshold stress intensities.

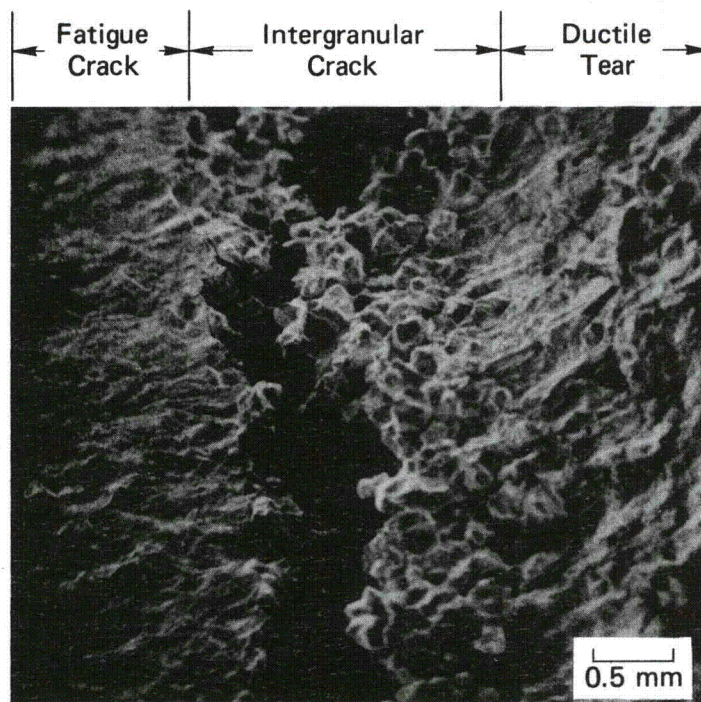
Optical and Scanning Electron Microscopy

All CT specimens were subjected to detailed posttest optical and scanning electron microscopic examinations to determine the actual final crack length, the planarity of the crack front, and the specific controlling crack advance mechanism(s). Because both specimens that exhibited cracking were very similar in appearance, we discuss only the specimen from Test 102.

Figure 6(a) shows an overall view of the crack plane. The fracture surface consists of three distinct zones. The dark, featureless zone



(a) Overall View of Crack Plane



(b) Scanning Electron Micrograph of Crack Tip

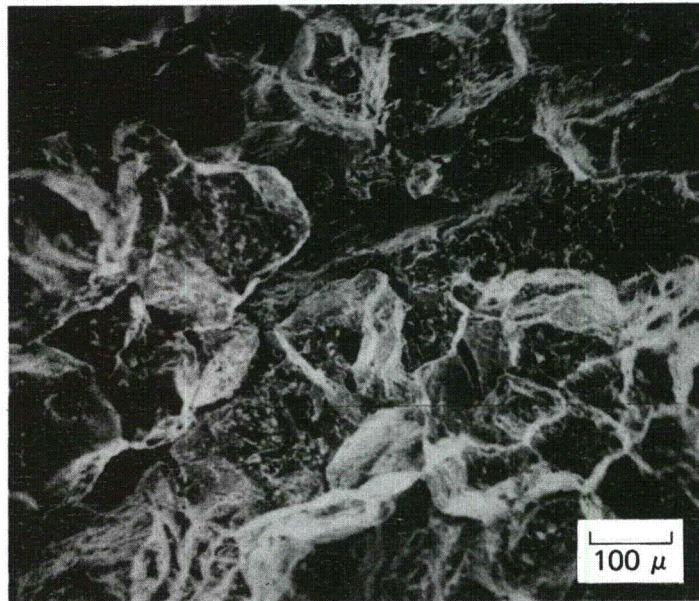
MP-8603-53

Figure 6. Microscopy on Specimen 8603-102, tested in 288°C, 8 ppm O₂ after LTS of 500°C for 24 hours.

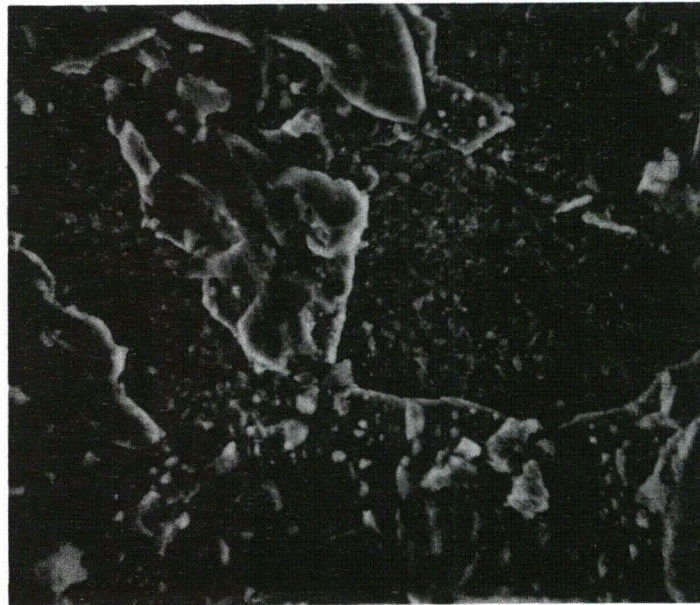
that starts at the notch root is the fatigue precrack. The shiny, rumpled zone is the ligament that was torn when the specimen was broken open after testing. The thin, dark, rumpled zone between the fatigue crack and the torn ligament is the zone of intergranular crack growth. This zone is 1.2 ± 0.1 mm wide and corresponds to the crack length calculated from the compliance measurements within the accuracy of the measurements. Note also that the intergranular crack front is reasonably straight and the crack surface is planar. Thus, the crack appeared to grow as fast at the edges of the specimen as at the center, and the crack propagated normal to the load axis. The plastic deformation visible on the sides of the specimen in Fig. 6(a) occurred when the specimen was torn open for the posttest examination. We conclude that, at least for crack extensions of about 1 to 2 mm, side notches for planar crack propagation are not necessary.

Figure 6(b) is a scanning electron micrograph of the fracture surface showing quite clearly all three zones: the fatigue crack growth zone, the intergranular crack growth zone, and the ductile tear zone. The crevice running along the boundary between the fatigue crack and the intergranular crack is another crack that initiated at the tip of the fatigue crack. However, it extended only a few grains and stopped because there were no additional sensitized grain boundaries nearby. This suggests that there was some crack tip branching before the propagation of the main intergranular crack.

Figure 7(a) is a higher magnification scanning electron micrograph of the intergranular crack growth zone showing that it is indeed intergranular with extensive separation between the individual grains. Figure 7(b) details the substructure visible on individual grain facets. This substructure consists of alternating smooth, featureless areas and rough areas. The boundaries between these areas appear to be well defined. There are two possible explanations for this surface appearance. First, the smooth areas are part of the actual crack surface exposed by the propagating crack, and the rough areas are corrosion products deposited on this crack surface at a later time. The alternative explanation is that the rough areas are



(a) Note Extensive Intergranular Separation



(b) Detail of One Intergranular Facet

MP-8603-51

Figure 7. Detailed views of intergranular crack on Specimen 8603-102.

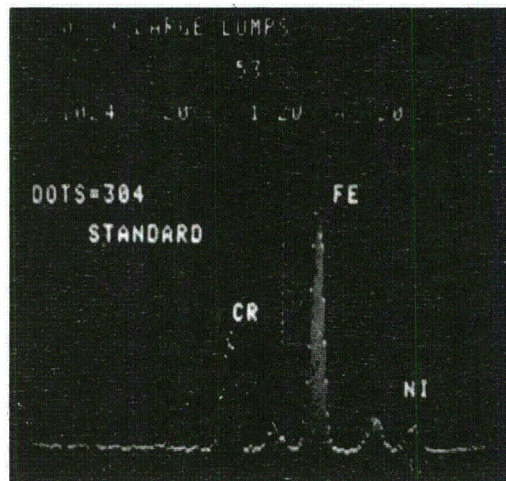
$M_{23}C_6$ grain boundary precipitates and the smooth areas represent exposed material. If the first explanation is correct, then the crack propagates primarily along the precipitates/matrix interface. If the second explanation is correct, then the crack propagates primarily through the matrix adjacent to the precipitates (i.e., through the depleted zone).

We performed energy dispersive X-ray analyses on the fracture surface of this specimen to determine which of the above crack advance mechanisms is correct. The results of these analyses are shown in Fig. 8. The count times were adjusted to yield the same iron peaks, thereby allowing direct comparison of chromium peak heights. As expected, both regions contain primarily iron, nickel, and chromium. The chromium content in the rough areas is significantly less than the iron content and is even less than the bulk chromium content of Type 304 stainless steel (dotted line). If the rough areas were fractured carbides, then the chromium peak should at the least, be higher than the Type 304 stainless steel standard and closer to the iron peak. A low chromium content is, however, expected in a corrosion product. The chromium content in the smooth areas, on the other hand, is much higher than the 304 standard, indicating that in these regions the chromium content is much higher than the matrix chromium content. This is expected if the smooth areas were actually the surface of fractured $M_{23}C_6$ precipitates. The smooth areas are certainly not depleted in chromium. Therefore, it appears that, in LTS-treated material, the intergranular cracks propagate primarily along the carbides/matrix interface rather than through the depleted zone in the matrix material itself.

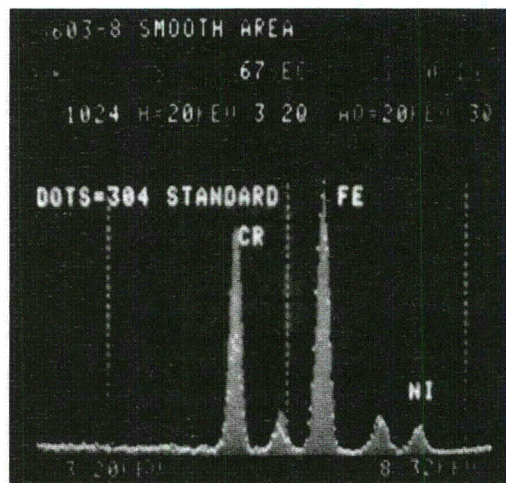
CONCLUSIONS

The following conclusions can be made from the results of this study.

- LTS heat treatments accelerate the initiation of intergranular cracks in welded specimens. Extrapolation of incubation time data collected during CERT predicts that, in the presence of appropriate environmental and stress conditions, initiation of IGSCC can occur in weld HAZs in as little as one month at 288°C.
- LTS-treated CT specimens exhibit crack growth rates that are independent of crack tip stress state over a range of applied stress intensities. The stress intensity at which the transition from stress-independent to stress-dependent growth occurs varies with the test environment. Also, the magnitudes of the growth rates in the stress-independent regime (Stage II) depend on the environment, suggesting that the stress-independent growth is electrochemically controlled.
- The Stage II crack growth rates in LTS-treated weld HAZs are an order or magnitude lower than those reported by other workers on Type 304 stainless steel sensitized at 600°C.
- Intergranular stress corrosion cracks in LTS-treated weld HAZs seem to propagate along the carbide/matrix interface rather than through the chromium-depleted zone in the matrix itself.
- The limited CT data and the microscopy studies imply that a different mechanism is controlling the growth of intergranular cracks through LTS-treated Type 304 stainless steels HAZs. The chromium depletion model,^{13,14} usually associated with growth through Type 304 stainless steel sensitized in the $M_{23}C_6$ precipitation range does not seem to fit the data on LTS-treated material. However, there are insufficient data at this time, particularly at very low sensitizing temperatures (<400°C), to clearly identify what mechanism is controlling crack advance in LTS-treated weld HAZs.



(a) Rough Areas in Figure 7(b)



(b) Smooth Areas in Figure 7(b)

MP-8603-52

Figure 8. Energy dispersive X-ray records of intergranular crack on Specimen 8603-102.

ACKNOWLEDGMENTS

The authors would like to acknowledge the financial support of the Electric Power Research Institute, Palo Alto, California, under Contract T-110-1, for this research. They would also like to acknowledge the valuable assistance of D. Cubicciotti, Electric Power Research Institute, and S. Wing and K. Borg, SRI International, during this work.

REFERENCES

1. M. J. Povich, Corrosion, 1978, Vol. 34, p. 60.
2. M. J. Povich and P. Rao, Corrosion, 1978, Vol. 34, p. 296.
3. R. D. Caligiuri et al., "Low Temperature Sensitization--Phase I," Semiannual Progress Report 2 on Project T-110-1, submitted to Electric Power Research Institute, Palo Alto, CA, July 1980.
4. R. D. Caligiuri et al., "Low Temperature Sensitization--Phase I," Semiannual Progress Report 2 on Project T-110-1, submitted to Electric Power Research Institute, Palo Alto, CA, July 1980.
5. U. Cihal, Prot. Met. (USSR), 1968, Vol. 4, p. 563.
6. American Society for Testing and Materials, "Standard Methods of Tension Testing of Metallic Materials," Specification E8-69, 1978 Annual Book of Standards.
7. American Society for Testing and Materials, "Standard Test Method for Plain Strain Fracture Toughness of Metallic Materials," Specification E399-78, 1978 Annual Book of Standards.
8. A. Saxena and S. Hudak, Jr., Inst. J. Fracture, 1978, Vol. 14, p. 453.
9. J. Y. Park and W. L. Shack, "Corrosion Studies of Nuclear Piping in BWR Environments, "Semiannual Report on Project T-117-1, submitted to Electric Power Research Institute, Palo Alto, CA, July 1980.
10. R. M. Horn et al., "The Growth and Stability of Stress Corrosion Cracks in Large Diameter BWR Piping," Semiannual Report 2 on Project T-118-1, submitted to Electric Power Research Institute, Palo Alto, CA, June 1980.

11. F. P. Ford, "Effects of Oxygen-Temperature Combinations on the SCC Susceptibility of SA533-6 Carbon Steel in BWR Quality Water," Semiannual Report on Contract 1248-1, submitted to Electric Power Research Institute, Palo Alto, CA, May 1979.
12. P. L. Andresen, "Investigation of Benefits of BWR Oxygen Control," Semiannual Report 2 on Project T-115-3, submitted to Electric Power Research Institute, Palo Alto, CA, December 1980.
13. C. Stawström and M. Hillert, J. Iron Steel Inst., January 1967, p. 77.
14. F. P. Ford and M. Silverman, "Mechanisms of Environmentally Enhanced Cracking in Alloy/Environment Systems Peculiar to Power Generation Industries," First Semiannual Report on Contract RP1332-1, submitted to Electric Power Research Institute, Palo Alto, CA, June 1979.

IAEA - SPECIALISTS MEETING ON SUBCRITICAL CRACK GROWTH
FREIBURG FEDERAL REPUBLIC OF GERMANY
13-15 MAY 1981

EFFECTS OF PWR ENVIRONMENT ON THE FATIGUE
CRACK GROWTH OF DIFFERENT STAINLESS STEELS AND
INCONEL TYPE ALLOY

C. AMZALLAG* - G. BAUDRY** - J.L. BERNARD**

Abstract :

The FCGR of the main materials (Ni base alloys, and stainless steels) in contact with the primary coolant of pressurized water reactors have been investigated. Attention was paid to environmental (temperature, reactor coolant hot water, frequency) and metallurgical parameters (grain size, delta ferrite content, thermal aging).

Depending on the type of materials, different behaviours were found. In general, temperature and PWR environment appears as the more important parameters for FCGR.

* CREUSOT-LOIRE - CENTRE DE RECHERCHES - 42701 FIRMINY FRANCE

** FRAMATOME - Tour FIAT Cédex 16 - 92084 PARIS LA DEFENSE

1. INTRODUCTION

The main materials in contact with the primary coolant of Pressurized water Reactors (PWR) are :

- Ni base alloys of INCONEL type
- austenitic and austenitic-ferritic stainless steels.

These materials are used as forgings, castings, claddings, and weldments.

The safety analyses require the knowledge of the fatigue crack growth rates (FCGR) of these materials taking into account the reactor environment and metallurgical parameters. For this purpose, the influence of the following parameters on FCGR of these materials was studied :

- Environmental and operating parameters : temperature, reactor coolant hot water, frequency
- Metallurgical parameters : grain size, delta ferrite content, thermal aging.

In order to insure that results are as representative as possible, tests have been carried out on specimens taken from actual components or from materials having chemical and mechanical properties representative of these components.

2. MATERIALS

The materials studied and their main applications are :

a) Ni base alloys :

- Wrought material (INCONEL 600), mainly used for partition plate of steam generators, weldments, and cladding, also used in these components,

b) Stainless steels :

- Austenitic wrought material, (Z3 CND 17-12, with low carbon content and controlled nitrogen, close to AISI 316).

This grade is mainly used for primary coolant piping.

Materials with 2 grain sizes (coarse and standard) were studied ;

- Austenitic-ferritic cast materials : Z4 CN 20-09, similar to CF8 mainly used for pump casings, and Z4 CND 19-10, similar to CF8M used for elbow pipes.
- Austenitic-ferritic welds, used for joining these elements. The welds studied are made in 308L, and in 316L.

The austenitic-ferritic materials were studied in unaged and aged states. The aging treatments were performed in order to closely simulate the thermal service conditions during the life of the reactor.

The chemical compositions, heat treatments, and mechanical properties of all the materials studied are given in table I to IV.

3. EXPERIMENTAL PROCEDURES

All the tests were performed at CREUSOT-LOIRE UNIEUX Laboratory. They have been conducted on hydraulic testing machines with C.T. precracked specimens. Tests were conducted at low R ratio : P_{min} / P_{max} ($0,05 \leq R \leq 0,1$).

In PWR environment, tests are performed in autoclaves mounted on testing machines. The crack growth is monitored continuously through the measure of compliance by a LVDT attached to the lips of the specimen, inside the autoclave. In order to get a calibration curve relating the crack opening to the crack length, beach marks are produced during the test, by cycling at high frequency with the maximum load constant and increased minimum load. Most of the tests were performed in a water corresponding to the composition given in table V.

4. Ni BASE ALLOYS-EFFECT OF TEMPERATURE, HOT WATER ENVIRONMENT, AND TYPE OF MATERIAL ON FCGR

The test matrix for Ni base alloys is presented in table VI. For the case of the welded metal and the cladding orientation is given in Fig.1. For wrought base metal orientation was LT.

The results obtained on base metal and on weldment in air and in PWR environment are given respectively in fig. 2 and 3. It can be noticed that :

- For a given environment, there is no significant difference between the FCGR of the base metal and weld metal
- In air environment there is a slight effect of temperature,
- there is a significant effect of PWR environment at low frequency (4 cpm).

The results obtained in air environment are in good agreement with those reported by JAMES [1] on wrought materials in the same temperature range.

In PWR environment, tests were conducted with 2 different Cl⁻ contents :

Cl⁻ = 0,15 ppm for the weld metal and 0,5 ppm for the base metal. Very similar crack growth rates were obtained for both materials. This shows that the level of Cl⁻ content does not influence significantly the FCGR in the range investigated.

Two other tests in hot water environment were performed on a cladding in the same conditions, (Cl⁻ content < 0.15 ppm). The FCGR results obtained are given in fig. 4 and compared to those obtained on the base metal and on the weld metal. It can be seen that :

- the upper results for the cladding are closed to the results on the base metal and on the weld metal,
- the lower results are slightly above those obtained in air at 320° C.

HALE et al [2] have performed similar fatigue crack growth tests on INCONEL 600 in BWR environment in the same frequency range with a skewed sawtooth waveform. For purpose of comparison, the scatter band of their results is graphically reported on fig. 5. Our results are located in the upper part of their scatter band.

The overall results indicates a definite but likely limited effect of PWR environment on FCGR in Nickel base alloys.

5. RESULTS ON STAINLESS STEELS

5.1. Wrought austenitic stainless steels - Influence of temperature, pressurized hot water, frequency, and grain size

The influence of these parameters on FCGR was investigated on Z3 CND 17-12. Results have been presented earlier [3.4]. In order to serve as reference for the comparison with austenitic-ferritic stainless steels, it is useful to recall them :

- Temperature (320° C) has a significant influence on FCGR of Z3 CND 17-12. The FCGR is enhanced by a factor of about 3 between room temperature and 320° C. Similar results were reported in the literature [5] on 316 stainless steel. Frequency was found to have no significant influence in air in the 300° C temperature range.
- It was found that pressurized hot water environment have no significant influence on the FCGR of Z3 CND 17-12 at low frequency (4 cpm). Results of tests at very low frequency (4 cph) show a slight increase of crack growth rate. Some enhancement of FCGR with decreasing frequency from 5 cpm to 0,3 cpm was also noticed by HALE et al [2] in the case of 304 and 304 L in BWR environment.

In the primary circuit piping, grain size is usually 4 to 6 (ASTM), but coarse grain can be found. Due to this variability the possible effect of grain size on FCGR in PWR environment was investigated. Two materials with fine (7 ASTM - 30 μ m) and coarse (1-2 ASTM, 75,250 μ m) grain sizes were tested at 4 cpm in PWR environment. No effect was found.

In summary, for this type of material, temperature appears to have a definite effect on FCGR. The other parameters investigated, such as PWR environment frequency, and grain size have no significant or a slight effect.

5.2. Cast austenitic-ferritic stainless steels effect of temperature, environment, ferrite content, and aging on FCGR

The table VII presents the tests performed on the two cast stainless steels studied, i.e. Z4 CN 20 09 (CF8) and Z4 CND 19.10 (CF8M).

The fig. 6 and 7 show the effect of the temperature in air environment on FCGR for the two materials. One can notice a less pronounced effect of temperature on FCGR than for wrought materials. In particular, this effect seems negligible for the

lowest values of $\Delta K \lesssim 30 - 35 \text{ MPa } \sqrt{\text{m}}$). A similar behaviour can be observed from the results obtained by JAMES for CF8 [6].

The effect of PWR environment on FCGR has been investigated for these steels at low frequency (4 cpm for Z4 CN 20.09 and 1 cpm for Z4 CND 19.10).

The results obtained are presented in fig. 8 and 9, and compared with those obtained in air. In the case of Z4 CN 20.09, fig. 8 exhibits a significant effect of PWR environment essentially for $\Delta K \lesssim 25.30 \text{ MPa } \sqrt{\text{m}}$. For higher values of ΔK , crack growth rates become similar. Results obtained on Z4 CND 19.10 (fig. 9) show also the same trend.

The delta ferrite content of the cast components of PWR reactors is specified and allowed to vary between 10 and 25 %. In order to know its influence on FCGR in PWR environment, two heats of Z4 CN 20.09 with 12.5 and 17.5 F.N. (ferrite number) according to SCHOEFER'S diagram [7] were tested. The fig. 8 shows that the ferrite content doesn't have a significant effect on FCGR at 4 cpm for the range studied.

The ferrite contained in these alloys is submitted to Fe-Cr decomposition during aging at temperatures below 550°C [8]. The influence of this decomposition on tensile properties and charpy energy were described elsewhere by BAUDRY and PICHARD [8]. An aging treatment was applied on Z4 CND 19-19 [8].

Aging at 400°C during 7,500 h was performed, in order to fairly obtain the material in the end of the life condition for a plant. In air environment, the aging has no significant effect on FCGR at R.T. and 320°C (fig. 7). These results are consistent with those obtained by LANDERMAN and BAMFORD [10], and BERNARD et al. [4] on centrifugally cast austenitic-ferritic stainless steels.

The overall results on cast austenitic-ferritic materials essentially shows that :

- temperature effect is less pronounced than for wrought austenitic materials,
- PWR environment has a slight effect,
- ferrite content in PWR environment and aging in air environment have no significant effect.

V.3. Austenitic-ferritic weldmetal-effect of temperature, environment, and aging on FCGR

The matrix of tests performed on the weldmetal (308 L, manual welding, and 316 L, automatic welding) is presented in table VII. Fig. 10 indicates the crack orientation in the weld.

The results obtained in air environment at R.T. and 320° C are presented in fig. 11. It appears that there is no significant difference between the two types of weldmetal. This is in good agreement with the results of JAMES[11], who does not found any significant influence of the welding process on the FCGR on 308 weldmetals. The effect of temperature is slight. A little increase of FCGR can be noticed at 320°C essentially for $\Delta K \geq 30 \text{ MPa } \sqrt{\text{m}}$.

The effect of PWR environment were studied on 308 L. The results obtained at 4 cpm in water are compared with those found in air at the same temperature in fig. 12. They show a slight effect, if any, of PWR environment on FCGR. This is consistant with the results obtained by BAMFORD on a 316 weldmetal [12].

Austenitic-ferritic weldments are sensitive to aging at temperatures below 500°C for the same reasons as for castings (see § V.2.). The 308 L weldment was aged for 10,000 h at 400° C to simulate the material condition at the end of the life of the reactor. Fig. 13 shows that the FCGR at R.T. is very similar for aged and unaged material. This behaviour is not surprising, since weldments are generally not so sensitive to aging than castings[9], and since aging has no significant effect on FCGR of Z4 CND 19-10 cast stainless steel (§ V.2.).

The synthesis of all the results on weldments indicates a slight effect of temperature and PWR environment. Aging and welding procedure have no significant effect in air environment.

6. CONCLUSION

The primary emphasis of this work was to get informations on the effect of reactor environment on FCGR for the main materials in contact with the primary coolant of pressurized water reactors. Particular attention was paid to metallurgical parameters

Significant results have been obtained. They can be summarized as follow :

- For all materials, a significant effect of temperature was found in air environment however this effect was smaller for austenitic-ferritic cast stainless steels.
- At low frequency (1 to 4 cpm), pressurized hot water environment have a significant effect on FCGR of Ni base alloys. This effect was less pronounced for austenitic and austenitic-ferritic stainless steels.
- The other parameters investigated (thermal aging in air environment, frequency, ferrite content, and grain size in PWR environment) seems to have no sensitive effect.

The overall results allows a better knowledge of the CGR for the components of the primary circuit.

REFERENCES

- 1 JAMES, L.A., "Fatigue - Crack propagation behaviour of INCONEL 600", Int. J. Pres. Wes. and Piping, 5, 1977, pp 241-259.
- 2 HALE, D.A., C.W. JEWETT, J.N. KASS, "Fatigue crack growth behaviour of four structural alloys in high temperature high purity oxygenated water" Journal of Engineering Materials and Technology", July 1979, Vol. 101, pp 191-198.
- 3 BERNARD, J.L., HOUSSIN, B., SLAMA, G., "Validation des caractéristiques de calcul des matériaux constituant le circuit primaire des réacteurs à eau sous pression", In Reliability Problems of reactor pressure components, Vol. I, IAEA, Vienne 10 - 13 october 1977, pp 251-287.
- 4 BERNARD, J.L., SLAMA, G., AMZALLAG, C., RABBE, P., "Influence of P.W.R. environment on fatigue crack growth behaviour of stainless steels", IAEA Technical Committee Meeting on Time and Load Dependent Degradation of Pressure Boundary Materials, Innsbruck, Austria, 20-21 November 1978.
- 5 SHAHINIAN, P., SMITH, H.H., WATSON, H.E., "Fatigue crack growth in type 316 stainless steel at high temperature", Journal of Engineering for Industry, November 1971, pp 976-980.
- 6 JAMES, L.A., "Fatigue crack propagation in a cast stainless steel in a pressurized water reactor environment", ASME Paper 77-PVP 34, 1977.
- 7 SCHOEFER, "Constitution diagram for stainless steel castings", Metal Progress, Feb. 1976- p. 55.
- 8 GROBNER, P. J., "The 475° C Embrittlement of ferritic stainless steels", metallurgical Transactions, Vol. 4, January 1973, pp 251-260.
- 9 BAUDRY, G., PICHARD, C, "Evolution lors de maintiens de longue durée entre 300 et 450° C des caractéristiques mécaniques des aciers moulés et des joints soudés austéno-ferritiques utilisés dans les centrales nucléaires à eau pressurisée", Congrès des Appareils à Pression, AFIAP, Paris, octobre 1980.

- 10 LANDERMAN, E.I., BAMFORD, W.H., "Fracture Toughness and fatigue characteristics of centrifugally cast type 316 stainless steel pipe after simulated thermal simulated thermal service conditions", ASME meeting, "Ductility and Toughness-consideration in elevated temperature service". San Francisco 10-15 Déc. 1978 - p 99 - 127.
- 11 JAMES, L.A., "Crack Propagation behaviour in type 304 stainless steel weldments at elevated temperature", welding J. Research Supp., 52, 4, 173 s, (1973).
- 12 BAMFORD, W.H., "Fatigue crack growth of stainless steel reactor coolant piping in a pressurized water reactor environment, ASME Paper 77 PVP - 34, 1977.

TABLE I - Ni base alloy type INCONEL - characterization

I.a) Chemical composition

	C	Mn	Si	S	P	Ni	Cr	Fe	Cu	Co	Ta + Nb
wrought material	0.060	0.31	0.33	0.003	0.009	73.29	16.50	9.49	0.001	0.005	-
weldmetal	0.056	7.82	0.31	0.011	0.004	66.11	15.64	7.87	0.003	0.016	2.17
cladding	0.008	3.45	0.54	0.002	0.002	72.25	18.51	2.50	0.16	0.02	1.96

I.b) Heat treatment

wrought material	air quenched - 950°C
weldment	-
cladding	-

I.c) Tensile properties

Température	material	R _{0.002} (N/mm ²)	R _m (N/mm ²)	A (%)	Z (%)
R.T.	wrought material	242 262	657 673	47 47	
	weldmetal	401 411	578 636	14 23	26 36
320°C	wrought material	185 216	596 611	42 40	
	weldmetal	299 325	592 581	30	47

TABLE II - Cast austenitic-ferritic stainless steel - Z4CN20.09
Characterization

II.a) Chemical composition and ferrite content

heat	Chemical Composition (%)											ferrite content	
	C	Mn	Si	S	P	Ni	Cr	Mo	Cu	N	Co	calculated SCHOEFFER (FN)	measured (%)
A	0.034	0.710	0.68	0.010	0.024	8.46	19.69	0.12	0.098	0.046	0.042	24	10
B	0.027	0.700	0.55	0.011	0.024	8.58	19.27	0.14	0.092		0.045	12,5 *	7.5
C	0.040	0.750	0.50	0.012	0.023	8.58	21.20	0.08	0.105		0.035	17,5 *	17.5

* with N estimated ~ 0.045 %

II.b) Heat treatment

waterquenched - 1100°C

II.c) Tensile properties

Température	heat	R _{0.002} N/mm ²	R _m N/mm ²	A %	Z %
R.T.	A	263 288	493 520	50 45	81 80
	B	300 288	521 545	40 44	76 70
	C	253 243	501 510	47 52	71 73
320°C	A	156 140	352 354	32 31	62 52
	B	156 159	372 364	29 31	49 60
		174 174	391 407	28 29	68 55

TABLE III - Cast austenitic-ferritic stainless steel - Z4CND19.10
Characterization

III.a) Chemical composition and ferrite content

Chemical composition (%)											ferrite content	
C	Mn	Si	S	P	Ni	Cr	Mo	Cu	N	Co	calculated SCHOEFER (FN)	measured (%)
0.040	0.80	0.81	0.016	0.021	10.56	20.76	2.48	0.10	0.042	0.040	17.5	19

III.b) Heat treatment

waterquenched - 1100°C

III.c) Tensile properties

Température	state	R _{0.002} (N/mm ²)	R _m (N/mm ²)	A (%)	Z (%)	KCU (daJ/cm ²)
RT	unaged	293	573	40	76,5	17,2 17,6
	aged 7500 h at 400°C	313 329	747 753	30 25.5	49 35	3,6 2.8
343°C	unaged	179 188	454 469	25.5 30	49 43	-
	aged 7500 h at 400°C	214 232	664 663	21 ≥20.5	24 24	-

TABLE IV - Austenitic-ferritic stainless steel weldmetal 308 L and 316 L -
Characterization

IV.a) Chemical composition and ferrite content

Grade	Welding	Chemical composition (%)										ferrite content	
		C	Mn	Si	S	P	Ni	Cr	Mo	Cu	N	calculated ASME S 75 (FN)	measured (%)
308L	manual	0.013	1.43	0.61	0.007	0.016	10.59	19.24	0.010	0.050	0.040	7	5.5
316L	automatic	0.019	0.86	0.70	0.011	0.024	10.59	18.68	2.28	0.065	0.066	14	6.5

IV.b) Tensile properties (as welded)

Température	Type	State	R _{0.002} (N/mm ²)	R _m (N/mm ²)	A (%)	Z (%)	KCU (daJ/cm ²)
R.T.	316 L automatic	unaged	465	613	29	36	6.4 7.6
	308 L manual	"	439 452	541 544	43 46	59 62	6.2 6.4
	"	aged 10.000 h at 400°C	417	586	37	51	6.2 5.8
343°C	316 L automatic	unaged	375	474	17.5	35	
	308 L manual	aged 10.000 h at 400°C	344 363	391 390	27 27	58 62	

TABLE V - Characterization of PWR fluid

Température : 320°C

pressure : 155 bars

pH at R.T. : 5.1

O₂ < 0.10 ppm

Cl < 0.15 ppm

F < 0.15 ppm

boric acid (exprimed in ppm of boron) : 2500 ppm

LiOH : necessary quantity for ajustement of pH

Electrical conductivity : 2 - 40 µmho/cm

TABLE VI - Ni base Alloys - Tests of FCGR

material	environment	fréquency
base métal	air - R.T	10 hz
	air - 320°C	"
	PWR *	4 cpm
weldmetal	air - RT	10 hz
	air - 320°C	10 hz
	PWR	4 cpm
cladding	PWR	4 cpm

* $\text{Cl}^- = 0,5 \text{ ppm}$

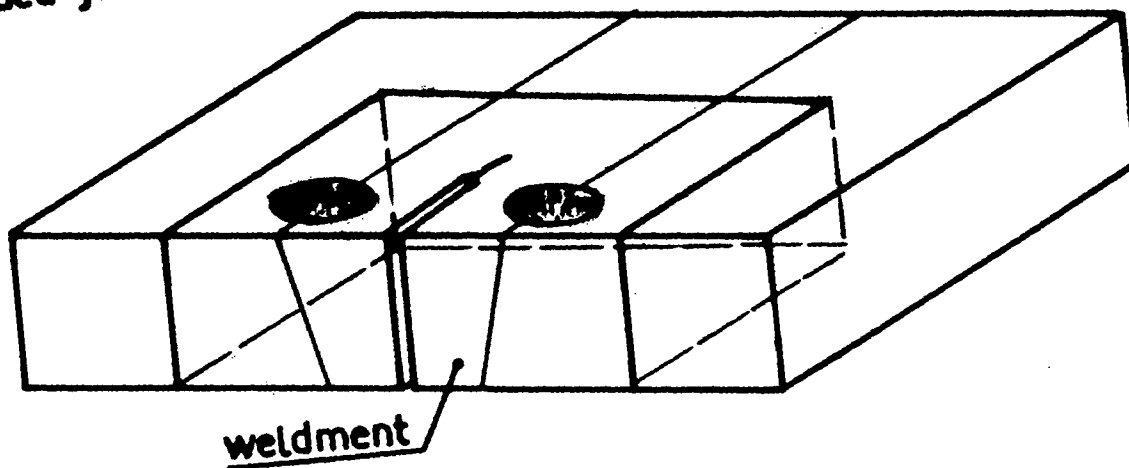
TABLE VII - Cast stainless steel-tests of FCGR

material	environment	ferrite content (FN) (SCHOEFER)	aging	frequency
Z4CN20.09 (CF8)	air - RT	14	no	10 hz
	air - 320°C	14	"	"
	PWR	12,5	"	4 cpm
	"	17,5	"	"
Z4CND19.10 (CF8M)	air - RT	17,5	no	20 hz
	air - 320°C	"	"	10 hz
	PWR	"	"	1 cpm
	air - RT	"	7.500 h at 400°C	20 hz
	air - 320°C	"	"	10 hz

TABLE VIII - Austenitic - ferritic weldmetal-tests of FCGR

grade	type of welding	environment	aging	frequency
308 L	manual	air amb	no	10 hz
		air 320°C	"	5 hz
		PWR (Cl ~ 0,17 ppm, B ~ 2800 ppm)	"	4 cpm
		air amb	10.000 h at 400°C	10 hz
316 L	automatic	air amb	no	10 hz
		air 320°C	"	5 hz

1.a welded joint



1.b cladding

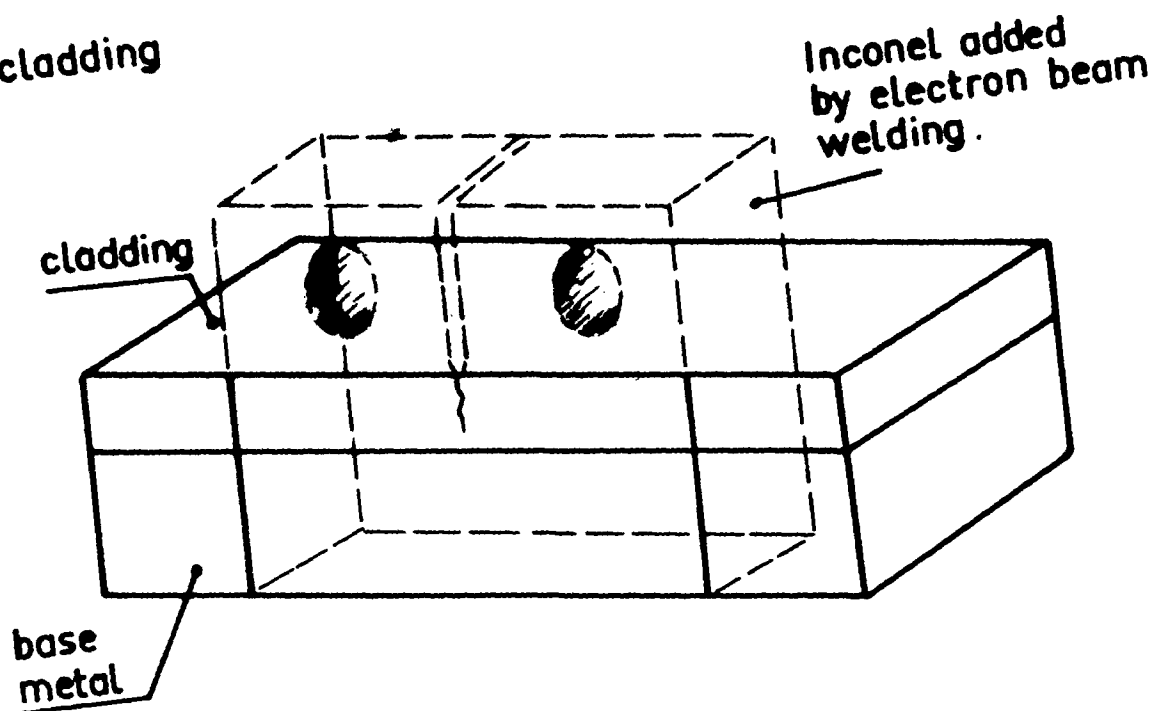


FIG. 1 - Ni base alloy - Position of CT specimens.

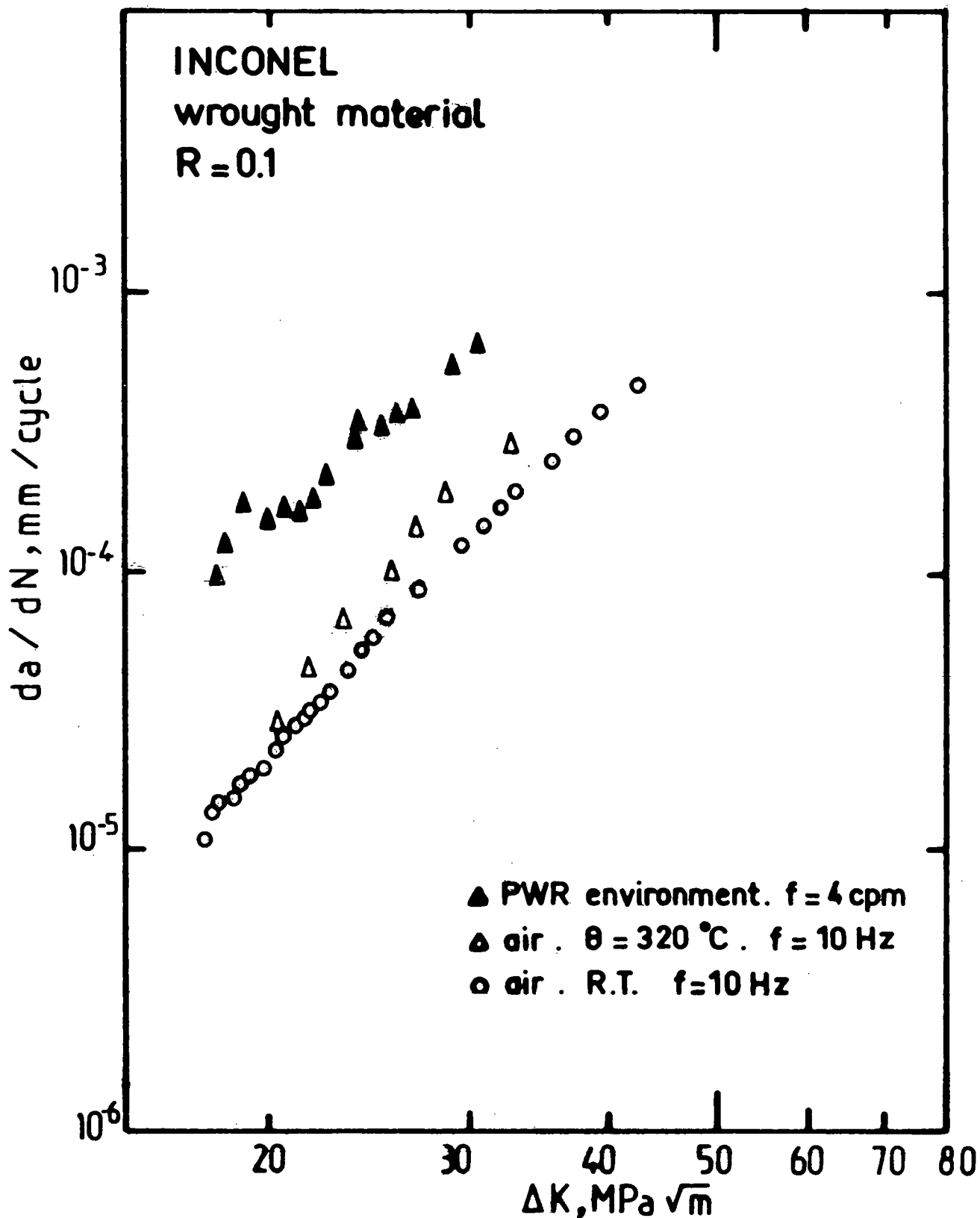


FIG. 2 - INCONEL - Wrought material - Effect of temperature and PWR environment on FCGR.

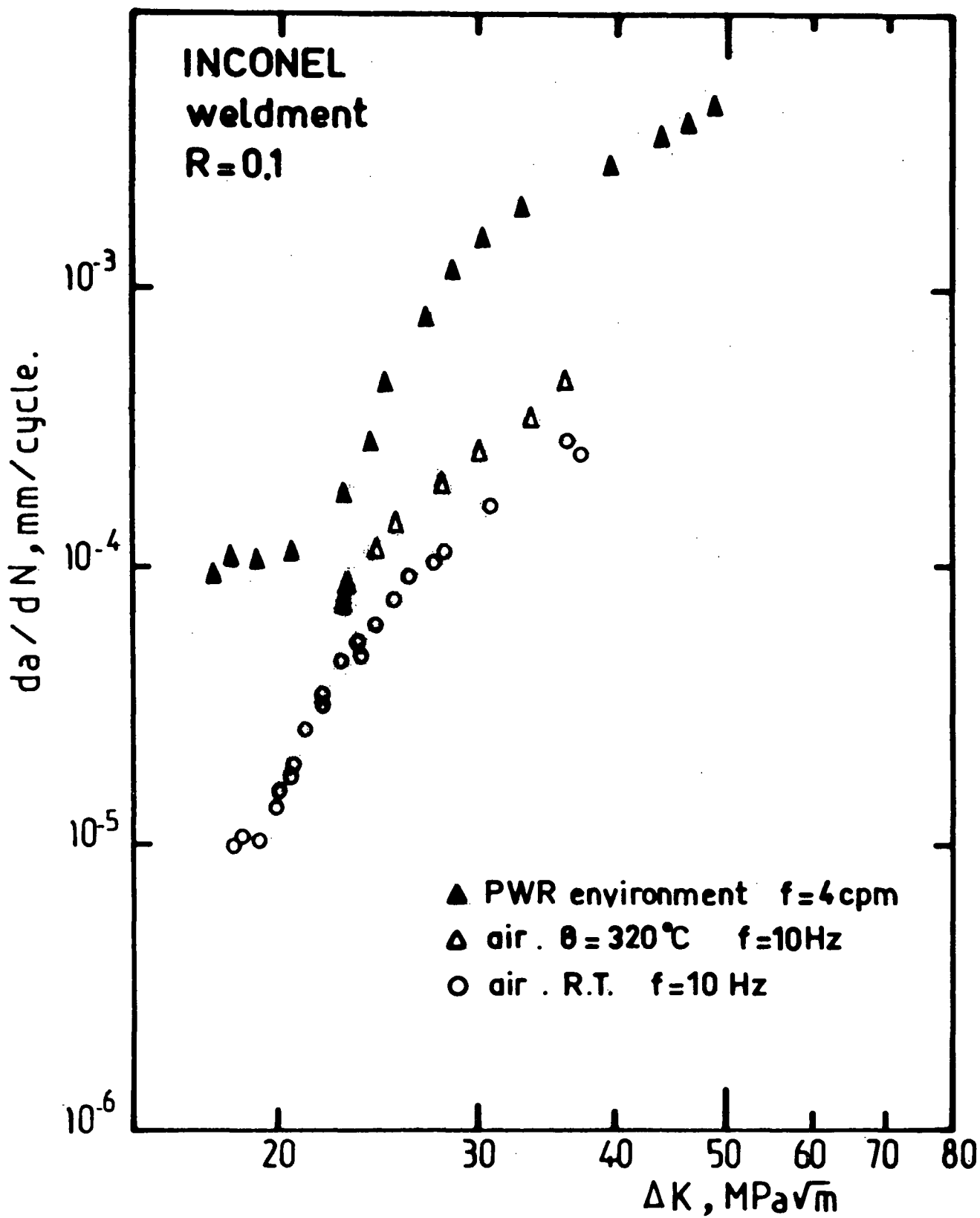


FIG. 3 - INCONEL - Weldment (MMA) - Effect of temperature and PWR environment on FCGR.

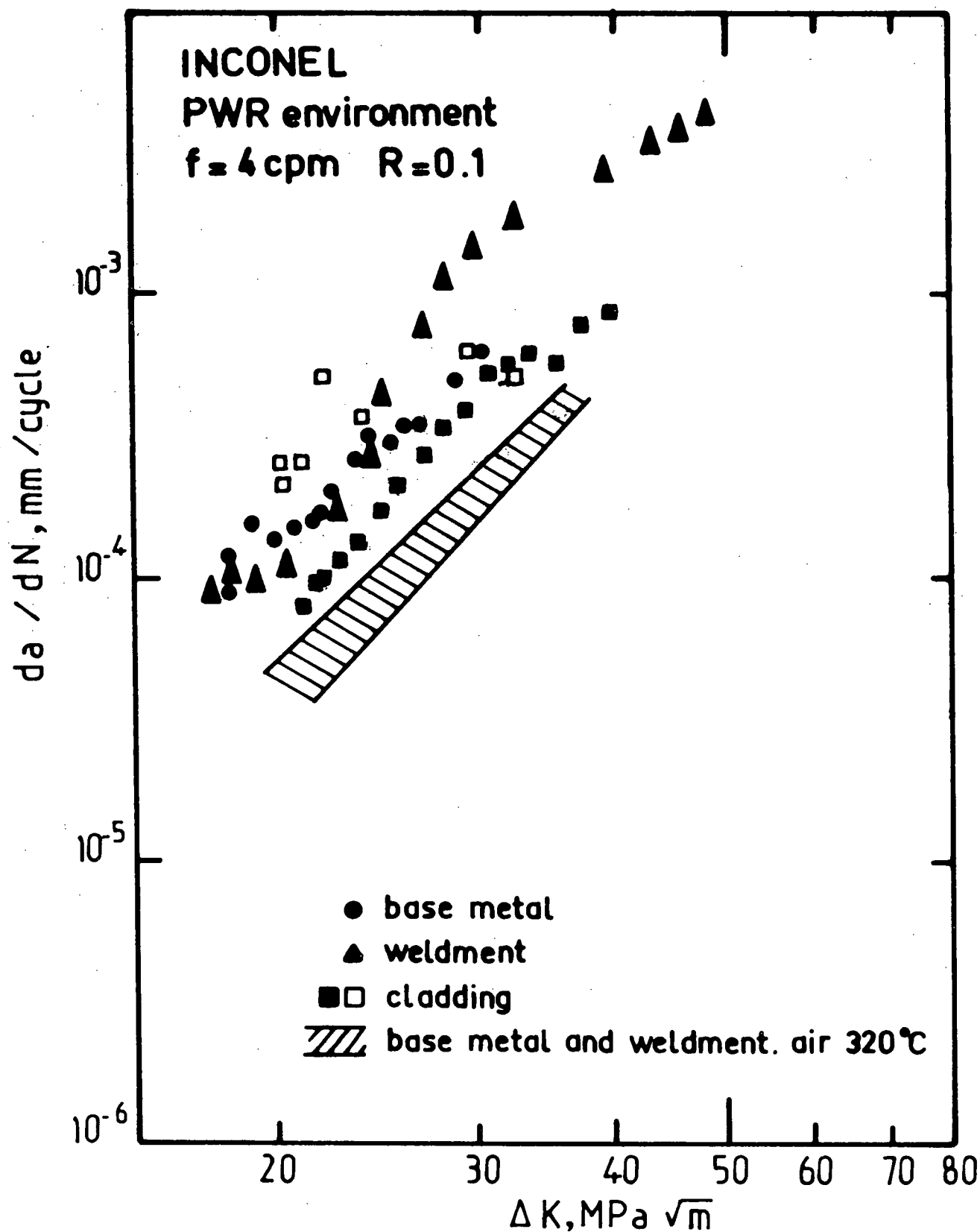


FIG.4 - INCONEL - Comparaision of FCGR obtained on different types of materials in PWR environment and in air.

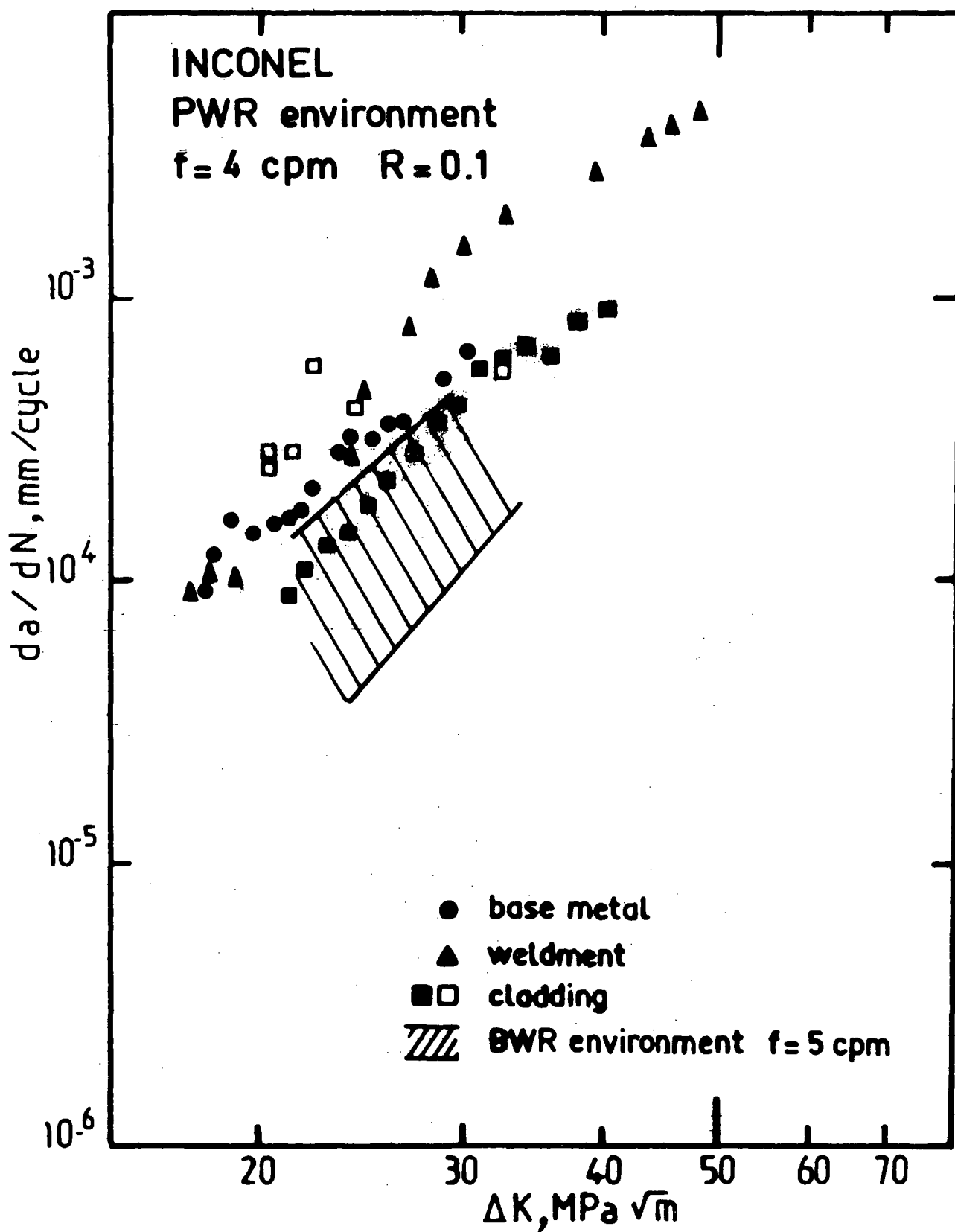


FIG. 5 - INCONEL - Comparison of FCGR obtained in PWR and BWR environment.

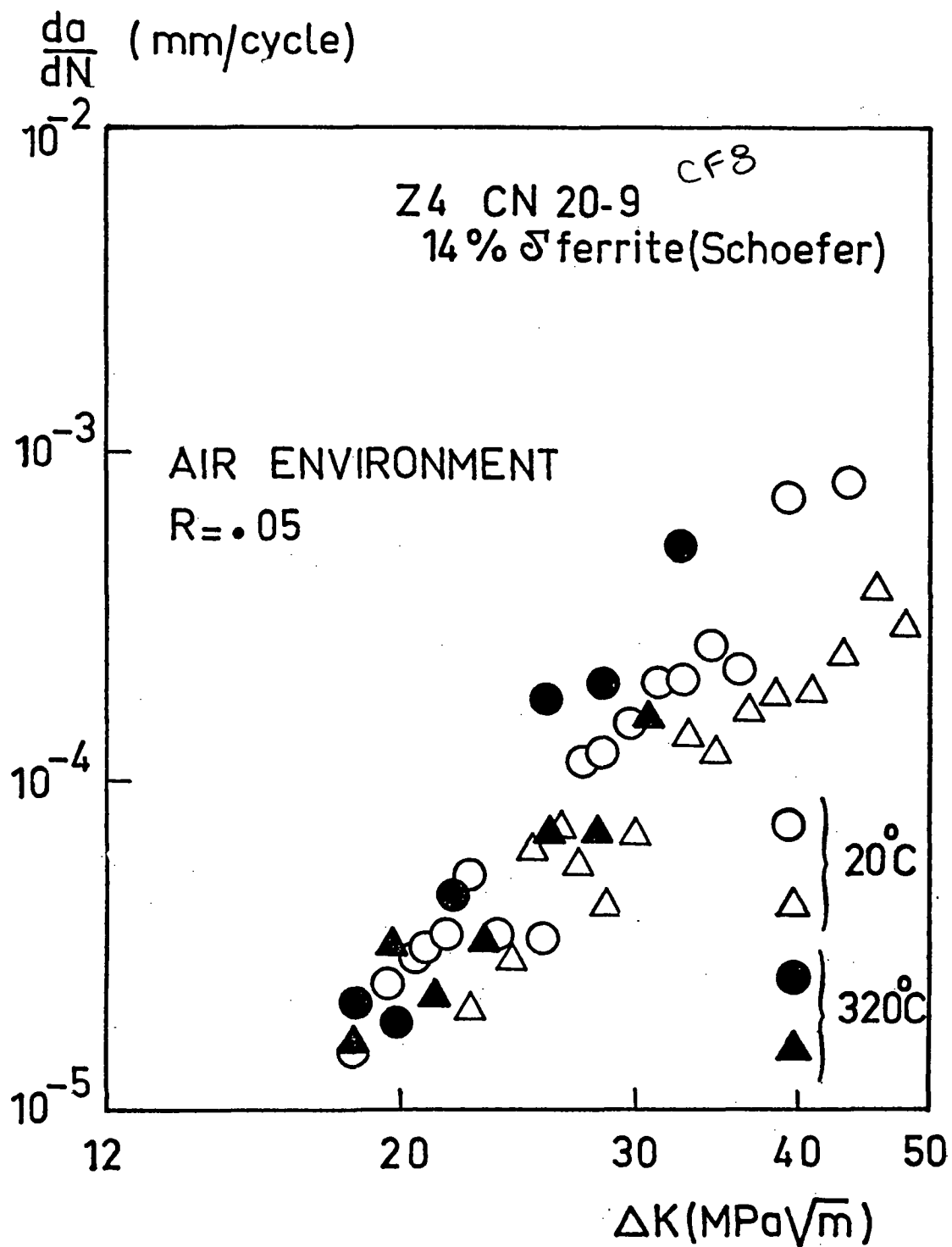


fig. 6 INFLUENCE OF TEMPERATURE ON
FATIGUE CRACK GROWTH RATE OF Z4 CN 20-9
STAINLESS STEEL

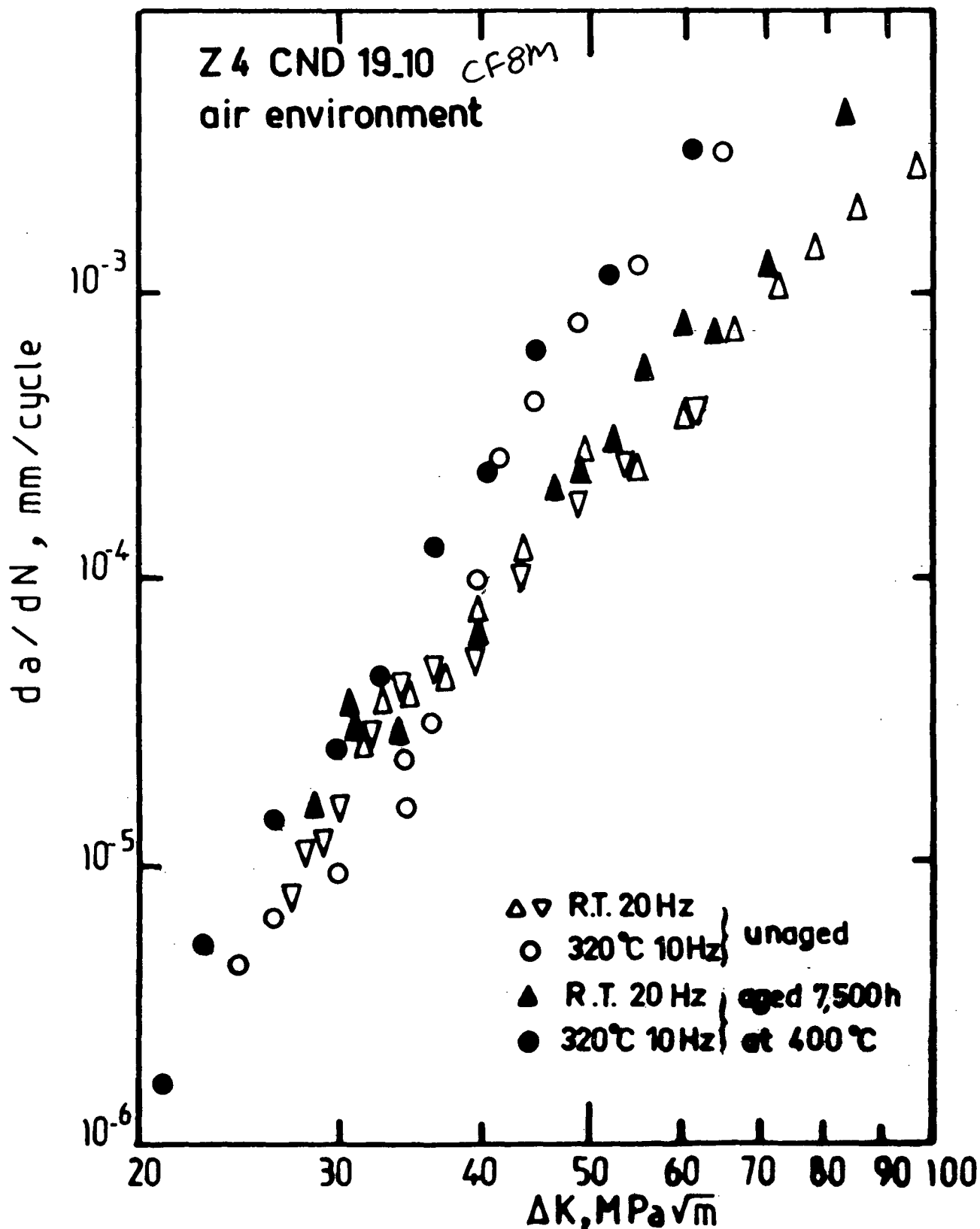


FIG. 7 - Z 4 CN D 19.10 - Air environment.
Effect of test temperature and aging.

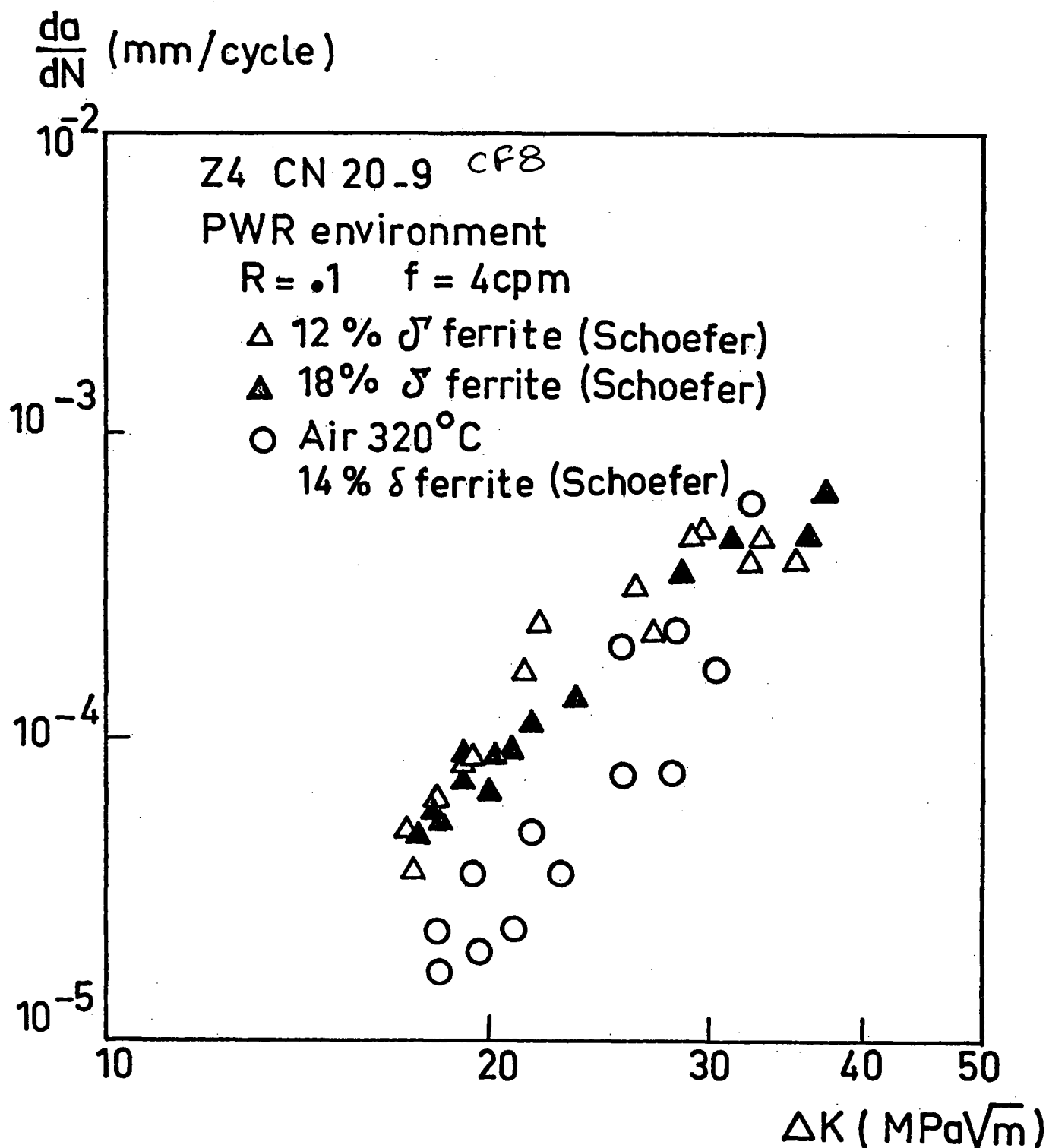


fig.8 FATIGUE CRACK GROWTH RATE OF THE Z4 CN 20-9 STEEL IN PWR ENVIRONMENT

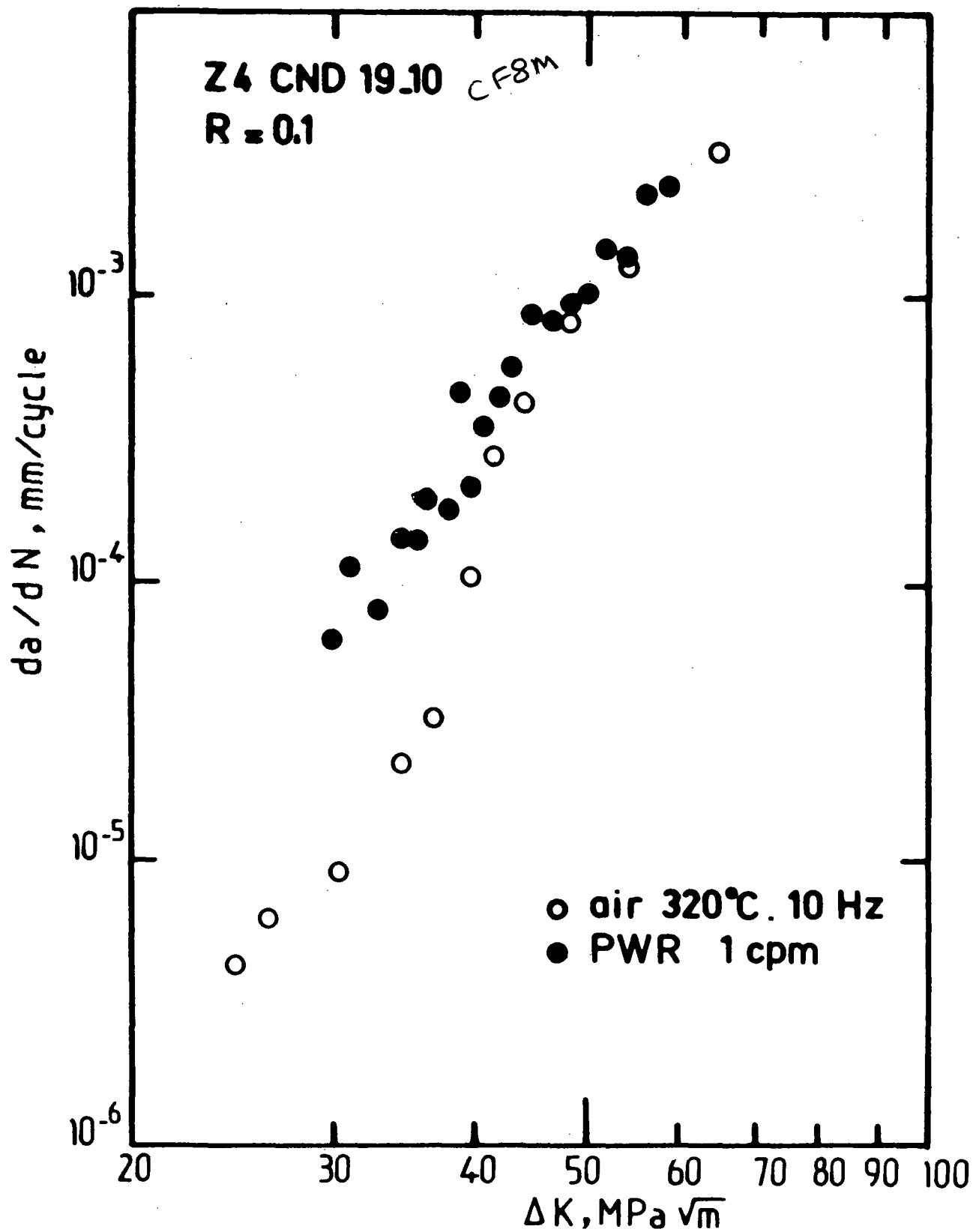


FIG. 9 - Z 4 CN D 19.10 - ● = 320°C
 Effect of PWR environment.

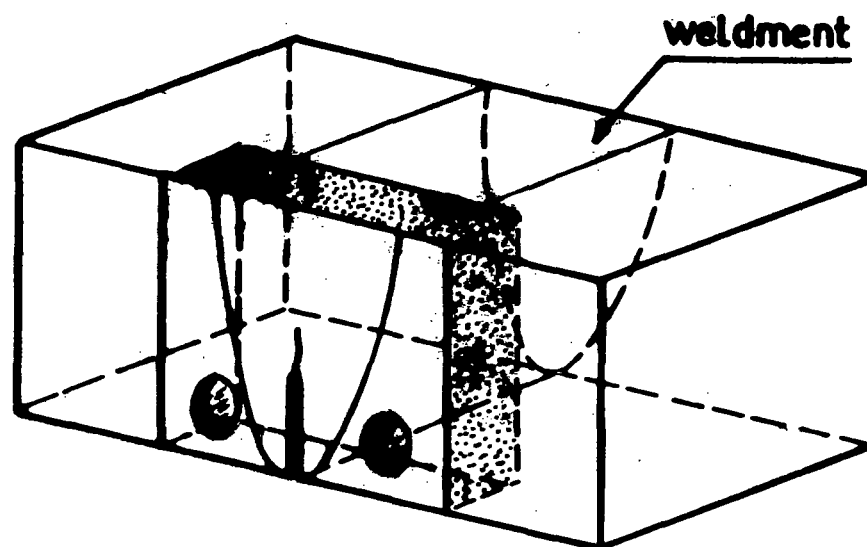


FIG. 10 - Austeno-ferritic weldments.
Position of C.T. specimens.

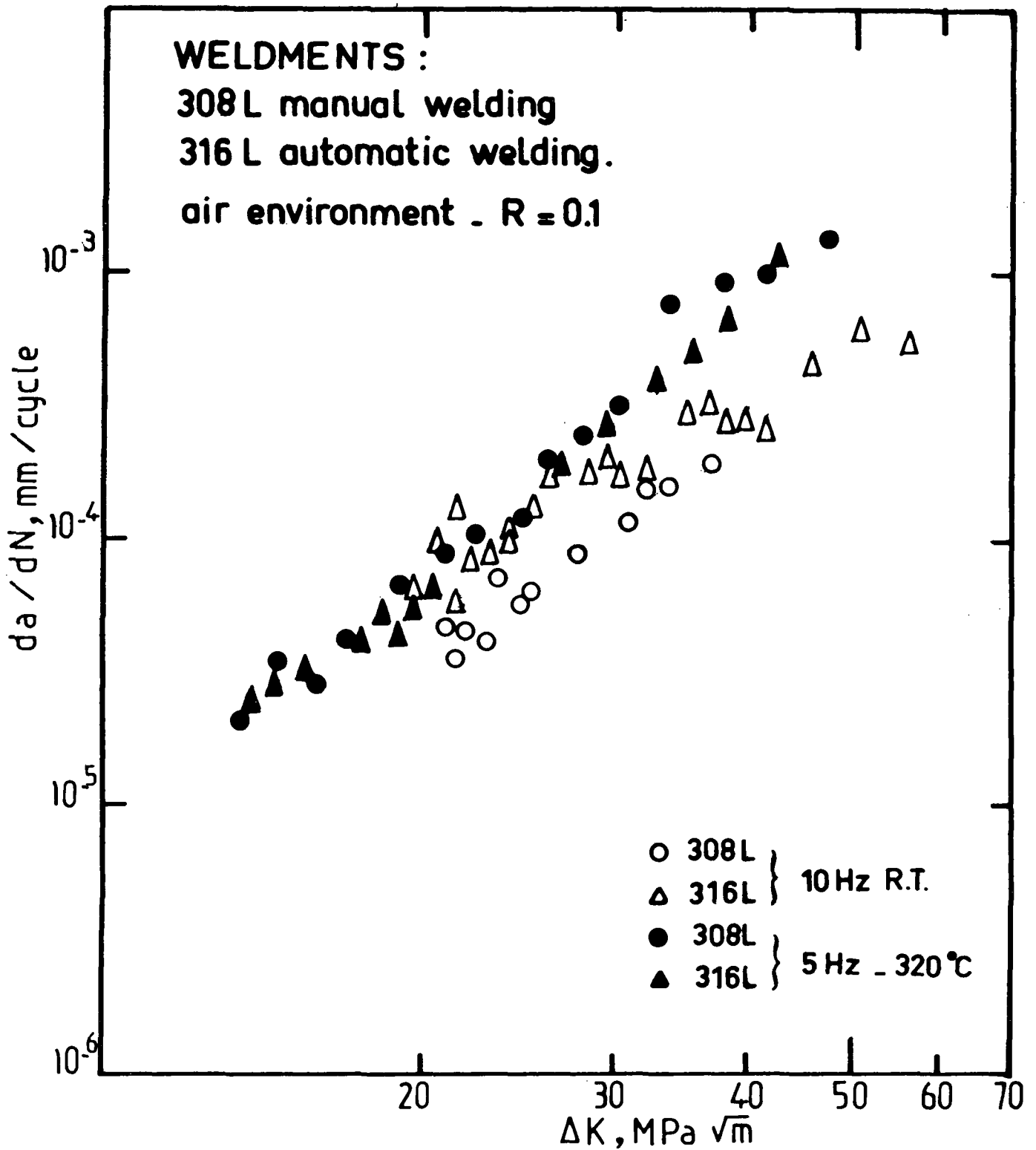


FIG. 11 - Weldments - air environment. Effect of type of weldment and temperature.

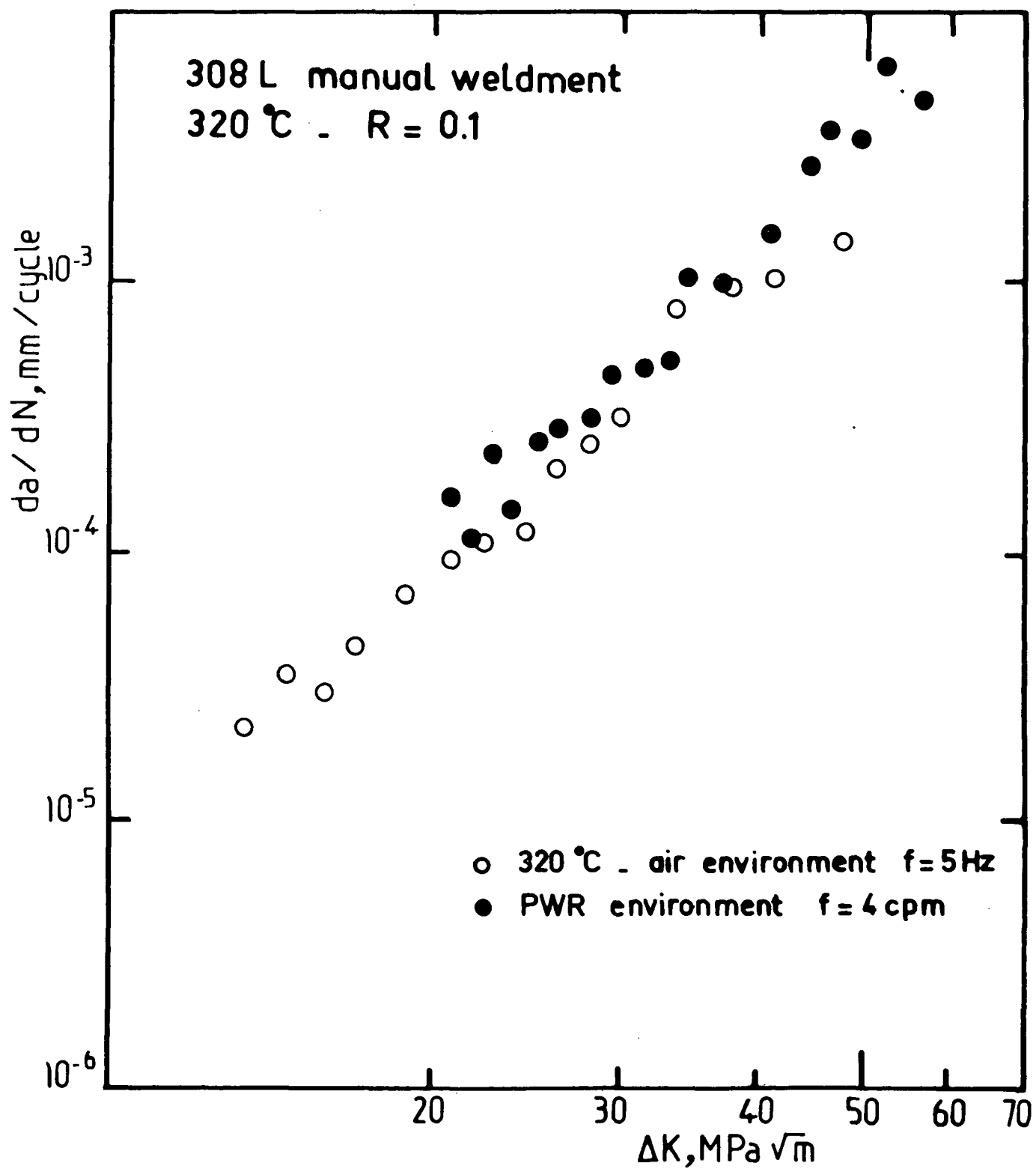


FIG. 12 - 308L manual weldment - $\theta \approx 320^\circ$ - Effect of PWR environment.

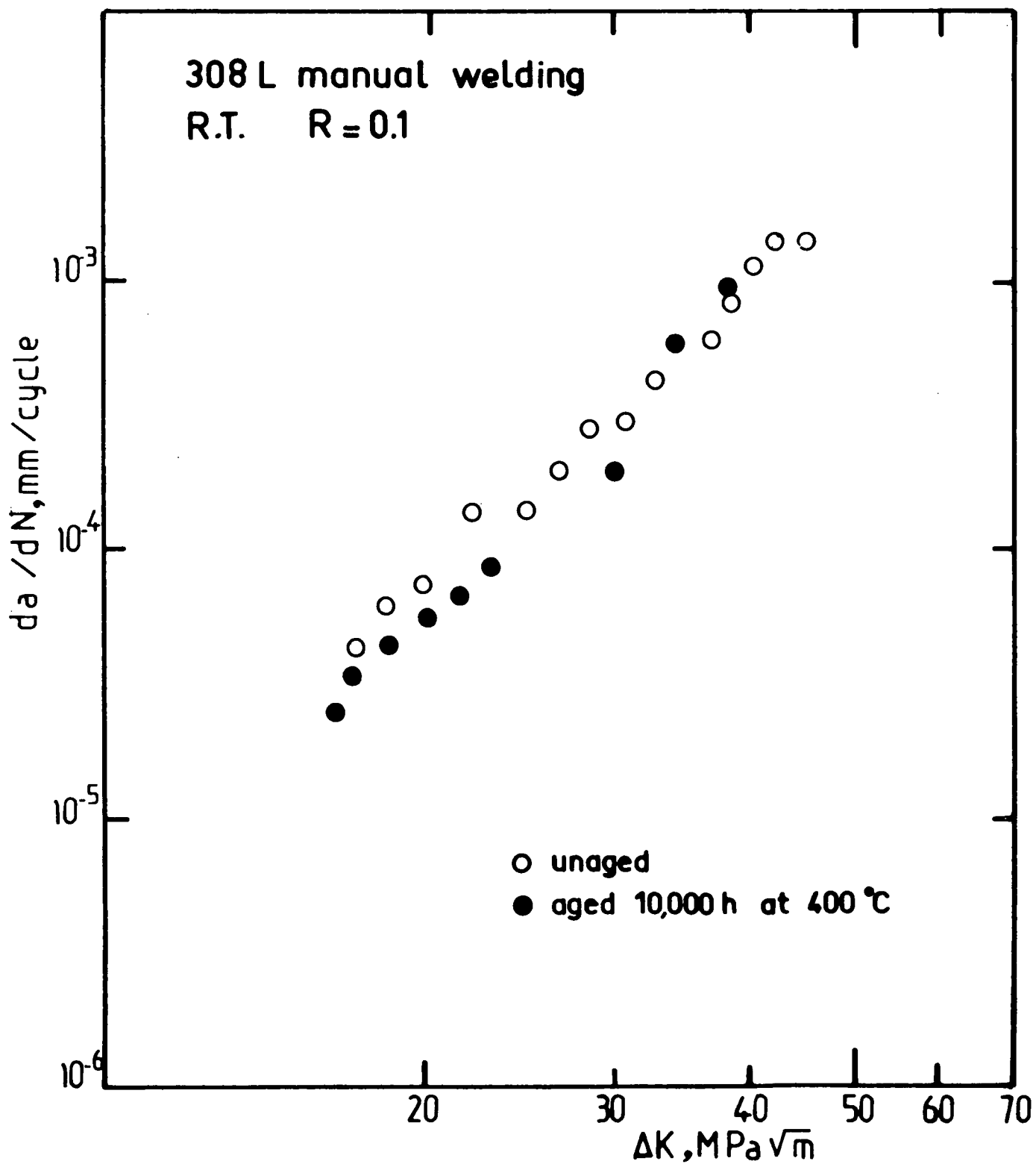


FIG. 13 - 308L manual weldment. R.T. effect of aging.

THE ROLE OF UNCERTAINTY IN THE
MEASUREMENT OF CRACK LENGTH BY
COMPLIANCE TECHNIQUES

R.G. Ballinger*, R.M. Latanision**, W.C. Moshier*,
R.M.N. Pelloux**

*Research Assistants, Massachusetts Institute of Technology,
Cambridge, Massachusetts, U.S.A.

**Professors, Department of Materials Science and Engineering,
Massachusetts Institute of Technology, Cambridge,
Massachusetts, U.S.A.

ABSTRACT

An experimental program is underway to investigate the effect of thermal treatment and electrochemical potential on the cyclic crack growth behavior of Inconel-600 and Inconel X-750 in deoxygenated high purity water at 290°C. As part of the program an investigation has been conducted to determine an approximation for the degree of uncertainty in the elastic compliance technique used for determining crack length. Preliminary results indicate that for room temperature-air crack growth measurements an uncertainty of approximately 1.5% can be expected for the value of measured compliance. For the specimen geometry used this translates to an uncertainty in the effective crack length of 0.25 mm. In an aqueous environment at 290°C, 10.34 MPa the estimated uncertainty in compliance measurement can be as much as 6.5% which translates to a crack length uncertainty of 1.83 mm. These uncertainty values have a significant impact on the measurement intervals required for statistically meaningful crack growth rate data generation.

1. INTRODUCTION

Failure of components by environmentally assisted fatigue cracking is a significant problem in the nuclear industry. Failures which have at least been assisted by a fatigue loading interactions include Inconel-600 steam generator tubes, and Inconel X-750 fasteners, for example. Fatigue is also of concern in predicting life expectancy of heavy section nuclear components such as pressure vessels. It is important that accurate data be available for fatigue crack growth rates in the actual operating environments so that sound design decisions can be made.

With the above concerns in mind the Electric Power Research Institute is funding a program at the Corrosion Laboratory at the Massachusetts Institute of Technology whose aim is to obtain fatigue crack growth rate data for Inconel-600 as a function of thermal treatment and electrochemical potential in environments which simulate that which may exist in both Pressurized Water Reactors (PWR's) and Boiling Water Reactors (BWR's). The fatigue cracking study is part of a larger study which, in addition, is concerned with investigating the effect of variables such as trace element segregation and grain boundary chemistry on the fatigue cracking behavior of Inconel-600 and Inconel X-750.

The measurement of fatigue crack growth rates in a simulated PWR or BWR environment cannot be accomplished by direct optical techniques. Techniques which have been used in the past for indirect crack growth measurement include potential drop (AC or DC) and compliance measurement. In an environment where the electrochemical potential is a controlled variable the use of potential drop techniques are precluded leaving only the compliance technique.

The use of elastic compliance has an advantage in that its calculation requires the measurement of only two fundamental quantities, load and displacement. Compliance calibrations exist for several specimen geometries and displacement measurement point locations. [1,2] Under ideal circumstances both load and displacement can easily be measured with sufficient accuracy to allow prediction of crack length. However, when conditions deviate from the ideal, it is important that an estimate be made of the possible error in crack length which may result from errors in the measurement of compliance. This paper will discuss results of an investigation of sources of uncertainty and their impact on crack length prediction in simulated PWR or BWR environments.

II. DESCRIPTION OF EXPERIMENTAL APPARATUS

The experimental equipment for the measurement of fatigue crack growth rates at high temperatures consists of an autoclave system installed in a servohydraulic

fatigue machine. Crack opening displacements are measured using a Linear Variable Differential Transformer (LVDT) attached directly to the specimen. The autoclave system is constructed entirely of titanium and operates at a temperature of 290°C, a pressure of 10.34 Mpa, and a flow rate of 3.7 liters per hour.

The specimen type used for the experimental program is of the compact tension (CT) design with demensions conforming to the recommendations of ASTM E647-78T, "Tentative Test Method for Constant-Load-Amplitude Fatigue Crack Growth Rates Above 10^{-8} m/cycle". The specimen width (w) is 5.08 cm and thickness is 1.27 cm.

Due to the desire to exercise electrochemical potential control, electrical isolation of the specimen from the rest of the system is required. This isolation is achieved as follows:

- * Specimen pin holes are enlarged from 1.27 cm to 1.524 cm to allow the use of a zirconia bushing between the loading pin and the specimen.
- * Zirconia washers are used to insure that the sample sides do not contact the grips at any time.
- * The LVDT is insulated from the specimen through the use of a zirconia standoff.

- * The entire specimen, with the exception of a .635 cm wide strip on each side of the specimen parallel to the expected crack growth plane, is plasma sprayed with magnesium zirconate.

III. COMPLIANCE MEASUREMENT AND CRACK LENGTH DETERMINATION

Compliance measurement is achieved by measuring crack opening displacement with an LVDT attached directly to the specimen front face and measuring specimen load with a load cell external to the autoclave. The LVDT used is a Schaevitz Model 100XS-ZTR with a linear displacement range of $\pm .254$ cm. Compliance measurements are made at selected intervals by stopping the test and then measuring the slope of the displacement versus load curve upon unloading. This information is combined with materials constants to determine the elastic compliance:

$$C = BE \frac{dv}{dp} \quad (1)$$

where B is the specimen thickness, E is the elastic modulus, and dv/dp is the slope of the displacement-load curve.

Once the compliance is measured the crack length can be inferred by using either an empirically determined compliance-crack length relationship or making use of theoretical compliance-crack length relationships such as that derived by Newman [2]. In general experimental and theoretical compliance-crack length relationships agree quite well, usually within one percent when the experimental calibration curve is derived under as close to ideal conditions

as possible, using accurately machined cracks of varying lengths.

IV. IMPORTANCE OF UNCERTAINTY ESTIMATES

The crack length data generated is used to construct a relationship between the crack tip stress intensity factor, K , and the rate of crack growth per cycle, da/dn . The crack tip stress intensity factor is a function of crack length, load, and materials parameters. The simplest technique for determining da/dn is to simply measure the change in crack length over a selected number of fatigue cycles. To obtain statistically meaningful data, crack length measurements must be made at intervals which insure that a significant change in crack length has occurred. In addition, crack length measurements must be made at small enough intervals to insure that the crack tip stress intensity factor has remained essentially constant over the interval. To insure that the above requirements are met ASTM E647-78T lists the following recommendations:

Crack length should be measured at the following intervals:

$$\Delta a \leq 0.02 W \text{ for } .25 \leq a/w \leq .6$$

$$\Delta a \leq 0.01 W \text{ for } a/w > .6$$

The minimum Δa should be 0.25 mm or ten times the crack length measurement precision, whichever is greater.

In the case of the compliance technique, the crack length is not directly measured and the important parameter is the calculated compliance. Figure 1 shows a typical compliance vs. crack length plot. In this case, the plot is of dimensionless compliance vs. dimensionless crack length a/w for a displacement measurement location 3.493 cm from the load line at the specimen front. For a specimen of width of 5.08 cm, this yields a dimensionless measurement location of

$$x/w = 3.493/5.08 = - .6877$$

Figure 1 illustrates the fact that the required measurement precision for a given change in crack length is a function of the instantaneous crack length. This is particularly true, in the range of crack length of from 1-3 cm (a/w from .2 - .6) when the slope of the compliance-crack length curve is the shallowest. Unfortunately, this is precisely the range of crack lengths where most of the measurements are made.

V. SOURCES OF UNCERTAINTY IN CRACK LENGTH MEASUREMENT

The sources of error or uncertainty in crack length measurement using the compliance technique in a system such as the one described previously can be divided into three basic categories; (1) electronics uncertainties, (2) uncertainties due to system design, and (3) uncertainties due to nonideal materials behavior.

Uncertainties associated with system electronics are usually the most easily quantifiable and therefore the easiest to deal with. Modern measurement instruments for load and displacement usually are capable of achieving sufficient accuracy so as to affect the analysis only to second order. However, system operating characteristics can have a negative impact on an instruments effective accuracy in a given environment. As an example, the LVDT used for the study could be calibrated externally to a precision of $0.05087 \pm .0007$ mm/volt at room temperature. However, when calibrated in the autoclave system at temperature and pressure the best that could be obtained was $0.052 \pm .003$ mm/volt. This illustrates the importance of calibration of instrumentation under the actual conditions of the experiment.

System design and operational characteristics which affect the overall accuracy of the system include (1) system temperature fluctuations and their effect on electronics fluctuations, (2) system pressure fluctuations and their effect on overall specimen load, (3) load train alignment problems and their effect on specimen load, (4) frictional loads introduced due to pull rod feed through design. All of the above items with the possible exception of item 3 are unique to the high temperature, high pressure environment.

Uncertainties introduced by "non-ideal" materials behavior result from the fact that (1) cracks don't always grow straight, (2) seldom does there exist, except during calibration, a true case of plane stress or plane strain which leads to (3) crack tunneling.

An estimate of the uncertainty introduced by "non-ideal" materials behavior other than an upper bound is almost impossible from a practical point of view. Using the compliance technique allows one to ignore the problem if one accepts the concept of an effective through thickness straight crack. However, in reality one does not really have anything close to the ideal case of a straight crack especially for tough materials. This fact introduces an unknown error which should be considered when using data generated by the compliance technique for design.

Required Compliance Precision

An estimate can be made of the required precision in compliance measurement for a given crack length if we use as a base the recommendations put forth in ASTM E647-78T. Accordingly, we place the following requirements on an analysis for a specimen of width 5.08 cm.

°The crack length measurement interval should be

~~.25~~ ~~2.5~~ mm or ten times the measurement precision
whichever is greater.

°Crack length measurement interval should be

$$\Delta a \leq 1.02 \text{ mm for } .25 \leq a/w < 0.6$$

$$\Delta a \leq .51 \text{ mm for } a/w > 0.6$$

For an a/w of from .25 to .6 the ten times precision requirement results in a required measurement precision of .102 mm. Table 1 shows the required compliance measurement precision for various normalized crack lengths for a displacement measurement location of $\sim .6877$. One can see that, as pointed out earlier, the required precision is quite high for low values of a/w and indeed is quite high when compared to what can be reasonably obtained under ideal conditions.

Actual Estimated Uncertainty in Crack Length Measurement

The experimental system described earlier was analyzed to obtain an estimate of the expected uncertainty in crack length measurement. The analysis was carried out in two steps. First, the analysis was conducted for room temperature, air conditions using the same experimental set up with regard to

TABLE 1

Required Compliance Measurement
Precision to Meet ASTM-E647-78T
Requirements

Normalized Crack Length (a/w)	Approximate Compliance (BEV _x /P)	Required Accuracy of Compliance Measurement as Per ASTM E647-78T
0.2	32.6	0.4 %
0.3	42.7	0.5 %
0.4	58.8	0.7 %
0.5	85.5	0.8 %
0.6	134.0	1.0 %
0.7	241.0	1.2 %
0.8	600.0	2.3 %

grips, fixtures, etc. as that for the high temperature, high pressure work. Once this was done, the same procedure was carried out at temperature and pressure. The basic equations for propagation of errors are given by Bevington (3) for a dependent variable which is calculated as a combination of several independent variables. For the simplified case where the uncertainties in individual independent variables are uncorrelated the variance of the dependent variable can be expressed as

$$\sigma_x^2 = \sigma_u^2 \left(\frac{\partial x}{\partial u} \right)^2 + \sigma_v^2 \left(\frac{\partial x}{\partial v} \right)^2 + \dots \quad (2)$$

where $x = uv$

$$\left(\frac{\partial x}{\partial u} \right), \quad \left(\frac{\partial x}{\partial v} \right) = \text{partial derivatives} \quad (3)$$

$$\sigma_x^2, \sigma_u^2, \sigma_v^2 = \text{variances in associated variables}$$

The assumption of uncorrelated variances between independent variables is a reasonable one for the room temperature - air case. However, for the high temperature, high pressure case it is expected that some degree of correlation will exist. However, the uncorrelated assumption yields an upper ~~band~~^{bound} in this case.

The basic relationship for the compliance calculation is given by equation (1)

$$C = BE \frac{dv}{dP}$$

which can be approximated by

$$C = BE \frac{\Delta V}{\Delta P}$$

Equation (4) can be further expanded to

$$C = BE \left(\frac{\Delta V}{\Delta S} \right) (\Delta S) \left(\frac{1}{\Delta P} \right) \quad (5)$$

where $\frac{\Delta V}{\Delta S}$ = calibration constant to convert LVDT output to displacement

ΔS = LVDT output voltage change for a given displacement

ΔP = change in load for a given ΔV

B = specimen thickness

E = Youngs Modules

If the uncertainties in the individual terms in (5) are uncorrelated the following formula applies for the variance of the compliance.

$$\sigma_c^2 = \sigma_B^2 \left(\frac{\partial C}{\partial B} \right)^2 + \sigma_E^2 \left(\frac{\partial C}{\partial E} \right)^2 + \sigma_{\frac{\Delta V}{\Delta S}}^2 \left(\frac{\partial C}{\partial \frac{\Delta V}{\Delta S}} \right)^2 + \sigma_{\Delta S}^2 \left(\frac{\partial C}{\partial \Delta S} \right)^2 + \sigma_{\Delta P}^2 \left(\frac{\partial C}{\partial \frac{1}{\Delta P}} \right)^2 \quad (6)$$

$$\frac{\sigma_C}{\sigma_B} = E \left(\frac{\Delta V}{\Delta S} \right) (\Delta S) \left(\frac{1}{\Delta P} \right) \quad (7)$$

$$\frac{\sigma_C}{\sigma_E} = B \left(\frac{\Delta V}{\Delta S} \right) (\Delta S) \left(\frac{1}{\Delta P} \right) \quad (8)$$

$$\frac{\sigma_C}{\sigma \left(\frac{\Delta S}{\Delta V} \right)} = BE \Delta S \left(\frac{1}{\Delta P} \right) \quad (9)$$

$$\frac{\partial C}{\partial \Delta V} = BE \left(\frac{\Delta S}{\Delta V} \right) \left(\frac{1}{\Delta P} \right) \quad (10)$$

$$\frac{\partial C}{\partial \Delta P} = -BE \left(\frac{\Delta S}{\Delta V} \right) \left(\frac{1}{\Delta P} \right)^2 \Delta S \quad (11)$$

Equation (6) requires estimates for the variances of the specimen thickness (B), the elastic modulus (E), the LVDT calibration constant $\left(\frac{\Delta V}{\Delta S} \right)$, the displacement as measured by the LVDT (ΔS), and the specimen load (ΔP). An estimate of the above mentioned variances was obtained as part of the overall system calibration procedure.

Uncertainties in Band E

The uncertainty of the specimen thickness (B) was estimated to be $\pm .25$ mm based on measurements of several tens of specimens. The uncertainty of the elastic modulus was assumed to be zero for this analysis.

UNCERTAINTIES IN LVDT CALIBRATION ($\frac{\Delta s}{\Delta V}$)

An estimate of the uncertainties in the LVDT calibration was obtained by calibrating the LVDT using a capacitance gauge as a standard with an accuracy of $\pm .0005$ mm. For the room temperature case the LVDT, was attached directly to the calibration fixture and calibrated over a 0.5 mm interval in steps of 0.025 mm. This calibration procedure was repeated until twenty sets of twenty measurement are made. The calibration constant was found to be $.05087 \pm .0007$ mm/volt.

The high temperature calibration was performed by attaching the LVDT to the specimen grips with no specimen attached and bringing the system to operating temperature and pressure. The capacitance gauge was then attached to the fatigue machine actuator was then assumed to be equal to the displacement of the LVDT ~~case~~ ^{Coax}. The calibration procedure was then carried out as described earlier. The calibration constant for the operating environment was found to be $.0521 \pm .0035$ mm/volt. The operating environment resulted in a factor of 5 increase in the measurement uncertainty.

UNCERTAINTY IN SYSTEM LOAD MEASUREMENT (ΔP)

Uncertainties in specimen load are due to several factors. The design of the system pressurization system makes use of a positive displacement reciprocating pump and a back pressure regulator. The nature of the pump operation results in a system pressure fluctuation with a frequency corresponding to the speed of rotation of the pump. The pressure pulsations are damped out to the maximum extent possible by using a pulsation damper on the pump discharge. In spite of this there is a finite pressure fluctuation which results in a load fluctuation

on the specimen which is not fully compensated for by the fatigue machine electronics.

Another source of load uncertainty is due to friction between pullrods and autoclave seals as well as load train miss-alignment. The system design tends to minimize the load-train miss-alignment. This condition is illustrated by the fact that the fatigue cracks remain in the plane perpendicular to the load line and the front and back surfaces of the crack remain aligned. Load uncertainties due to seal friction was estimated to be $\pm .034$ Mpa by recording the load fluctuation during ~~actual measurement~~ ^{actuator movement} without a specimen installed. An overall uncertainty in load was estimated to be $\pm .069$ Mpa due to friction and system pressure fluctuations.

UNCERTAINTY IN DISPLACEMENT MEASUREMENT (ΔS)

The uncertainty in displacement measurement was determined for each compliance measurement during a test. The change in displacement for a given change in load was measured by interrupting a test and recording load and displacement for a series of unloading steps. The unloading measurement procedure was performed 5 times for each compliance measurement. The uncertainty in displacement measurements varied slightly from specimen to specimen measurement but averaged .0056 volt.

VI. COMPLIANCE CALIBRATION

As pointed out earlier, the uncertainty analysis was carried out as part of the compliance calibration procedure. The compliance calibration was performed using specimens with accurately machined cracks of specific lengths as well as with specimens which were beach marked at specific intervals during a fatigue crack growth test. Compliance calibration

was performed at both room temperature as well as operating conditions. Figures 2, 3 show the compliance calibration results for two measurement locations for the case where specimens with accurately machined cracks were used. The upper curve corresponds to a condition of plane stress while the lower curve corresponds to a condition of plane strain with a poisson's ratio of 0.3. The calibration data at both room temperature and operating conditions agree with the theoretical curve for plane stress to within 2.5%.

Figure 4 shows the calibration data for beach marked specimens. For this case the influence of non-ideal materials behavior becomes evident. For the actual fatigue cracking case the fatigue crack does not remain straight but grows under a mixed mode between plane stress and plane strain depending on whether you are at the specimen edge or center. For the specimen size and loading conditions in question the dominant mode is one of plane strain as indicated by the minimum shear lip formation. This fact is illustrated in Figure 4 by the closeness of the data to the plane strain curve. The data points in Figure 4 represent data generated at room temperature as well as operating temperature and pressure.

VII. UNCERTAINTY IN COMPLIANCE MEASUREMENT

When one combines the estimates of the uncertainties in the estimated values of each component in equation 5, an estimate of the overall uncertainty of the compliance is obtained. When this is done, we estimate that for room temperature air measurement and a range of a/w of from 0.2 to 0.4 that there will be approximately a 1.5%

uncertainty in the compliance estimate. This translates to an estimated uncertainty in crack length measurement of $\pm .25$ mm. When one compares this with the estimated requirements listed in Table 1 we can see that these requirements are hard to meet for short cracks.

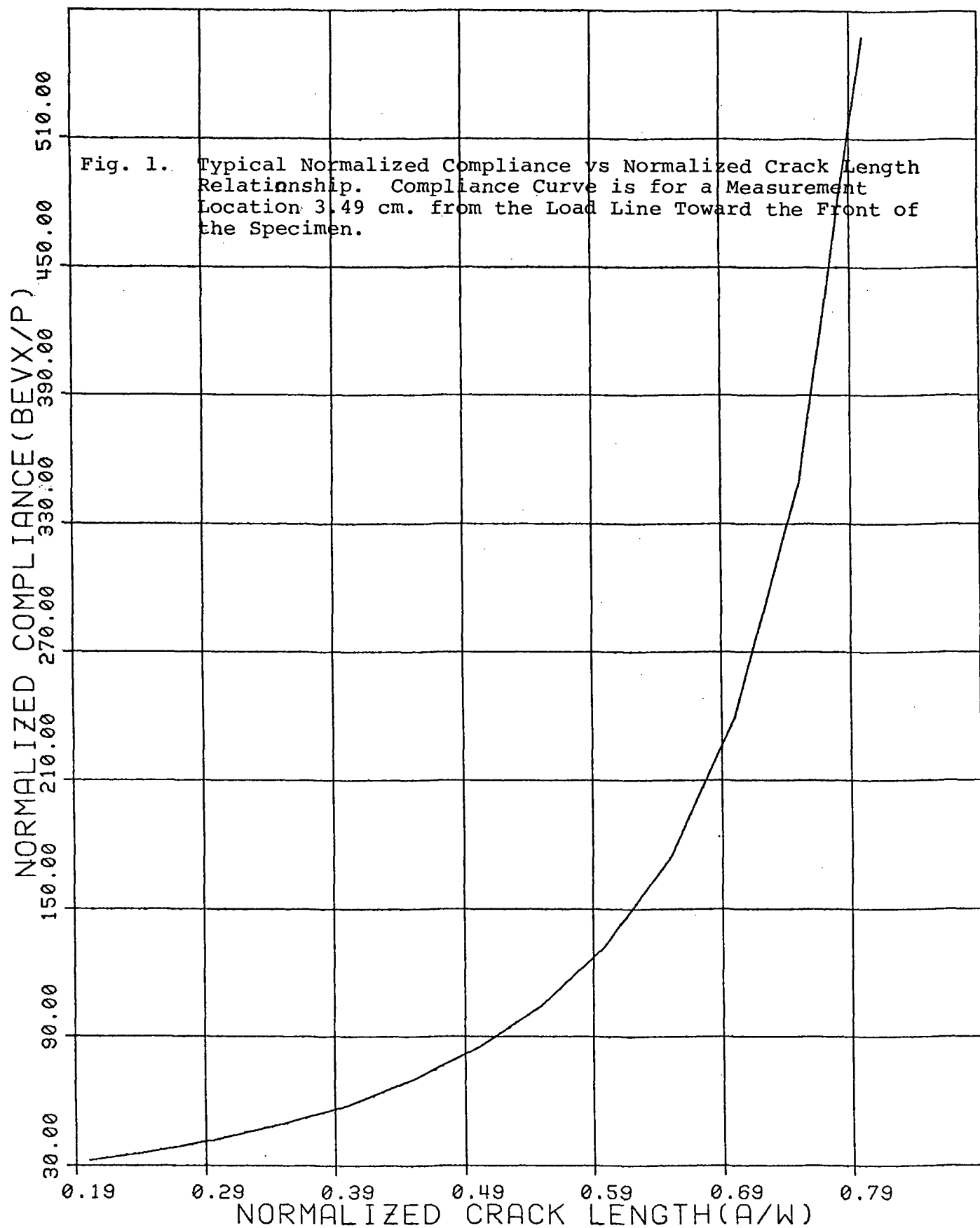
For the case of high temperature and pressure the estimated uncertainty estimate increases to an average of 6.5% which translates to an uncertainty in crack length of ± 1.83 mm which, if correct, is unacceptable.

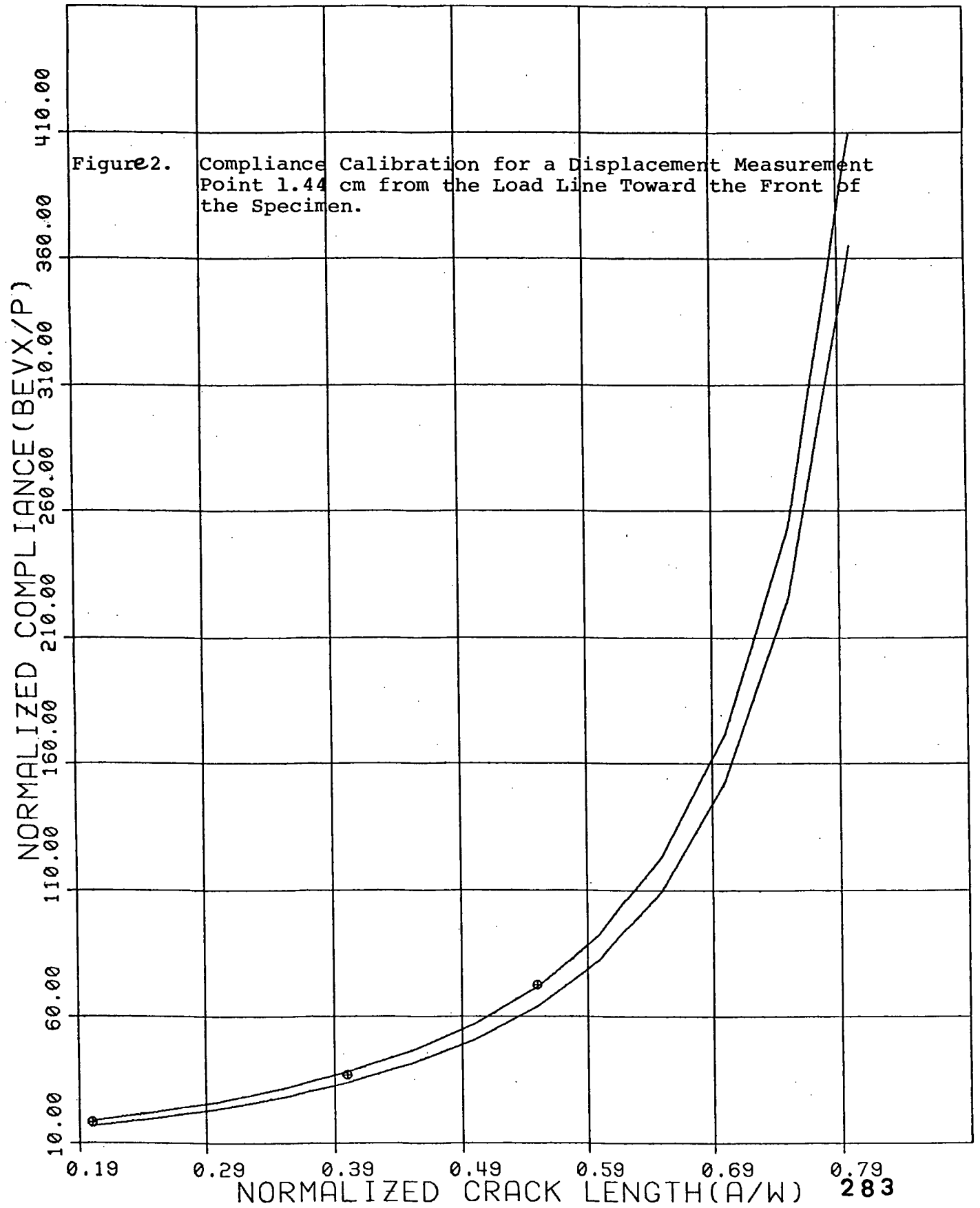
As pointed out earlier, it is anticipated that the individual variances for the high temperature case will exhibit some degree of correlation by the very nature of the calibration procedure. The LVDT calibration procedure was carried out under the influence of the system pressure fluctuations. Such correlations can be expected to reduce the actual uncertainty. But in no case can the uncertainty be reduced to less than that for the air calibration case. Another indication that the uncertainty may be lower than estimated is illustrated by the closeness with which both the air and high temperature calibration data fit the theoretical compliance curve of Figure 4. Further work needs to be done especially with regard to estimating the degree of correlation between variables but, nevertheless, the analysis indicates that care should be exercised when generating and interpreting crack growth data under actual experimental conditions. From a practical standpoint the

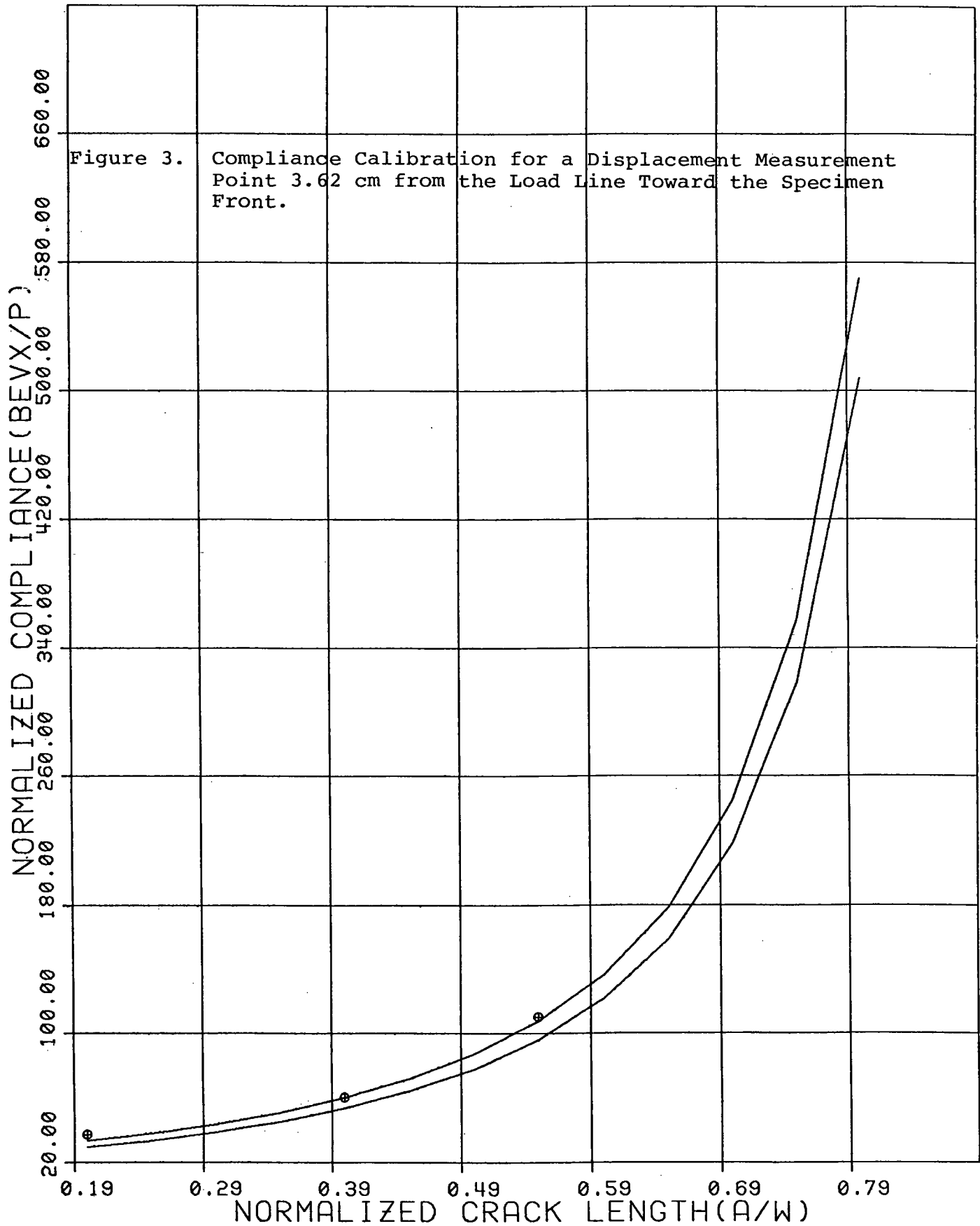
required measurement precision in order that the criteria of ASTM E 647-78T be met, cannot be achieved, at least for our experimental setup. The alternative is to increase the crack measurement interval to the maximum extent possible consistent with a reasonably constant stress intensity factor over that interval.

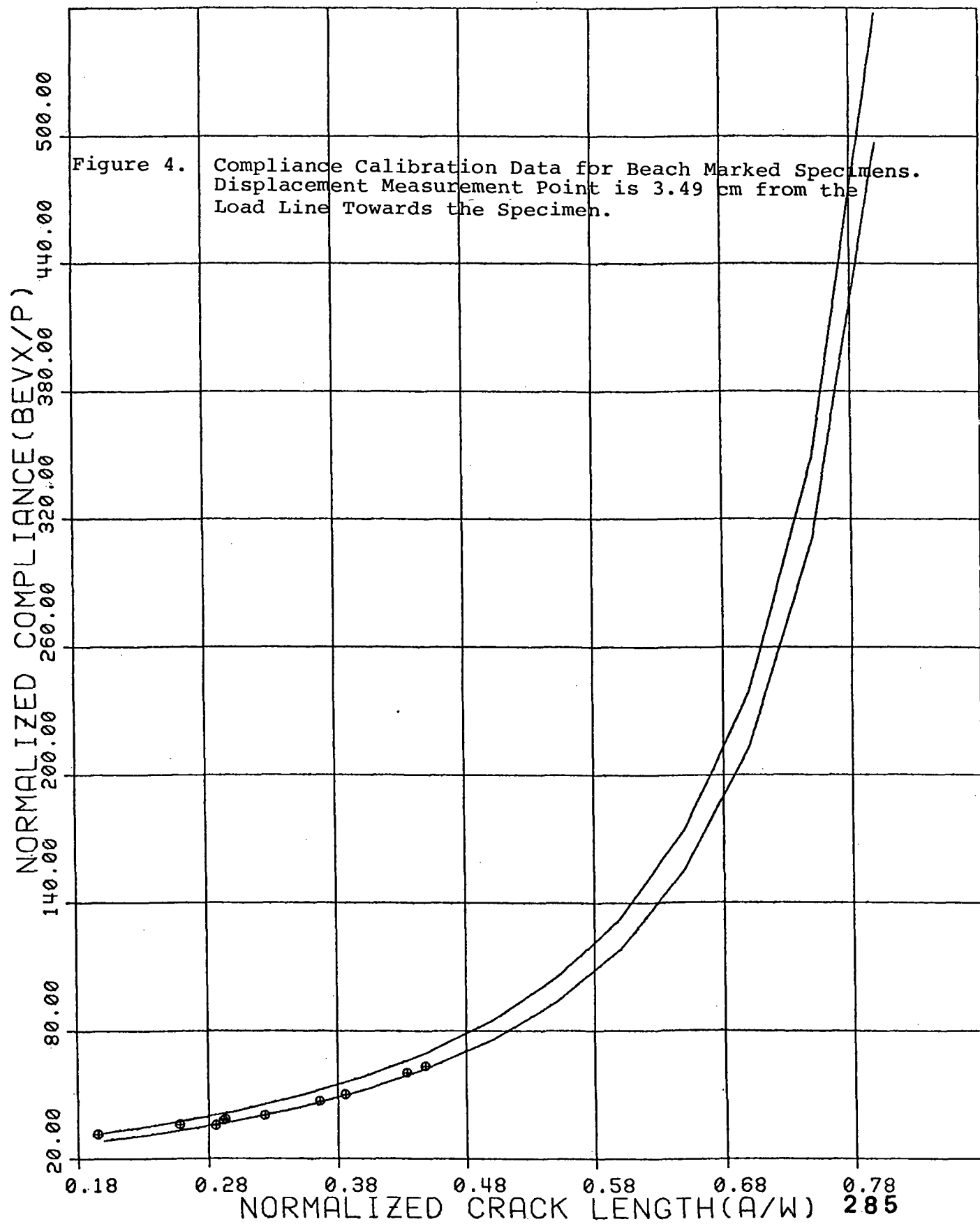
References

1. A. Saxena and S. J. Hudak, Jr., Review and Extension of Compliance Information for Common Grade Growth Specimens, Int. J. of Fracture, Vol. 14, No.5. Oct. 1978.
2. J. C. Newman, Jr., Stress Intensity Factors and Crack Opening Displacements for Round Compact Specimens, NASA Technical Memorandum 80174.
3. P. R. Bevington, Data Reduction and Error Analysis for the Physical Sciences, McGraw-Hill, 1969.









NRC FORM 335 (7-77)		U.S. NUCLEAR REGULATORY COMMISSION BIBLIOGRAPHIC DATA SHEET		1. REPORT NUMBER (Assigned by DDC) NUREG/CP-0044, Vol. 1 MEA-2014	
4. TITLE AND SUBTITLE (Add Volume No., if appropriate) Proceedings of the International Atomic Energy Agency Specialists' Meeting on Subcritical Crack Growth				2. (Leave blank)	
				3. RECIPIENT'S ACCESSION NO.	
7. AUTHOR(S) Edited by W. H. Cullen				5. DATE REPORT COMPLETED MONTH April YEAR 1983	
9. PERFORMING ORGANIZATION NAME AND MAILING ADDRESS (Include Zip Code) Materials Engineering Associates, Inc under contract to: 9700B George Palmer Highway ENSA Lanham, MD 20706 3320 Bailey Avenue Buffalo, NY				DATE REPORT ISSUED MONTH May YEAR 1983	
				6. (Leave blank)	
12. SPONSORING ORGANIZATION NAME AND MAILING ADDRESS (Include Zip Code) Division of Engineering Technology Office of Nuclear Regulatory Research U.S. Nuclear Regulatory Commission Washington, D.C. 20555				8. (Leave blank)	
				10. PROJECT/TASK/WORK UNIT NO.	
13. TYPE OF REPORT Conference Proceedings				11. CONTRACT NO. NRC FINB8133	
				PERIOD COVERED (Inclusive dates)	
15. SUPPLEMENTARY NOTES				14. (Leave blank)	
16. ABSTRACT (200 words or less) This report is a compilation of papers which were presented at the IAEA Specialists' Meeting on Subcritical Crack Growth, held at the Fraunhofer-Institute for Fracture Mechanics, Freiburg, Federal Republic of Germany, May 13-15, 1981. These papers describe the experimental procedures for and interpretation of results of fatigue crack growth rate testing of pressure vessel and piping steels in pressurized, high-temperature water.					
17. KEY WORDS AND DOCUMENT ANALYSIS			17a. DESCRIPTORS		
17b. IDENTIFIERS/OPEN-ENDED TERMS					
18. AVAILABILITY STATEMENT Unlimited			19. SECURITY CLASS (This report) unclassified		21. NO. OF PAGES
			20. SECURITY CLASS (This page) unclassified		22. PRICE \$

UNITED STATES
NUCLEAR REGULATORY COMMISSION
WASHINGTON, D.C. 20555

OFFICIAL BUSINESS
PENALTY FOR PRIVATE USE, \$300

FOURTH CLASS MAIL
POSTAGE & FEES PAID
USNRC
WASH. D. C.
PERMIT No. G-62